Universidade do Minho
Escola de Engenharia

Chirita Georgel Maricel

Mechanical and Fatigue Properties of Functionally Graded Aluminium Silicon Alloys

Fevereiro de 2011

Mechanical and Fatigue Properties of Functionally Graded Aluminium Silicon Alloys
Chirita Georgel Maricel
UMinho | 2011

Universidade do Minho
Escola de Engenharia

Chirita Georgel Maricel

Mechanical and Fatigue Properties of Functionally Graded Aluminium Silicon Alloys

Tese de Doutoramento
Área de Mecânica de Materiais / Ramo de Engenharia Mecânica

Trabalho efectuado sob a orientação de
Professor Doutor Filipe Samuel Silva
Universidade do Minho, Guimarães, Portugal
Ioan I. Stefanescu
Universidade Dunarea de Jos, Galati, Romania

Fevereiro de 2011

This thesis is dedicated to my wife Mioara,

for her love, endless support

and encouragement!

ACKNOWLEDGMENTS

During the development of my doctoral studies in the University of Minho several persons from different departments have collaborated directly and indirectly with my research. That is why I wish to dedicate this section to recognize their support.

I want to start expressing a sincere acknowledgement to my advisor, Dr. Filipe Samuel Silva because he gave me the opportunity to research under his guidance and supervision. I received motivation, encouragement and support from him during all my studies. Special thanks I owe Dr. Ioan Stefanescu for the opportunity of working under his support and guidance. I would like to thank to Dr. Delfim Soares for his valuable advices, constructive discussion and interpretation of some results presented in this thesis.

I also owe my appreciation to many other members of Mechanical Engineering Department from Minho University for the encouragement, advices and suggestions of the work. Here are the names of those who have substantially contributed to the successful completion of this particular work: Dr. Nuno Costa, Mr. Fernando Araújo, Vitor Neto, Dr. Joaquim Barbosa, Engineer Daniela Cruz, Dr. Helder Puga, Dr. Eurico Seabra, Miguel Abreu, Mr. Julio Caldas.

Finally, I gratefully acknowledge the FCT - Fundação para a Ciência e a Tecnologia for their financial support throughout the BD-Bolsa de Doutoramento (PhD Grant) with the reference SFRH/BD/19618/2004.

MECHANICAL AND FATIGUE PROPERTIES OF FUNCTIONALLY GRADED ALUMINIUM SILICON ALLOYS

ABSTRACT

Many structural components encounter service conditions and, hence, required materials performance, which vary with location within the component.

It is well known that abrupt transitions in materials composition and properties within a component often result in sharp local concentrations of stress, whether the stress is internal or applied externally. It is also known that these stress concentrations are greatly reduced if the transition from one material to the other is made gradual. By definition, functionally graded materials are used to produce components featuring engineered gradual transitions in microstructure and/or composition, the presence of which is motivated by functional performance requirements that vary with location within a part. With functionally graded materials, these requirements are met in a manner that optimizes the overall performance of the component.

The research on functionally graded materials (FGMs) is encouraged by the need for properties that are unavailable in any single material and the need for graded properties to offset adverse effects of discontinuities for layered materials. Centrifugal casting is a very common method for obtaining functionally graded materials, mainly composite materials or metallic materials which has high differences of density and low solubility on different phases or different materials of the same alloy. The present work is emphasizing the fact that the centrifugal process could be successfully used for obtaining functionally graded materials also for metallic materials (alloys) with moderate solubility and small differences of density of the different phases, as is the case of most aluminum alloys.

The first approach of the problem was to isolate the effects of the centrifugal casting technique (the centrifugal pressure effect, the fluid dynamics and the inherent vibration effects) in order to identify the reason of mechanical properties improving. To have a reference for comparison, castings obtained by both centrifugal casting technique and gravity casting technique were tested.

To isolate the vibration effect, experimental equipment was designed and constructed in order to be able to cast within a certain level of vibration equivalent with the vibration level of the centrifugal casting equipment. The results are confirming that there is a correlation of improving mechanical properties with the vibration of the melt during solidification.

The difference of the mechanical properties of castings obtained by gravity casting technique and by centrifugal casting technique could be explained by the fact that, the vibration due to the inherently vibration of the equipment, the fluid dynamics and the centrifugal pressure make the melt, during solidification, to initiate more nuclei of solidification. Then, the centrifugal pressure moves the nuclei of solidification to the furthest point of the mould (where the pressure is higher) fact that explains the obtained results which are higher on one side of the ingots which corresponds with the side of the mould where the pressure is higher and smaller on the other side where the pressure is smaller. This causes several differences in microstructures in both sides of the ingot.

The mechanical and fatigue properties are largely influenced by microstructure and the presence of material inhomogeneities. Pores, inclusions or secondary phase particles are common sites for fatigue crack nucleation in aluminium alloys. The constituent particle's size and shape are also important characteristics that influence crack nucleation.

This study intends to assess also the problem of fatigue life prediction by establishing a relation within some of the characteristics of the micro structural features of studied aluminium silicon alloys such as: micropores, secondary dendrites arm spacing (SDAS), volume fractions of phases (α-Al phase, eutectic and intermetallic phases), the size of silicon lamellas in interdendritic eutectic regions and the size and shape of silicon particles. This evaluation was performed along the ingots gradients for different aluminum alloys.

PROPRIEDADES MECÂNICAS E DE FADIGA DE LIGAS DE ALUMÍNIO-SILÍCIO COM GRADAÇÃO FUNCIONAL

RESUMO

Muitos componentes estruturais, nas suas condições de serviço, requerem desempenhos que variam com a localização dentro do componente.

É sabido que transições bruscas de composição química dos materiais no componente muitas vezes resultam em acentuadas concentrações de tensão locais. É também sabido que estas concentrações de tensões são muito reduzidas/atenuadas se a transição de um material para outro é feita gradualmente. Por definição, materiais com gradiente funcional de propriedades são usados para produzir componentes de engenharia com transições graduais na microestrutura e / ou composição química, cuja presença é motivada por exigências de desempenho funcional, que variam com a localização de cada parte do componente. Com materiais com gradiente funcional, estes requisitos são cumpridos de uma forma que otimiza o desempenho geral do componente.

A pesquisa sobre materiais com gradiente funcional (FGMs) é incentivada pela necessidade de propriedades que não estão disponíveis em qualquer material único ou em componentes obtidos pelas junção de partes diferentes materiais onde existe o efeito negativo da sua junção.

A fundição centrífuga é um método muito comum para a obtenção de materiais com gradiente funcional, principalmente materiais compósitos ou materiais metálicos, que tem grandes diferenças de densidade e baixa solubilidade em diferentes fases ou em diferentes materiais da mesma liga. O presente trabalho visa enfatizar o fato de que o processo de fundição centrifuga pode ser utilizada com sucesso para a obtenção de materiais com gradiente funcional também para materiais metálicos (ligas) com solubilidade moderada e pequenas diferenças de densidade das diferentes fases, como é o caso da maioria das ligas de alumínio. A primeira abordagem do problema foi isolar os efeitos da técnica de fundição centrífuga (o efeito das pressões centrífugas, a dinâmica dos fluidos e os efeitos da vibração inerente), a fim de identificar o motivo da melhoria das propriedades

mecânicas. Para ter uma referência para comparação, foram obtidos e testados provetes de vazamentos por ambas as técnicas, quer de fundição centrífuga quer de fundição por gravidade. Para isolar o efeito da vibração, um equipamento experimental foi projetado e construído de modo a ser capaz de reproduzir um determinado nível de vibração equivalente ao nível de vibração do equipamento de fundição centrífuga. Os resultados confirmam que há uma correlação entre a melhoria das propriedades mecânicas com a vibração da liga durante a solidificação. A diferença das propriedades mecânicas de peças fundidas obtidas pela técnica da gravidade e pela técnica de fundição centrífuga poderia ser explicada pela vibração inerente do sitema, pela dinâmica dos fluidos e pel pressão centrífuga, que originam, durante a solidificação, mais núcleos/germens de solidificação. A pressão centrífuga move os núcleos de solidificação para o ponto mais afastado do eixo de rotação (onde a pressão é maior) que explica que os resultados obtidos são mais elevados nessa zona do que do lado mais próximo do eixo de rotação, que corresponde ao lado do molde em que a pressão é menor. Isto causa substanciais diferenças de microestrutura e mambos os lados dos lingotes.

As propriedades mecânicas e de fadiga são grandemente influenciadas pela microestrutura assim como pela presença de inomogeneidades no material. Poros, inclusões ou partículas de fases secundárias são responsáveis pela nucleação de fendas de fadiga em ligas de alumínio. O tamanho das partículas e a sua forma são também características importantes que influenciam a nucleação da fenda. Este estudo pretende avaliar a previsão da vida à fadiga através de correlações com características microestruturais das ligas de alumínio-silício estudadas tais como: microporos, espaçamento entre braços das dendrites (SDAS), frações volumicas de fases ou constituintes(α primária, eutético e intermetálicos), a espessura das lamelas do silicio eutéctico e dimensões de partículas de silicio eutéctico. Esta avaliação é feita para diferentes diferentes zonas ao longo do gradiente de propriedades dos lingotes das diferentes ligas de alumínio.

KEYWORDS

FUNCTIONALLY GRADED MATERIALS
GRAVITY CASTING
CENTRIFUGAL CASTING
VIBRATING CASTING
MECHANICAL PROPERTIES
FATIGUE LIFE

PALAVRAS-CHAVE

MATERIAIS COM GRADAÇÃO FUNCTIONAL
FUSÃO COM GRAVIDADE
FUSÃO CENTRÍFUGO
FUSÃO VIBRATÓRIA
PROPRIEDADES MECÂNICAS
FADIGA

TABLE OF CONTENTS

LIST OF FIGURES

CHAPTER 1 – INTRODUCTION

CHAPTER 4 – RESULTS

CHAPTER 5 – FURTHER RESULTS

CHAPTER 6 – DISCUSIONS

CHAPTER 7 – CONCLUSIONS

LIST OF TABLES

NOMENCLATURE

Latin symbols

Symbol	SI-Unit	Eq	Description
C		2.1	Constants related to material
n		2.1	Constants related to material
ts	s	2.1	Local solidification time
K	-	2.3	Constant
V_V^{α}	mm^3	2.4	Volume fraction of aluminium phase
V_V^{Si}	mm^3	2.4	Volume fraction of silicon phase
k, k_2, k_3	-	2.6	Constants
Hv	Kgf/mm^2	2.9	Vickers Hardness
DAS	μm	2.2	Dendrites Arm Spacing
$\sqrt{area}$	μm	2.10	Square root of pore area
Ra	μm		Surface roughness
$k_{1\ stress}$ $k_{1\ strain}$		6.1	Factors that introduces the influence of SDAS, primary silicon particles size; intermetallics type, size, and distribution
$k_{2\ stress}$ $k_{2\ strain}$		6.1	Factors that introduces the influence of phase morphology and distribution on the eutectic constituent
T_P			Total number of points
P_F	%		Point fraction
P_{avg}	%	3.4	Average Point fraction
Vf	%	*3.4*	volume fraction
V_T	%	*3.1*	Total volume
V_A	%	*3.1*	Volume of A
P(A)		*3.1*	Probability of the point hitting the A phase
Qi	MPa		Quality Index

Symbol	SI-Unit	Eq	Description
UTS	MPa		Ultimate Tensile Strength
Vf_{eut}	%		Volume fraction of eutectic
Vf_{dend}	%		Volume fraction of aluminum phase
Vf_{int}	%		Volume fraction of intermetalic
th_{eut}	μm		Thickness of eutectic
th_{int}	μm		Thickness of intermetalic

Greek symbols

Symbol	SI-Unit	Eq	Description
γ	μm	2.6	The size of silicon lamellas in interdendritic eutectic regions
λ	μm	2.6	Secondary dendrite arm spacing
ε	-		Rupture Strain
σ	MPa	2.4	Tensile stress
σ_{Si}	MPa	2.4	Tensile stress of silicon phase
σ_u	MPa	2.8	Ultimate static strength
σ_w	MPa	2.8	Fatigue limit
σ_α	MPa	2.4	Tensile stress of aluminium phase
σ_f	MPa	6.5	Fatigue limit

Abbreviations

Symbol	Description
3D	Three Dimensions
Al- Si	Aluminium Silicon alloys
ASTM	American Society for Testing And Materials
CC	Centrifugal Casting
CNC	Computer Numerical Control
E-N	Strain-life
EPS	Expandable Polystyrene
FCT	Fundação para a Ciência e a Tecnologia
FEM	Finite Element Method
FGM	Functionally Graded Material
GC	Gravity Casting
HDSI	High-pressure Direct Spark Injection
HIP	Hot Isostatic Pressing
LM25	Al-Si7Mg0.5
LM6	Al-Si12
RT	Room Temperature
SAE	Society of Automotive Engineers
SDAS	Secondary Dendrites Arm Spacing
SEM	Scanning electron microscope
SF	Strain to failure
S-N	Stress-life
T6	Solution heat treated and artificially aged
TDC	Top Dead Center
TEM	Transmission Electron Microscopy
UTS	Ultimate Tensile Strength
VGC	Vibrating Gravity Casting
YS	Yield Strength
α-Al	Primary Aluminum Phase
ΔK	Stress intensity

CHAPTER 1

INTRODUCTION

MATERIALS are selected and used as a result of a match between their properties and the needs dictated by the intended application. In this sense, the properties should be defined broadly and include fabricability, required maintenance, costs associated with the original materials and maintenance, and the behavioural characteristics associated with the function of the item within the overall design [1]. Material specific properties such as density, thermal conductivity, fatigue behaviour and wear resistance, as well as creep and deformation properties must also be taken into account.

1.1 Background

Engine pistons are one of the most complex components among all automotive or other industry field components. There are lots of research works proposing, for engine pistons, new geometries, materials and manufacturing techniques, and this evolution has undergone with a continuous improvement over the last decades and required thorough examination of the smallest details.

Piston materials and designs have evolved over the years and will continue to do so until fuel cells, exotic batteries or something else makes the internal combustion engines obsolete.

The piston is one of the most stressed components of an entire vehicle – pressures at the combustion chamber may reach about 180–200 bar [2] – a few years ago this value was common only for heavy-duty trucks but nowadays it is usual in HDSI engines. To reach speeds of about 25 m/s the temperatures at the piston crown may reach about 400 ^{0}C [2].

The temperature of the engine piston parts becomes higher with the increasing of the specific power output (Figure 1.1)[3]. As one of the major moving parts in the power-transmitting assembly, the piston must be so designed that it can withstand the extreme heat and pressure of combustion. Pistons must also be light enough to keep inertial loads on related parts to a minimum.

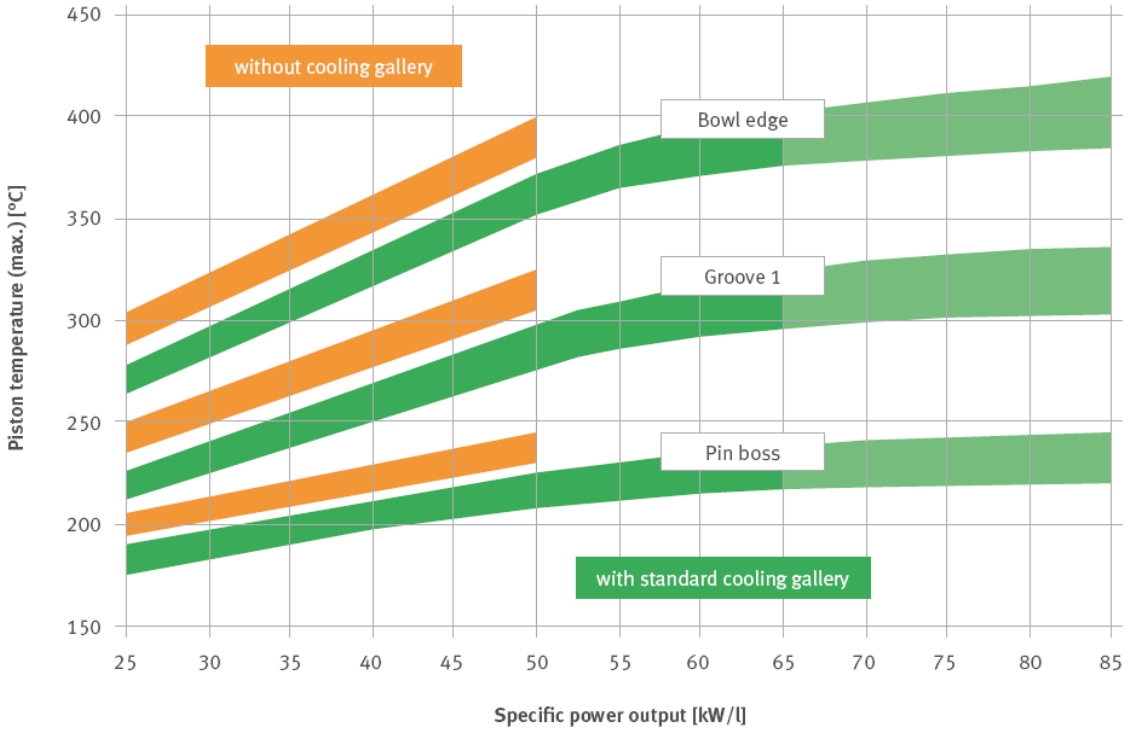

Figure 1.1 - Temperature in a diesel engine piston as a function of engine power output [3]

The piston also aids in sealing the cylinder to prevent the escape of combustion gases. It also transmits heat to the cooling oil and some of the heat through the piston rings to the cylinder wall.

The pistons take up and transmit to their connecting rods the forces resulting from the gas pressure in the cylinders, and also participate in all the operations constituting the working cycle of the engine. The pistons are exposed to high temperatures and pressures, and move with significant velocities inside the cylinders. Accordingly, their material must be adequately strong and wear-resistant; it must be light in weight and conduct heat well.

Therefore, the pistons in modern engines are cast in a light-weight, but sufficiently strong aluminium alloy.

The structural components of the pistons (Figure 1.2)[4] are: 1) the head, 2) ring grooves 3) lands 4) piston pin and 5) skirt ; however, not all piston look like the typical one shown here. Some have differently shaped heads. Diesel engine pistons usually have more ring grooves and rings than the pistons of a gasoline engine. Some of these rings may be installed below as well as above the wrist or piston pin. The pistons of diesel engines are made with recesses (cavities) in their tops, whose shape depends on the method of mixing the fuel with air and the arrangement of the valves and fuel injectors.

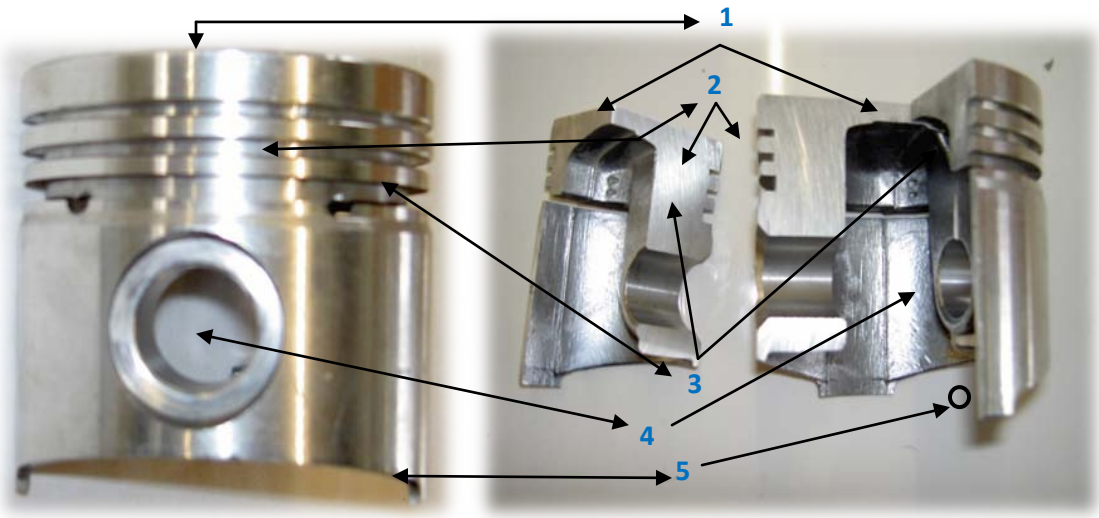

Figure 1.2 - Engine piston parts: 1. piston head, 2. piston rings grooves, 3. lands 4. piston pin, 5. skirt, [4].

The outer surface of the piston head and skirt is provided with grooves to accommodate compression and oil-control rings, respectively. The number of the rings installed on a piston depends on the engine type and the crankshaft rotation frequency. In some engines, a metallic-bonded steel groove insert is used for the top compression ring in order to improve the wear resistance of the ring-to-groove joint, and thus increase its durability. Oil-ring grooves have through holes drilled in their backs around the periphery of the piston to drain the oil scraped off by the rings into the engine crankcase.

On the inside of the piston skirt, there are two bosses 4 with holes to fit the piston pin (also known as the gudgeon pin). The piston pin bosses are joined with the piston crown by intermediate supporting webs, which improve the strength of the piston. Annular grooves cut in the pin holes serve to accommodate piston pin lock rings, or retainers. The piston skirt is relieved on the outside opposite the piston pin bosses, so that oil pockets – "coolers" – are formed where oil is accumulated to facilitate the cooling of the thickened part of the piston and prevents it from becoming stuck in the cylinder. The latter end is also attained with pistons machined to a special form, which is both tapered in profile (the skirt diameter is greater than the head diameter) and oval in contour (the major axis of the skirt is disposed in the direction across the piston pin).

1.1.1 Function of engine piston in an engine

The piston may be the hardest-working part in the internal combustion engine. Following is just a brief outline of the piston's function and construction.

Three Jobs

The piston does three important jobs. It is a bearing, receiving loads from combustion and transferring them straight and true through the connecting rod to the crankshaft. The piston is also a seal, as it seals combustion's forces and compression's trapped air. Finally, the piston is a heat conductor, transferring some of the cylinder's heat to the outside. In fact, nearly 80 percent of the cylinder's excess heat is drawn away by just the piston's rings.

Piston Parts

The piston is made of essentially seven parts. The piston's top or *crown* takes the brunt of combustion's forces and heat. Consequently, the crown is the hottest part of the engine after the spark plug. It must therefore be quite thick so as to not collapse, though it is not always the thickest part of the piston. Moving down the piston, the next thing is the *ring groove*. The closely manufactured groove accepts the third part, the precisely made *piston ring*. In the four-stroke engine, natural harmonics cause the ring to rotate as the piston goes up and down in the cylinder. This helps the groove stay clean of carbon. The solid pieces between the grooves are called *ring lands.* They are similar to the lands in a gun barrel. They

support the shock loads the rings receive during combustion. The next part is the *piston pin hole*. This hole accepts a pin that connects the piston to the connecting rod. The hole is offset from the piston's center slightly so that when the piston and rod reach TDC (Top Dead Center), they do so at slightly different times. This spreads the shock loads at high rpm, easing stresses on the connecting rod and eliminating a noise called "piston slap." Surrounding the hole *inside* the piston are *pin bosses*, thick masses of metal that support the pin when it is inserted in the hole. The pin bosses are sometimes the thickest part of the piston. In some cases, they are not as thick as the crown. In either case however, the thickness of these two parts is important, as it determines much about how the piston deals with heat. Lastly, we come to the *piston skirt*. The skirt is the bearing portion of the piston. It slides against the cylinder wall, bearing the force of combustion on the power stroke and the loads of compression on the compression stroke. There are also stresses involved with rpm that the piston and cylinder are designed together to deal with. The skirt is the part of the piston most in need of lubrication. Thus most lubrication problems show up on the piston skirt first.

Piston Shapes

There are two important ways in which pistons are shaped. First, the piston is not round, but elliptical in shape. The reason is the afore-mentioned pin bosses. The bosses' mass makes them absorb a lot of heat, which makes them expand more than any part of the piston. If the piston was instead made round, it would not be when fully warmed up. That would be a problem. Therefore, the width of the piston at the area of the bosses is narrower than it is elsewhere. The resulting shape (looking downward onto the piston crown) is an ellipse (an oval). The other (second) shape that all pistons have is *taper*. That is, the diameter of the piston at its crown is considerably smaller than its diameter at the skirt. The reason is the same as for the piston's ellipse. Only this time it is the crown, not the pin bosses, that necessitates the shape. The crown absorbs so much heat that it must be made smaller so that when fully heated, the piston will be straight.

Piston Manufacturing Methods

Pistons are manufactured in one of two ways. Those two ways are the cast piston and the forged piston. The *cast* piston is made of molten aluminium. The alloy is flowed into a mould having the shape of the finished product, in much the same way that many other cast parts are made. Piston moulds are permanent *dies*, intricately made multiple-piece steel shapes. The molten aluminium is vacuum drawn into the mould. So accurate is the process that the resulting casting requires minimal machining. The *forged* piston is made very differently. The metal is not molten, but heated somewhat. A blob of this hot aluminium alloy called an ingot is placed in a female mould, and a male ram is pounded into it. The result is not a piston, but a piston blank, which must then undergo many machining operations before it resembles a piston. These two methods of making pistons continue today.

1.1.2 Service loads and failures experienced by engine piston

Even if technological evolution riches high levels, there are still a significant number of damaged pistons. Damages may have different origins: mechanical stresses; thermal stresses; wear mechanisms; temperature degradation, oxidation mechanisms etc.

Piston damages are mostly attributed to wear and lubrication sources, but fatigue is also responsible for a significant number of piston damages. Fatigue exists when cyclic stresses/deformations occur in an area on a component. The cyclic stresses/deformations have mainly two origins: load and temperature. Traditional mechanical fatigue may be the main damaging mechanism in different parts of a piston depending on different factors. High temperature fatigue (which includes creep) is also present in some damaged pistons. Thermal fatigue and thermal–mechanical fatigue are also present in other damaged pistons. For a better understanding of the damaging mechanism different analytical tools, such as finite element analysis, fractographic analysis, metallurgical analysis, etc., will be used whenever they are necessary for a clear understanding of the damaging mechanism.

1.1.2.1. Mechanical and high temperature mechanical fatigue

Piston head and piston pin hole

By mechanical fatigue it is meant that in a piston a crack will nucleate and propagate in critical stressed areas. The stresses in this context are due to the loads acting externally on the piston. Although stresses on pistons change with piston geometries and engine pressures; Figures 1.3 a) and b) show a typical stress distribution on an engine piston when pressure is applied on the piston head area and restraints on the piston pin holes.

It is clear that there are mainly two critical areas: the top side of piston pin hole and two areas at the piston head. Stress analyses on diesel pistons show the same critical areas. If holes or grooves are introduced on the pin hole it is possible to introduce critical stressed areas on those discontinuities.

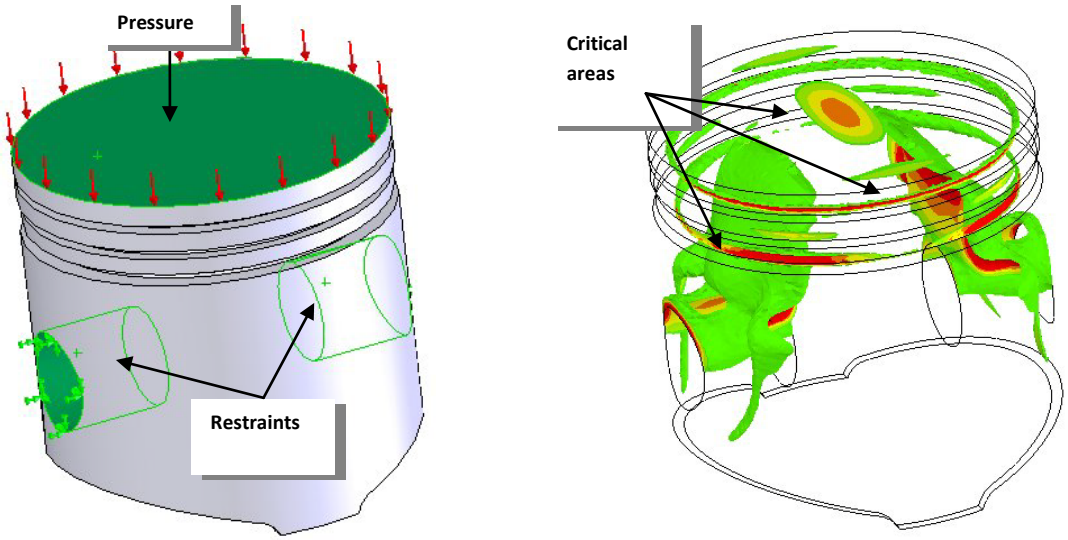

Figure 1.3 - a) Pressure on the piston head area and restraints on the piston pin holes b) typical stress distribution on an engine piston [4]

On piston in figure 1.4 it seems by fractographic analysis that the crack initiated at the pin-hole. On pistons in figure 1.5 and figure 1.6 the cracks initiated on the piston head near the combustion chamber. From the plot of typical stress distribution (Figure 1.3 b) is easy to observe that the stressed points on the piston are the head and the topside of the pin.

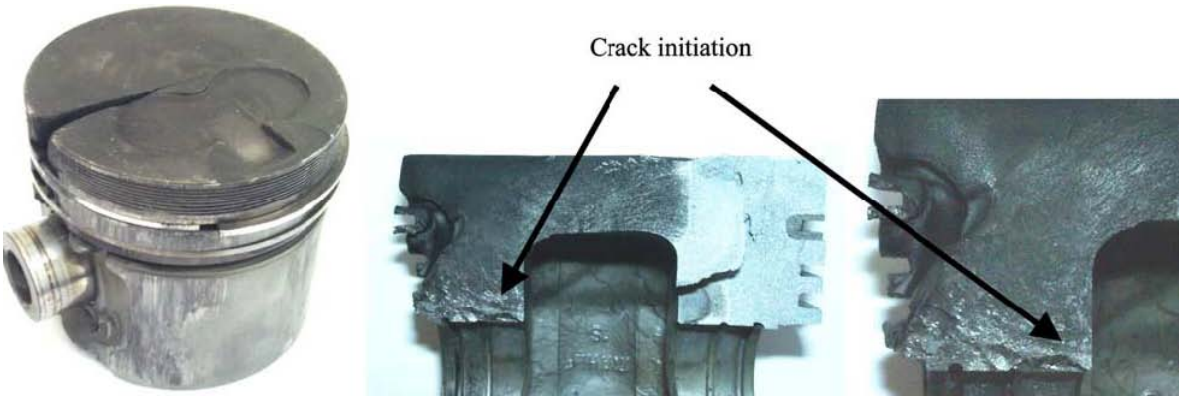

Figure 1.4 - Petrol engine piston with a crack from one side of the pin hole to the head.

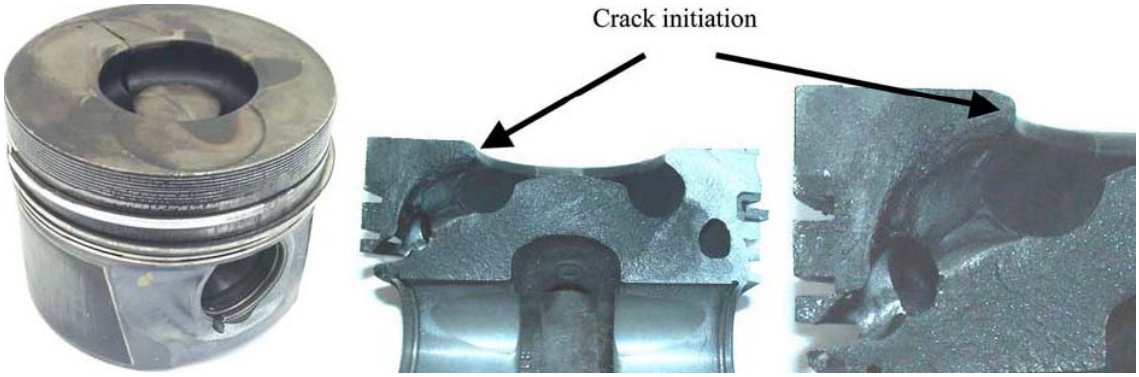

Figure 1.5 - Diesel engine piston (with cooling gallery) with a crack from one side of the pin hole to the head.

Figure 1.6 - Diesel engine piston with a crack from one side of the pin hole to the other pin hole going through the head of the piston.

A FEM analysis (Figure 1.7) was made to piston from figure 1.6 and the results show that in pistons with a bowl combustion chamber, besides the pin holes (and in this particular case on the curvature radius on the inner side of the piston top) there are also two regions at the piston head where there exist stress concentrations.

These two areas are located on the same vertical plane that contains the pin holes.

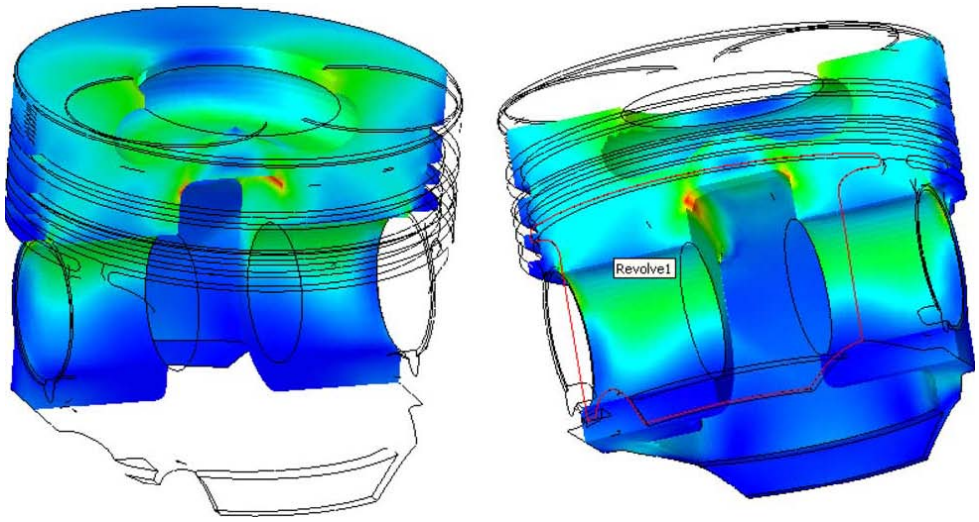

Figure 1.7 - Linear static stress distribution of piston from figure 6.[5]

The stresses at the piston head are higher – at the same vertical plane (Figure 1.7) conducting to initiation of cracks almost always on that plane which contains the pin holes (see Figures. 1.5 and 1.6)

In pistons of figure 1.5 and figure 1.6, both broken by the piston head, there is only one visible crack, and this is typical of mechanical fatigue. Due to the different temperature distribution along the vertical axis of the piston the head is always hotter than the bottom and the pin hole area. If it's combined the effect of the temperature with the static stresses, there are two critical areas – those on both sides of the bowl rim area on the same vertical plane that contains the pin holes - this result of a superposition of static stresses (Figure 1.3) with temperature distribution (Figure 1.14).

Piston compression grooves

In figure 1.8 it is presented one damaged piston by another typical fatigue damage that occurs on piston compression grooves. This happens because of the stress concentration

on a stress radius of the groove when the compression ring is not inside the groove – the inner side of the ring is located at mid distance of the groove depth.

The simulation of the maximum Von Misses stress with the ring inside the groove (close to the piston wall) presented a maximum stress of about one third of the one shown in figure 1.9 b, where the inner side of the ring is located at mid distance of the groove depth. When the clearance between the piston and cylinder wall becomes high (due to wear of the cylinder wall) there is an increase of the pressure acting on the ring (because the ring comes out of the groove – see Figure 1.9 b) and consequently a stress increase on the compression groove. The stresses at that particular curvature radius at the compression ring groove seem to be enough to initiate fatigue cracks on the piston. Thus the main reason for this damage is related to the clearance between the piston and the cylinder wall.

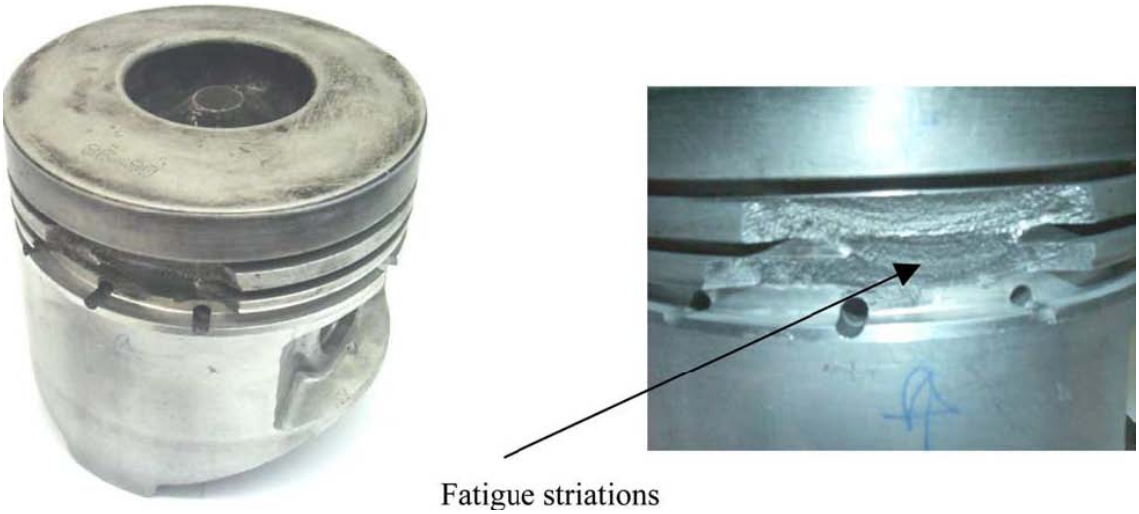

Figure 1.8 - Engine piston with damaged grooves: (a) piston; (b) detail of damaged grooves. [5]

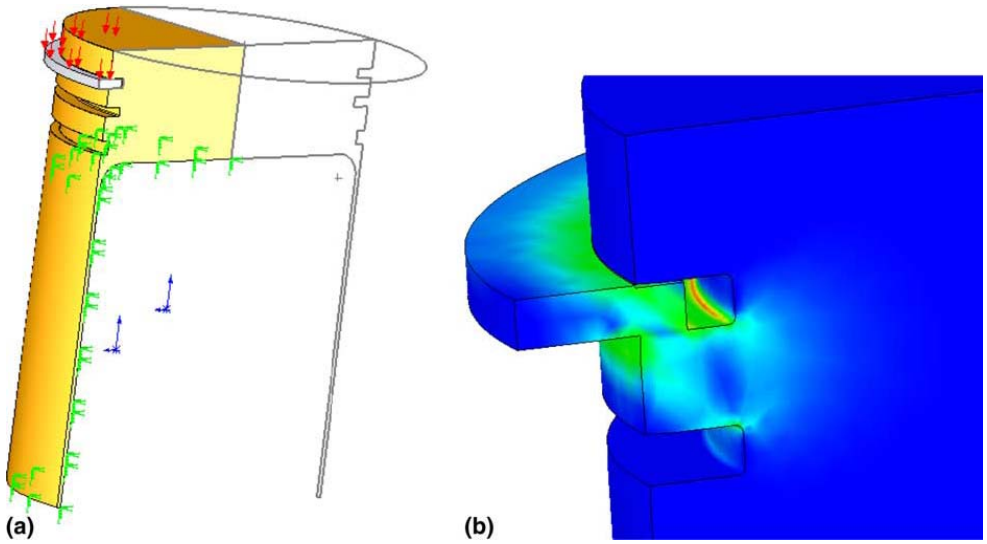

Figure 1.9 - Typical stress distribution on stress radius on the grooves. [5]

Piston skirt

Another zone where the piston breaks is the skirt (Figure 1.10) mainly due to the stresses that act on the curvature radius of some skirt geometries (Figure 1.11). The main reason for this damage is related to the clearance between the piston and the cylinder wall which allow the piston to rotate and to contact the cylinder wall mainly in two points: the bottom part of the skirt and the top part of the piston head. These contacts introduce a flexural load on the piston skirt that increases the stress concentration areas shown in figure 1.11.

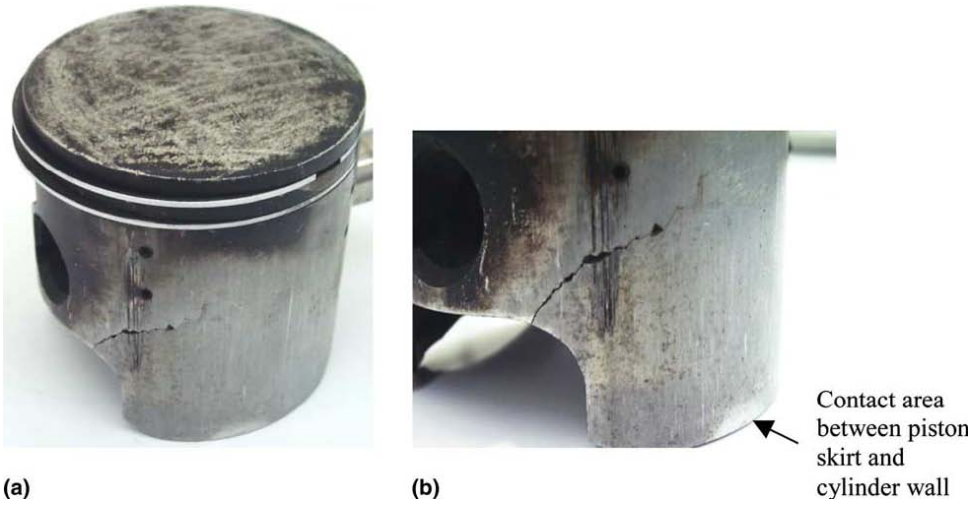

Figure 1.10 - Engine piston with damaged skirt: (a) piston; (b) detail of damaged skirt. [5]

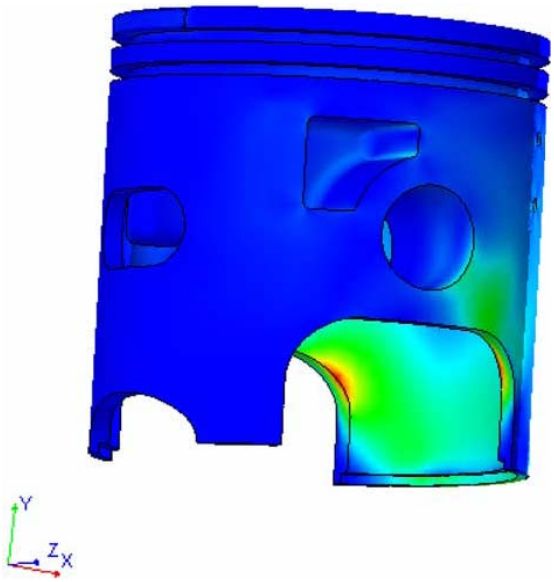

Figure 1.11 - Typical stress distribution on engine skirt with a big clearance. [5]

Thermal/thermal–mechanical fatigue

Thermal fatigue cracks are easy to identify because they usually show a particular feature. Typically there are some visible fatigue cracks on the areas with cyclic thermal gradients as can be seen on brake disks and other components under thermal fatigue [6].

Thermal stresses are difficult to simulate because there are, in a piston, two kinds of thermal stresses (see Figure 1.12):

(a) Thermal stresses due to the „vertical" distribution of the temperature along the piston – high temperatures at the top and lower temperatures at the bottom.

(b) Thermal stresses due to the different temperatures at the head of the piston due to the flow of the hot gases or to fuel impingement (related to high-pressure injection).

Thermal fatigue is related to the stresses in the material induced by thermal gradients in the component. Figure 1.13 shows two train pistons with several cracks at the piston head.

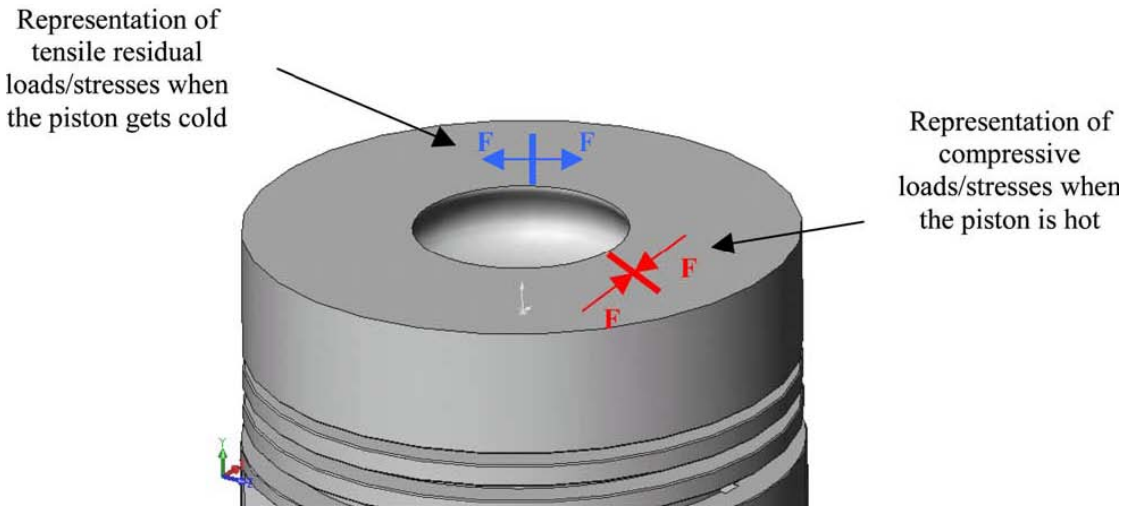

Figure 1.12 - Sketch of an example of thermal stresses at the top of a piston and forces, F, acting on the material. [5]

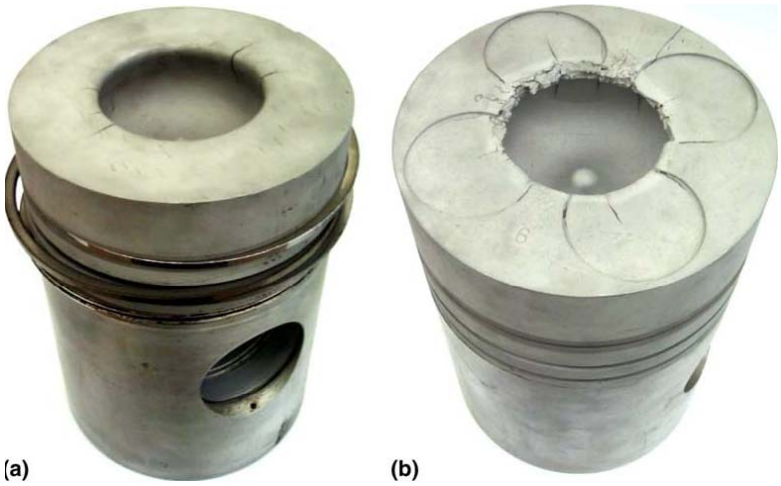

Figure 1.13 - Train engine pistons with damaged head: (a) piston 1; (b) piston. [5]

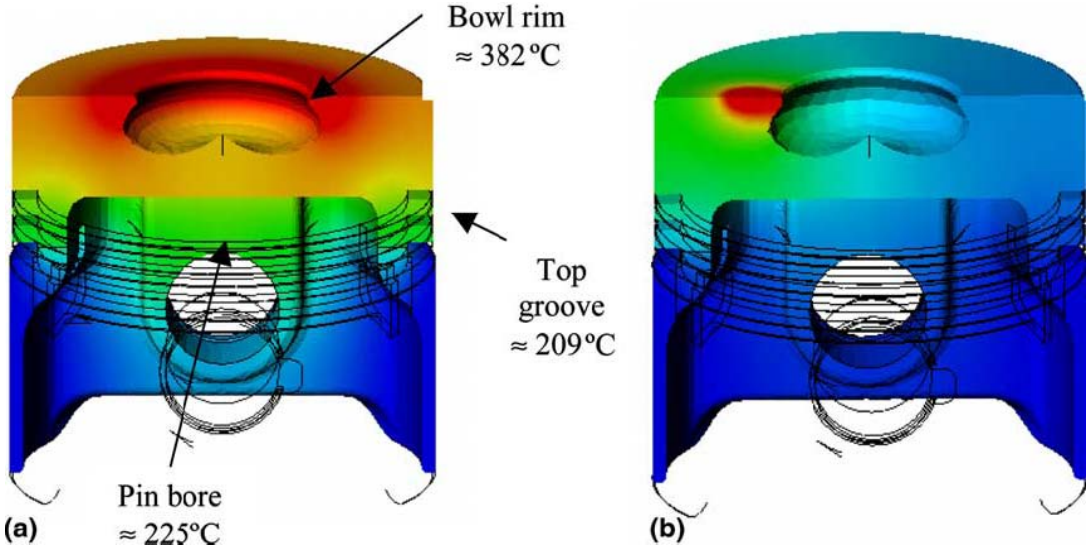

Figure 1.14 - Schematic thermal distribution at a piston: (a) homogeneous; (b) localized [5]

Cracks distributed along the bowl rim clearly shows that the main mechanism was thermal fatigue due to an homogeneous temperature distribution can be seen on figure 1.13 b and cracks located in opposite sides at the piston crown in figure 1.13a.

1.2 Motivation and Objectives of the Study

Selecting the "ideal" material for the respective application is extremely important for the function of the piston system. In the material selection, engine - and application specific must be taken into consideration aspects such as the thermal load, exposure to wear and required running time. Material specific properties such as density, thermal conductivity, fatigue behaviour and wear resistance, as well as creep and deformation properties must also be taken into account. Due to time constraints, the development of the material must be completed before the start of a project since it is extremely cost - and time - intensive. It is therefore all the more important to pursue continuous developments in this field and search for new solutions.

Many structural components encounter service conditions and, hence, required materials performance, which vary with location within the component.

It is well known that abrupt transitions in materials composition and properties within a component often result in sharp local concentrations of stress, whether the stress is internal or applied externally. It is also known that these stress concentrations are greatly reduced if the transition from one material to the other is made gradual. By definition, functionally graded materials are used to produce components featuring engineered gradual transitions in microstructure and/or composition, the presence of which is motivated by functional performance requirements that vary with location within a part. With functionally graded materials, these requirements are met in a manner that optimizes the overall performance of the component.

The primary goal of this work is to develop and implement suitable methodologies for prediction of mechanical properties and fatigue life of aluminium silicon cast alloys and functionally graded materials covering a range of percentage of silicon from 6.5% to 19%.

An introduction and an overview of the thesis are provided in the **First Chapter**.

The remainder of this dissertation consists of six chapters, dealing with the different aspects of casting techniques: gravity, vibrating gravity, centrifugal and functionally graded materials.

The First Chapter also provide information about the function of engine piston in an engine along with the service load and failures of the engine piston. Different types of mechanical and fatigue failure of engines pistons are exemplified by suggestive analysis and pictures.

Chapter Two is a general literature review starting with the evolution of the engine piston followed by functionally graded materials description and Al-Si casting alloys. There are presented the two main casting techniques used in this research like gravity and centrifugal casting and one secondary: vibrating gravity casting.

In **Chapter Three,** the experimental procedures are described. This research is divided into four general parts, each dealing with the folowing aspect : i) the fabrication and heat treatment of the samples, ii) the metallographic study, iii) the mechanical and fatigue properties testing, iv) the quantitative analysis.

Chapter Four present the results of this research starting with the metalurgical caracterization – secondary dendrite arm spacing for all three alloys studied, eutectic silicon thickness and length, and equivalent diameter for eutectic silicon particle and pores. Than for each alloy studied (alloy A- hypoeutectic aluminium silicon alloy with 7% of silicon, alloy B - eutectic aluminium silicon alloy with 12% of silicon and alloy C- hypereutectic aluminium silicon alloy with 18% of silicon) the mechanical analysis results are presented (rupture strength, rupture strain, Young modulus and hardness) followed next by the chemical composition analysis and microstructure analysis. In the end of this chapter the fatigue analysis results are presented as a comparison of gravity and centrifugal casting for all alloys.

In **Chapter Five**, the influence of the inherent vibration over the mechanical properties is assesed. This study was split in two: the first one used differrent vibration frequncies to establish the optimal of vibration influence over mechanical properties and the second one isolate the vibration effect and compare the mechanical properties between gravity, vibrating gravity casting and centrifugal casting.

The **Sixth Chapter** brings some explanation of the results obtained and present some models that can be used to predict the mechanical and fatigue behaviour of some aluminium silicon alloys.

In the **last Chapter**, the main conclusions of the present research work are presented and also are sketched the important direction that must be folowed for continuing this research.

CHAPTER 2

LITERATURE REVIEW

2.1 Evolution of Engine Piston

It's hard to believe the piston engine has been around for 143 years. Nicholaus August Otto invented the first such engine in 1866, one year after the Civil War ended. Given that much time, you'd think the pistons inside today's engines would be radically different from those of their ancestors.

The materials and designs of pistons have evolved over the years and will continue to do so until fuel cells, exotic batteries or something else makes the internal combustion engine obsolete. But until that happens, pistons will continue to power the vehicles we drive.

The basic function of a piston is one thing that has not changed over the years. The piston forms the bottom half of the combustion chamber and transmits the force of combustion through the wrist pin and connecting rod to the crankshaft. The basic design of the piston is still pretty much the same, too. It's a round slug of metal that slides up and down in a cylinder. Rings are still used to seal compression, minimize blow by and control oil.

So what has changed? The operating environment. Today's engines run cleaner, work harder and run hotter than ever before. At the same time, engines are expected to

last longer than ever before, too: up to 250000 km or more – and with minimal maintenance. Consequently, heat management is the key to survival of the fittest.

Today, everything is modelled in 3D on a computer, and then evaluated with finite element analysis software before anything is made. That speeds up the design and testing process, reduces the lead time to create new piston designs, and produces a better product.

Hot Pistons

The most critical area for heat management is the top ring area. One of the "tricks" engine designers came up with to reduce emissions was to move the top compression ring up closer to the top of the piston. A decade ago, the land width between the top ring groove and piston crown was typically 7.5 to 8.0 mm. Today that distance has decreased to only 3.0 to 3.5 mm in many engines.

The little crevice around the top of the piston between the crown and top ring creates a dead zone for the air/fuel mixture. When ignition occurs, this area often does not burn completely leaving unburned fuel in the combustion chamber. The amount isn't much, but when you multiply the residual fuel in each cylinder by the number of cylinders in the engine times engine speed, it can add up to a significant portion of the engine's overall hydrocarbon emissions.

One of the consequences of relocating the top ring closer to the top of the piston is that it exposes the ring and top ring groove to higher operating temperatures. The top rings on many engines today run at close to 315°C, while the second ring sees temperatures of 150°C or less. These extreme temperatures can soften the metal and increase the danger of ring groove distortion, micro welding and pound-out failure. The reduced thickness of the land area between the top of the piston and top ring also increases the risk of cracking and land failure.

The evolutionary advances that enable today's pistons to handle this kind of environment include changes in piston geometry, stronger alloys, anodizing the top ring groove and using tougher ring materials.

Anodizing has become a popular method of improving the durability of the top ring groove and is now used in many late model engines. Anodizing reduces micro welding between the ring and piston to significantly improve durability. But it can't work miracles: an anodized piston can still fail if it gets too hot.

Anodizing is done by treating the ring groove with sulphuric acid. The acid reacts with the metal to form a tough layer of aluminium oxide, which is very hard and wear-resistant. Part of the layer is below the surface of the metal and part is above. On average, the layer is about 20 microns thick so the piston manufacturer compensates for the added thickness when the top ring groove is machined.

Another approach some piston manufacturers have used to improve top ring durability is to weld nickel alloy into the top ring groove.

Low Tension Rings

To further complicate the problem of heat management, rings have been getting smaller. Starting in the 1980s, "low tension" piston rings began to appear in many engines. Typical ring sizes today are 1.2 mm for the top compression ring, 1.5 mm for the second ring, and 3.0 mm for the oil ring. Some are even thinner, shallower to improve fuel economy because the rings account for up to 40 percent of an engine's internal friction losses. Thinner rings produce less drag and friction against the cylinder walls. But the downside is they also reduce heat transfer between the piston and cylinder because of the smaller area of contact between the two. Consequently, pistons with low tension rings run hotter than pistons with larger rings.

Low tension rings also present another problem. They are less able to handle bore distortion. To maximize compression and minimize blow by, the cylinder must be as round as possible. This often requires the use of a torque plate when honing to simulate the bore distortion that is produced by the cylinder head.

Piston Geometry

Changes in piston geometry have also been made to improve their ability to survive at higher temperatures. Piston manufacturers used to grind most pistons with a straight taper profile. When the piston got too hot, it would contact the cylinder along a narrow area producing a thin "wear strip" pattern on the side of the piston. Now are used CNC machining to do a barrel profile on pistons. The diameter of the piston in the upper land area is smaller to allow for more thermal expansion and to spread any wall contact over a larger area.

Pistons are getting shorter and lighter. In the 1970s, a typical small block piston and pin assembly weighed around 750 grams. The same parts in a late models engine weigh only about 600 grams.

Part of the weight reduction has been achieved by reducing piston height and using shorter skirts. The distance from centre of the wrist pin to the top of the piston (called "compression height") used to be 38.1 mm to 43.18 mm back in the 1970s. Today, wrist pins are located higher up. On today's engines, the compression height is between 30.4 mm to 33.02 mm.

Moving the location of the wrist pin higher up on the piston also allows the use of longer connecting rods, which improve torque and make life easier on the bearings and rings.

Some aftermarket pistons are now available with wrist pins that have been relocated upward slightly to compensate for resurfacing on the block and heads. The other alternative is to shave the top of the piston if the block has been resurfaced, but this reduces the depth of the valve reliefs which may increase the risk of detonation and/or valve damage.

Pistons used to have long tail skirts (which sometimes cracked or broke off). Now most pistons have "mini-skirts." Instead of a 63.5 skirt length, the piston may only have 38 mm skirt. Shorter skirts reduce weight but also require a tighter fit between the piston

and cylinder bore to minimize piston rocking and noise. Consequently, today's piston clearances are much less than before (typically 0.0254 to 0.0127 or less). Some have a zero clearance fit or even a slight interference fit (made possible by special low friction coatings).

Piston Materials

The alloy from which a piston is made not only determines its strength and wear characteristics, but also its thermal expansion characteristics. Hotter engines require more stable alloys to maintain close tolerances without scuffing.

Many pistons used to be made from "hypoeutectic" aluminium alloys like SAE 332 which contains 8.5 to 10.5 percent silicone. Today we see more "eutectic" alloy pistons which have 11 to 12 percent silicone, and "hypereutectic" alloys that have 12.5 to over 16 percent silicone.

Silicone improves high heat strength and reduces the coefficient of expansion so tighter tolerances can be held as temperatures change. Hypereutectic pistons have a coefficient of thermal expansion that is about 15 percent less than that for standard alloy pistons. Because of this, the pistons can be installed with a much tighter fit – up to 0.012 mm less clearance may be needed depending on the application.

Hypereutectic alloys are also slightly lighter (about 2 percent) than standard alloys. But the castings are often made thinner because the alloy is stronger, resulting in a net reduction of up to 10 percent in the piston's total weight.

Hypereutectic alloys are more difficult to cast because the silicon must be kept evenly dispersed throughout the aluminium as the metal cools. Particle size must also be carefully controlled so the piston does not become brittle or develop hard spots making it difficult to machine. Some pistons also receive a special heat treatment to further modify and improve the grain structure for added strength and durability. A "T-6" heat treatment, which is often used on performance pistons, increases strength up to 30 percent.

Machining hypereutectic pistons is also more difficult because of the harder alloy. Consequently, hypereutectic pistons typically cost several dollars more than standard alloy pistons. That's why most Original Equipment Manufacturers have gone back to eutectic alloy pistons in their late model engines.

Piston Coatings

Survival of the fittest also requires a high degree of scuff resistance. Cold starts without adequate lubrication can cause piston scuffing. The same thing can happen if the engine overheats. Piston-to-cylinder clearances close up and the piston scuffs against the bore. The initial start-up of a freshly built engine is also a risky time for scuffing and is of special concern to engine builders because that's when many warranty problems occur.

Applying a permanent low friction coating to the sides of the pistons provides a layer of protection against scuffing. Many rebuilders have found that using coated pistons has virtually eliminated warranty problems due to scuffing.

Many late model use pistons with graphite molly-disulfide coatings on the piston skirt to improve scuff resistance. Most aftermarket piston manufacturers also offer some type of coated replacement pistons to rebuilders who want them. Coatings typically add a small amount to the price of a replacement piston, but the added scuff protection and reduction in warranty claims more than offsets the higher cost say many engine builders who use them.

"Thermal barrier" ceramic-metallic coatings for the tops of pistons are another type of coating that has been used on some diesel pistons and performance pistons. Improving heat retention in the combustion chamber improves thermal efficiency and makes more power. It also helps the piston run cooler. But too much heat in the combustion chamber also increases the risk of detonation and preignition, which is not a problem with diesel but is with gasoline engines. So when a coating is used, ignition timing must usually be retarded several degrees to reduce the risk of detonation.

Piston Crowns

The shape and finish on the tops of pistons has also been changing. Flat top pistons have been replaced by dished pistons, domed pistons and pistons with intricate contours to swirl the fuel mixture and promote better fuel atomization.

Some piston crown designs can be very complex because they are designed to produce the lowest possible emissions with the best overall fuel efficiency. The shape of the crown controls the movement of air and fuel as the piston comes up on the compression stroke. This, in turn, affects the burn rate and what happens inside the combustion chamber. Replacement pistons for stock engines with complex piston designs should be the same as the original to maintain the same emissions and performance characteristics.

With performance pistons, designs can be even more specialized. Manufacturers have developed special "fast burn" configurations that allow engines to safely handle more compression without detonating.

An "Attenuator-Groove" is used on some pistons to enhance the valve reliefs. The groove removes two potential hot spots in the combustion chamber and improves air flow and wet flow atomization.

Another unique design feature is the "Mini-Grooves" machined into the top ring land on performance pistons. If the piston gets too hot, the top of the piston swells causing the mini-grooves to contact the cylinder. This momentary contact helps cool the piston to reduce the danger of detonation and piston destruction.

Piston Pins

Piston pin holes have also been changing. Rather than being round and straight, pin bores are taking on new shapes. Some are oval and some are trumpet-shaped, flaring out toward the inside edges of the pin bosses. The reason for these shapes is to accommodate wrist pin bending and becoming oval. These variances from straight and round are quite small, measured in tenths of a thousandth, but have proven to extend piston life.

Future development

Pistons may continue to get shorter and lighter, but most engineers believe rings can't get much smaller than they are today. Some do think, though, that the two ring piston may not be too far away. Some Indy racing motors are already running two ring pistons quite successfully.

Other design innovations that may shape the direction of future piston development include lightweight alloy wrist pins, more anodizing and/or the use of ceramic coatings on the tops of pistons and upper ring groove to improve heat resistance and wear, and maybe top rings with no end gaps.

The best indication of what's coming down the road is to look at today's state-of-the-art racing pistons: super lightweight designs with almost no skirts, holes machined into the sides to reduce weight, and various design tricks to control thermal expansion and detonation under high load.

Can be seen some exotic graphite reinforced pistons for certain high output engines similar to ones that are now being used in diesel engines. The development of direct injection gasoline engines in the market will likely require complex fuel bowls in the tops of pistons similar to those now used in many diesel engines. Direct injection, which is starting to come on strong in Europe, allows extremely lean air/fuel mixtures (up to 40:1) and much better fuel economy. But it also requires precise control of airflow in the combustion chamber for reliable ignition and complete combustion.

If hybrid gasoline/electric or diesel/electric vehicles become more common in the not-too-distant future (which many predict will happen), no big changes in piston design will be needed because most such systems use the same basic engine designs as today.

The biggest change in piston design will occur if and when fuel cells become a competitive power source for automotive applications. In that case, there will be no need for pistons and they'll be on the endangered species list.

Most experts believe fuel cell technology is still years away. And when it does go into production, volumes will be very limited because of high costs. Eventually the cost will come down.

But even if fuel cells do eventually take over, many experts believe piston engines will continue to be produced for smaller, economy vehicles as well as heavy-duty vehicles.

There will also be an ongoing replacement market for pistons as long as piston-powered vehicles remain on the road.

Abrupt transitions in materials composition and properties within a component often result in sharp local concentrations of stress, whether the stress is internal or applied externally. These stress concentrations are greatly reduced if the transition from one material to the other is made gradual. Functionally graded materials are used to produce components featuring engineered gradual transitions in microstructure and/or composition, the presence of which is motivated by functional performance requirements that vary with location within a part. With functionally graded materials, these requirements are met in a manner that optimizes the overall performance of the component.

2.2 FUNCTIONALLY GRADED MATERIALS

In materials science **functionally graded material (FGM)** may be characterized by the variation in composition and structure gradually over volume, resulting in corresponding changes in the properties of the material. Functionally graded materials can also be defined as materials having graded transition in mechanical properties, either continuous or in fine, discrete steps, across the interface [7-9]. This type of materials can be designed for specific function and applications. Various approaches based on the bulk (particulate processing), preform processing, layer processing and melt processing are used to fabricate the functionally graded materials.

The FGM concept originated in Japan in 1984 during the space plane project, in the form of a proposed thermal barrier material capable of withstanding a surface temperature of 1726^{o}C and a temperature gradient of 727^{o}C across a cross section <10 mm. Since 1984, FGM thin films have been comprehensively researched, and are almost a commercial reality.

A functionally graded material (FGM) is a two-component composite characterized by a compositional gradient from one component to the other. In contrast, traditional composites are homogeneous mixtures, and they therefore involve a compromise between the desirable properties of the component materials. Since significant proportions of an FGM contain the pure form of each component, the need for compromise is eliminated. The properties of both components can be fully utilized. For example, the toughness of a metal can be mated with the refractoriness of a ceramic, without any compromise in the toughness of the metal side or the refractoriness of the ceramic side.

However, in functionally graded materials (FGMs), the property of one side differs from that of the other side. Thus, it arise different functions within a material. For example, one side may have high mechanical strength and the other side may have high thermal resistant property; thus, there are "two aspects" in one material.

FGM's are materials that can be purposefully processed to obtain higher superficial hardness and adequate internal toughness. Special processing is required to produce these materials in order to exhibit characteristics that are not attainable by monolithic or homogeneous materials [10].

It is now well known that abrupt transitions in materials composition and properties within a component often result in sharp local concentrations of stress, whether the stress can be internal or applied externally. It is also known that these stress concentrations are greatly reduced if the transition from one material to the other is made gradual.

These considerations form the essential elements of the logic underlying the majority of functionally graded materials. By definition, functionally graded materials are used to produce components featuring engineered gradual transitions in microstructure and/or composition, the presence of which is motivated by functional performance requirements that vary with location within the part. With functionally graded materials, these requirements are met in a manner that optimizes the overall performance of the component.

This new concept of materials engineering hinges on materials science and mechanics due to the integration of the material and structural considerations into the final design of structural components. Because of the many variables that control the design of functionally graded microstructures, full utilization of the FGMs potential requires the development of appropriate modelling strategies for their response to combined thermo-mechanical loads.

The processing of graded materials is revealing a very wide spectrum of methods available. As a consequence of this diversity, much work to date is largely developmental or exploratory in nature, and aimed most often at providing proof of the viability of a given processing route toward FGM production.

Some common threads can, however, be found in this wide variety of processes. According with Surresh and Mortensen [8] can be distinguish two principal classes of methods for the production for FGMs containing a metallic phase: (i) processes where the graded material is constructed spatially, layer by layer and according to essentially any pre-chosen distribution, and (ii) processes wherein natural transport phenomena, such as

fluid flow, atomic diffusion, or heat conduction, are exploited towards the creation of macroscopic gradients in composition and microstructure (Figure 2.1). For each process class, different subclasses exist.

In the first class of processes, the FGM is constructed layer by layer, in a manner that starts with an appropriate distribution of constituents of the FGM, often in a precursor of the component. These techniques are named constructive processes because the gradients are literally constructed in space. Constructive processes are, thus, ones which are amenable to computer-control of the gradients produced, and represent largely an outgrowth of the tremendous advances that have been made over the past decades in automation of materials processing: such meticulous distribution of phases would otherwise be absurdly expensive.

Constructive processes are distinguished from a second class of FGM processes, which rely on natural transport phenomena to create gradients within a component. These transport-based processes use the flow of fluid, the diffusion of atomic species, or the conduction of heat, to create gradients in local microstructures and/or compositions that are useful. Both heat and mass diffusion have been used for centuries to create functional, microstructural, and/or compositional gradients in steel. Fluid flow, interfacial segregation, and solid state diffusion during solidification are responsible for macrosegregation in single crystals and alloy castings. Although generally viewed as a problem in the processing of homogeneous materials, these are naturally segregative phenomena which can be used to create tailored gradients within a component. If these processes are quantitatively understood and harnessed, gradients produced can still be optimized, albeit within a narrower window of possible structures.

Transport phenomena, of fundamental importance in the latter class of FGM processes, must also be considered in the context of constructive processes because these tend to erase gradients incorporated early in the FGM process cycle. It is therefore generally instructive, in the processing of FGMs, to consider approximate time or velocity scales for each of heat, solute, and liquid transport.

The centrifugal casting method is one of advantageous transport-based techniques to fabricate functionally graded materials such a cylindrical composite parts as its main

functions like strength and thermal expansion coefficient vary along the wall thickness of a cylinder in some conveniently gradient fashion.

The previous studies on the functionally graded materials obtained by centrifugal casting method have mainly treated the case where dispersion-hardening particles in the composite have a higher density than that of the matrix substance, so that they segregate on the outer side of the cylinder wall [11-13]. The Al-Si base functionally graded materials obtained by centrifugal casting method studied in the present research are however different from the previous ones in the respect that Si particle as the dispersion-hardening phase has a lower density than that of the Al enriched matrix.

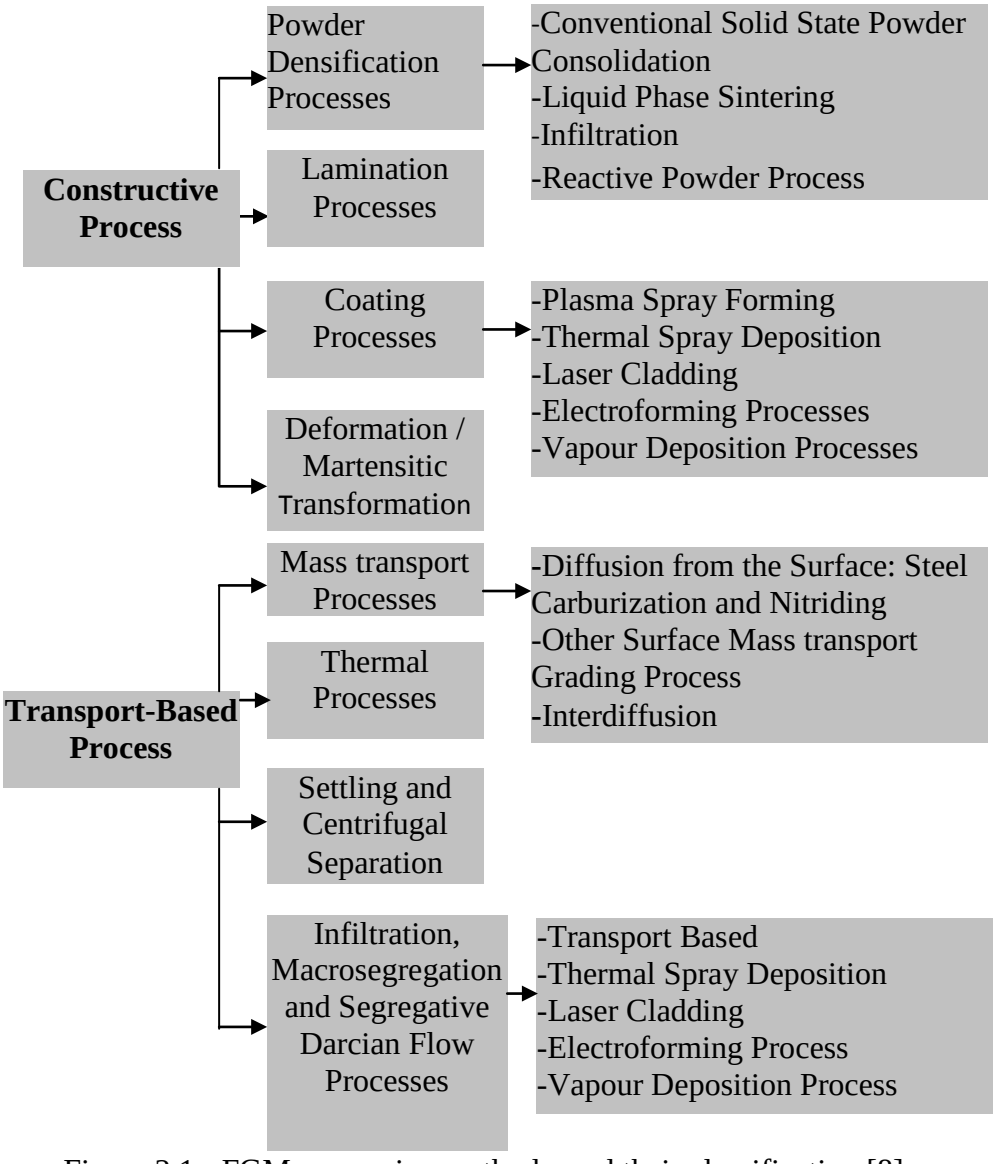

Figure 2.1 - FGM processing methods, and their classification [8].

Many processing methods have been proposed to fabricate FGMs, such as chemical vapour deposition, the plasma spray technique and various powder metallurgy techniques. The centrifugal method was introduced recently and has attracted a lot of attention due to its unique merits [14]. In particular, Al based FGMs fabricated by the centrifugal method showed interesting properties that are not obtained in conventional monolithic materials, such as gradual changes in hardness, wear resistance, Young's modulus, etc [15].

FGMs offer great promise in applications where the operating conditions are severe. For example, wear-resistant linings for handling large heavy abrasive ore particles, rocket heat shields, heat exchanger tubes, thermoelectric generators, heat-engine components, plasma facings for fusion reactors, and electrically insulating metal/ceramic joints. They are also ideal for minimizing thermo-mechanical mismatch in metal-ceramic bonding.

Most of studies in the domain of functionally graded materials (FGMs), obtained by centrifugal casting deal with functionally graded composites where an alloy is reinforced with a solid phase as for example silicon particles [17-20]. In these cases the gradation as well as the improvement of mechanical properties is attributed to the reinforcement. Moreover in some cases it is possible to obtain FGMs with metallic materials where there is a high difference of density and low solubility of different phases or different materials of the same alloy. In this last case the phases with higher density move in the radial direction to the outer surface of the casting due to the centrifugal force [16, 21].

However, in this study, an aluminium alloy, without reinforcement, and with very close densities between phases, is used. It will be shown that the casting may be very influenced by the centrifugal effect and functionally graded castings may be obtained. In order to understand why a homogeneous alloy, with similar densities between phases, may give rise to an FGM, by using the centrifugal effect, an analysis of the most important effects of the centrifugal casting process on metallurgical features is necessary.

In this research the mechanical and also the fatigue properties were obtained the same way as for the homogenous materials with the particularity shown in chapter 3 that the samples were obtained by cutting the ingots by layers to be able to characterise the functionally graded material along the gradient of properties.

2.3 CASTING OF AL-SI ALLOY

Aluminium is amongst those metals which can be ‘cast’ by every process used in metal casting. These processes, in descending order of quantity of aluminium casting are: die casting, permanent mould casting, sand casting, plaster casting, investment casting, centrifugal casting and continuous casting. The casting process is selected on the basis of factors such as cost, feasibility, quality, etc.

An excellent combination of castability, mechanical properties, good corrosion resistance and weldability, make cast aluminium alloys one of the most important materials used in aerospace and automotive industries.

Furthermore the relatively low coefficient of thermal expansion, mainly in hypereutectic AlSi alloys, and fluidity, made this alloy family as candidate materials for a large number of automotive applications such as pistons, cylinder blocks and liners [16, 22-24]. Perhaps the main drawback is that under the conventional solidification conditions in cast Al-Si alloys, the Si phase often exhibits a coarse microstructure that leads to poor mechanical properties. Recent results have demonstrated that rapid solidification processes may substantially modify the morphology of the Si phase as compared to those found in conventionally processed materials [25, 26].

Cast aluminium alloys are important construction materials, which are used in various fields of technology. Because of their low density, relatively low melting point, good heat and electrical conduction, low thermal expansion coefficient, good castability and low casting shrinkage, they are mainly used in car manufacturing as: piston castings, cylinder head castings, engine blocks, structural supporting reinforcements and elements absorbing crash impact.

The mechanical properties and fracture behaviour of cast aluminium alloys are strongly dependent on secondary dendrite arm spacing (SDAS), the amount of eutectic phase and, in particular, the size and shape of eutectic silicon particles or lamellas and Fe-rich intermetalics. Thus, not only the chemical composition but, more important, some micro structural features in the microstructure have a strong influence on mechanical and fatigue properties of Al-Si cast alloys [27, 28].

To control this micro structural features there are different solutions, for example by introducing special elements to refine the grain [29-32]. However to improve mechanical

properties of cast aluminium-silicon alloys the most common solution is by cast technology [33-37].

The influence of processing and process parameters plays a key role for the aluminium foundry and transport industries as it affects the quality and soundness of the cast products. Particularly, the choice of a process chain in aluminium foundry, otherwise of process parameters, influences the reject rates, hence casting costs, the process yield and the production rate. The process chain is a complex sequence of processes and the final casting quality depends on many parameters. Several aspects of this subject are still not fully understood. The motivation of the research presented in this doctoral research work was, therefore, to fill this gap of knowledge. The study has aimed at understanding the influence of various processes and process parameters of foundry on the quality of aluminium alloy castings and, in particular, Al-Si based castings.

2.3.1 Casting techniques

An obvious advantage of aluminium is its comparatively low melting point (660^{o}C when pure), as well as its easy melting point and pouring in air without any protective flux covering or inert gas atmosphere, since the oxide surface skin that forms on the molten metal prevents excessive oxidation. The production of aluminium semifabricated products begins with the solidification of a molten alloy in the shape of a casting with the right characteristics for subsequent processing and fabrication. The casting operations, tailored to each product, can be grouped under three main headings:

- **static** (or mould) **casting** (high pressure die casting, permanent mould casting, sand casting, investment casting, centrifugal casting, etc) to obtain products (foundry ingots) of near-net final shape and high mechanical properties,
- **semi-continuous casting** (direct chill and electromagnetic casting) to obtain products, mainly extrusion billets and sheet ingots, of substantial cross-sectional area, of length restricted to several meters (ten at most), used as the starting point in traditional processing and fabrication processes,
- **continuous casting** (thin coiled sheet, strip, twin rolled casting) yielding a rough casting of dimensions fairly close to those of the end-product, thus making it

possible to employ downstream processing facilities which are “lighter” and hence cost less than the more traditional processes.

These can be also classified based on the mould material, method of producing the mould and the pressure on molten metal during filling (gravity, centrifugal force, vacuum, low pressure, high pressure). Permanent or metal moulds are used in gravity and pressure die casting processes, suitable for producing a large number of components. In expendable mould processes (sand, shell and investment), a new mould is required for every casting or a bunch of castings with a common gating and feeding system produced in the same mould. Expendable moulds can be made using either permanent pattern or expendable pattern. Permanent pattern can be made from wood, metal or plastic. In expendable pattern processes (also called investment processes), each pattern produces only one casting. Such patterns are made of wax, expandable polystyrene (EPS) or other polymer materials.

2.3.1.1 Gravity casting

The casting process that poured the molten metal under the gravitational force is called gravity casting and can be mainly divided function of the mould type: sand casting and permanent mould casting.

1. Sand Casting consists basically of pouring molten metal into appropriate cavities formed in a sand mould. The sand may be natural, synthetic, or an artificially blended material. All types of metals can be sand cast. Shape complexity of sand cast parts can be quite complex. There is no limit on part size, but small size parts are very hard to cast because of the difficult of maintaining gating and regulating metal flow into these cavities. The accuracy of tolerances of sand cast parts is lowest when compared to all other methods of casting. Typical surface finishes range from 5-25 μm. Lastly, one sand mould is usually made for one part. As an expendable mould, the sand mould is destroyed after casting. The sand material is typically reusable. The grain development in sand casting has dendrite grains and must be heat treated.

2. Permanent mould casting sometimes referring to as gravity die casting is the process when a metal mould consisting of two or more parts is repeatedly used for the production of many castings of the same form. The liquid metal enters the mould by

gravity. Simple removable cores are usually made of metal, but more complex cores are made of sand or plaster. When sand or plaster cores are used, the process is called semi permanent mould casting. Permanent mould casting is particularly suitable for the high-volume production of castings with fairly uniform wall thickness and limited undercuts or intricate internal coring. The process can also be used to produce complex castings, but production quantities should be high enough to justify the cost of the moulds. Compared to sand casting, permanent mould casting permits the production of more uniform castings, with closer dimensional tolerances, superior surface finish, and improved mechanical properties. Wherever quantities are in the range of 500 pieces or more, permanent-mould casting becomes competitive in cost with sand casting, and if the design is simple, runs as small as 200 pieces are often economical. Production runs of 1000 pieces or more will generally produce a favourable cost difference.

Permanent mould castings are gravity-fed and pouring rate is relatively low, but the metal mould produces rapid solidification. Permanent mould castings exhibit excellent mechanical properties. Castings are generally sound, provided that the alloys used exhibit good fluidity and resistance to hot tearing.

2.3.1.2 Centrifugal Casting

Centrifuging is a method of forcing metal into a mould by centrifugal force. Steel baked sand, plaster, cast iron, or graphite moulds and cores are used for centrifugal casting of aluminium. Metal dies or moulds provide rapid chilling, resulting in a level of soundness and mechanical properties comparable or superior to that of gravity-poured permanent mould castings.

The centrifugal casting process, which involves the pouring of molten metal into a rapidly rotating metallic mould, was developed by A.G. Eckhardt of Soho, England, in 1809. The method was soon adopted by the pipe foundries and was first used in Baltimore, Maryland, in 1848. Sir Henry Bessemer, famed for his converter, used centrifugal casting to remove gases and was the first to pour two or more metals into a single rotating mould. The centrifugal casting of steel was first attempted in 1898 at the plant of the American Steel Foundries in St. Louis, Missouri. Railroad car wheels were spun cast in 1901 at a rotation speed of 620 rpm.

The process uses spins a mould about an axis of rotation. Moulds are typically made of graphite, steel or iron. All types of metals can be cast in this method. Often the inside of the mould cavity is coated with a refractory lining to reduce mould wear. Typical parts cast in this method are pipes, gun barrels and street posts.

Centrifugal cast parts have high degree of accuracy and very little porosity. The surface finish will range from 2-10 mm. Maximum part weight is above 5000 kg. The cost of the mould and equipment is quite expensive so only large volume runs are economically feasible.

The question will immediately arise: "Why pour castings in a machine when they may be successfully cast statically?" The primary reasons are (a) to obtain better quality castings, (b) to produce castings more economically and (c) to cast a part which cannot be satisfactorily cast statically. These reasons do not necessarily go hand in hand as certain castings are centrifugally cast to increase the yield or to decrease cleaning room expense without having any idea of affecting the quality. Usually, however some improvement in quality results. Another advantage is that the percentage of rejected castings is reduced. Bad castings come from human errors and are no more prevalent in centrifugal casting than in static casting. Moreover, centrifugal force assists in counteracting some human errors which otherwise would result in a bad casting.

Among the different aluminium casting techniques centrifugal casting is an example of a casting technology used with success to obtain improved mechanical results. Although in some studies the materials used are aluminium matrix composites where the improvement of mechanical properties is attributed to the reinforcement, it is documented that the centrifugal casting process can give an important contribution to improve the mechanical properties of aluminium alloys even if it is applied to alloys without reinforcement [33-35].

Traditionally the centrifugal casting process has been mainly used for obtaining cylindrical parts. There are essentially two basic types of centrifugal casting machines: the horizontal types, where the die rotates around a horizontal axis, and the vertical type, where the die rotates around a vertical axis. Horizontal centrifugal casting machines are generally used to make pipes, tubes, bushings, cylinder sleeves (liners), and cylindrical or tubular castings that are simple in shape. The range of applications of vertical centrifugal casting machines is considerably wider: gear blanks, pulley sheaves, wheels, impellers,

electric motor rotors, valve bodies, plugs, yokes, brackets. Castings that are not cylindrical or even symmetrical can be obtained by vertical centrifugal casting. Centrifugally cast parts have a high degree of metallurgical cleanliness and homogeneous microstructures, and they do not exhibit the anisotropy of mechanical properties evident in rolled/welded or forged parts. Directional solidification provides for clean, dense castings with physical properties that are often superior to those of the static casting processes.

The effect of the vertical centrifugal process on castings can be due to one or more of the following three main features: centrifugal pressure; fluid dynamics; intrinsic vibration of the process [33]. The effect of each of these variables may be responsible for the enhancement found in both mechanical and metallurgical properties of the castings. Although the beneficial effect of the centrifugal casting process is well accepted an explanation for the reasons of that occurrence are not fully explored yet.

Thus, in order to understand whether the centrifugal effect is due to the inherent vibration of the process or to the centrifugal pressure and fluid dynamics, three different tests were performed: gravity casting as a baseline process, gravity casting with vibration in order to simulate the additional effect of the inherent vibration of the vertical centrifugal process, and vertical centrifugal casting in order to evaluate all the full process variables, e.g. the effect of fluid dynamics, centrifugal pressure, and inherent vibration.

One application of centrifugal casting is in FGM fabrication. In this method, a centrifugal force applied to a homogeneous semi-liquid composite, (containing ceramics or intermetallic compound particles) drives the formation of the desired gradient. The resulting composition gradient is produced by the difference in density between the molten metal and the particles under the same centrifugal force. Compared to other techniques, the centrifugal method is potentially applicable to mass production of both small and large FGM components at a low cost. Mechanical properties of FGMs fabricated by this method have been investigated using relatively large samples [38].

2.4. METALLURGICAL PROPERTIES

As the majority of cast components have complex geometries, a variety of microstructures may arise within a single casting. Considering that mechanical properties are a function of the microstructure, they will tend to change as the microstructure changes, thus any study of the properties of cast aluminium must take into account all the factors which may influence the microstructure. The two principal phases present in Al-Si casting alloys are primary aluminium based α-Al which, as the phase with the largest volume fraction, acts as the matrix for the alloy, and the silicon phase, which is found largely in two forms: primary 'blocky' silicon and 'plate like' eutectic silicon.
The goal of microstructural analysis is to develop a quantitative description of microstructure that can be used to establish its relationship to properties and processing.

The most significant microstructural features involved are second phase particles and grain structure; the second-phase particles of concern here are: (i) coarse, insoluble particles formed during casting, or coarse particles of normally soluble phases formed during casting or subsequent processing; (ii) smaller intermediate particles formed during homogenization; and (iii) aging precipitates.

Microstructural factors also have important influence in these cases: microstructural refining, defects like porosity and oxides, silicon modification, fractions of eutectic, precipitates and intermetallics [41-45]. Efforts have been done to improve the performance of these materials by controlling the microstructure, for example, in the cooling rate, aiming at reducing the secondary dendrite arms spacing's and porosity [46-48].

Phase's description of the Al-Si alloy

The Al-Si casting alloys contain two principal phases: aluminium based α-Al as the phase with the largest volume fraction, acts as the matrix for the alloy, and the silicon phase, which is found largely in two forms: primary 'blocky' silicon and 'plate like' eutectic silicon. To fully assess the role of phases, an alloy containing a different amount of Si (7%, 12% and 18%) has been investigated in this work.

α-aluminium phase

In each of the alloys studied in this project aluminium comprises 81.5-92.5 wt% and hence Al-based solid solution strengthened α-Al phase acts as the matrix for the alloys. This phase usually has a dendritic structure [53] but this is known to be dependent on the solidification conditions of the casting [83]; for example the temperature gradient across the sample and the thickness of the sample. A high temperature gradient is known to give elongated or columnar aluminium dendrites [56, 57], with a small secondary dendrite arm spacing (SDAS) [84]. The dendrites grow along the direction of the heat flow. More equiaxed dendrites form when the temperature gradient is lower e.g. in the centre of thicker sections of a casting.

Grain size is similarly affected by the cooling conditions, but may also be influenced by the addition of alloying elements [82]. The mechanism by which some elements like Ti, B, Zr and V work as grain refiners is not certain [57]. However, grain refiners are generally thought to provide inoculants particles, which do not dissolve in the melt, so that when the melt cools they provide sites for heterogeneous nucleation and therefore promote the growth of grains [59]. In Al-Si casting alloys fatigue cracks have been observed to be retarded at grain boundaries [78]. This retardation is usually attributed to the difference in the crystallographic orientation between grains, which inhibits the movements of dislocations ahead of the crack tip [50, 73]. If grains are large compared with other microstructural features (for example: dendrite or particle size) then their effect on crack propagation is less pronounced [61].

Al-Si casting alloys can be age hardened because the α-Al phase is a solid solution, which contains Cu and Mg. Under the correct aging conditions, these elements precipitate out of the α-Al, forming precipitates such as Al2Cu [76] and Mg2Si [74, 79] .The peak aging time for Al-Si casting alloys is approximately thirty minutes at a temperature of 230°C [49].

Etching of the aluminium phase in a 0.5% HF in water solution gives the matrix a characteristic yellow colour [57] .The shape of the aluminium dendrites formed is usually identifiable because the intermetallic and Si phases form at the tips of the dendrites and between the dendrite arms. The dendrites in eutectic alloys are less obvious because the primary and secondary phases are distributed more evenly throughout the matrix.

Silicon phases

The amount of silicon that is present in the alloys investigated in this study varies from 7 wt% to 18 wt%. In eutectic Al-Si casting alloys (which contain approximately 12 wt% Si), two types of silicon may be found: primary silicon and secondary, eutectic silicon [52, 53, 57]. Primary silicon is known to have a blocky morphology [60] but should not form in hypoeutectic alloys. Eutectic silicon usually has a plate or flake like morphology but this can be modified to have a much finer structure. Upon etching with a 0.5% HF in water solution, silicon has a grey colour. The size, volume fraction and morphology of the silicon phase are determined by the casting conditions, the chemistry of the alloy (for example the amount of Si and the other alloying additions) and the heat treatment [84]. The size of Si particles can vary from 2 μm [77] to greater than 100 μm [69]. Increasing the Si content up to the eutectic level (approximately 12 wt %) improves the castability of the alloy by reducing the melting temperature and the temperature range of the 'mushy' zone [71]. As a result of a more fluid cast, smaller interdendritic pores form which can improve the fatigue life of the alloys [51]. The addition of Si to Al also reduces the coefficient of thermal expansion [71]; this is important for a piston because it limits expansion in the engine and ensures the smooth movement of the piston when the engine warms up from resting temperature to the operating temperature. The more the material expands, the smaller the part must be produced so that it can expand in the cylinder and then the greater the possibility of piston slap. This has been understood since the early part of the 20th century [66, 70].

Silicon is a relatively hard, brittle phase and so improves the wear resistance of the resulting alloy [62, 80]. However, this does make the alloy more difficult to machine and so can increase production costs. Si is also added to improve the strength and elastic modulus of these materials [56] and these properties are dependent on the morphology and size of the silicon phases [67]. It has been demonstrated that a finer eutectic silicon structure with a spherical morphology improves both the tensile strength and the

percentage elongation of the alloy, whilst coarser particles are more detrimental to these properties [68]. Silicon particle shape and size may be altered through heat treatments such as hot isostatic pressing (HIPping) and solutionizing [75, 79], which produces a spherodised Si morphology (in a 2-D cross-section), or by the addition of alloying elements [70].

Sr [74] and Na [81] are typical alloying elements added to Al-Si alloys to alter the morphology of eutectic Si from large plates to finer particles [51], which may form part of an interconnected fibrous network of Si particles [72]. Additions of Sr and Na are thought to produce finer Si particles because they lower the eutectic temperature and therefore restrict the growth of Si nuclei [23].

Other phases

There are two elements added to Al-Si casting alloys able to increase their high temperature strength [80] are Ni and Cu. The mechanism by which they do this is unclear but work by [63] indicates that Al-Si alloys containing higher quantities of these elements are more resistant to stress relaxation at 350C. This may be attributed to a greater number of large particles, which can both inhibit the movement of dislocations and increase load transfer [58], which shields the matrix phase. Ni and Cu combine with Al to form three different phases [57]; these are the Al3Ni, Al3(NiCu)2 and the Al7Cu4Ni phases. Whilst the name of the Al3Ni phase suggests that it contains no Cu it actually contains approximately 10 wt% Cu and 29 wt% Ni. The Al7Cu4Ni contains 37 wt% Cu and 18 wt% Ni and so the principal difference between the alloys is the Ni:Cu ratio. The phases cannot be easily differentiated by a characteristic morphology. However, with etching in a solution of 0.5% HF in water solution the phases can be separated by colour which is generally related to the Ni:Cu ratio: a dark brown/grey colour indicates a phase with a high Ni:Cu ratio and a lighter grey colour signifies a low Ni:Cu ratio. These three phases often form adjacent to one another and are usually interconnected [52].

The AlP and Al3Ti phases have a indirect effect on the material properties, by altering the principal microstructural features: P is added to these alloys so that the AlP phase forms which acts as a nucleation site for primary ‘blocky’ Si particles [57] inhibiting the formation of large Si plates. In micrographs this phase appears as a small

black dot (approximately 1 μm2) in the centre of a primary Si particle. Ti is added to Al-Si alloys to act as a nucleant for the α-Al phase and encourage small, regular grains to form [57].

In Al-Si casting alloys, containing the required levels of Mg or Cu and under the correct aging conditions, Mg2Si and Al2Cu phases can be precipitated out of the α-Al matrix [74, 76, 79]. The state of these precipitates is known to play an important role in the strength of Al alloys [71] and so, depending on the aging conditions these precipitates are likely to have a direct effect on the material properties. However, these phases may also form during the cooling period of the casting process and form larger secondary phases that have a 'Chinese script' or lacy appearance [53, 57]. The effect of these larger phases on the mechanical or other properties of Al-Si casting alloys was not found in a review of the literature.

Due to the steel equipment used in the casting processes may be found on the microstructure some traces of Fe present as impurity [65] and as a result Fe-containing phases are commonly found in Al-Si casting alloys. Several Fe containing phases have been observed in these alloys including the β(AlFeSi), Al9FeNi, π(Al8FeMg3Si6) and α(AlFeMnSi) phases [53, 57]. The β phase is thought to be the most detrimental of the Fe-containing phases to the mechanical properties [54] and is also detrimental to the fatigue properties [69]. It forms large flakes and is reported [85] to provide a good 'nucleation site' for pores as it restricts the flow of the cast. To limit the effect of the β-phase, alloying additions such as Mg and Mn [85] are added to promote the growth of the other Fe-containing phases. The π and α phases have a 'Chinese script' morphology and are often smaller than the β-phase [53] although [55] indicates that the improved properties obtained by the addition of Mg may be due to the formation of Mg2Si precipitates and not because the π-phase is less deleterious. The Al9FeNi phase is not often mentioned in the literature since Al-Si casting alloys (for example A356 and A357) do not contain large quantities of Ni. However, the Al9FeNi phase was previously observed by Edwards [57] and Joyce [64]. Al9FeNi does not exhibit a 'Chinese script' or flake morphology like the other Fe-phases and so it is not yet established whether this

phase is preferable in terms of mechanical and fatigue properties. The Fe-containing phases have a grey/brown appearance after etching in 0.5% HF in water solution.

Grain size

The size of the grains within a material has an important influence over the strength of the material. The boundary between grains acts as a barrier to dislocation movement and the resulting slip because adjacent grains have different orientations. Since the atom alignment is different and slip planes are discontinuous between grains. The smaller the grains, the shorter the distance atoms can move along a particular slip plane. Therefore, smaller grains improve the strength of a material. The size and number of grains within a material is controlled by the rate of solidification from the liquid phase.

According to the amount of silicon, industrial Al-Si alloys are divided into three groups: hypoeutectic alloys with Si content between 5 and 10 wt%, eutectic alloys with 11-13 wt% Si, and hypereutectic alloys, commonly with Si content between 14 and 20 wt%.

To be easier to understand the formation of the microstructure, the phase diagrams are briefly explained at three different compositions of elements Al and Si, and how their microstructures will differ because of their positions on the phase diagram. First a hypoeutectic alloy, which is an alloy with composition situated on the left of the eutectic point, will be considered. Then compositions of the eutectic and hypereutectic will be discussed. At this point, only the condition of slow cooling, which will allow the alloy to solidify into it equilibrium condition, will be considered. The microstructure can be controlled by manipulating the speed of cooling the alloy.

Hypoeutectic Alloys

First, consider an alloy of Al and Si that has an overall composition that places it to the left of the eutectic point (Figure 2.2.). When an alloy falls to the left of the eutectic point it is called a hypoeutectic alloy. At location 1, the alloy is at a temperature that is high enough to put it in a fully liquid phase.

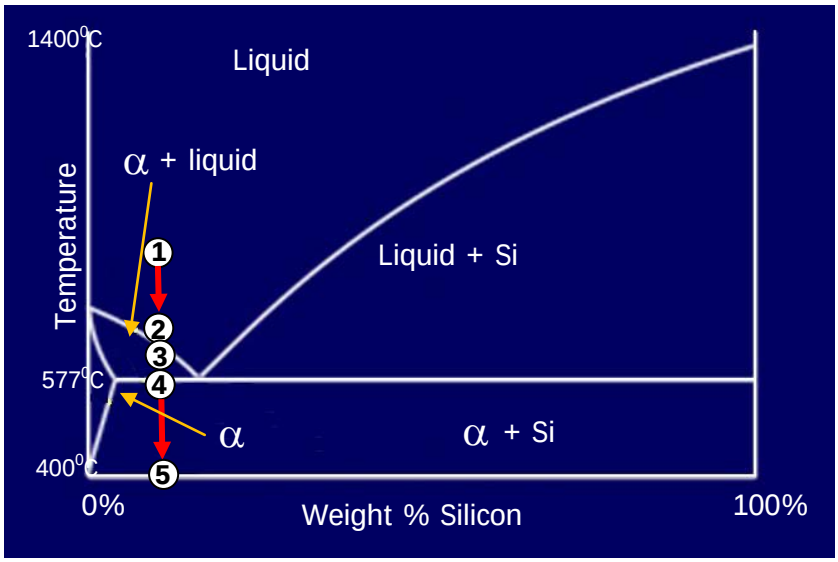

Figure 2.2 - Solidification diagram of hypoeutectic Al-Si alloy

When the alloy is cooled, it remains in the liquid state until it reaches the temperature where it crosses the liquidus line (location 2). At this temperature, the alpha phase starts to solidify at any favourable nucleation sites. The alpha solidifies as dendrites which grow to become grains of alpha. The first solid phase to form is called the primary phase so, in this case, primary alpha is formed.

As the alloy continues to cool (location 3) the existing nucleation sites will grow as dendrites and further nucleation sites will form within the liquid part of the mixture. The melt will have that mushy consistency of chunks in liquid while it is in the “alpha + liquid” region of the phase diagram. Since the alpha phase is mostly Al (with a small amount of Si atoms in solid solution), the remaining liquid becomes slightly richer in Si as the liquid cools, which is indicated by the liquidus line. The composition of the solid alpha phase also becomes slightly richer in Si atoms as the solid solution line shows.

This primary alpha phase growth and the accompanying phase composition shifts continue until enough aluminium atoms have been removed so that the remaining liquid is of eutectic composition. This composition is achieved at the point where the temperature crosses the eutectic line (location 4). At this point the primary alpha phase stops forming. The remaining liquid starts to solidify into the lamellar (alternating layers of alpha and beta phases) structure of a eutectic composition. The microstructure configurations in the points that correspond to points from solidification diagram of hypoeutectic Al-Si alloy are presented in figure 2.3. The eutectic structure will grow; adding alpha to the layers of alpha and beta to the layers of beta in the eutectic regions, and new solidification sites will continue to form. Remember that solidification occurs rapidly and without the need for a further decrease in temperature once the liquid reaches the eutectic line. At this point, the entire alloy has solidified into a mixture comprised of grains of alpha and grains of eutectic mixture (alpha and beta). The microstructure from this point at the eutectic line down to ambient temperature will look something like that shown in micro 5.

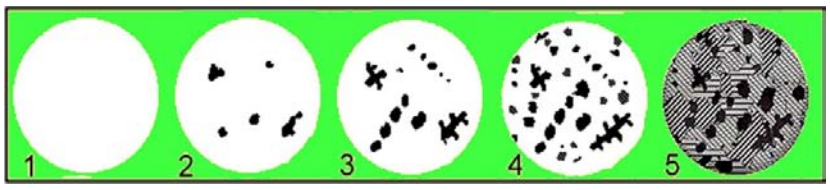

Figure 2.3 - Microstructure configuration in the points from solidification diagram of hypoeutectic Al-Si alloy

Diffusion occurs as the alloy cools since the amount of Si in the alpha phase changes with temperature. This occurs exactly like it did for the eutectic alloy. Diffusion must also occur in the grains of pure alpha, as the composition of alpha phase also changes with temperature.

Eutectic Alloys

Next, consider the eutectic alloy of elements Al and Si as it is cooled from a temperature at location 1 to location 4 on the phase diagram (Figure 2.4.). At location 1, the alloy is at a high enough temperature to make the mixture fully liquid. The circles below show a representation of the alloy's microstructure at each of the locations numbered on the phase diagram.

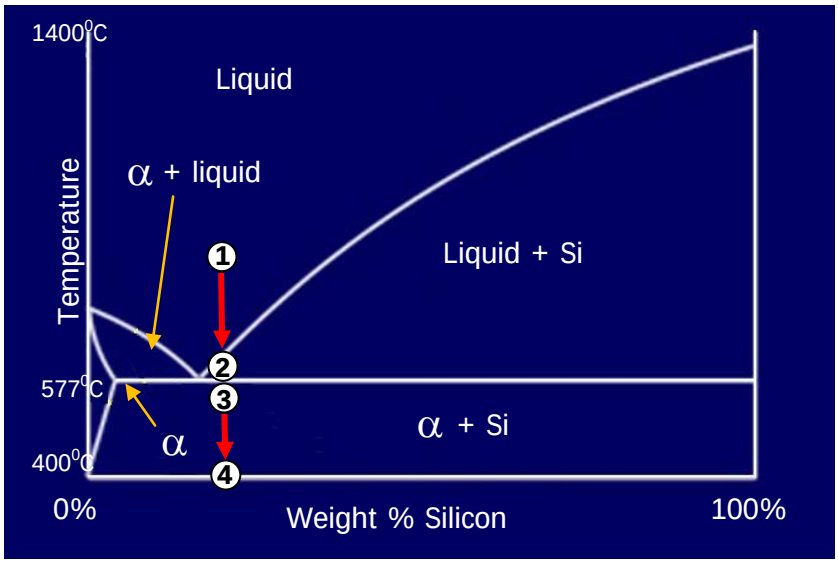

Figure 2.4 - Solidification diagram of eutectic Al-Si alloy

At location 1, there is nothing of interest as the alloy is completely liquid. As the alloy is slow cooled, it remains liquid until it reaches the eutectic temperature (location 2) where it starts to solidify at any favourable nucleation sites. From the microstructure image 2, it can be seen that as the alloy solidifies it forms into alternate layers of alpha and beta phase. This layered microstructure is known as lamellar microstructure and the layers are often only of the order of 1 micron across. The reason that a eutectic alloy forms in this way has to do with the diffusion times required to form the solid.

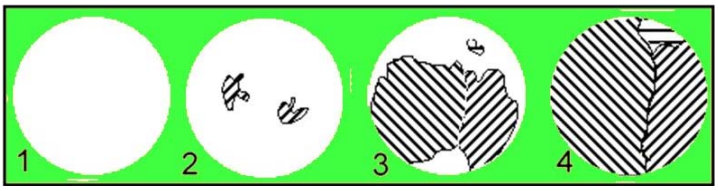

Figure 2.5 - Microstructure configuration in the points from solidification diagram of eutectic Al-Si alloy

The grains grow by adding alpha to alpha and beta to beta until they encounter another grain (location 3). Further nucleation sites will also continue to form within the liquid parts of the mixture. This solidification happens very rapidly as any given volume of liquid in the melt reaches the eutectic temperature. It has to be noticed that a eutectic composition solidifies at a single temperature like a pure element and not over a temperature range. The microstructure configurations in the points that correspond to points from solidification diagram of eutectic Al-Si alloy are presented in figure 2.5. As the now solid alloy cools to location 4, the composition of the layers of alpha and beta continue to change as it cools. Atoms of Al and Si will diffuse between the two phases to produce the equilibrium compositions of alpha and beta phase at a given temperature. By drawing tie lines at various temperatures the eutectic point on the phase diagram, it can be seen that the solubility of Al in the beta phase and Si in the alpha phase decreases as the temperature decreases. Since this phase composition change is due to diffusion, which is a relatively a slow process), it is important that eutectic alloys be allowed to cool slowly to produce the correct microstructure.

Hypereutectic Alloys

Finally, consider an alloy of Al and Si that has an overall composition that places it to the right of the eutectic point (Figure 2.6). When an alloy falls to the right of the eutectic point it is called a hypereutectic alloy. This alloy will solidify like the hypoeutectic alloy did except it will pass through the “beta + liquid” region of the phase diagram rather than the “alpha + liquid” region. This will result in a microstructure comprised of grains of beta and grains of eutectic mixture (alpha and beta) rather than

grains of alpha and grains of eutectic mixture (alpha and beta) as the hypoeutectic alloy had.

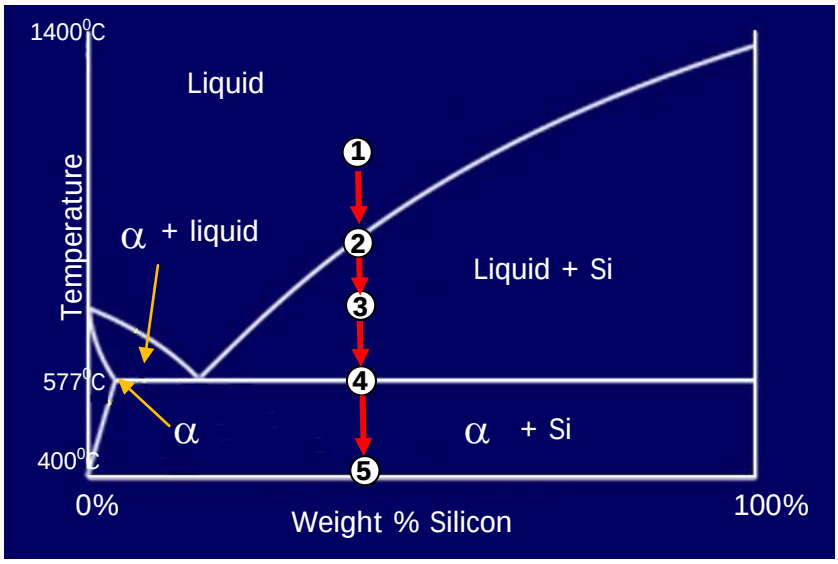

Figure 2.6 - Solidification diagram of hypereutectic Al-Si alloy

At location 1, the alloy is at a temperature that is high enough to put it in a fully liquid phase. When the alloy is cooled, it remains in the liquid state until it reaches the temperature where it crosses the liquidus line (location 2). At this temperature, the beta phase starts to solidify at any favourable nucleation sites. The beta solidifies as particles which grow to become grains of beta. The first solid phase to form is called the primary phase so, in this case, primary beta is formed.

As the alloy continues to cool (location 3) the existing nucleation sites will grow as dendrites and further nucleation sites will form within the liquid part of the mixture. Since the beta phase is mostly element Si, the remaining liquid becomes richer in Al as the liquid cools, which is indicated by the liquidus line.

This primary beta phase growth and the accompanying phase composition shifts continue until enough Si atoms have been removed so that the remaining liquid is of eutectic composition. This composition is achieved at the point where the temperature

crosses the eutectic line (location 4). At this point the primary beta phase stops forming. The microstructure configurations in the points that correspond to solidification diagram of hypereutectic Al-Si alloy are presented in figure 2.7. The remaining liquid starts to solidify into the lamellar (alternating layers of alpha and beta phases) structure of a eutectic composition. The eutectic structure will grow; adding alpha to the layers of alpha and beta to the layers of beta in the eutectic regions, and new solidification sites will continue to form. At this point, the entire alloy quickly solidifies into a mixture of beta grains and eutectic mixture (alpha and beta) grains. The microstructure from this point at the eutectic line down to ambient temperature will look something like that shown in location 5.

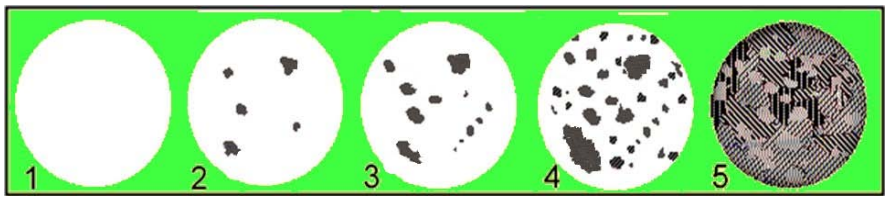

Figure 2.7 - Microstructure configuration on the points from solidification diagram of hypereutectic Al-Si alloy

Diffusion occurs as the alloy cools since the amount of element Si in the alpha phase changes with temperature. This occurs exactly like it did for the eutectic alloy. Diffusion must also occur in the grains of pure alpha, as the composition of alpha phase also changes with temperature.

Secondary Dendrite Arm Spacing (SDAS)

Secondary Dendrite Arm Spacing (SDAS) is the linear distance between two of the secondary α-Al dendrites or arms. As this SDAS is governed by the solidification conditions, it thus provides a direct measurement of the solidification rate in the local casting area. In general, the mechanical properties of aluminium castings tend to correlate better with the SDAS than with the grain size; all other things being equal, higher solidification rates yield finer spacing, which in turn provide better mechanical properties [93]. Each grain contains a family of aluminium dendrites originated from the same nucleus. Dendrite arm spacing (DAS) is determined by the cooling rate through the

mushy zone, with slower cooling which then results in larger DAS values. The grain size in aluminium foundry alloys varies between 1-10 mm, while DAS values vary from 10-150 μm and the eutectic silicon may be found in the form of plates of up to 2 mm in length or in rounded particles of less than 1 μm in diameter [93-95].

The SDAS is described by some researcher, as a function of local solidification time, equation 1 [86, 87], depicting the fineness of the microstructure constituents where ts is the local solidification time, and C and n are constants which are related to the material:

$$SDAS = C * ts^{n} \quad (2.1)$$

Porosity

Porosity is a major defect in cast aluminium alloys; it may be observed in the form of pores, voids, or cavities which arise in the interior of a casting during solidification. In general, porosity has three sources. The first is poor casting design which prevents the casting from filling properly; this defect is commonly referred to as *macroshrinkage.* The next source of porosity is gas which is entrapped or dissolved in the liquid metal during casting; this is called *gas porosity* or *microporosity.* The third source of porosity develops from the natural volume contraction which occurs when a liquid solidifies; this is often referred to as *microshrinkage* porosity [97]. The presence of porosity is crucial in that it lowers the soundness of a casting and thereby its mechanical properties.

Factors that influences the solidification diagram

Solidification of a melt is able to proceed from the edge of the casting inwards by extraction of heat at the surfaces of the casting. The extraction of heat generates thermal gradients in the casting by which heat can be extracted from the central regions of the casting. The solidification behaviour is heavily influenced by the thermal gradient in the liquid and the velocity with which the solidification front moves through the casting.

Recent results have demonstrated that rapid solidification processes and mechanically based microstructure refinement may changing the normal route of solidification formation of the microstructure showed above, modifying substantially the morphology of the Si phase when compared to that found in conventionally processed

materials [88, 89, 92] namely those where the lamellar to fibrous Si modification is achieved by strontium, sodium or antimony addition [90, 91].

There are three principal methods for achieving grain refinement in Al alloys [96]:

a) Rapid cooling during solidification *(i.e.* chill grain-refinement);

b) Agitation of the melt, *e.g.* as occurs during semi-solid metal processing;

c) Addition of a grain refiner to the melt.

A fine grain structure is formed by varying the solidification conditions such as cooling rate and temperature gradient in the casting. This is due to shortening of grain growth during the solidification process. In the second method, grain refinement is obtained by mechanical or electromagnetic agitation, by forced convection, and by breaking up the dendrites in the semi-solid state. The fragmented parts are thereupon transported into the bulk and become effective nucleants. This type of refinement mechanism is the one in which the required stirring is applied during the formation of the semi-solid structure.

Processing the metal in its molten state is the activity wherein the most gains can be achieved. Molten metal processing is an opportunity for refining and quality enhancement. For example, processes such as alloying, degassing, filtration, fluxing, and grain refinement and modification in aluminium are usually carried out in the liquid metal prior to casting. The mass transfer rates and the kinetics are such that these reactions are carried out much more effectively in the melt.

Mechanical mould vibration

It is documented that the application of mechanical vibration to the mould during solidification has an effect on the microstructure and consequently on mechanical properties of the casting [27, 98]. The lamellar spacing tends to reduce and silicon morphology becomes fibrous with the increase of the vibration amplitude as compared to gravity casting. However, exceeding a critical value of acceleration (relationship between frequency and displacement amplitude), the silicon tends to coarsen [98]. Fragmented primary dendrites with higher arm thickness and reduced solidification time were obtained on Al–8Si with rectilinear vibration at 100 cycles/min (~2 Hz). The same level of vibration was applied to Al–12Si and it was reported a reduction of the eutectic cell size from 5 to 1.6 mm and a coarsening tendency of the eutectic Si [99]. Another study on

the effect of the very low frequency vibration (100 and 200 cycles/minute) concluded that mechanical vibrations improve the density, hardness, UTS and elongation of the cast components [103]. They attributed these improvements to the enhanced coagulation of hydrogen bubbles and their escape from the melt brought about by vibrating the mould. Thus porosity was reduced and wetting of the mould walls by the melt was enhanced, this in turn promoted faster heat transfer and fragmentation of the solids formed on the mould wall [102]. Metal vibration at a constant frequency of 100 Hz and amplitudes from 18 to 199 μm was reported to increase the alloy elongation between 19 and 68% and a slight increase around 3% in the ultimate stress [98]. The increase in elongation was correlated with the increase in the amount of eutectic composition compared to the non-vibrated case [98]. Moreover, significant reduction in gas content was obtained with low frequency melt agitation in Al–20Si [100]. Nevertheless, in another study the volume fraction and size of pores increased in LM25 (Al–7Si) and LM6 (Al–12Si) alloys with increasing frequencies between 15 and 41.7 Hz and amplitudes between 0.125 and 0.5 μm [101].

A research focused on the effect of mechanical vibrations on the grain refinement and mechanical properties on pure aluminium, Al7%SiMg and Al12%Si alloys along with other non-ferrous alloys was done by Dommaschk et all [104]. The same research team was also reported that the dependence of the castings' wall thickness on casting characteristics could be minimized with the use of mechanical vibration [104-106].

Thus, it is clear that vibration may promote changes in microstructure and consequently in mechanical properties, either increasing or decreasing it. However the mechanisms under which those changes occur are still unclear. This work proposes a mechanism that is able to explain the reason for the shift on metallurgical and mechanical properties with vibration acceleration.

Fluid dynamics

The fluid dynamics of aluminium alloys has a direct influence not only on material castability, but also on the casting properties. Fluid dynamics is a complex parameter that is affected by the properties of the molten metal and mould, pouring conditions and solidification mechanisms. Fluid dynamics has an important role on casting properties due mainly to the influence on solidification sequence.

The fluid dynamics is expected to be very different under gravitational force (gravity casting), gravitational force and vibrating movement (vibrating gravity casting) and under centrifugal pressure, gravity pressure and inherent vibration (centrifugal casting). It is expected that the turbulence of the melt in the centrifugal process is much higher inside the mould. According to [107], the first melt reaching the wall surface of the mould (where the first germens of solidification appear) will came backwards to the inside part of the mould cavity increasing the number of solidification sites in the inner part of the casting and consequently promoting a quicker solidification and a refined microstructure, as compared to the gravity casting process [33].

Centrifugal pressure

During solidification the molten alloy is subjected to external forces that influence the solidification behaviour as, for example, gravitational force in gravity casting, lateral forces due to vibration movement in vibrating gravity casting and also the combined effect of vibration and centrifugal pressure in the case of centrifugal casting.

The centrifugal pressure applied on the melt during solidification can significantly decrease the percentage of porosity, increase the density, decrease the grain size of α-Al, and modify the eutectic Si [34, 36, 37]. It is also important to highlight that the centrifugal pressure may have an influence on the positioning of the densest phases during solidification, which have tendency to move to the outer part of the casting due to the centrifugal force [35]. Thus it is expected that in alloys where phases with different densities coexist the densest ones will concentrate on the outer part of the casting.

This is what happens with most of composite particle reinforced materials obtained by centrifugal casting [108] (also called functionally graded materials). In this research, the effect of both the inherent vibration of the centrifugal process as well as the centrifugal pressure and fluid dynamics on the mechanical properties of the castings will be evaluated.

2.5. MECHANICAL PROPERTIES EVALUATION

Several factors have to be considered when examining the physical properties of aluminium silicon casting alloys. The mechanical properties are affected by the casting method, eutectic modification, and grain refinement. Based upon similar casting parameters, casting methods and micro-alloying additions that promote fine grain structure (e.g. rapid undercooling due to high heat transfer rates, and the addition of titanium or boron) and peak modification of the silicon structure in the eutectic (i.e. the addition of sodium or strontium) give the best mechanical properties.

Different techniques are used to characterize the functionally graded materials mainly depending on the process of obtaining the FGM's. For example: depth sensing indentation is a widespread technique for mechanical characterization of materials obtained mainly by constructive processes (figure 2.1) by determining hardness and the Young's modulus. In the case of constructive methods can be used along with indentation, hardness testing methods almost all 'classical' methods on different gradual depths of the material by cutting slices and extract specimens from gradual positions.

The use of aluminium–silicon casting alloys as structural materials is determined by their physical properties (primarily influenced by their chemical composition) and their mechanical properties (influenced by chemical composition and microstructure). The high specific tensile strength of aluminium alloys is very strongly influenced by their composed poly-phase microstructure. The mechanical properties of a specific alloy (hypoeutectic, eutectic or hypereutectic) can be attributed to the individual physical properties of its main phase components (a-aluminium solid solution and silicon crystals) and to the volume fraction and morphology of these components. According to [115] the tensile properties and fracture behaviour of cast aluminium alloys A356 and A357 strongly depend on secondary dendrite arm spacing (SDAS), Mg content, and, in particular, the size and shape of eutectic silicon particle and Fe-rich intermetalics. Thus, mechanical properties of Al–Si cast alloys depend not only on chemical composition but, more important, on micro structural features such as morphologies of dendritic a-Al, eutectic Si particles and other intermetalics that are present in the microstructure. There are different solutions to control these microstructural features, for example by

introducing special elements [116, 117] to refine the grain. However the most common solution to improve mechanical properties of cast aluminium–silicon alloys is by cast technology [22]. Each technology has particular aspects that interfere on microstructure and consequently on mechanical properties.

Tensile properties are an important mechanical properties used routinely in design calculations being controlled by the microstructure, as well as the formation of porosity and intermetallics. In general, the relation between porosity and any of the mechanical properties is non-linear [114]. The shape of the non-linear graphs gives an indication of the pronounced influence of porosity on all the properties.

Among the properties measured, ultimate tensile strength (UTS) appears to be the one most affected by porosity, followed by yield strength (YS) and then percentage elongation. An increase in the volume fraction and size of intermetallics also lead to a decrease in tensile and impact properties.

The mechanical properties of cast aluminium alloys are very sensitive to composition, casting process, which encounters mould filling and solidification behaviour, and post-processing such as thermal treatment. The coarseness of the microstructure and the type of intermetallic compounds that form and precipitate during solidification, are fundamental to the material behaviour. This contribution aims to predict the mechanical and fatigue properties of three aluminium cast alloys component produced with various casting processes, in heat treated conditions. The simulation of the casting processes, gravity and centrifugal casting, and the resulting microstructure and mechanical properties, permits a reduction of experimental testing and providing the best solution of process and material selections, thereby making the design and development process more cost efficient.

However, the mechanical properties of aluminium alloy cast components are strongly dependent on the local microstructure, which is directly related to the chemical composition and the solidification conditions imposed by the casting system (mould, cores, cooling circuit, coolers, etc.) [86, 115, 118-134]. Many studies demonstrated that solidification defects (such as gas pores, cavity shrinkages and oxide films) strongly affect the mechanical behaviour, and mainly fatigue resistance, of cast aluminium alloys

[121-128]. A number of papers have been published about the relationship between casting defects and fatigue resistance of A356 (AlSi7Mg0.3) and A357 (AlSi7Mg0.6) aluminium alloys [123-127]. Continuous improvement in casting techniques, however, has led to a decrease in casting defects. As a result, other microstructural parameters, including the secondary dendrite arm spacing (SDAS), the grain size, the size and morphology of eutectic Si particles, as well as the shape and distribution of intermetallic compounds, have to be considered in order to predict the mechanical behaviour of cast aluminium alloys [115, 129-134].

2.5.1. Models to predict mechanical properties

Some authors believe that DAS is the most important factor, which determines the characteristic mechanical strength of aluminium casting alloys [138-140], but some others believe that the effect of eutectic silicon phase morphology [137], volume, size and morphology of microporosity [143], have the same or more importance. DAS has often a proportional relationship with the solidification rate [139, 140, 142]. It is also roughly proportional to the resulted mechanical properties [138, 140] by improvement of ultimate tensile and yield strength, as well as elongation percentage. Alloy chemical composition has generally been found to influence the spacing, although the effect is usually small compared with that obtained by solidification time [140].

Khomamizadeh [144] assumed that the final mechanical properties of cast alloy resulted from the sharing effect of three mentioned microstructural major components and a linear relationship can be obtained by regression analysis of quality index versus DAS, spheroicity of eutectic silicon particle and the 2-D microporosity area as follows:

$$Qi\ (MPa) = 213 - 0.081 * DAS\ (\mu m) + 126 * \text{spheroicity} - 24.0\ \text{porosity}(\%) \quad (2.2)$$

The “quality index" correlates the tensile strength rate and the increasing percent of elongation, as well as the contribution of different microstructural constituents on the mechanical properties [141, 145]. This parameter is defined as follows:

$$Qi = UTS + K \log(\text{Elongation}) \quad (2.3)$$

In this equation, the constant K, for the alloy A356, is equivalent to 150 MPa [141, 145].

Another way to predict both mechanical properties as well as the fatigue life the material component is based on some metallurgical characteristics of the obtained casting.

A number of papers have been published showing several relations that estimate the tensile stress with other different microstructure characteristics. For example, Bernsztejn proposed a relation to calculate the average stress as a linear function of the volume fraction of silicon [146]:

$$\sigma = \sigma_{\alpha} \cdot V_V^{\alpha} + \sigma_{Si} \cdot V_V^{Si} \tag{2.4}$$

where σ_{α} and σ_{Si} are stresses in the volume unit.

This formula neglects the influence of the morphology, the average size, and the distribution of brittle particles, that is, silicon precipitates and also the volume fraction of constituents which can differentiate the properties of materials of similar value of the silicon volume fraction to an important degree.

A correlation between tensile strength (σ) and silicon particle size for aluminium-silicon alloy containing 17-27% Si, was presented by Mandal et al.[147]:

$$Tensile\ strength\ (MPa) = 252.8 - 3.73 \times particle\ size\ (\mu m) \tag{2.5}$$

Another relationship between ultimate tensile strength and secondary dendrite arm spacing and the size of silicon lamellas in interdendritic eutectic regions, was proposed [22]:

$$\sigma = k + k_2 \cdot \gamma^{-\frac{1}{2}} + k_3 \cdot \lambda^{-\frac{1}{2}} \tag{2.6}$$

where: σ is the ultimate tensile strength, k, k_2 and k_3 are empirical constants, γ is the size of silicon lamellas in interdendritic eutectic regions and λ is the secondary dendrite arm spacing.

Secondary dendrite arm spacing is also in attention of researcher and generates several models to estimate tensile strength: [148]

$$UTS = -1{,}4399 * SDAS + 34 \text{ [MPa]} \tag{2.7}$$

In order to optimize the design of the cast components based on local properties it is necessary to know the local metallurgical properties which gave the mechanical properties that may help to estimate the failure of the component.

Even if the relations 2.2 to 2.7 are able to estimate with sufficient accuracy the ultimate rupture strength they could not be used for entire range of silicon percentage contained in aluminium alloys. That's why one of the goals of the present research was to find a general equation that could predict ultimate rupture strength for a large range of the silicon percentage of aluminium alloys.

2.6 FATIGUE PROPERTIES

Fatigue analysis refers to one of three methodologies: local strain or strain life, commonly referred to as the crack initiation method, which is concerned only with crack initiation (E-N, or sigma nominal); stress life, commonly referred to as total life (S-N, or nominal stress); and crack growth or damage tolerance analysis, which is concerned with the number of cycles until fracture.

Fatigue is failure under a repeated or varying load, never reaching a high enough level to cause failure in a single application. The fatigue process embraces two basic domains of cyclic stressing or straining, differing distinctly in character. In each domain, failure occurs by different physical mechanisms:

1. Low-cycle fatigue—where significant plastic straining occurs. Low-cycle fatigue involves large cycles with significant amounts of plastic deformation and relatively short life. The analytical procedure used to address strain-controlled fatigue is commonly referred to as the Strain-Life, Crack-Initiation, or Critical Location approach.
2. High-cycle fatigue—where stresses and strains are largely confined to the elastic region. High-cycle fatigue is associated with low loads and long life. The Stress-Life (S-N) or Total Life method is widely used for high-cycle fatigue applications—here the applied stress is within the elastic range of the material and the number of cycles to failure is large. While low-cycle fatigue is typically

associated with fatigue life between 10 to 100,000 cycles, high-cycle fatigue is associated with life greater than 100,000 cycles.

In the case of functionally graded materials the fatigue properties are obtained in the same way as for normal materials, for different layers on the direction of gradation to be able to characterize the whole materials.

Pistons are typically produced from multi-component Al-Si casting alloys. These alloys exhibit a complex, multiphase microstructure comprising α-aluminium as the matrix with silicon particles and several intermetallic phases. Previous research reported on literature on Al-Si casting alloys has demonstrated that porosity is detrimental to fatigue life as cracks initiate freely at pores. Casting defects have a detrimental effect on fatigue life by shortening not only fatigue crack propagation but also the initiation period. The decrease in fatigue life is directly correlated to the increase of defect size. There exists a critical defect size for fatigue crack initiation, below which fatigue crack initiates from other competing initiators such as eutectic particles and slip bands. Castings with defects show at least an order of magnitude lower fatigue life compared to defect-free materials. Porosity is more detrimental to fatigue life than oxide films.

However, with improved casting techniques porosity can be greatly reduced and other microstructural features influence fatigue life. In particular, Si particles have been shown to play an important role in the initiation and subsequent propagation of fatigue cracks. Pores, Si particles and intermetallic phases were shown to cause fatigue crack initiation.

It was reported on literature that fine microstructures (DAS = 15-30μm) produces long (75% of total life) crack initiation times. A very coarse microstructure (DAS > 50μm) produces short (15% of total life) crack initiation times. In coarse microstructure (DAS > 30μm) pores are the dominant crack initiation site, whereas for finer microstructure (DAS < 27μm) the eutectic phase are dominant. These effects are more dominant in high cycle fatigue [205].

Primary silicon particles in hypereutectic Al-Si casting alloys influence their fatigue behavior. These particles are hard and brittle in nature, and act as favored sites for crack initiation an also for crack propagation. The crack is attracted towards them, increasing the crack growth rate. The damage and decohesion of primary silicon particles during cyclic loading results in facilitating the fatigue crack propagation and, as a consequence, lowers the fatigue life. The number of cycles to produce a crack that leads to failure also depends heavily on grain size, with the finest grains giving the best performance. Thus, fine grains appear to be best for resistance to fatigue initiation, and coarse grains appear to be best for resistance to crack propagation for long cracks. In fact, it may be shown that there is a crossover in endurance limit for very short cracks versus long cracks.

2.6.1. Effect of microstructure on fatigue of aluminium

Microstructural, manufacturing, and environmental factors can cause high local stresses and therefore act as initiation sites. It is noted that fatigue is a cascade of processes of crack formation and growth that depends on the hierarchical morphology of phases or grains, as well as the presence of nonmetallic inclusions in cast or wrought alloys.

Microstructure plays a role in establishing ‘‘connectivity” of slip within the microstructure that provides enhancement of driving force for small crack formation and growth. Typical microstructural factors in Al-Si alloys include brittle phases, for example primary Si particles [150], pores [149] and oxides [151]. Si particles have been shown to crack [150], and decohere at the particle/matrix interface [69] under cyclic loading and so act as initiation sites. Pores and other inclusions also act as stress raisers and are common artefacts of the casting process which reduce fatigue life [83].

2.6.1.1. Effect of porosity

Porosity (mixed or microshrinkage) is the major microstructural feature controlling fatigue properties because it introduces very high stress concentrations within fatigue specimens, serving as primary sites for fatigue crack initiation. Numerous studies have been conducted to investigate the effect of porosity on fatigue properties of cast aluminium alloys. It has been widely concluded that fatigue cracks initiate predominantly

from pores located at or close to the specimen surface. The number of cycles required to initiate a crack is small relative to the total fatigue life. Therefore, the fatigue life is dominated by the propagation of small cracks and the initiation life is generally considered to be negligible [170, 178, 180, 183, 184]. In hot isostatic pressed (HIP) aluminium, where porosity is greatly reduced, the initiation periods are finite; therefore the total fatigue life will be longer than that of non-HIP aluminium. A comparison of the HIP and non-HIP results [177] shows that the presence of porosity significantly decreases the fatigue resistance. Similarly, a study on A356-T6 [185] found that for specimens with similar secondary dendrite arm spacing (SDAS) but different porosity levels, the fatigue lives tested at 138 MPa differ by approximately a factor of 10.

Porosity is the term used for the voids or cavities that form within a casting during solidification. It is the most common defect found in Al–Si casting alloys and is the major cause of rejection of such castings, as it often results in poor mechanical properties such as limited strength and ductility, variable fracture toughness, irregular crack initiation and crack propagation characteristics, as well as a lack of pressure tightness [93, 154-156].

Two major fundamental effects contribute to the formation of porosity in solidifying Al–Si casting alloys: (i) shrinkage resulting from the volume contraction accompanying solidification, as well as inadequate liquid metal mobility (bad feeding), and (ii) gas evolution (mainly hydrogen) resulting from the decrease in gas solubility in solid metal compared to the liquid [85, 157-160].

Fatigue is considered to be the most common mechanism by which engineering components fail, and it accounts for at least 90% of all service failures attributed to mechanical causes. Failure occurring under conditions of dynamic loading is called fatigue failure, and is particularly insidious because it occurs without any obvious warning, resulting in sudden or catastrophic failure [1]. Fatigue can be defined as “the process of progressive localized permanent structural change occurring in a material subjected to conditions that produce fluctuating stresses and strains at some point or points and that may culminate in cracks or complete fracture after a sufficient number of fluctuations” [161]. Three basic factors are necessary to cause fatigue failure: maximum tensile stress of sufficiently high value, a large variation or fluctuation in the applied stress, and a sufficiently large number of cycles of the applied stress [1]. The fatigue

fracture surface generally consists of three main regions that correspond to fatigue crack initiation, fatigue crack growth, and fast fracture [154].

Several studies [75, 123, 154, 162-172] have shown that porosity is the key factor which controls the fatigue properties in Al–Si casting alloys. Pores are preferential sites for crack initiation in these alloys, and thus constitute the main factor influencing fatigue performance, independently of the loading conditions and of the stress applied. Compared with porosity, the eutectic structure and intermetallic phases play a minor role in crack initiation.

The effect of porosity on fatigue life has been summarized as follows: pores reduce the time for crack initiation by creating a high stress concentration in the material adjacent to the pores; because of this, most of the fatigue life is spent in crack growth.

Porosity has been classified according to the importance of crack initiation as follows: a single shrinkage pores close to or at the surface is considered the most critical, whereas a gas pore at the surface is considered the least critical [154]. Porosity is the microstructural feature most detrimental to fatigue life. It overrides any influence from other factors such as oxide films, eutectic particles and slip bands [83].

There exists a critical defect size, [83], (in Sr modified cast A356 alloy, the critical defect size is in the range of 25-50 μm) for fatigue crack initiation, below which the fatigue crack initiates from other intrinsic initiators such as eutectic particles and slip bands.

Compared with porosity, the eutectic structure and intermetallic phases play a minor role in crack initiation. The effect of porosity on fatigue life has been summarized as follows: pores reduce the time for crack initiation by creating a high stress concentration in the material adjacent to the pores; because of this, most of the fatigue life is spent in crack growth [125]. Typically, fatigue endurance is reduced when the size of porosity increases [83, 170, 174, 175]. Casting defects have a detrimental effect on fatigue life by shortening not only fatigue crack propagation, but also the initiation period. The decrease in fatigue life is directly correlated to the increase of defect size [83].

The negative effect of oxide films on fatigue life becomes pronounced in the absence of porosity, Compared with materials failed from porosity, the fatigue lives of specimens failed from oxide films are 4 to 5 times longer. However, even when the oxide films are

crack initiators there is little improvement in fatigue data scatter. For defect-free specimens, fatigue cracks are usually initiated from slip bands and eutectic particles. The fatigue lives of these specimens are 25 times longer than those associated with specimens failed from porosity. In addition, the specimens failed from slip bands shows slightly less scatter in fatigue life.

Murakami *et al.* [179] showed that fatigue resistance mainly depends on pore size and its location, not its shape and volume fraction. Similar results were reported by Wang *et al.* [83]. Murakami *et al.* [179] recommend characterizing the size of pores as the square root of the projected two-dimensional area normal to the loading direction. In general, fatigue life increases with decreasing pore size because large pore sizes decrease the number of cycles that needs to fail the specimens. Decreasing the pore size is certainly beneficial; however, this holds true only up to the point when other fatigue crack initiators (e.g. oxide films, eutectic particles and PSBs) become dominant. The size of the critical pore for fatigue crack initiation is related to the material microstructure and loading conditions. A critical pore size of about 100 μm has been proposed for a 319 alloy [186] and 25 μm for a Sr-modified A356 alloys [83]. In addition, the distribution of initiating pore size does not show a distribution of all pore sizes in the material but a distribution of sizes of the largest pores. In the study of fatigue of cast 319 alloys, Boileau [177] found that the initiating pores were significantly larger than those observed on the metallographic surface. Major *et al.* [77] found that the fatigue life was sensitive to the maximum pore size.

Pore location is also an important factor that determines fatigue life of aluminium castings. For a given size pore, the stress intensity factor can be ~55% higher if the pore is located at the free surface rather than in the centre of the specimen [83]. A large pore, which is located in the centre of the casting, may not affect fatigue performance. However, a small isolated pore near a surface may have a significant impact. This is consistent with the work of Murakami *et al.* [179].

The effect of porosity on fatigue crack growth has rarely been reported. In one study on fatigue behaviour of A356-T6 aluminium cast alloys [83], it was found that the size and area fraction of porosity and oxide films on the fracture surface, particularly in the overloaded regions, was much higher than the area fraction determined by metallographic measurements. The authors attribute the higher fraction of porosity on the fracture surface

to the fact that the fatigue crack always seeks the weakest path and porosity provides an easy path for crack propagation. In addition, the higher stress concentration field around porosity also enhances microcrack initiation and further linkage to a macro-crack in front of the main fatigue crack. Gall *et al*. [183] believed that porosity has an "indirect" influence on fatigue crack growth rates. The porosity generally enhances the nominal stress field experienced by the microstructurally small cracks and this enhancement leads to relatively higher small crack growth rate even in the absence of explicit interaction between the small cracks and pores.

2.6.1.2. Effect of Silicon

Silicon content has an influence on the long fatigue crack growth behaviour of Al–Si–Mg alloys [181, 187]. Was found that lower the Si content, the better the fatigue crack growth resistance due to higher roughness-induced closure in the low Si content alloys [181]. Si particles encountered along the crack path change the local slip orientation and crack path selection. In alloys with low eutectic Si, the crack advances on certain slip systems until an obstacle, such as a grain boundary, causes an orientation change. The low Si alloys, exhibit extended planar slip behaviour that increases roughness. However, in higher Si alloys, the role of grain boundaries becomes less important. Instead, more frequent encounters with Si particles result in less variation in the crack path, lower overall roughness. Roughness level is also influenced by Si morphology. Unmodified alloys have higher fatigue crack growth threshold (high thresholds being associated with enhanced high-cycle fatigue properties), while modified alloys present higher fracture toughness (high fracture toughness involving better low-cycle fatigue behaviour) [181, 187]. At low ΔK *(stress intensity)*, the cracks in unmodified alloys show more path deflection, resulting in higher roughness-induced closure and thus high fatigue resistance. At high ΔK, once debonding and fracture of Si particles largely occur, the coarse morphology provides convenient paths for the crack to slide along or cut through. Sr-modified alloys have small and round eutectic silicon particles that offer more fatigue resistance. Overall, Sr-modified alloys show longer fatigue lives compared to unmodified alloys [188, 189].

2.6.1.3. Effect of intermetallics

Intermetallics were reported to act as the fatigue crack initiation site [182] when porosity is absent in the material.

Increasing Fe content decreases fatigue life [84], particularly for alloys with large secondary dendrite arm spacing (SDAS) values. The low fatigue life of high Fe content alloy was attributed to the increased amount and size of Fe-rich phases. Yi [190] found that increasing Fe-content reduces the fatigue life in the long lifetime regime ($>10^6$ cycles), however, Fe-content has no effect for medium fatigue life ($>10^5$ and $<10^6$ cycles) and it slightly increases the fatigue life in the short lifetime regime ($<10^5$ cycles). The existence of large plate-like Fe-rich intermetallic particles in high-Fe castings was found to promote fatigue crack initiation. However, these particles can cause retardation in the small crack growth stage when inclined to the crack growth path.

Increasing Mg content from 0.4% to 0.7% significantly decreases fatigue life of aluminium alloys [84]. The decrease of fatigue life with increasing Mg content can be attributed to the occurrence of microcracking. It is known that increasing the Mg content increases the eutectic particle size particularly in the Sr-modified alloy [55]. The increased eutectic particle size results in more particle fracture and thus shorter fatigue lives.

2.6.1.4. Effect of SDAS

The secondary dendrite arm spacing (SDAS) is an important factor defining the metallurgical structure of aluminium castings. SDAS is governed by the solidification rate and thus provides a direct measurement of the solidification rate in a local area of the casting. Higher solidification rates yield finer SDAS [93]. In general, the mechanical properties in aluminium alloy correlates better with the SDAS than the grain size.

Aluminium alloys with large SDAS are characterized by large α-Al dendritic regions, and large spacing between consecutively sampled Si regions. As a result, the crack roughness associated with these structures is higher than the roughness of small SDAS materials due to coarsely spaced fatigue crack-Si particle interactions, which results in higher closure, higher threshold, and better fatigue crack resistance in the near-threshold regime of long fatigue cracks.

However, at high ΔK levels, the size of eutectic regions and the Si particle morphology dictate the crack growth resistance. For coarse microstructures the eutectic regions as well as Si particle size are larger too, providing lower resistance to the crack advance. This behaviour results is higher growth rates at high ΔK and lower pseudo-fracture toughness for the large SDAS materials. Similar behaviour was experimentally observed for A356 [189, 191] and W319 [176] cast aluminium alloys.

2.6.2. Models to predict fatigue life

In terms of fatigue life, S–N curves and mainly fatigue limit, σ_w, there are basically three theories [113]. The first and probably the most common, correlates σ_w (fatigue limit) with ultimate static strength, σ_u, of the materials (equation 2.8). The second correlates σ_w with Vickers Hardness, H_v of the materials (equation 2.9). The third correlates σ_w with the size, (in terms of projected $\sqrt{area}$) of pores, impurities, or some fragile phases, of the materials. For aluminium alloys, this third theory (equation 2.10) it is used mainly to correlate σ_w with the size, ($\sqrt{area}$) of pores and, for some alloys, with the size of the silicon particles.

$$\text{1st theory:} \quad \sigma_w = 0.5\,\sigma_u; \tag{2.8}$$

$$\text{2nd theory:} \quad \sigma_w = 1.6H_v + 0.1H_v; \tag{2.9}$$

$$\text{3rd theory:} \quad \sigma_w = (\sqrt{area}) \tag{2.10}$$

Predicting fatigue life is a critical aspect of the design cycle because virtually every product manufactured will wear out or break down. The critical issues are whether the product/component/assembly will reach its expected life, and if damaged, whether the product/component/assembly will remain safely in service until the damage can be discovered and repaired. And as with most simulation analysis, the earlier fatigue analysis is deployed in the product development process, the more benefits will be realized, including safety and economic.

For example, fatigue analysis early in the design phase can locate areas that are likely to succumb to fatigue quickly, minimizing expensive and unnecessary prototypes and tests.

Access to fatigue information early in the design phase results in shorter time-to-market, improved product reliability, and customer confidence, as well as the elimination of costly recalls and premature product failures.

CHAPTER 3

MATERIALS AND EXPERIMENTAL METHODS

3.1 Introduction

This chapter describes the materials studied in this research and also the experimental methods used. The experimental methods were chosen for their suitability to investigate the link between microstructural features and mechanical and fatigue properties of the FGMs obtained by different casting techniques. Along with the tensile and fatigue tests of castings obtained by gravity casting (GC) and centrifugal casting (CC) another tests were done for the specimens obtained by vibrating gravity casting (VGC). To obtain these specimens a new device was design and manufactured to provide the vibration needed for casting to simulate the level of inherent vibrations from the centrifugal casting machine. Flat and round specimens extracted from ingots obtained be gravity, centrifugal and vibrating gravity casting techniques where used on tensile testing and fatigue testing respectively.

3.2 Materials

Three commercial aluminium silicon alloys have been investigated in this project. The materials were supplied by a portuguesse company named Rito Company Ltd, and are being considered for use in the pistons of automotive engines.

The compositions of the alloys used in this research may be found in table 3.1; the composition levels were obtained using transmission electron microscopy (TEM). The mainly difference between the alloys is the Si content: alloy A – AlSi7 which is an hypoeutectic aluminium silicon alloy, alloy B – AlSi12 is an eutectic aluminium silicon alloy and alloy C – AlSi18 which is an hypereutectic aluminium silicon alloy.

Other elements were present in amounts smaller than 0.01 wt.% in all three alloys studied.

Table 3.1- Compositions of the three aluminium silicon alloys studied**. (**alloy A – AlSi7, alloy B – AlSi12, alloy C – AlSi18**)**

Alloy	**Si (wt.%)**	**Mg (wt.%)**	**Cu (wt.%)**	**Ni (wt.%)**	**Fe (wt.%)**	**Mn (wt.%)**	**Ti (wt.%)**	Sb **(wt.%)**	Al **(wt.%)**
A - AlSi7	6.71 - 6.89	0.55-0.68	<0.07	<0.005	<0.15	<0.015	<0.12	<0,14	balance
B - AlSi12	11.8 - 12.3	1.32-1.37	<0.43	1.24-1.27	0.26-0.28	<0.15	<0.05	<0,05	balance
C - AlSi18	17.8 - 19.8	1.13-1.26	<0.49	1.34-1.4	0.85-0.95	<0.15	<0.04	<0,11	balance

The materials were melted at different temperature as follow: alloy A at 730 ^{o}C, alloy B at 630 ^{o}C and alloy C at 800 ^{o}C. After the alloys were completed melted were kept under vacuum for 3 minutes then poured into a permanent mould which was preheated at 130 ^{o}C. A high frequency induction furnace (Titancast 700 mP Vac, from Linn High Term, Germany) (Figure 3.1), equipped with a vacuum chamber, was used for melting.

Figure 3.1 - High frequency induction furnace: Titancast 700 mP Vac, from Linn High Term, Germany (Foundry Laboratory – Minho University)

A charge of approx. 240 g of material was used in each melting. The material melting was done inside of the vacuum chamber (Figure 3.5 a,b) . After melting in the induction furnace the material was kept 3 minutes under vacuum and then poured into the mould in three different ways of casting: a – gravity casting (see Figure 3.2 a), b – centrifugal casting (see Figure 3.2 b) and c – vibrating gravity casting (see Figure 3.3). The gravity vibrating casting was added in the research to isolate one of the inherent effects from the centrifugal casting trying to determine the influence of vibration over the properties.

All casting ingots before to be machined to obtain the specimens (see Figure 3.11) were heat treated as follows: AlSi7 – 8h at 540ºC, quenched in water and tempered at 4h at 160ºC; AlSi18 – tempered at 8h at 200ºC.

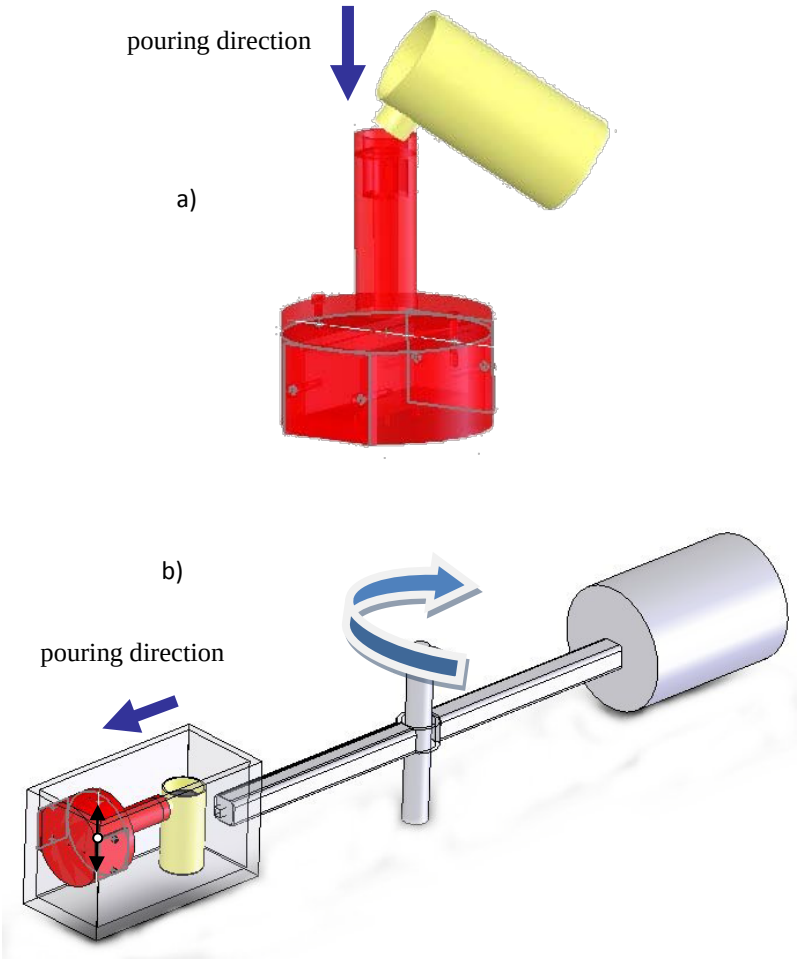

Figure 3.2 - Illustration of casting methods: a) GC – gravity casting, b) CC – centrifugal casting

To isolate the inherent vibration from the centrifugal casting system and to determine the influence of the vibration, the mould was attached on a system that provides the mechanical vibration due to the eccentric of the shafts (Figure 3.3) during the molten metal pouring. First step was to determine what the level of vibration on centrifugal casting machine is during the centrifugal casting. The level of vibration was measured with an accelerometer and was about 8Hz. The mechanical vibration was linearly applied with 0.5 mm amplitude for all castings and different frequencies, namely 0, 8 and 24 Hz. The analysis of the influence of vibration over the melt during solidification was done only for alloy C (Al18Si).

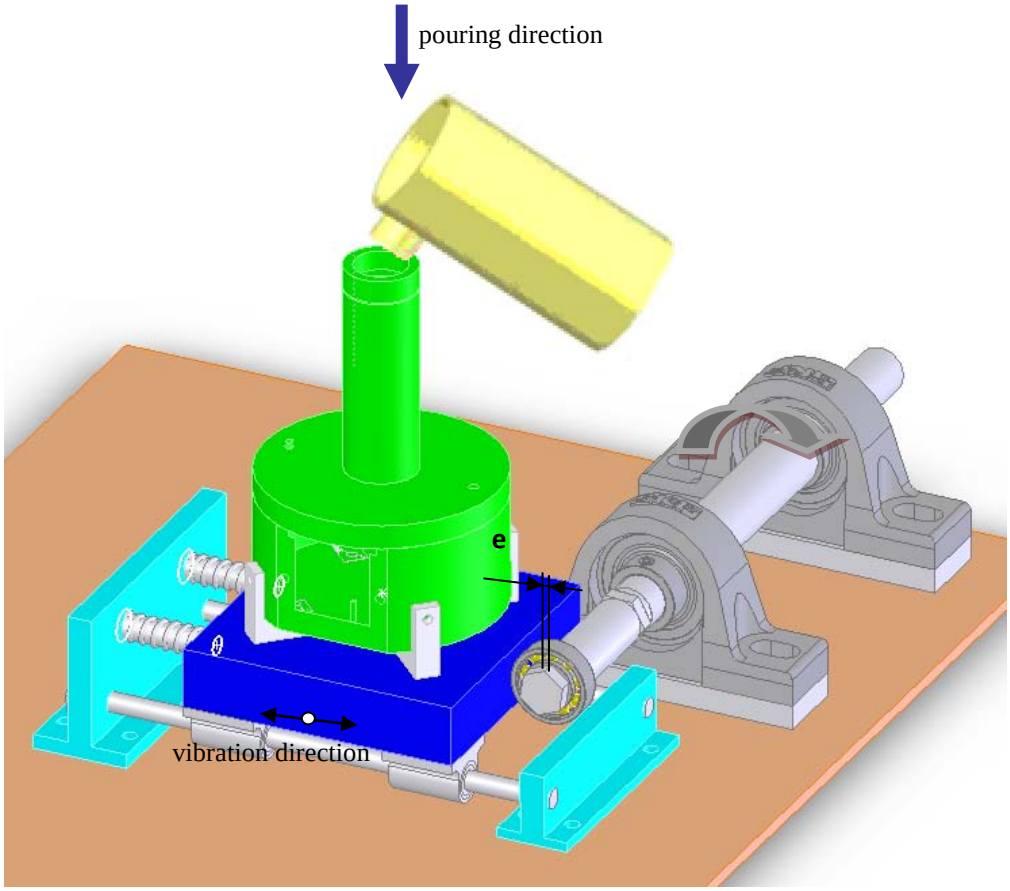

Figure 3.3 - VGC – vibrating gravity casting

As it is known the mechanical and fatigue properties are influenced by microstructure morphology which in turn is strongly influenced by casting process, more specifically by solidification conditions.

Thermocouples were inserted into the chill and through the wall of the refractory fibre tube so that the hot junctions of the thermocouples 1-5 were positioned on the central axis of the chill-mould arrangement and 6 and 7 on front side and back side of the mould respectively (Figure 3.7). Mineral insulated thermocouples type K with grounded hot junctions were inserted into holes drilled into the chill; the thermocouples inserted through the refractory mould wall were constructed of 0.2 mm diameter type K thermocouple wire with exposed hot junctions about 0.5 mm in diameter. The thermocouples were placed 2 mm from the inside mould wall (Figure 3.4), their temperatures recorded at 0.125 second intervals by a computer-controlled data logger. In

both cases, the thermocouples were selected to have a time response considerably less than the interval between temperature readings and to have a minimal effect on the temperature field of the casting and the chill.

The cooling curves were obtained by recording the temperature change as a function of time (Figure 3.5 and Figure 3.6) during solidification using a data acquisition system.

From these thermo-cycles graphs were extracted data regarding starting and ending of the solidification (Figure 3.6) and cooling rates on the points analyzed.

The temperature data acquisition system was attached during the casting on all three casting techniques analyzed in this work: centrifugal casting (Figure 3.8 a, b), vibrating gravity casting (Figure 3.9) and gravity casting (Figure 3.10).

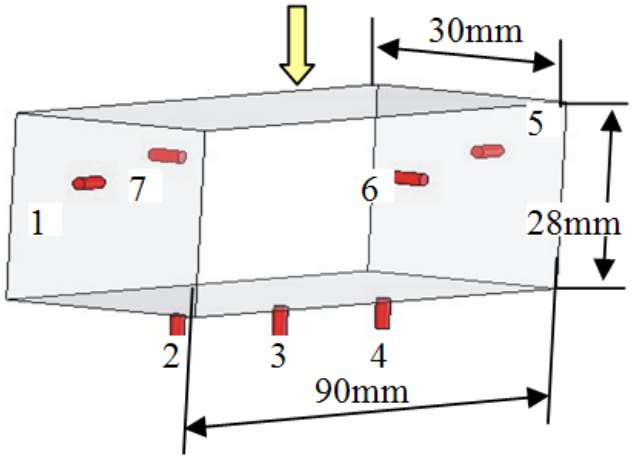

Figure 3.4 - Positioning of the thermo-couples on the ingot

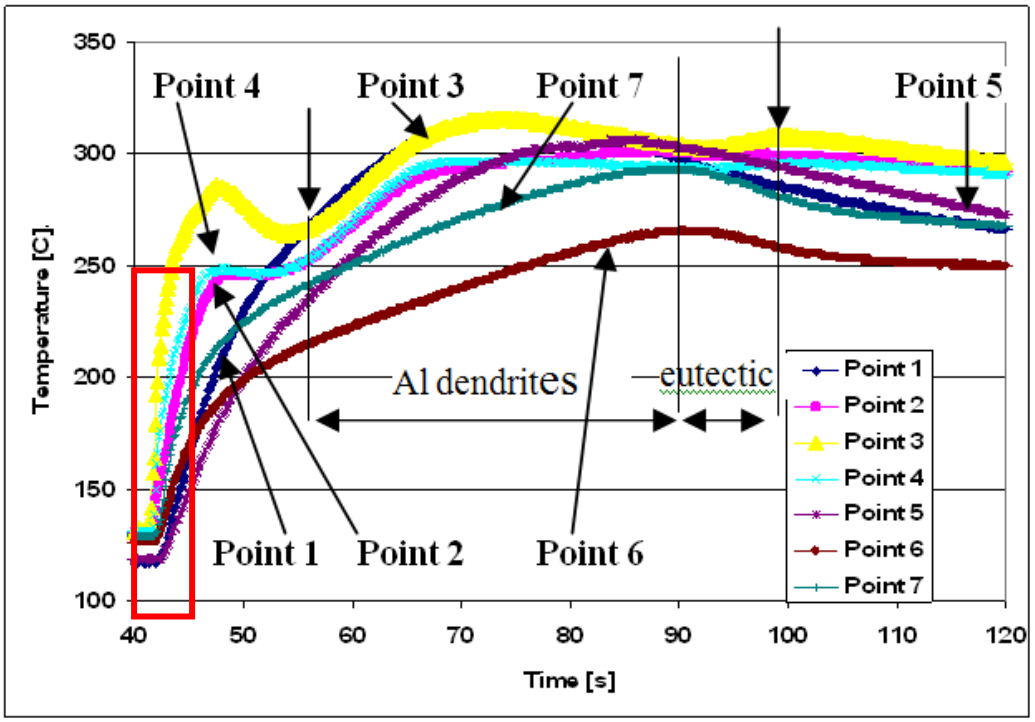

Figure 3.5 - Thermo-cycles on different positions

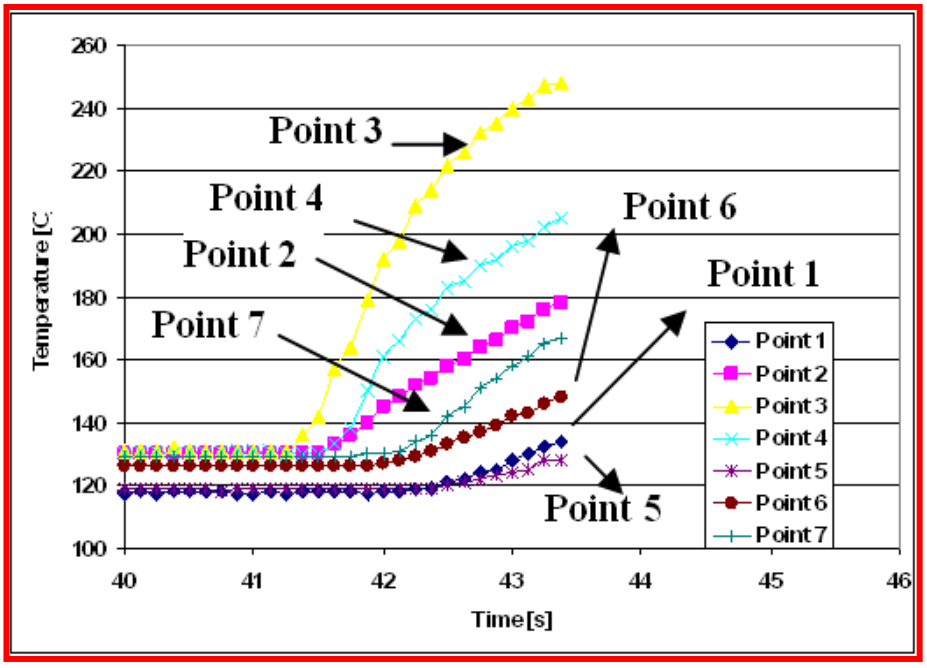

Figure 3.6 - Details of thermo-cycles on different positions of the mould

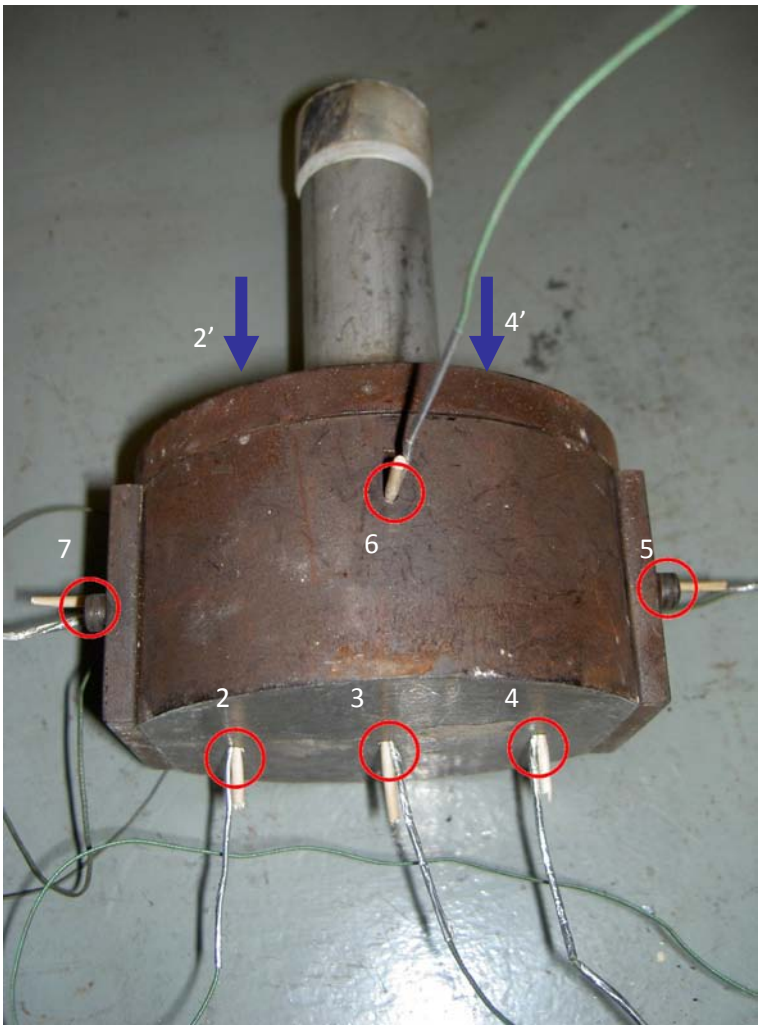

Figure 3.7 - Points of insertion of the K thermocouples in the mould

For much precise solidification characterization, the thermocouples 2 and 4 were moved on top position 2’ and 4’ in same plane with 1, 3 and 5 during few casting as it can be seen in figure 3.7.

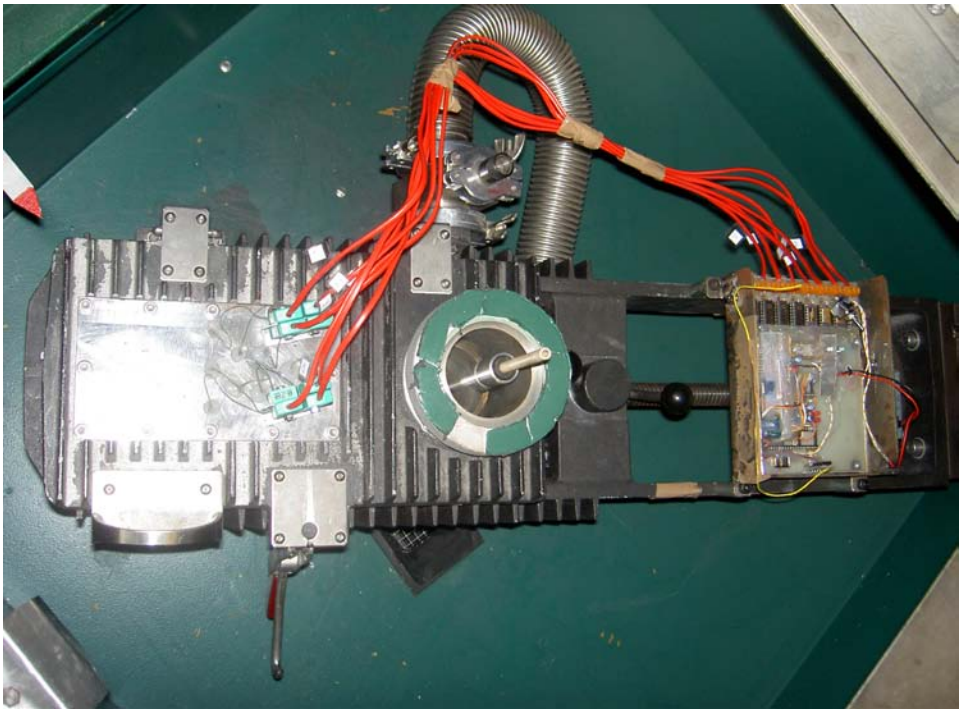

Figure 3.8 a - Temperature acquisition during centrifugal casting – vacuum chamber closed

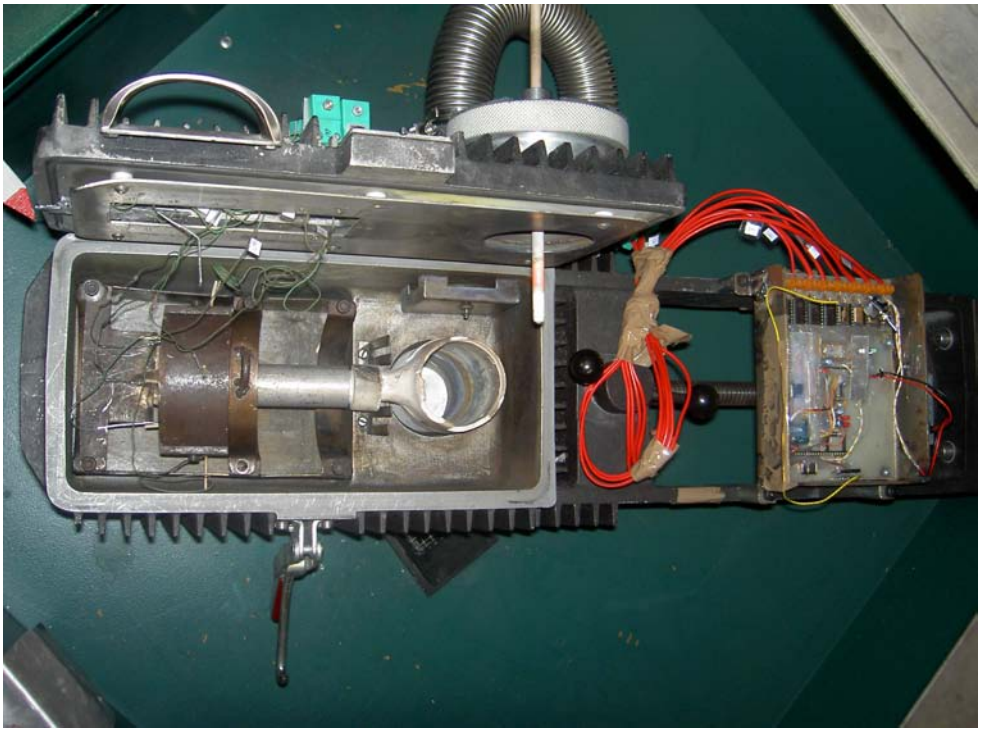

Figure 3.8 b - Temperature acquisition during centrifugal casting – vacuum chamber opened

Figure 3.9 - Temperature acquisition during vibrating gravity casting

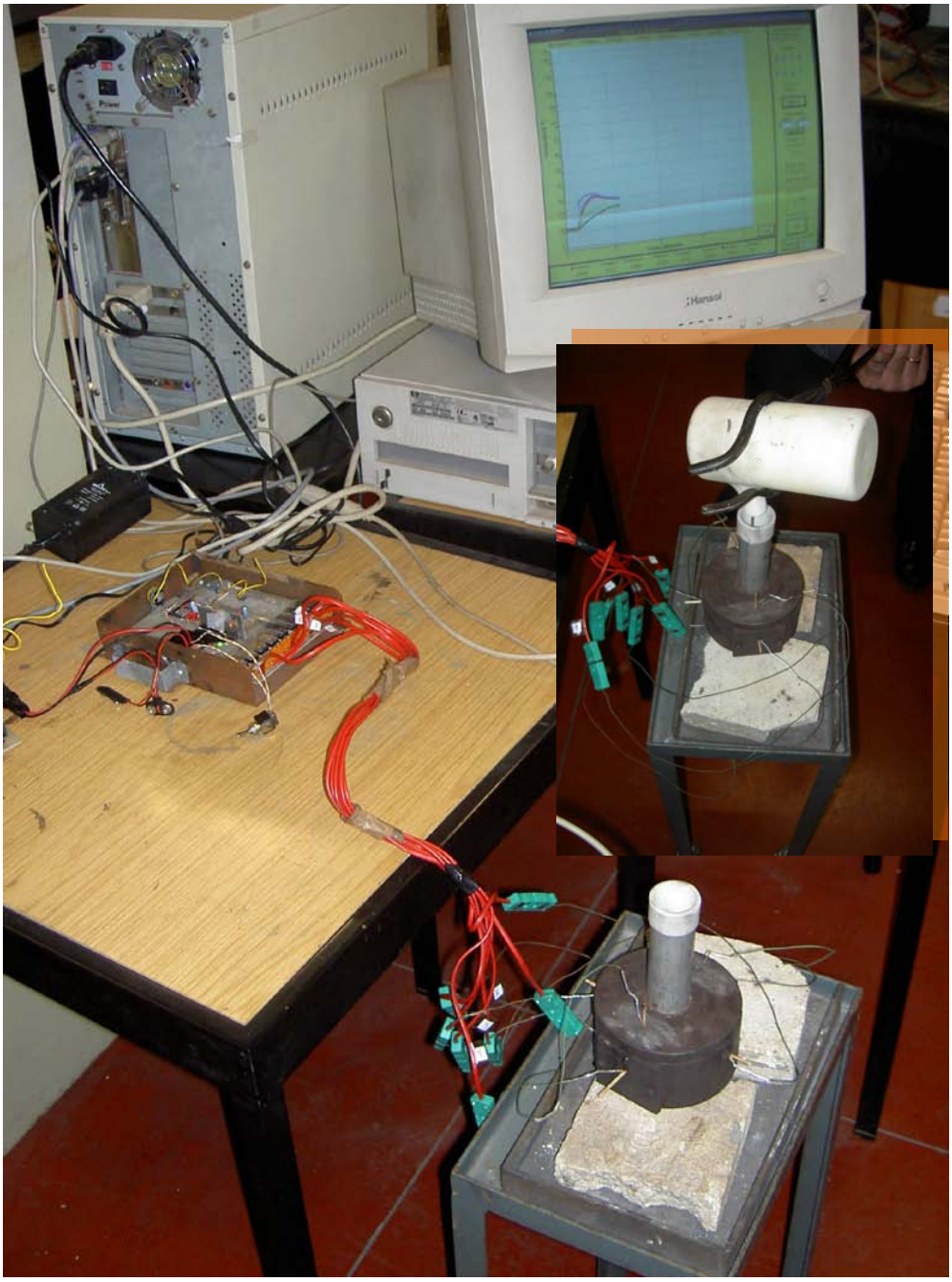

Figure 3.10 - Temperature acquisition system during gravity casting

3.3 Tensile tests

All tensile test samples were extracted from the casting ingots perpendicular to the feed direction (Figure 3.11). Three flat specimens from each casting ingot was extracted: one from exterior – position 1, one from middle – position 2 and one from interior – position 3. An electrical saw was used to cut the slices from casting ingots following the scheme presented in figure 3.13. The slices were than rectified to obtain the final parallel surfaces (Figure 3.12). The final dimension of the obtained tensile specimens from ingots is in figure 3.14.

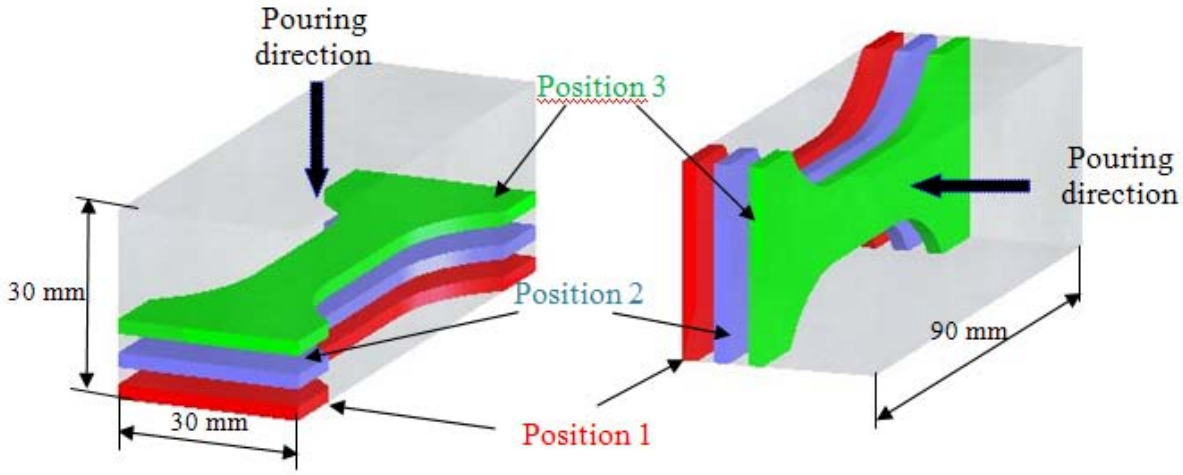

Figure 3.11 - Position from where tensile test specimens were taken: a) gravity ingots, b) centrifugal ingots

Figure 3.12 - Picture of flat tensile specimen

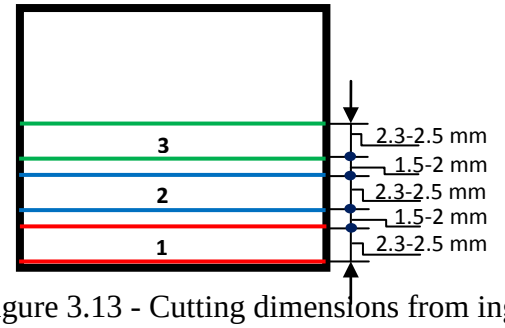

Figure 3.13 - Cutting dimensions from ingots

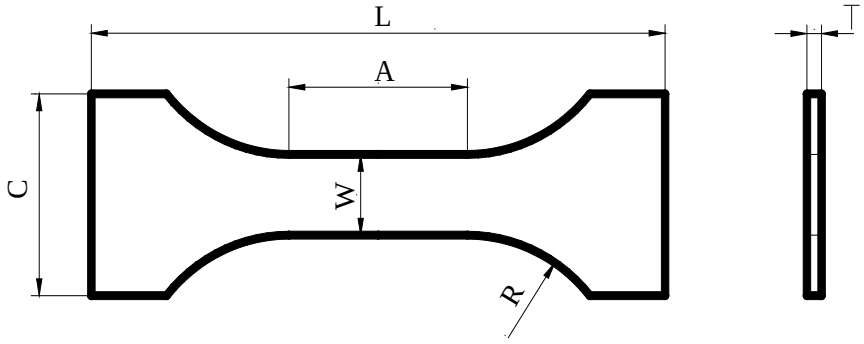

Figure 3.14 - Flat specimen dimensions

L— Overall length	90 mm
W— Width	12 mm
C— Width of grip section	30 mm
A— Length of reduced section	28 mm
R— Radius of fillet	25 mm
T— Thickness	2.3-2.5 mm

All tensile tests were carried out at room temperature (RT) using a loading rate of 1 mm/min. The load information was obtained from the calibrated load cells on the tensile test machines and the extension information was obtained by attaching an extensometer to the sample (Figure 3.17).

The equipment used for tensile tests was a Dartec servo-hydraulic tensile testing machine (Figure 3.15) from Material Testing Laboratory - Minho University, equipped with a data acquisition system (Figure 3.16) and an easy to use system of grips (Figure 3.17).

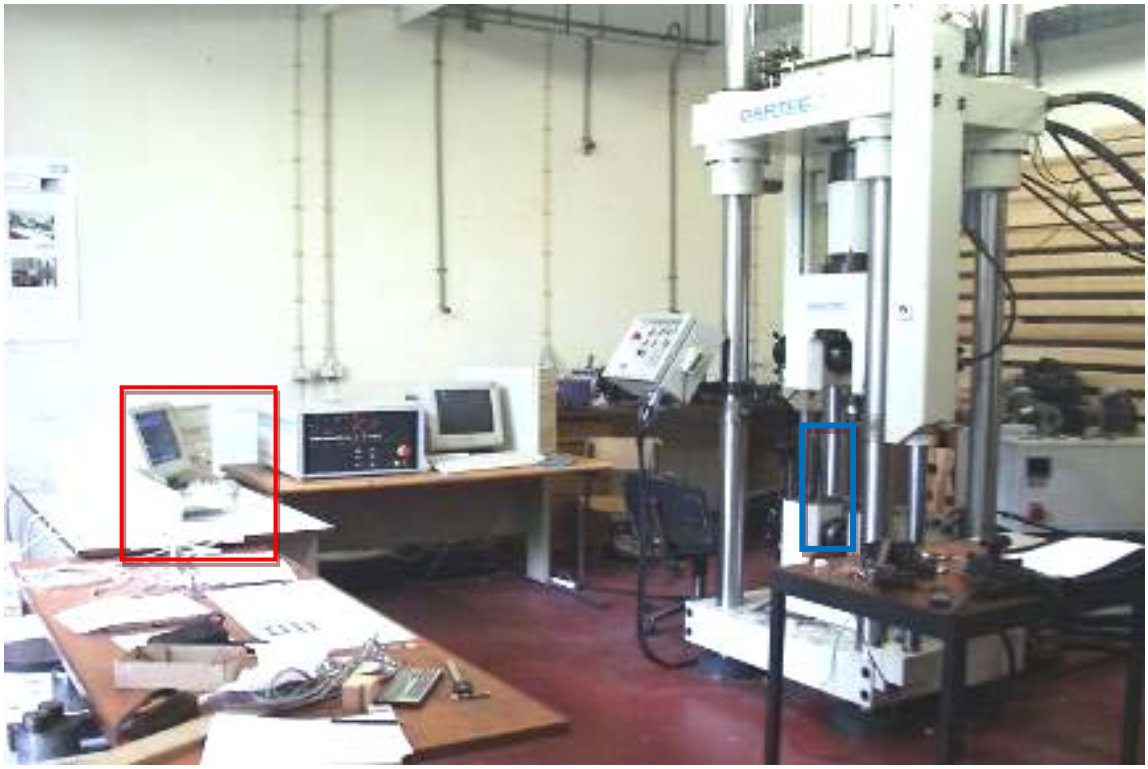

Figure 3.15 - Tensile testing servo-hydraulic equipment: Dartec (Material Testing Laboratory - Minho University)

Figure 3.16 - Data acquisition system: Dartec

Figure 3.17 - System of grips on Dartec machine

The data's from the acquisition system were imported in Microsoft Excel and build graphs like the one represented in figure 3.18 from which were extracted the following: 1.Ultimate Strength; 2. Yield strength, 3. Proportional Limit Stress. , 4. Rupture, 5. Offset Strain (typically 0.2%).

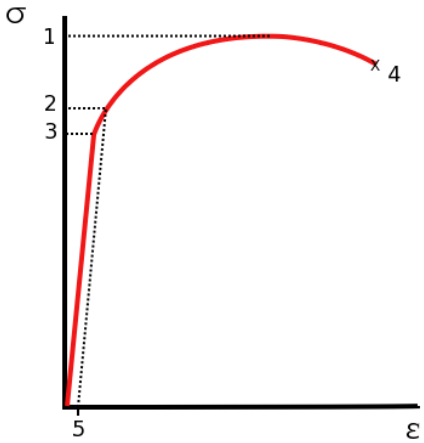

Figure 3.18 - Stress vs. Strain curve typical of aluminium

1.Ultimate Strength; 2. Yield strength, 3. Proportional Limit Stress, 4. Rupture,

5. Offset Strain (typically 0.2%).

Ten specimens of each position for all casting techniques studied (GC, VGC and CC) were produced and tested on Dartec machine. A total of 90 specimens were tensile tested.

3.4 Fatigue Tests

All rotating bending fatigue test samples were extracted from the casting ingots perpendicular to the feed direction (Figure 3.11). Two round specimens from each casting ingot was extracted. An electrical saw was used to cut the casting ingots. The parallelepipeds thus obtained were machined on a CNC tool to obtain the final rotating bending fatigue specimens (Figure 3.20). The final dimensions of the obtained tensile specimens from ingots are in figure 3.21.

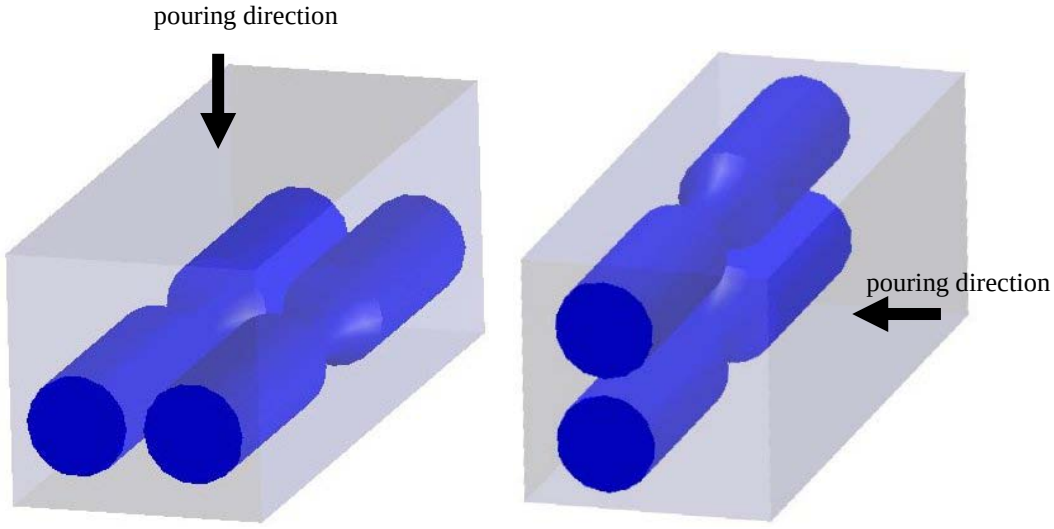

Figure 3.19 - Position from where fatigue test specimens were taken: a) gravity ingots (GC and VGC), b) centrifugal ingots (CC)

Figure 3.20 - Pictures of rotating bending fatigue specimen

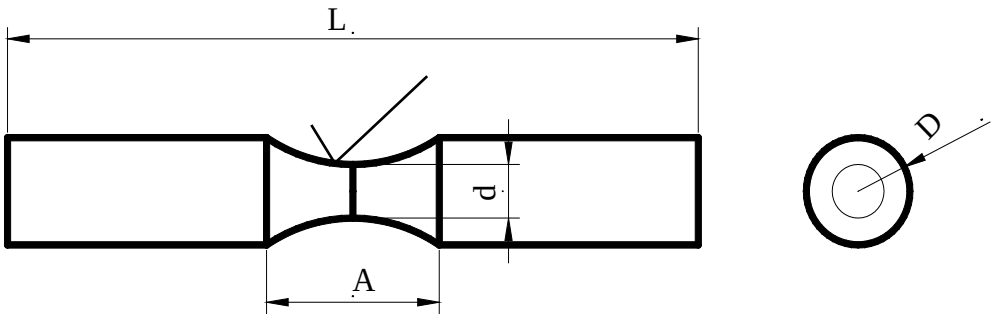

Figure 3.21 - Rotating bending fatigue specimen dimensions

L— Over-all length	80 mm
A— Length of reduced section	20 mm
d— Diameter of minimum reduced section	6 mm
D— Diameter of specimen	12 mm

The fatigue tests were performed on rotating beam fatigue machine from Material Testing Laboratory – Minho University (Figure 3.22).

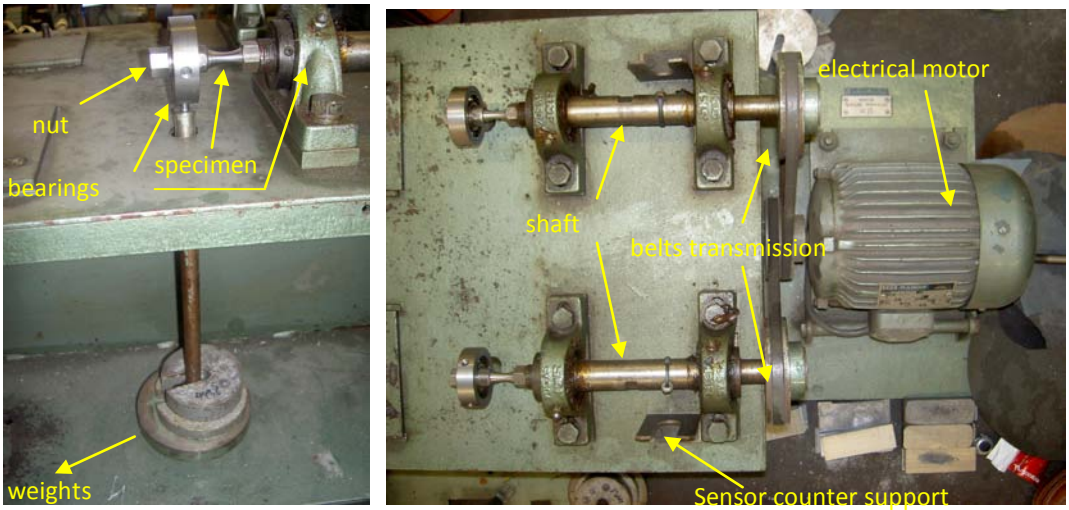

Figure 3.22 - Rotating bending fatigue machine (Material Testing Laboratory – Minho University)

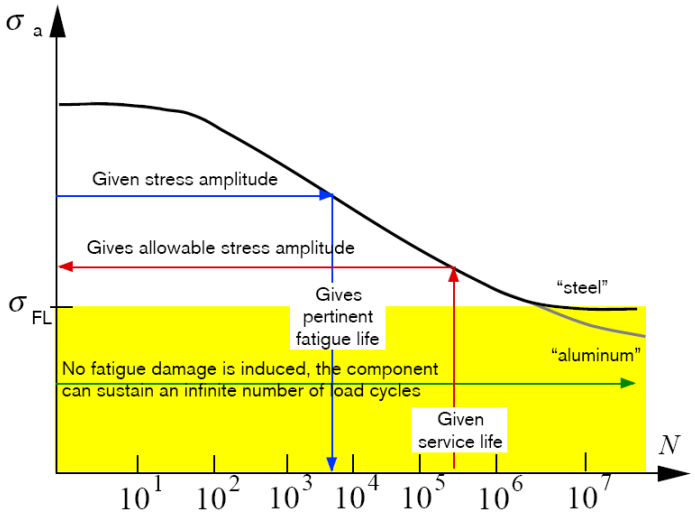

Figure 3.23 - Typical Wöhler curve

Twenty test samples of each casting techniques (GC, VGC and CC) were manufactured according to figure 3.21. The surface roughness (Ra value) and the smallest diameter were measured on all samples.

A Wöhler curve similar to the one represented in figure 3.23 was successfully constructed for each tested materials and are presented in the next chapter.

The usual procedure was done and was tested the first specimen at a high peak stress where failure was expected in a fairly short number of cycles. Then the test stress was decreased for each succeeding specimen until one or two specimens do not fail in the specified numbers of cycles, which is usually for these materials terminated after about 10^8 or $5x10^8$ cycles which is considered fatigue threshold (Figure 3.23).

3.5 Metallographic samples

Preparing the metallographic samples involves removing a small sample from the work-piece surface that are significant to be analysed (Figure 3.24). Small samples can be difficult to hold safely during grinding and polishing operations, and their shape may not be suitable for observation on a flat surface. They were therefore mounted inside a polymer resin block using two liquid components which become solid shortly after mixing. Cold mounting requires very simple equipment consisting of a cylindrical ring which serves as a mould and a flat piece which serves as the base of the mould. The samples are placed on the base within the cylinder and the mixture poured in and allowed to set cold mounting about 40 minutes. The obtained polymer blocks are presented in figure 3.24 a) for tensile specimen and figure 3.24 b) for rotating bending specimens.

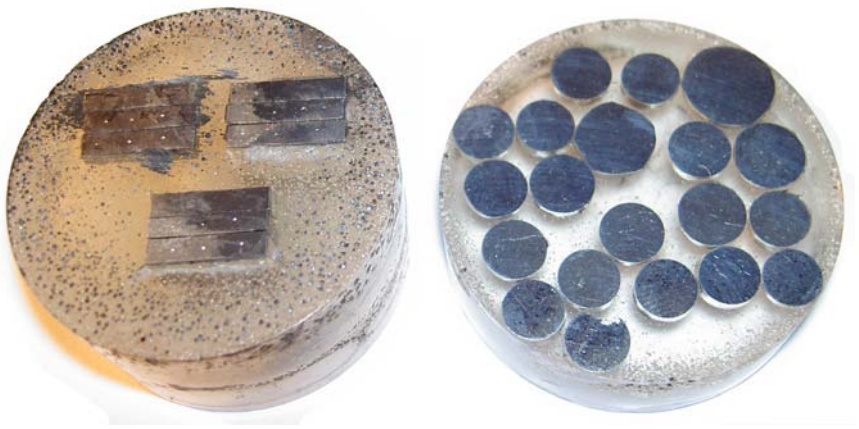

a) b)

Figure 3.24 - Samples mounted inside a polymer resin block: a) flat specimens b) round specimens

Figure 3.25 - Double Desk Polishing Machine DC Motor (Metallographic Laboratory – Minho University)

Double Desk Polishing Machine DC Motor from Metallographic Laboratory – Minho University was used for polishing the samples following the polishing route presented in table 3.2.

Table 3.2 - Polishing route

Abrasive/surface	**Lubricant**	**Speed [Rpm]**	**Force/ sample**	**Time**
180 grit SiC paper 360 grit SiC paper 600 grit SiC paper 800 grit SiC paper 1200 grit SiC paper	Water Water Water Water Water	300 300 300 200 200	3kg 3kg 3kg 3kg 3 kg	Until plane 4minute 3minute 3minute 3 minute
6 μm diamond on ATLANTIS polishing pad	Diamond Suspensions (water-based)	150	2 kg	4 minutes
1 μm diamond on NAPPAD polishing pad	Diamond Suspensions (water-based)	150	2 kg	8 minutes

3.6 Micro hardness tests

Micro hardness measurement was conducted with a diamond indenter using loads from as little as 5g. This produce very small indentations (between 0.01 and 0.1 mm across), which allowed individual grains/phases in an alloy and near surface regions in cross-sections to be measured.

Micro hardness measurements are conducted on Mitutoyo HM-122 (Figure 3.26) providing information on the changes in subsurface mechanical properties of the samples obtained by different casting processing.

Hardness measurements were done to assess the changes occurring in the microstructure (aluminum matrix and eutectic silicon) due to modification and heat treatment. The testing was performed using a Vickers hardness tester with a diamond indenter with an angle of 136^{o} and a load of 20 kg. The hardness tester was checked for calibration by taking five hardness readings on the test block. AlI values feIl within the range imprinted on the standard test block.

All samples pulled to determine the tensile properties were subjected to hardness tests, i.c four samples for each condition. Five hardness readings were taken from each sample and averaged, and for each condition the average of the four samples was calculated. Hardness indentations were made across the sample diameter and were well separated to ensure that there was no overlap of the deformation.

Figure 3.26 - Mitutoyo HM-122
(Metallographic Laboratory – Minho University)

3.7 Image analysis

Photomicrographs of the microstructure for all specimens of alloys studied A, B and C, obtained by centrifugal, gravity and vibrating gravity casting were obtained using Canon PowerShot A580 photo camera attached on an optical microscope belong to the Physical Laboratory – Minho University. Four to eight specimens were prepared for each material studied from each position and each casting techniques studied (GC, CC and VGC).

Quantitative image analysis was used to characterise the microstructures of the alloys studied. The main text used to inform this analysis is that of Underwood (1970) which is a useful guide to the background theory and practical use of quantitative stereology. The quantitative stereology has established relationships for the quantity of elements in three-dimensional space from observations on two-dimensional planes.

The point fraction analyses were performed on two-dimensional micrographs.

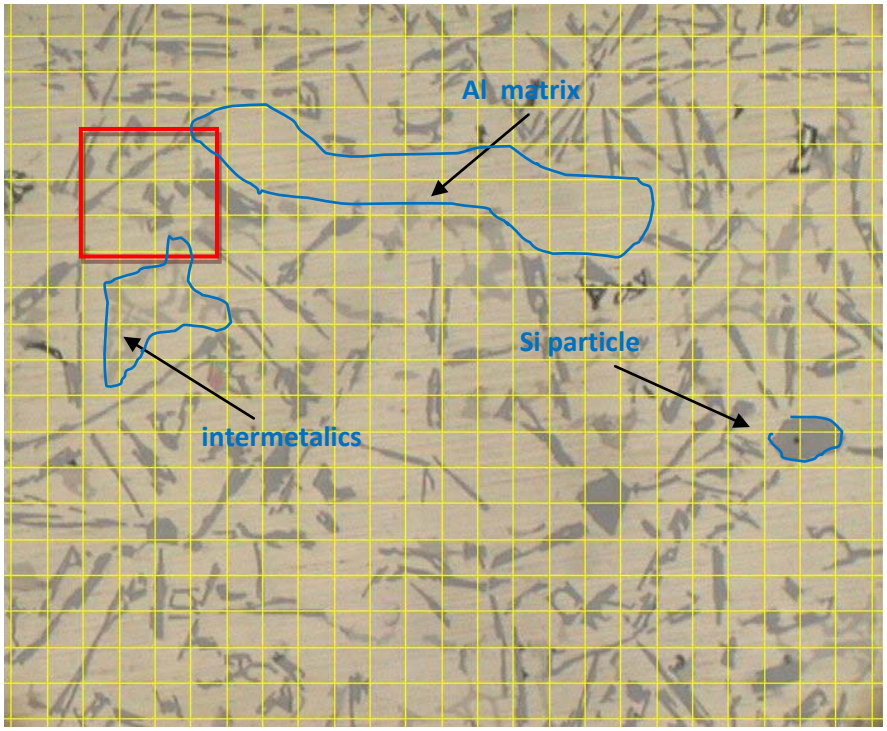

Figure 3.27 - Phases quantification using PaintShopPro 5 software

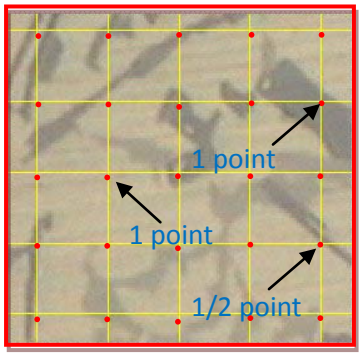

Figure 3.28 - Details of counting points

Point fraction analysis uses a grid of points (Figure 3.27) placed on a random but representative image of microstructure using the PaintShopPro 5 software. If a point falls on a phase of interest it counts as a 1 point and if it hits near the phase of interest count ½ point (Figure 3.28). Each point in the grid is assessed and the score added up. For quantification of phases done in this study was used a grid with 480 point (Figure 3.27). This score is divided by the number of points used in the grid (T_P) and gives a value for the point fraction (P_F) of the phase of interest. This process is repeated several times (in this study at least 10 times/picture) on other random samples of the microstructure and the average value of P_{avg} calculated.

Although this method is simple it is very useful because it can be used to estimate the volume fraction (*Vf*) of the phase of interest in the alloy. If a test point is placed at random in a test volume (V_T) containing a volume of A (V_A) the probability of the point hitting the A phase ($P(A)$) is:

$$P(A) = V_A / VT \tag{3.1}$$

For many randomly placed points (P_T) the expected number of points lying within the A phase (P_A) will be:

$$P_A = T_P * P(A) = T_P * (V_A / V_T) \tag{3.2}$$

and so can be seen that:

$$P_A / T_P = V_A / V_T \tag{3.3}$$

hence:

$$P_{avg} = Vf \tag{3.4}$$

The micrographs used in this study were taken at a magnification of 500x for quantification of phases, silicon particles and pores maximum dimensions, silicon eutectic thickness and 200x for measuring the SDAS secondary dendrites arm spacing's. Lower magnification images did not provide sufficient resolution to differentiate between some of the smaller microstructural features, particularly the Si particles in the aluminium silicon alloy. All the results of point fraction analysis presented in this study are the average of at least 10 measurements.

ImageJ software was used for measuring dimensions of the microstructure such as dimension and areas of different microstructure feature (Figure 3.29).

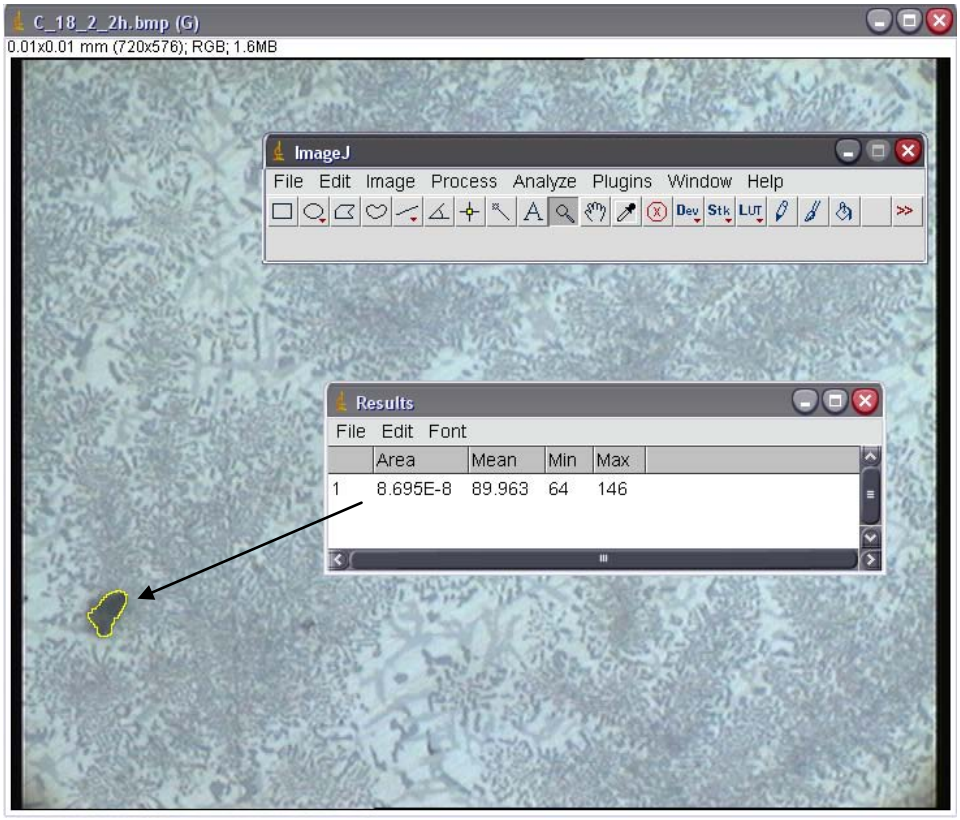

Figure 3.29 - ImageJ software used for measuring dimensions of the microstructure

3.8 Simulation of the casting processes

Simulation of the casting processes is widely used in modern foundry industry, as a tool in product design and process development. It helps in decision making, where industrial expertise is not enough or critical parameters of the process are missing, keeping the costs of development low to be competitive.

Different heat flow rates across the cast metal and mould surface regions affect the evolution of solidification and the micro-structural properties of the casting. Thus, the second issue is validation of the simulation results by comparing them with experimentally measured properties of the casting mainly with the results obtained through the temperature acquisition. This is the method used in the present work. In all cases both experiments and simulations were conducted and were determined the start and end of solidification, solidification interval, cooling rate and the characteristics of the melt dynamics during casting and solidification. The simulation of the casting processes was done in the Foundry Laboratory from Minho University using NovaSolid Software.

CHAPTER 4

RESULTS

4.1. Introduction

The mechanical and fatigue properties of cast aluminium alloys are very sensitive to composition, casting process, which encounters mould filling and solidification behaviour, and post-processing such as thermal treatment. The coarseness of the microstructure and the amount of the volume fractions of the phases that form and precipitate during solidification, are fundamental to the material behaviour. Mechanical properties are linked to the microstructure in the material which again is determined by chemical composition (trace elements, alloying elements), heat treatment parameters (time, temperature combinations) and casting conditions (solidification rate, temperature gradients, casting defect). With so many parameters influencing the microstructure and mechanical properties both individually and coupled, it is difficult to predict precisely the effect of a change in one or several parameters on the product properties.

As the majority of cast components have complex geometries, a variety of microstructures may arise within a single casting. Considering that mechanical properties are a function of the microstructure, they will tend to change as the microstructure changes, thus any study of the properties of cast aluminium must take into account all the factors which may influence the microstructure or as much of the factors that is possible to have the best results. The most significant microstructural features involved are second phase particles and grain structure; the second-phase particles of concern here are: (i) coarse, insoluble particles formed during casting, or coarse particles of normally soluble phases formed during casting or subsequent processing; (ii) smaller intermediate particles formed during homogenization; and (iii) aging precipitates.

4.2. Metallurgical Analysis

As it was stated on literature review chapter the tensile properties and fracture behaviour of cast aluminium alloys strongly depends on secondary dendrite arm spacing (SDAS), Mg content, and, in particular, the size and shape of eutectic silicon particle and Fe-rich intermetalics. Thus, mechanical properties of Al–Si cast alloys depend not only on chemical composition but, more important, on micro structural features such as morphologies of dendritic α-Al, eutectic Si particles and other intermetalics that are present in the microstructure.

The metallurgical analysis was done for all three alloys (alloy A - hypoeutectic aluminium silicon alloy with 7% of silicon, alloy B- eutectic aluminium silicon alloy with 12% of silicon and alloy C- hypereutectic aluminium silicon alloy with 18% of silicon) and the results of SDAS, eutectic silicon thickness and length are presented on figures 4.1 – 4.7.

Secondary dendrites arm spacing values for alloy A shows an decreasing tendency from position 3 to position 1 on both casting techniques; on position 3 the SDAS are bigger on centrifugal casting with about 20%. For alloy B it is noticed also a tendency of decreasing values of SDAS from position 3 to position 1 keeping a difference of about 8% between values of centrifugal and gravity casting in all three position.

Thickness and length of eutectic silicon particles of alloy A (Figures 4.3 and 4.4) present a decreasing slope tendency from position 3 to position 1 in both casting techniques studied, keeping an average difference of values of about 45% for thickness and 25% for length. In the case of alloy B a decreasing slope tendency from position 3 to position 1 of thickness and length of eutectic silicon particles in both casting techniques studied is obtained keeping an average difference of values of about 10% for thickness and 22% for length. Position 2 values make an exception registering almost the same values of thickness for both casting techniques. On alloy C was possible to measure only the thickness of eutectic silicon particle because of the coral like shapes (Figures 4.37-4.40). Around 13% lower thickness values of the eutectic silicon particles were obtained for centrifugal casting on all three positions of alloy C. The values of thickness on alloys C have the same tendency of decreasing form position 3 to position 1 for both casting processes.

In order to assess the main factors that contribute at the initiation of the fatigue crack, analysis of the equivalent area of the eutectic silicon particle and pores were done on the broken specimens from the rotating bending fatigue tests. The area of the irregular shapes of the silicon particle and pores was considered round and was calculated the diameter of round shape resulting the equivalent diameter. The results are presented on figures 4.8 and 4.9 showing that there is no significant difference on the pores dimension on all three alloys and casting processes; and significant decreasing values of silicon particle dimension of centrifugal casting on all three position, respectively: 20% on alloy A, 50% on alloy B and 250% on alloy C.

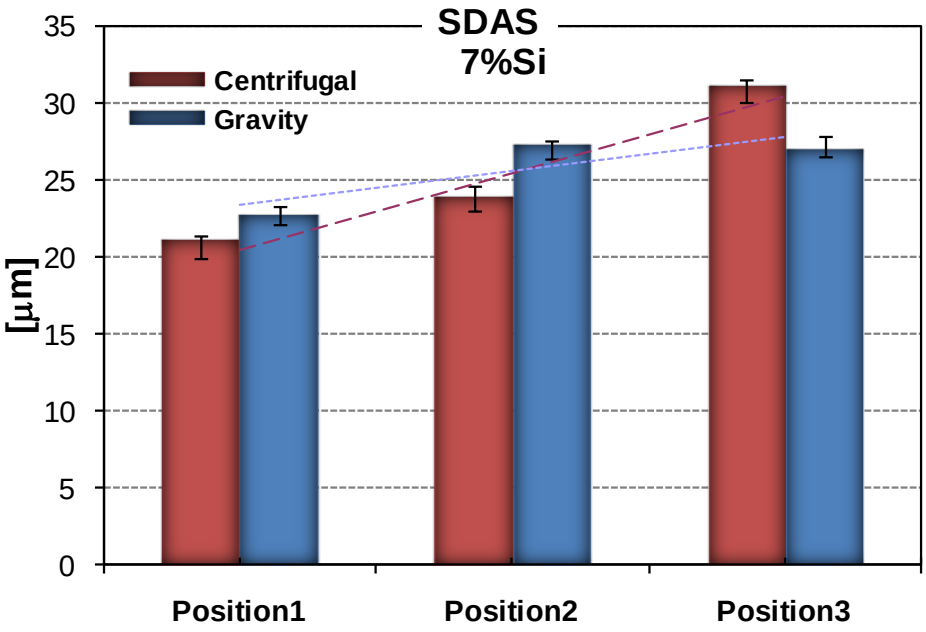

Figure 4.1 – Secondary dendrite arm spacing (SDAS) for centrifugal and gravity castings of alloy A in position 1, 2 and 3 of ingots.

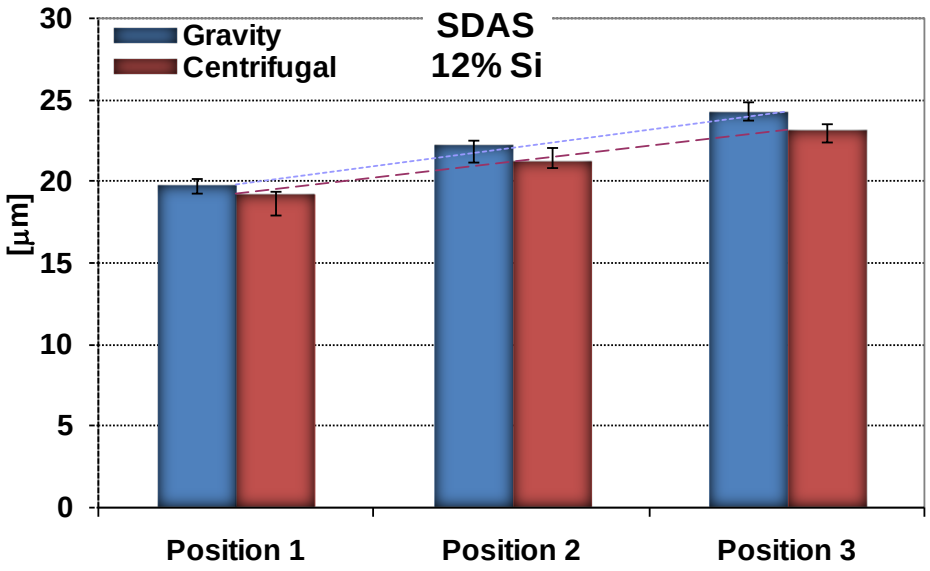

Figure 4.2 – Secondary dendrite arm spacing (SDAS) for centrifugal and gravity castings of alloy A in position 1, 2 and 3 of ingots

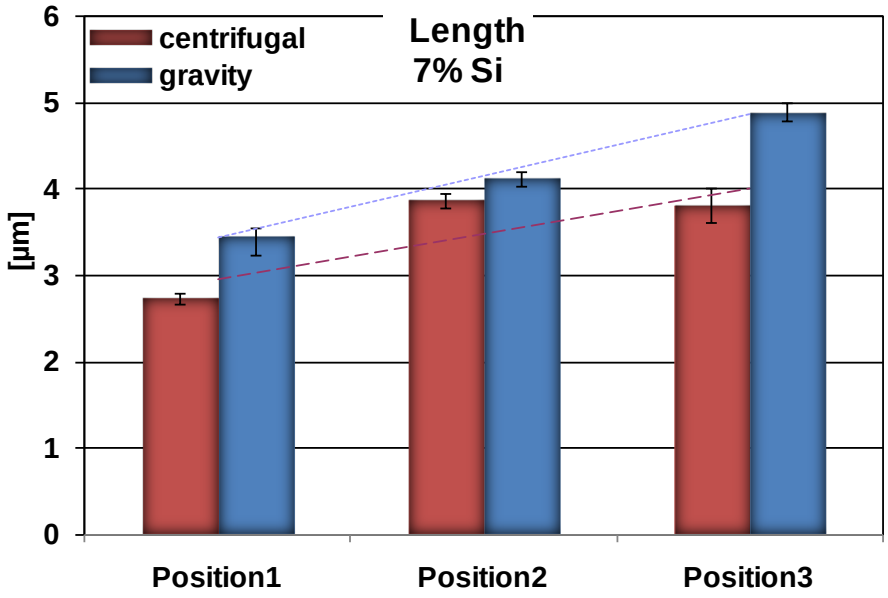

Figure 4.3 – Eutectic silicon length dimensions for centrifugal and gravity castings of alloy A in position 1, 2 and 3 of ingots

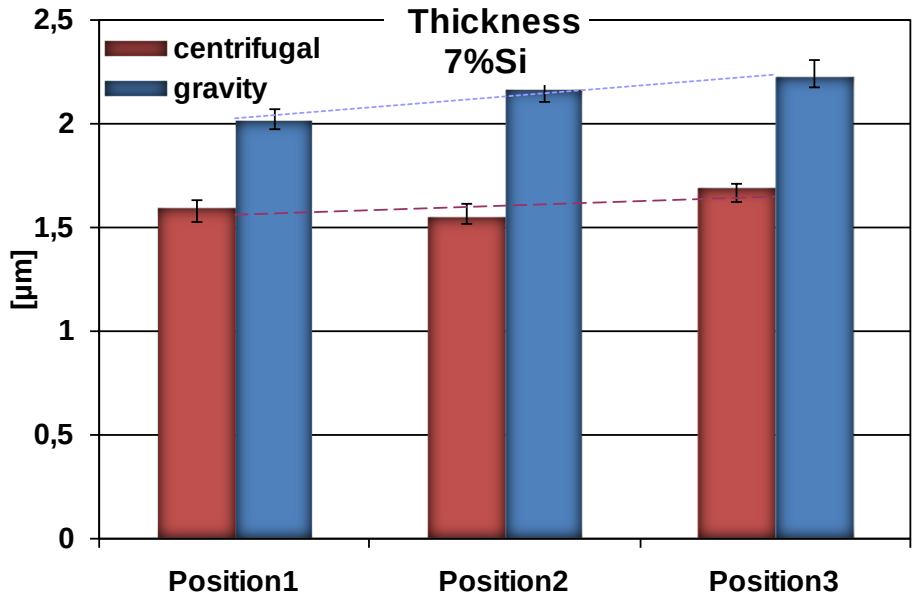

Figure 4.4 – Eutectic silicon thickness dimensions for centrifugal and gravity castings of alloy A in position 1, 2 and 3 of ingots

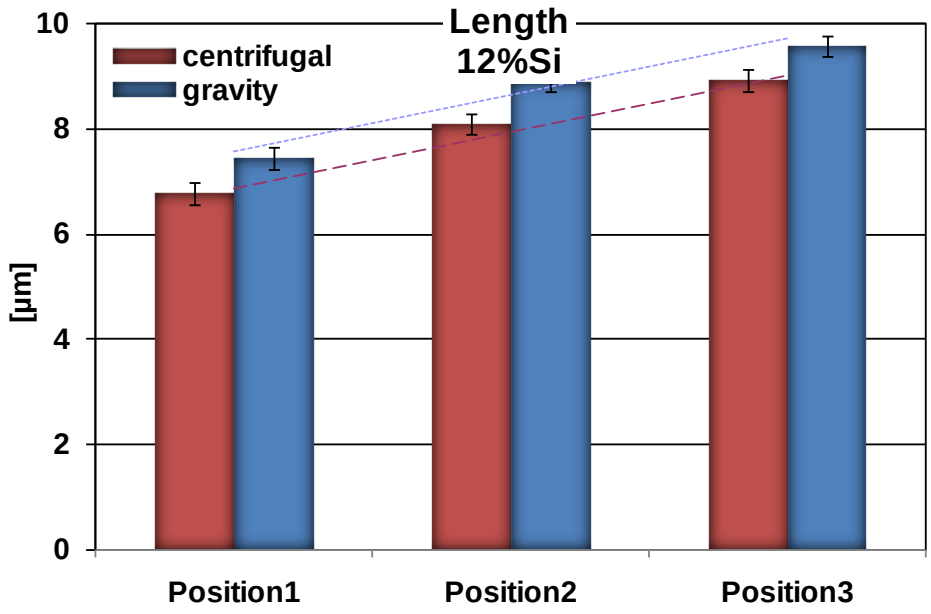

Figure 4.5 – Eutectic silicon length dimensions for centrifugal and gravity castings of alloy A in position 1, 2 and 3 of ingots

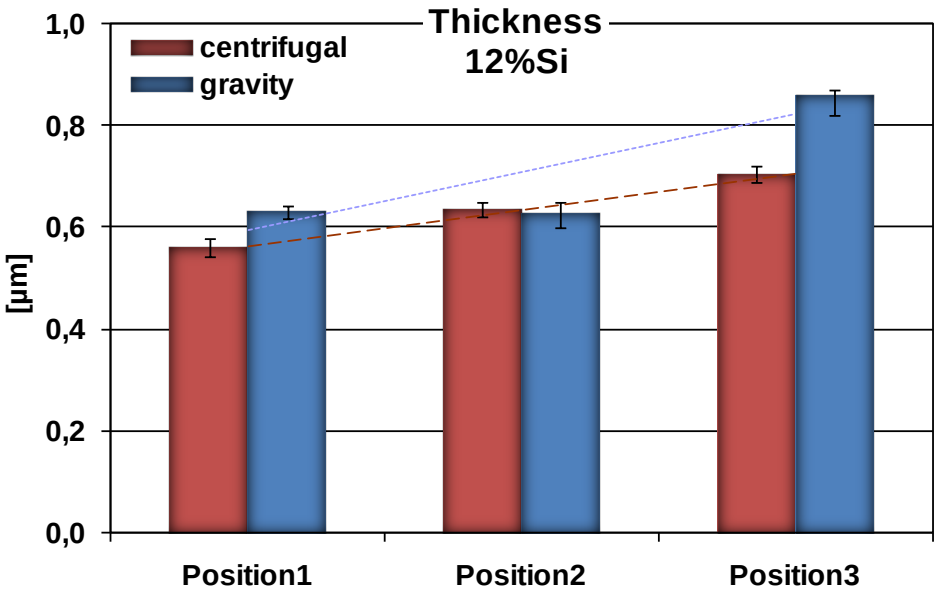

Figure 4.6 – Eutectic silicon thickness dimensions for centrifugal and gravity castings of alloy A in position 1, 2 and 3 of ingots

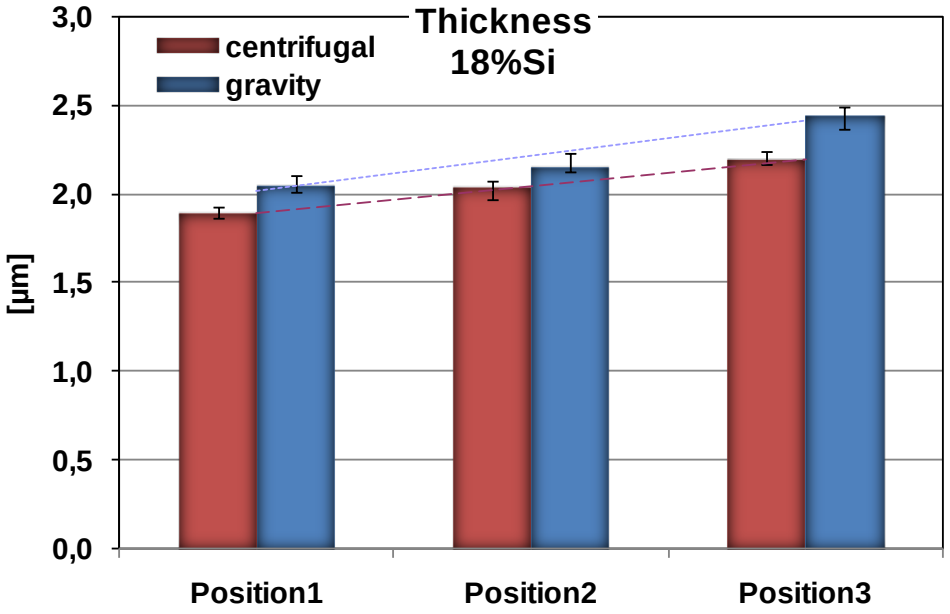

Figure 4.7 – Eutectic silicon thickness dimensions for centrifugal and gravity castings of alloy C in position 1, 2 and 3 of ingots

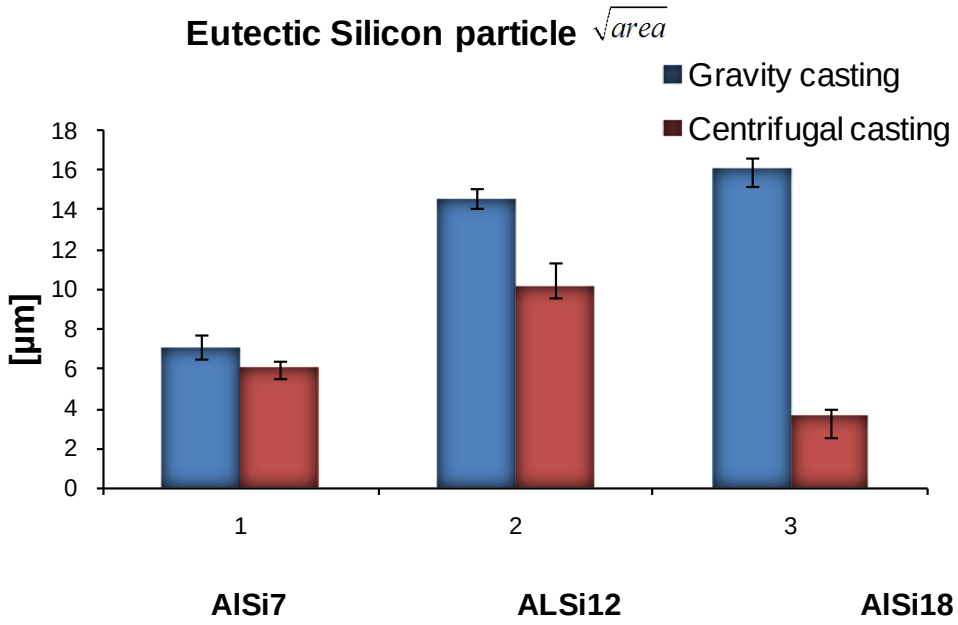

Figure 4.8 – Equivalent diameter for eutectic silicon particles for centrifugal and gravity castings of alloy A, B and C

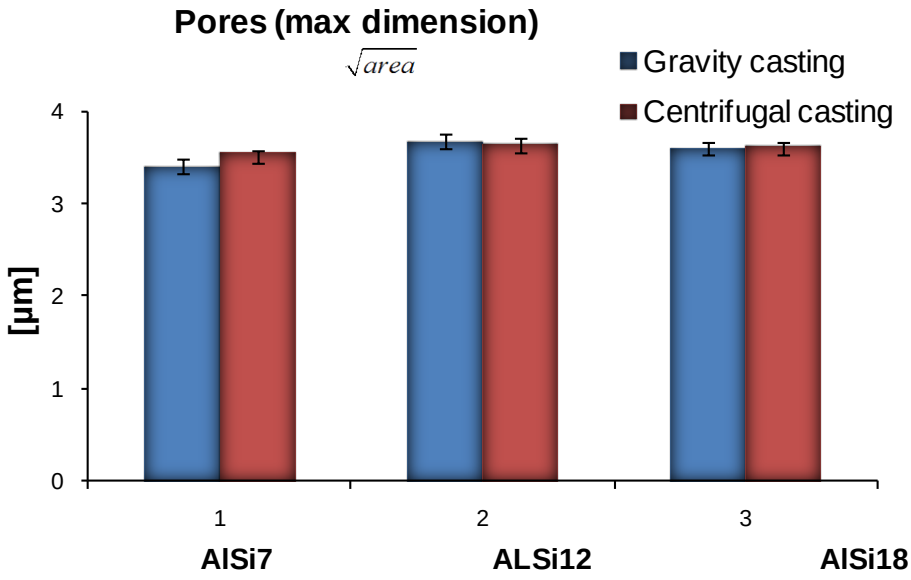

Figure 4.9 – Pores dimensions for centrifugal and gravity castings of alloys A, B and C

4.3. Mechanical properties results

Obtained results for the studied alloys, concerning mechanical properties, namely ultimate tensile strength, strain to failure, Young modulus and hardness, constituents' volume fraction and morphology, are presented in Tables 4.1 to 4.3 and Figures 4.10 to 4.40. In all graphs a linear global tendency among the positions 1, 2 and 3 (see Fig. 3.11) is presented.

The volume fractions of macro-pores presented in tables 4.1 to 4.3 is referring on pores with dimensions greater that 50 μm. The average dimensions of the micro pores were less than 10 μm, values that are situated under the threshold that could be considered as responsible for initiation of fatigue cracks according with some reported studies.

Alloy A (~7%Si)

Table 4.1 - Mechanical properties, constituents' volume fraction and morphology, pores volume fraction and hardness of an Al-7%Si alloy.

7% Si		**Mechanical properties**				**Volume fraction** (%)				
	Pos.	**σ (MPa)**	**ε (%)**	**E (GPa)**	**Hardness (HV)**	**(Al) dendrites**	**Eutectic**	**Int.**	**Macro-Pores**	**Micro-Pores**
Grav.	**1**	283±7.5	7.1±0.3	84.1±2.1	111±1.3	58.3±0.8	38.6±0.7	0.0	0.4	2.7±0.02
	2	282±5.5	4.7±0.4	71.3±1.5	107±0.6	61.3±0.5	35.6±0.5	0.0	0.1	2.7±0.03
	3	267±7.0	3.3±0.2	71.2±2.3	103±2.3	68.1±0.5	28.9±0.3	0.0	0.1	2.74±0.1
Cent.	**1**	321±4.0	10.2±0.4	71.5±0.8	127±1.3	51.4±0.6	46±0.4	0.0	0.1	2.37±0.03
	2	298±6.5	8.0±0.3	74.8±1.5	120±1.9	63.3±0.4	34±0.5	0.1	0.2	2.37±0.02
	3	285±4.0	4.0±0.3	66.6±1.8	115±2.3	66.3±0.8	31±0.3	0.2	0.0	2.5±0.05

Table 4.1 – cont.

7% Si		**Morphology** (μm)			
	Pos.	**Eutectic Si**		**SDAS**	**Pores**
		Thickness	**Length**		**Eq.Diam.**
Grav.	**1**	2±0.05	3.5±0.17	22.5±0.6	
	2	2.2±0.05	4.1±0.09	27.5±0.55	3.41±0.15
	3	2.25±0.07	4.85±0.1	26±0.65	
Cent.	**1**	1.6±0.05	2.7±0.07	21 ±0.7	
	2	1.55±0.05	2.85±0.09	24±0.7	3.56±0.3
	3	1.75±0.05	2.8±0.2	31±0.75	

For **alloy A** the results can be summarized as follows:

Ultimate tensile strength shows an increasing tendency from position 3 to position 1 in the case of centrifugal casting but no evident tendency is found on gravity castings between the three positions (Table 4.1, Figure 4.10). The increasing of the value of ultimate tensile strength on centrifugal casting in position 1 compared with position 3 is about 11%.

Strain to failure results shows also a tendency to increase from position 3 to position 1 in both casting processes with an accentuated effect in centrifugal castings (Table 4.1, Figure 4.11). Compared to gravity castings the values of ultimate tensile strength and strain to failure are higher in centrifugal castings in any position (Table 4.1, Figure 4.10 and Figure 4.11).

Young's modulus shows a smooth increasing tendency from position 3 to position 1 in both gravity and centrifugal castings (Table 4.1, Figure 4.12).

Hardness values shows an increasing tendency from position 3 to position 1 in the case of centrifugal casting and gravity castings between the three position (Table 4.1, Figure 4.13).

The percentage of aluminium and silicon contents is about the same in all positions and casting techniques as can be seen on Table 4.1 and Figure 4.14. Dendrites' volume fraction shows a decreasing tendency from position 3 to position 1 for both centrifugal and gravity castings (Table 4.1, Figure 4.15). Eutectic's volume fraction shows an increasing tendency from position 3 to position 1 for both centrifugal and gravity castings (Table 4.1, Figure 4.15). Intermetallics' volume fraction is not significant (always lower then 1%) for all positions and casting techniques (Table 4.1, Figure 4.15).

Microstructure shows a similar structure for both casting techniques but with different volume fractions and almost the same constituent's dimensions (Figure 4.16 and 4.17).

The microstructure configuration can be observed in SEM analysis with the magnification level of 500x on Figure 4.18 where can be noticed the well defined secondary dendrite arms spacing (SDAS) as well as in Figures 4.16 and 4.17, and 1000x on Figure 4.19 where can be seen the round and ovoid shapes of the eutectic silicon particles.

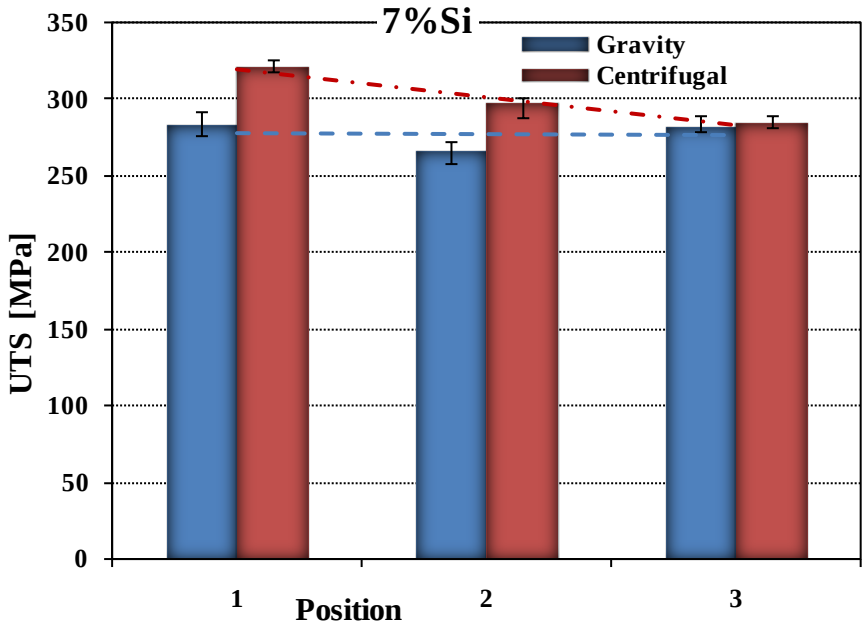

Figure 4.10 – Ultimate tensile strength results for centrifugal and gravity castings of alloy A in position 1, 2 and 3 of ingots.

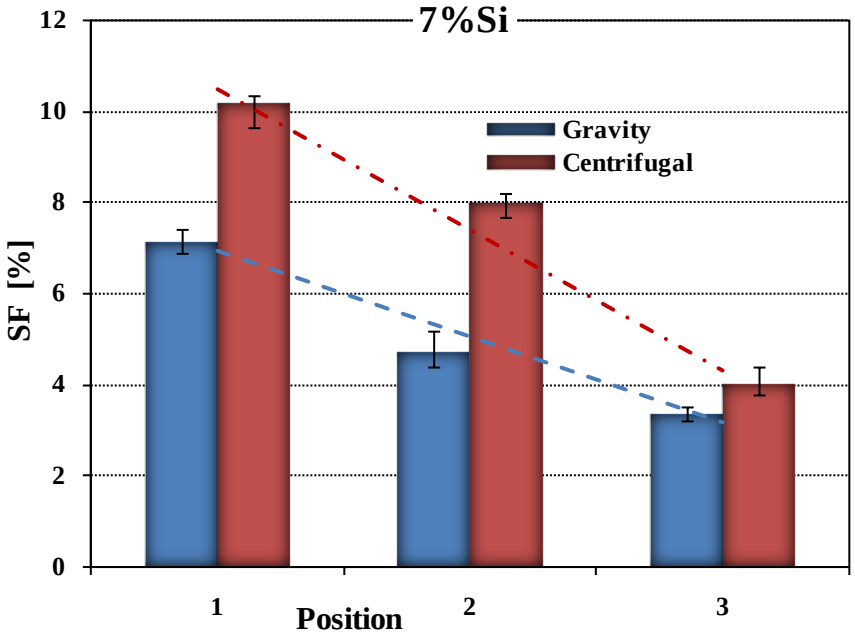

Figure 4.11– Strain to failure results for centrifugal and gravity castings of alloy A in position 1, 2 and 3 of ingots.

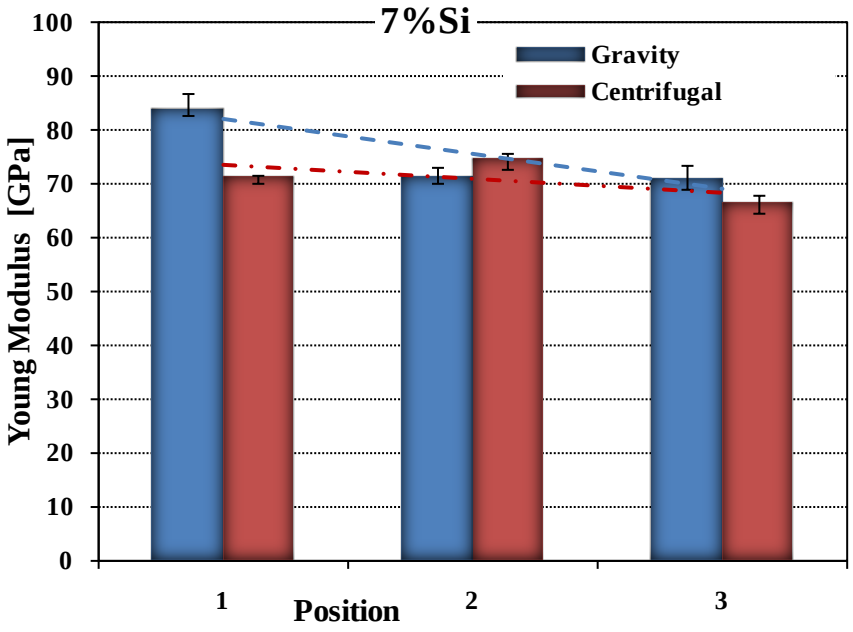

Figure 4.12 – Young's modulus results for centrifugal and gravity castings of alloy A in position 1, 2 and 3 of ingots.

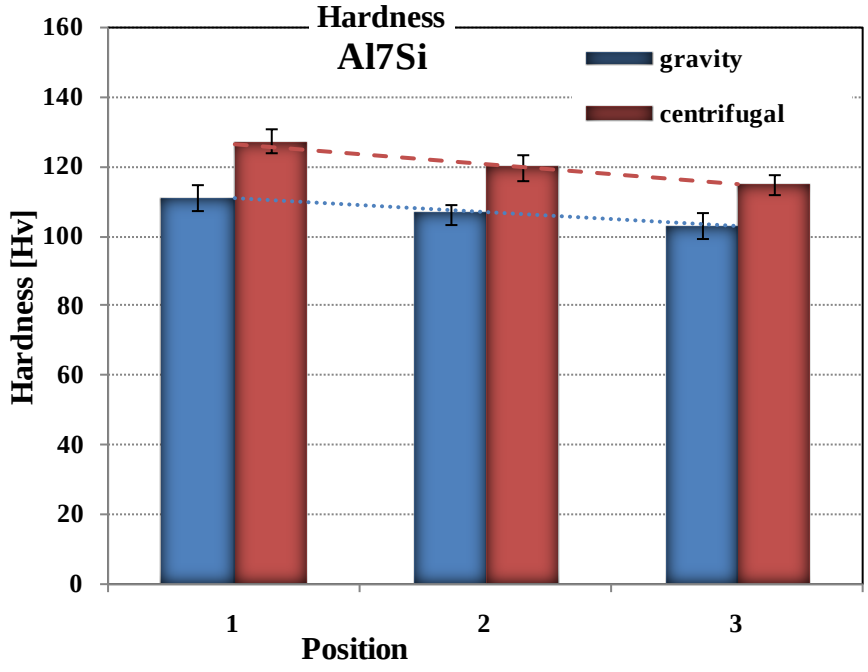

Figure 4.13 – Hardness values in position 1, 2 and 3 of ingots for gravity and centrifugal castings of alloy A

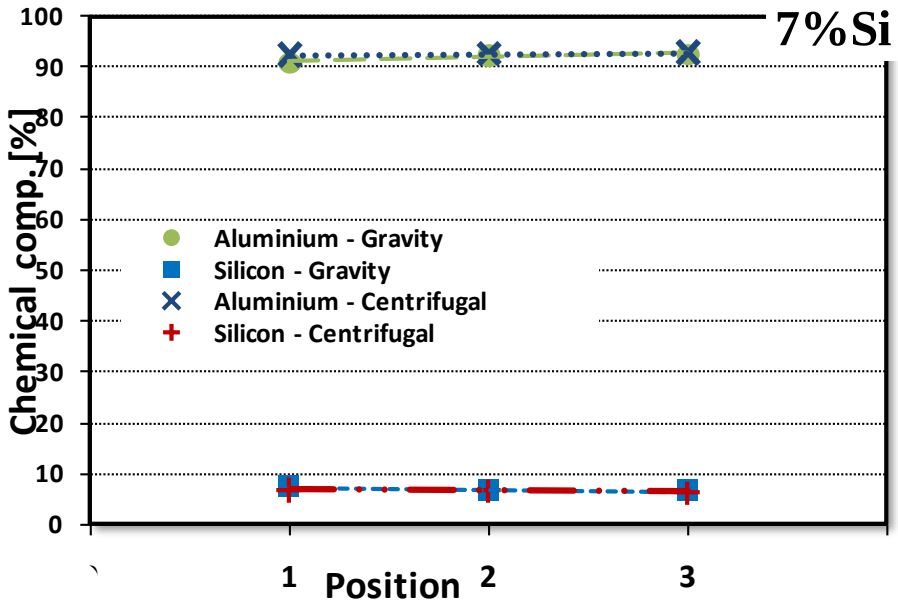

Figure 4.14 - Al and Si contents in position 1, 2 and 3 of ingots for gravity and centrifugal castings of alloy A

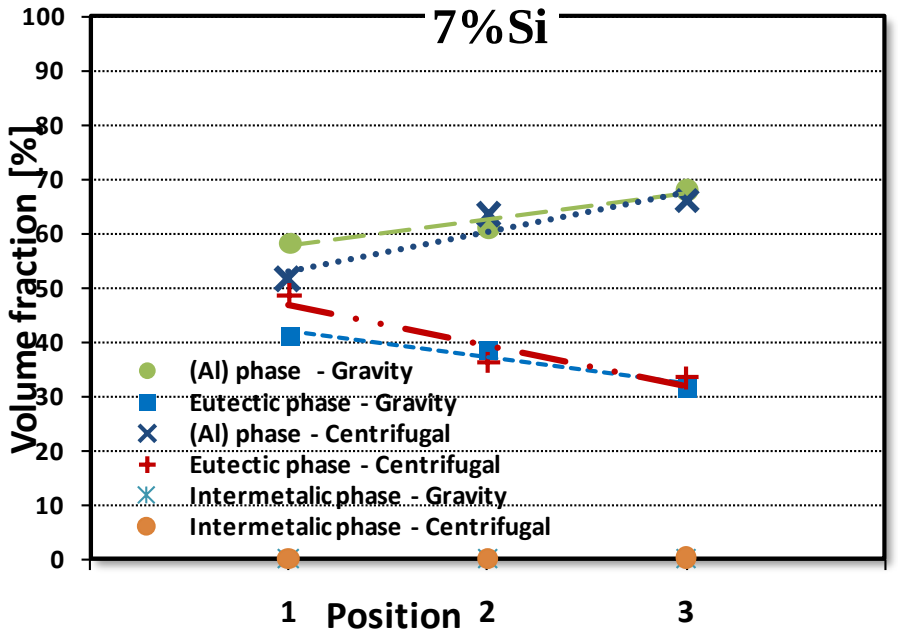

Figure 4.15 – Constituents' volume fraction in position 1, 2 and 3 of ingots for gravity and centrifugal castings of alloy A

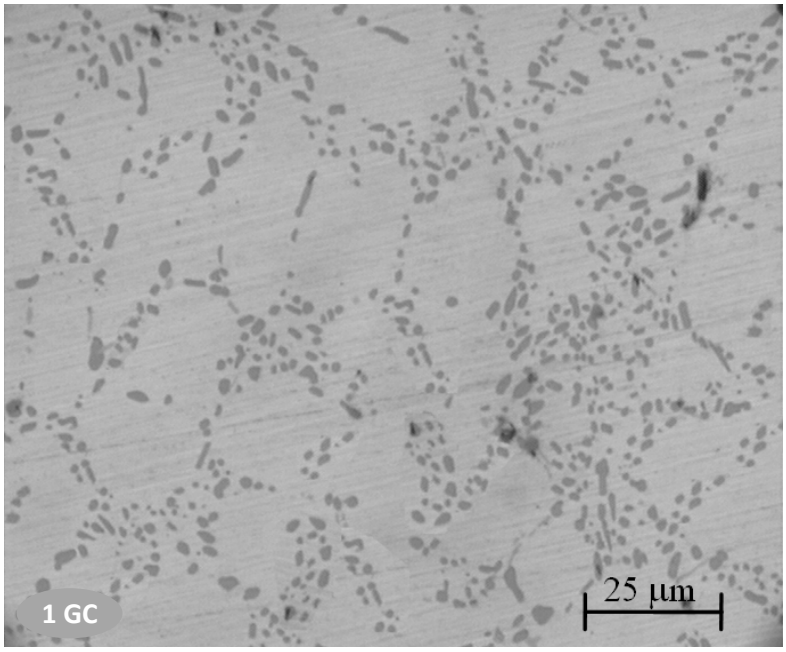

Figure 4.16 - Microstructures of gravity castings (GC) of alloy A on position 1 of the ingot.

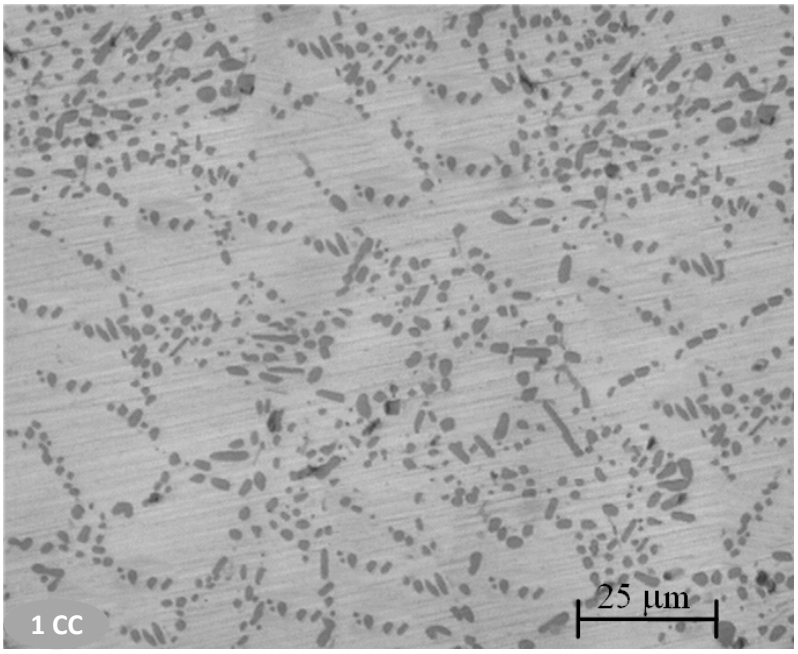

Figure 4.17 - Microstructures of centrifugal castings (CC) of alloy A on position 1 of the ingot.

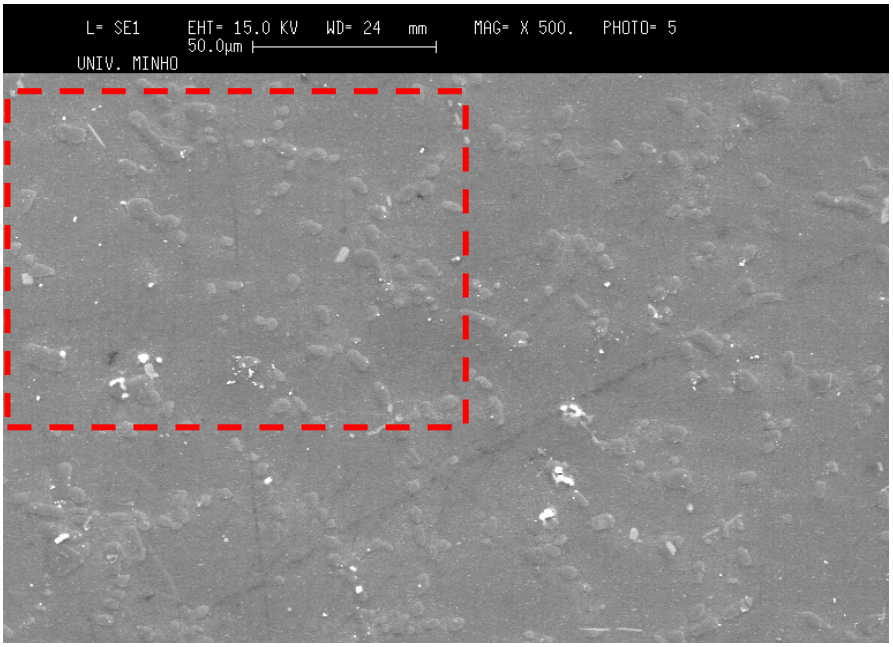

Figure 4.18 – SEM microstructure of centrifugal castings of alloy A in position 1: (500x)

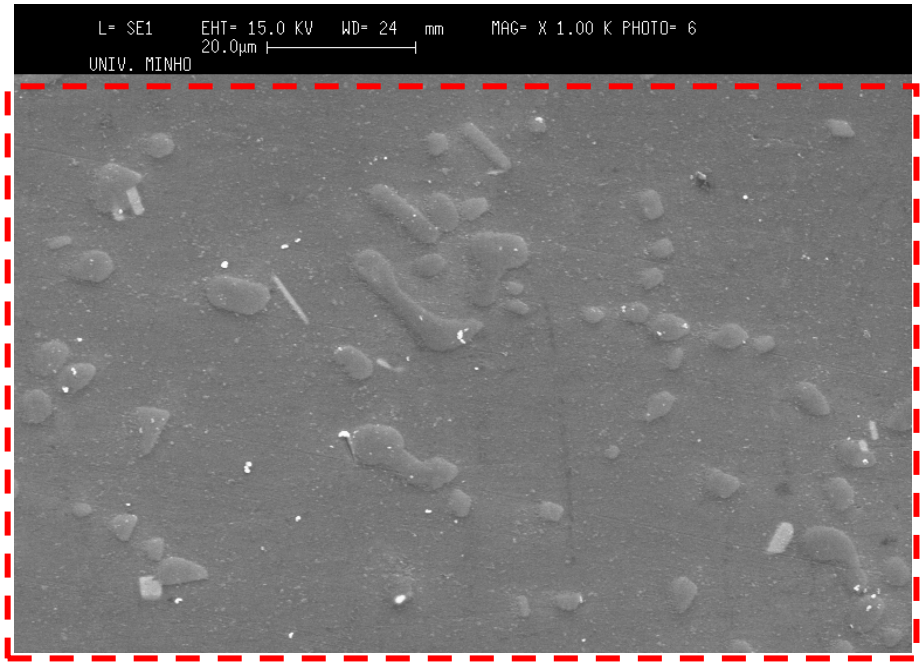

Figure 4.19– SEM microstructure of centrifugal castings of alloy A in position 1 (1000x)

Alloy B (~12% Si)

Table 4.2 - Mechanical properties, constituents' volume fraction and morphology, pores volume fraction and hardness of an Al-12%Si alloy.

12% Si		**Mechanical properties**				**Morphology** (μm)				
	Pos.	**σ (MPa)**	**ε (%)**	**E (GPa)**	**Hardness (HV)**	**Eutectic Silicon**		**SDAS**	**Int**	**Pores**
						Thickness	**Length**		**Thickness**	**Eq. diam.**
Grav.	**1**	226±7.0	0.9±0.05	82.9±1.5	109±1.2	0.62±0.013	7.3±0.22	19.5±0.45		
	2	208±5.5	0.7±0.04	82.7±2.7	106±1.0	0.61±0.025	8.9±0.22	22.3±0.66	3.84±0.5	3.68±0.04
	3	202±4.5	0.70±0.04	58.7±1.6	105±1.3	0.88±0.03	9.4±0.23	28.2±0.65		
Cent.	**1**	264±7.0	1.52±0.04	80.6±2.0	121±3.3	0.55±0.015	6.8±0.21	19.2±0.7		
	2	249±6.5	1.30±0.04	62.5±1.2	116±1.2	0.62±0.014	8.1±0.22	21.3±0.61	3.19±0.5	3.66±0.07
	3	227±4.0	0.91±0.05	70.1±2.0	114±1.2	0.70±0.010	8.9±0.21	23.2±0.60		

Table 4.2 – cont.

12% Si		**Volume fraction** (%)					
	Pos.	**(Al) dendrites**	**Eutectic**	**Interm.**	**(Si) particles**	**Macro-Pores**	**Micro-Pores**
Grav.	**1**	37.0±1.1	53.5±1.2	6.4±0.2	0.4±0.01	<0.1	2.7±0.02
	2	35.4±0.6	53.3±1.3	7.3±0.1	1.1±0.01	0.1	2.8±0.02
	3	38.6±0.7	49.0±0.8	7.7±0.1	1.8±0.01	<0.1	2.82±0.03
Cent.	**1**	25.6±0.3	66.1±0.5	5.7±0.15	0.0	<0.1	2.4±0.04
	2	27.9±0.2	62.1±0.9	6.8±0.18	0.1	0.1	2.51±0.03
	3	34.8±0.4	55.5±1.2	6.7±0.2	0.0	<0.1	2.6±0.05

Results, for **alloy B**, can be summarized as follows:

Centrifugal and gravity castings results show an increasing tendency of ultimate tensile strength from position 3 to position 1 (Table 4.2, Figure 4.20). In all three positions the ultimate tensile strength values are increased with about 15% on centrifugal casting compared with gravity casting results.

A substantial tendency of increasing gravity castings and in particular centrifugal castings it is obtained for strain to failure from position 3 to position 1 (Table 4.2, Figure 4.21). The maximum difference between casting techniques results on strain to failure is of about 47% on position 2 followed by position 1 with approximately 40% increasing.

Both gravity and centrifugal castings show a small tendency for the Young's modulus to increase from position 3 to position 1 (Table 4.2, Figure 4.22). There is no significant difference between analysed casting techniques.

Hardness values shows an increasing tendency from position 3 to position 1 in the case of centrifugal casting and gravity castings between the three position (Table 4.2, Figure 4.23). In all three positions the hardness values are increased with about 12% on centrifugal casting compared with gravity casting results.

The chemical composition analysis reveals as well as for alloy A that the aluminium and silicon contents are about the same in all positions and casting techniques (Table 4.2, Figure 4.24).

Decreasing tendency from position 3 to position 1 of the dendrites' volume fraction can be observed on both castings techniques (Table 4.2, Figure 4.25).

Eutectic's volume fraction shows an increasing tendency from position 3 to position 1 in both casting processes (Table 4.2, Figure 4.25).

Intermetallics' volume fraction shows a smooth increasing tendency from position 1 to position 3 on both casting techniques (Table 4.2, Figure 4.25). The decreasing/increasing on the three positions of the amount of the dendrites, eutectic and intermetallics volumes fractions can be observed as well on figure 4.28.

Microstructure shows a similar qualitatively structure (needle like eutectic silicon particles) for both casting techniques and positions but with different volume fractions and constituents dimensions (Figures 4.26 and 4.27).

The microstructure configuration can be observed in SEM analysis with the magnification level of 500x on figure 4.29 and 100x on figure 4.30, where can be better observed the intermetalic phases due to better contrast and also can be noticed the well defined secondary dendrite arms spacing (SDAS) as well as in figures 4.26 and 4.27.

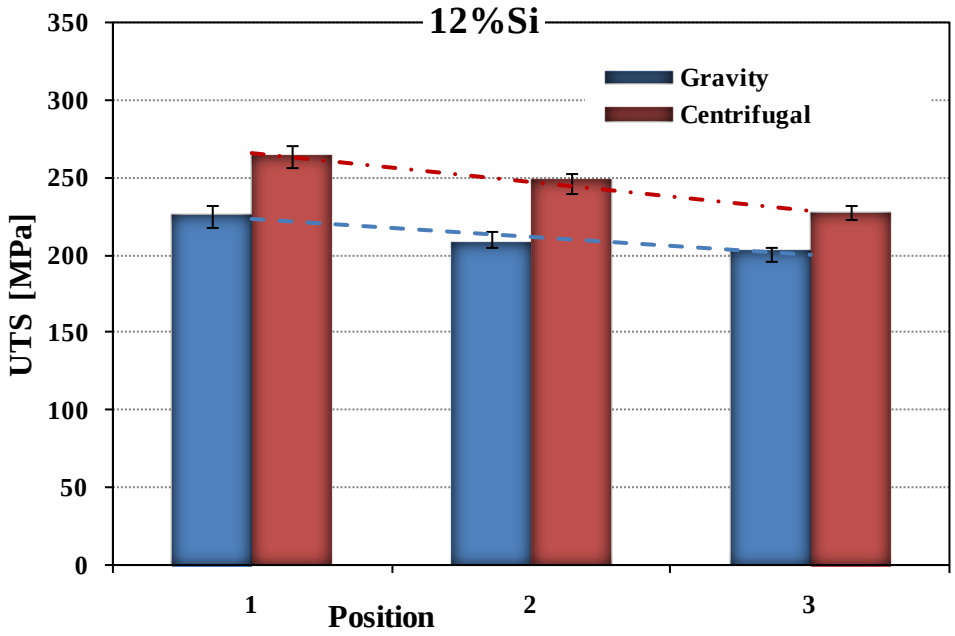

Figure 4.20 – Ultimate tensile strength results for centrifugal and gravity castings of alloy B in position 1, 2 and 3 of ingots.

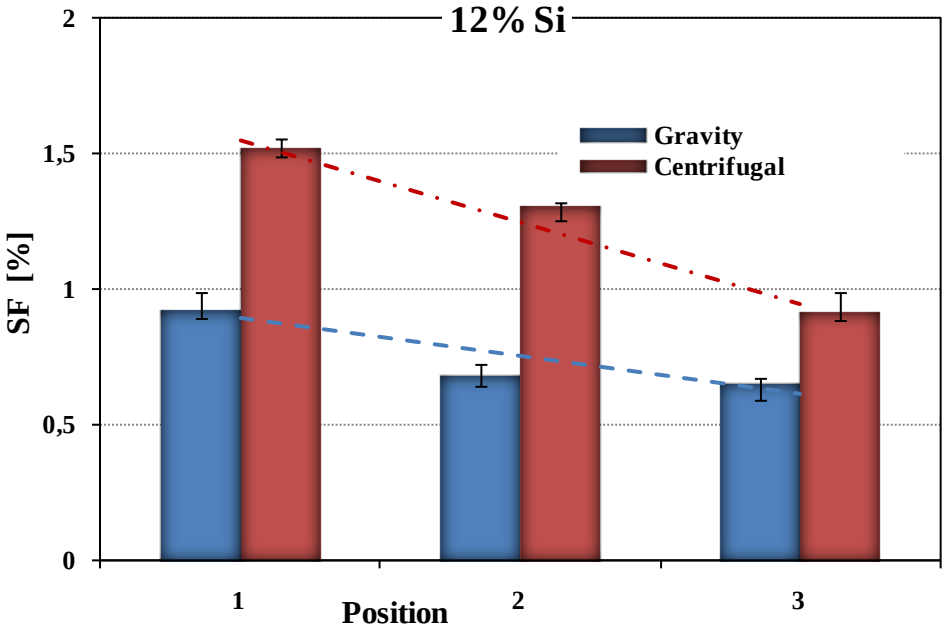

Figure 4.21 – Strain to failure results for centrifugal and gravity castings of alloy B in position 1, 2 and 3 of ingots.

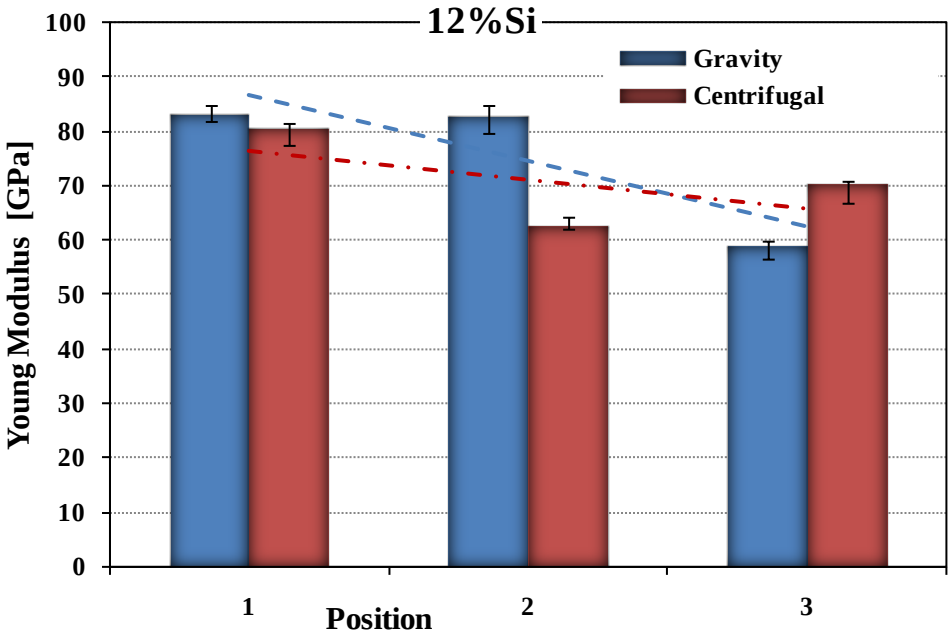

Figure 4.22 – Young's modulus results for centrifugal and gravity castings of alloy B in position 1, 2 and 3 of ingots.

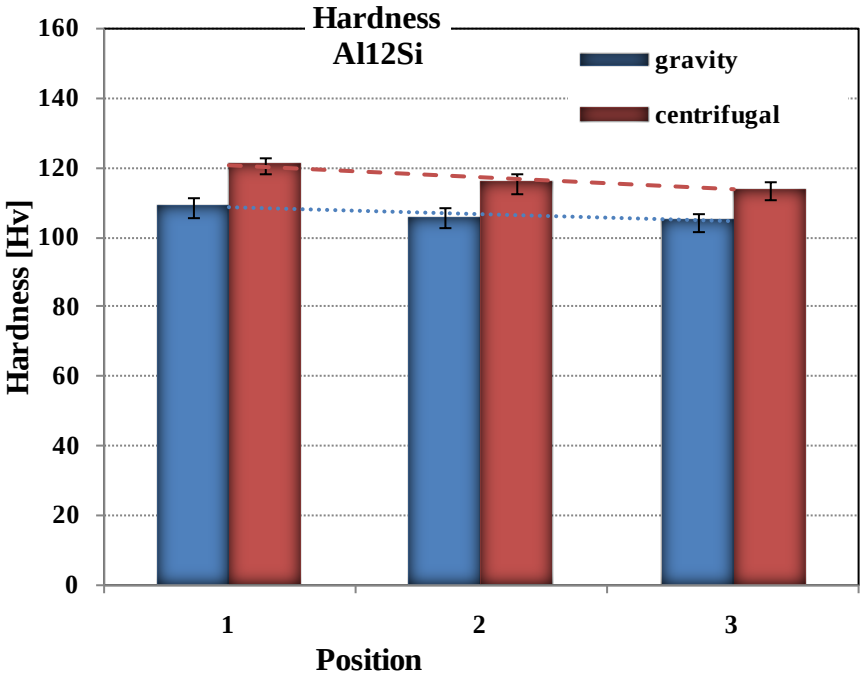

Figure 4.23 – Hardness values in position 1, 2 and 3 of ingots for gravity and centrifugal castings of alloy A

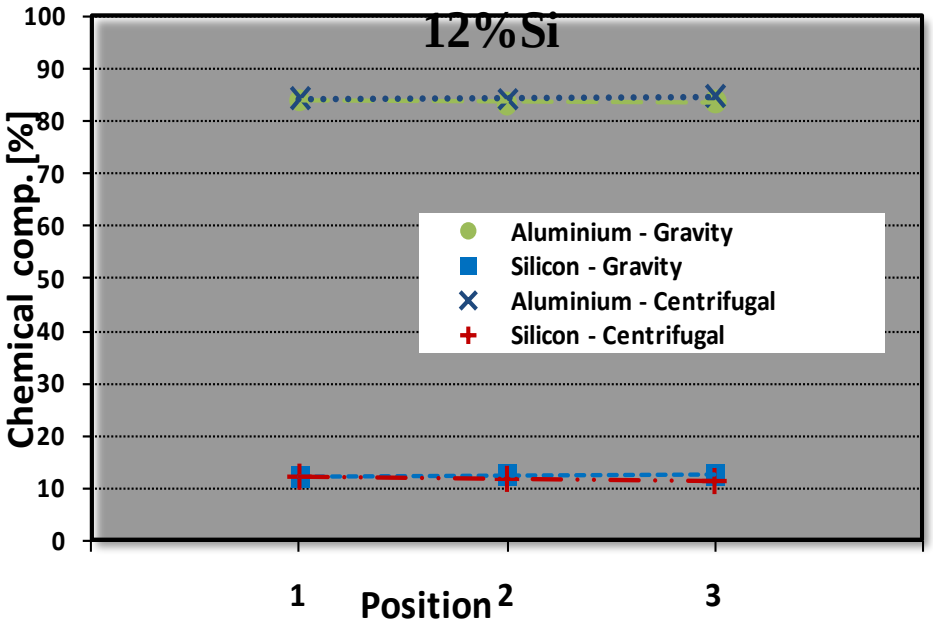

Figure 4.24 - Al and Si contents in position 1, 2 and 3 of ingots for gravity and centrifugal castings of alloy B

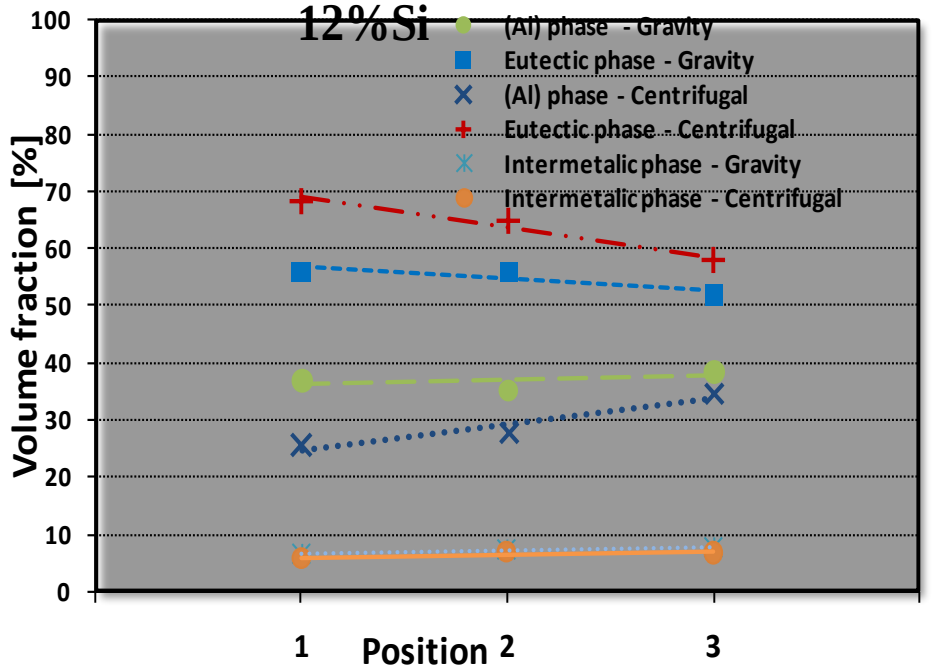

Figure 4.25 – Constituents' volume fraction in position 1, 2 and 3 of ingots fc gravity and centrifugal castings of alloy B

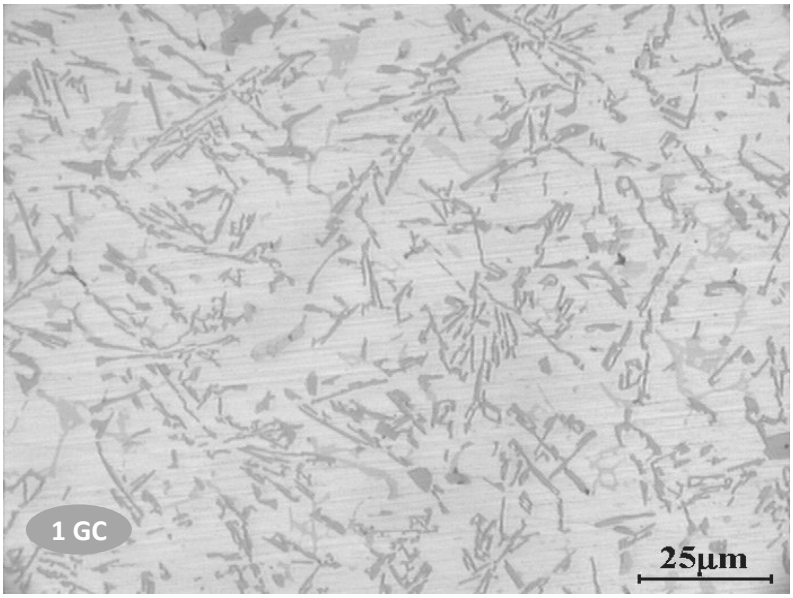

Figure 4.26 - Microstructures of gravity castings (GC) of alloy B on position 1 of the ingot.

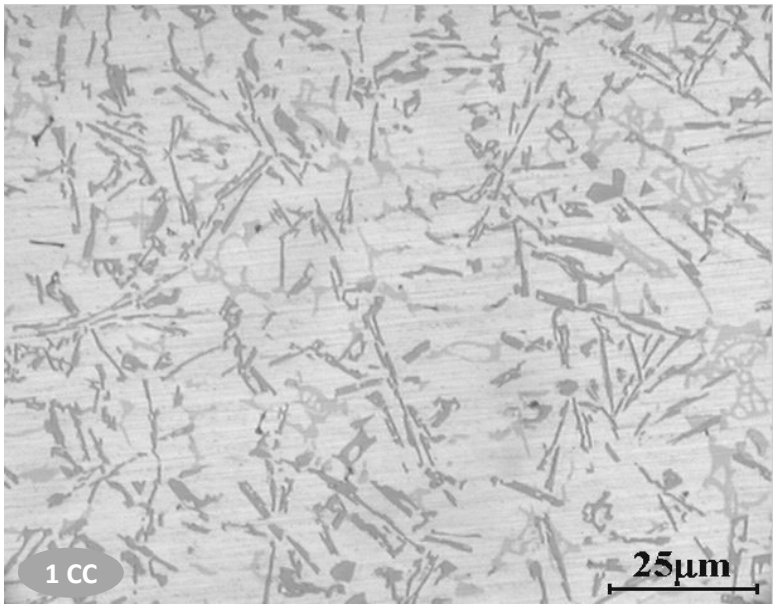

Figure 4.27 - Microstructures of centrifugal castings (CC) of alloy B on position 1 of the ingot.

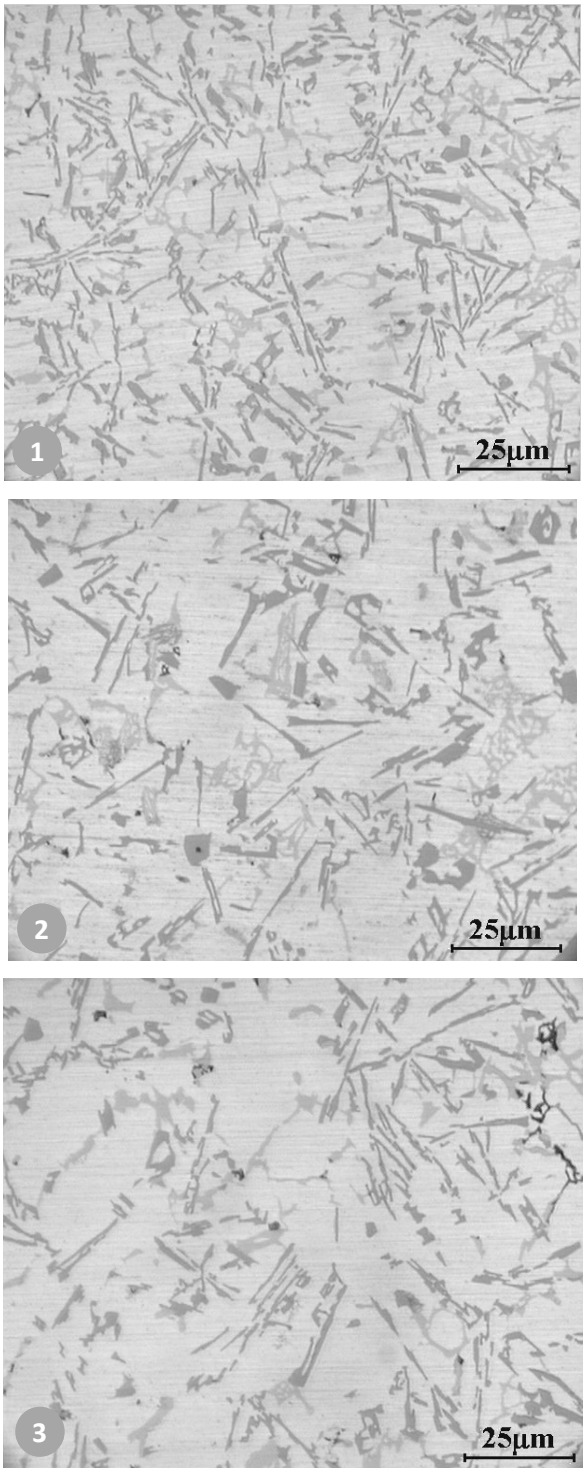

Figure 4.28 - Microstructures of centrifugal castings (CC) of alloy B on positions 1, 2 and 3 of the ingot.

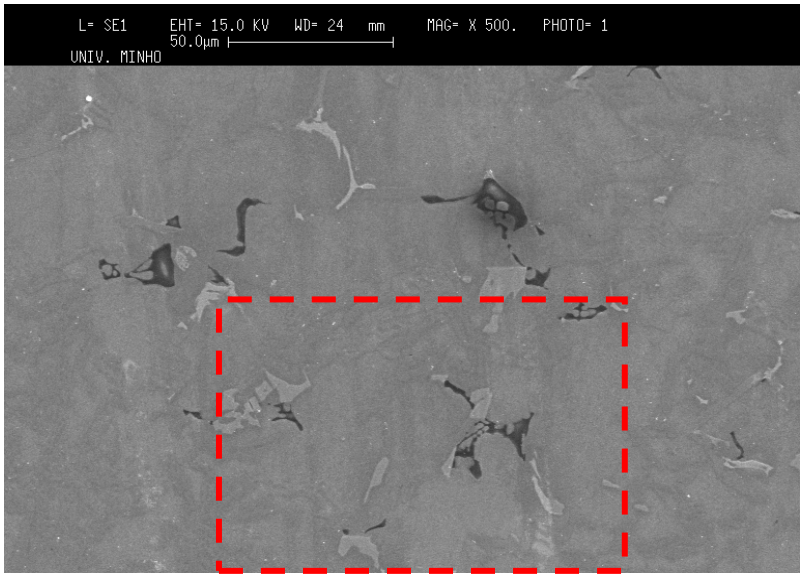

Figure 4.29 – SEM microstructure of centrifugal castings of alloy B in position 1: (500x)

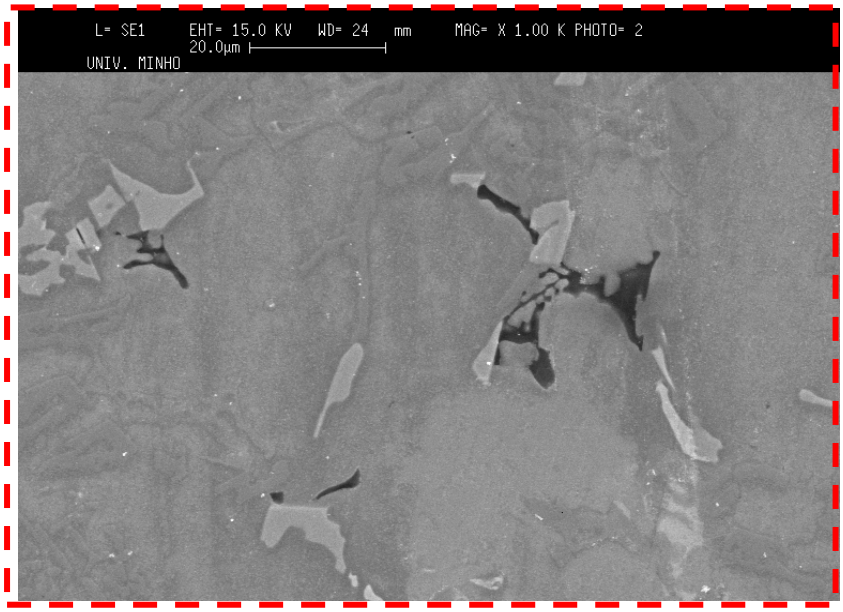

Figure 4.30 – SEM microstructure of centrifugal castings of alloy B in position 1 (1000x)

Alloy C (~18% Si)

Table 4.3 - Mechanical properties, constituents' volume fraction and morphology, pores volume fraction and hardness of an Al-18%Si alloy.

18% Si		**Mechanical properties**				**Morphology** (μm)			
	Pos.	**σ (MPa)**	**ε (%)**	**E (GPa)**	**Hardness (HV)**	**Si**		**Int**	**Pores**
						Particles	**Eutectic**	**Th**	
Grav.	**1**	169±10.0	0.4±0.04	80.5±1.4	110±2.5		0.20±0.05		
	2	165±7.0	0.4±0.05	85.3±1.7	102±2.1	3.5±0.5	0.22±0.45	3.52±0.5	3.6±0.5
	3	132±10.0	0.2±0.04	69.9±2.4	113±2.2		0.25±0.50		
Cent.	**1**	232±7.0	2.0±0.05	71.3±2.0	108±1.3		0.19±0.45		
	2	258±6.5	1.7±0.05	74.6±2.0	109±6.6	3.1±0.6	0.20±0.50	3.12±0.5	3.63±0.6
	3	212±4.0	0.9±0.05	79.1±1.5	111±0.6		0.22±0.50		

Table 4.3 – cont.

18% Si		**Volume fraction** (%)					
	Pos.	**(Al) α phase**	**Eutectic**	**Interm.**	**(Si) particles**	**Macro-Pores**	**Micro-Pores**
Grav.	**1**	10.4±0.5	65.1±0.9	19.9±0.6	0.6±0.03	0.1	3.3±0.04
	2	9.4±0.2	64.3±0.8	17.6±0.4	2.4±0.04	0.1	3.47±0.05
	3	14.7±0.3	61.3±1.1	12.9±0.5	7.4±0.06	0.2	3.5±0.06
Cent.	**1**	0.9±0.01	87.4±1.2	8.9±0.3	0	0.3	2.5±0.07
	2	0.8±0.02	81.5±0.8	14.5±0.5	0	0.3	2.79±0.06
	3	0.7±0.01	76.8±0.9	19.4±0.2	0	0.2	2.8±0.08

Results, for **alloy C**, can be summarized as follows:

Centrifugal and gravity castings shows an increasing tendency of ultimate tensile strength from position 3 to position 1 (Table 4.3, Figure 4.31). The maximum difference of ultimate tensile strength results between casting techniques is obtained in position 3 with approximately 60% followed by position 2 with 56% and position 1 with 37 % increasing values for centrifugal result.

Gravity castings and in particular centrifugal castings show a substantial tendency of strain to failure to increase from position 3 to position 1 (Table 4.3, Figure 4.32) obtaining more than 300% over the gravity strain to failure result in all 3 positions.

Young's modulus shows no clearly tendency even if in position 1 and 2 are obtained increased result for centrifugal castings with about 7% (Table 4.3, Figure 4.33).

Ultimate tensile strength and strain to failure show higher values for the centrifugal casting process in any position, when compared to gravity castings (Table 4.3, Figure 4.31 and Figure 4.32).

Hardness values shows an increasing tendency from position 3 to position 1 in the case of centrifugal casting and gravity castings between the three position (Table 4.3, Figure 4.34). There is no significant difference of hardness values between analysed casting techniques.

The aluminium and silicon contents are about the same in all positions and casting techniques with a small variation from position 3 to position 1 in centrifugal castings (Table 4.3, Figure 4.35).

(Al) phase volume fraction shows a decreasing tendency from position 3 to position 1 mainly in gravity castings (Table 4.3, Figure 4.36).

Eutectic's volume fraction shows an increasing tendency from position 3 to position 1 in both casting processes (Table 4.3, Figure 4.36).

Intermetallics' volume fraction shows an increasing tendency from position 1 to position 3 in centrifugal castings and from 3 to 1 in gravity castings (Table 4.3, Figure 4.36).

Microstructure shows a similar qualitatively structure with the same coral like eutectic form for both casting techniques but with different volume fractions and constituents dimensions (Figure 4.37 and Figure 4.38). In figure 4.39 it is presented the 500 magnification of SEM microstructure of centrifugal casting of alloy C in position 1 and in Figure 4.40 is a detailed view in which is observed the shape of eutectic clusters and intermetalic presence.

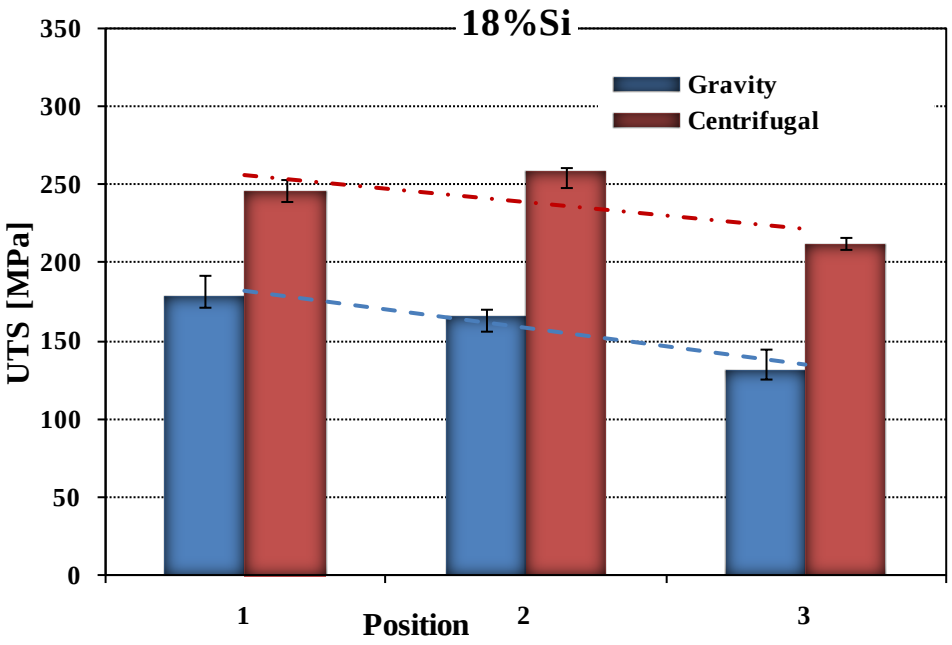

Figure 4.31 – Ultimate tensile strength results for centrifugal and gravity castings of alloy C in position 1, 2 and 3 of ingots.

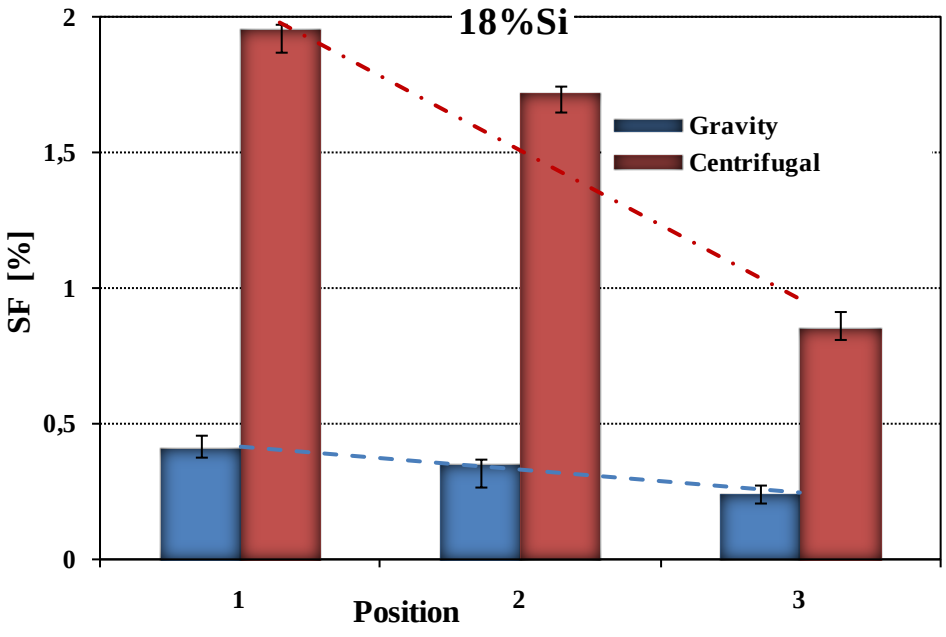

Figure 4.32 – Strain to failure results for centrifugal and gravity castings of alloy C in position 1, 2 and 3 of ingots.

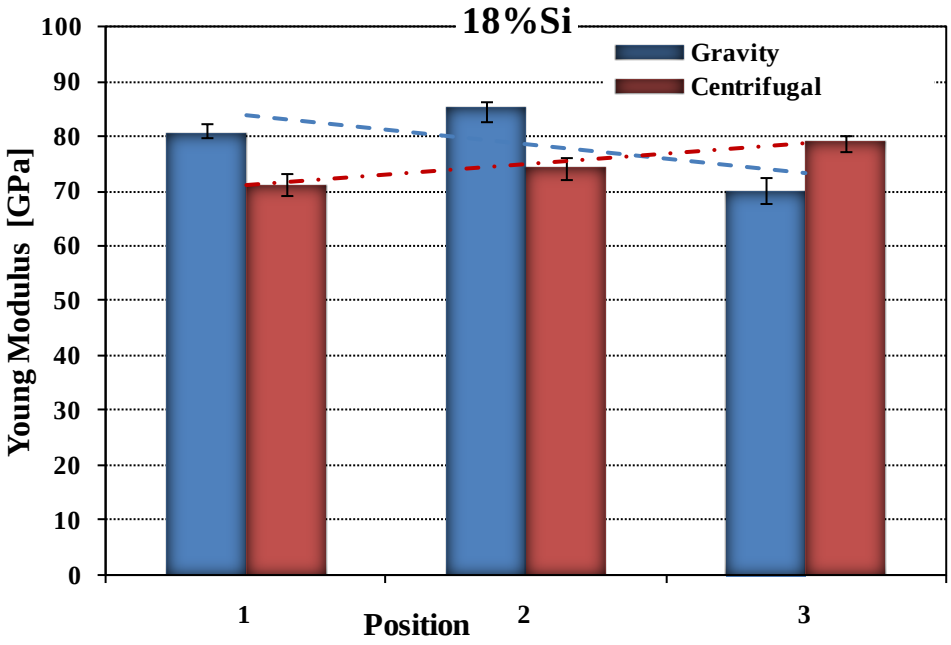

Figure 4.33 – Young's modulus results for centrifugal and gravity castings of alloy C in position 1, 2 and 3 of ingots.

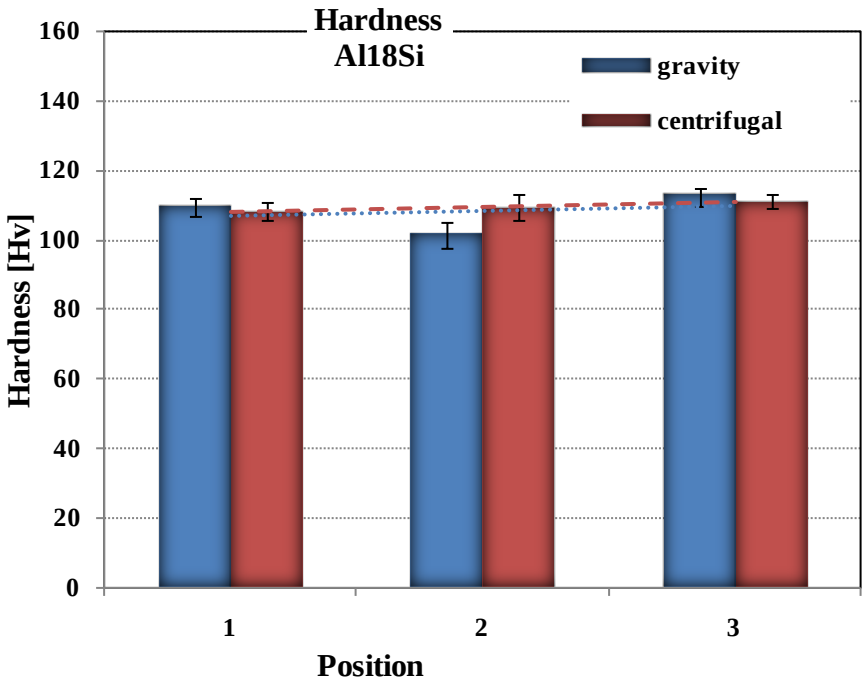

Figure 4.34 – Hardness values in position 1, 2 and 3 of ingots for gravity and centrifugal castings of alloy A

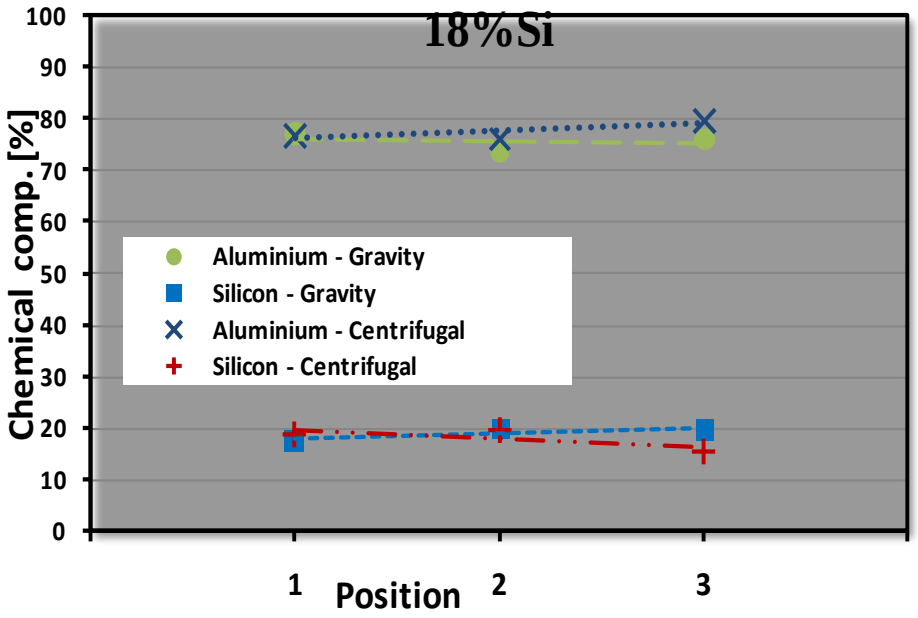

Figure 4.35 - Al and Si contents in position 1, 2 and 3 of ingots for gravity and centrifugal castings of alloy C

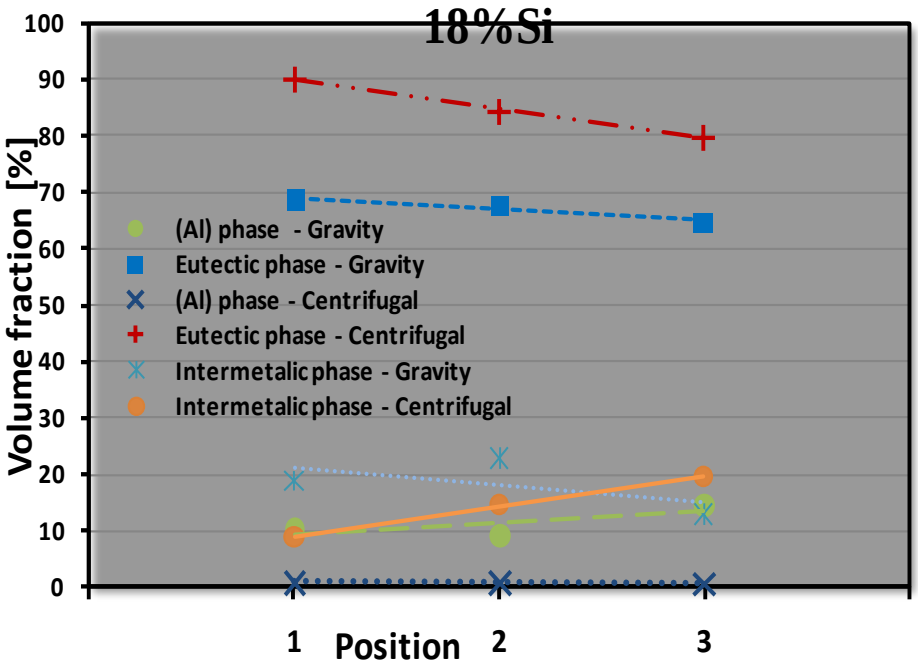

Figure 4.36 – Constituents' volume fraction in position 1, 2 and 3 of ingots for gravity and centrifugal castings of alloy C

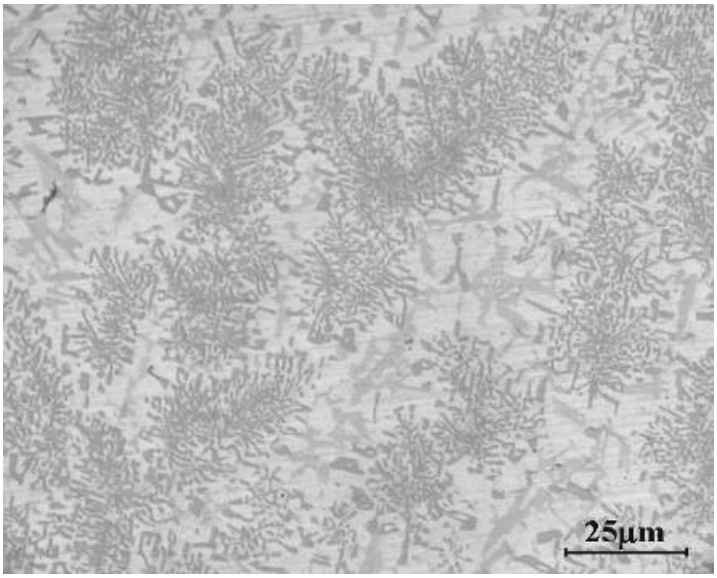

Figure 4.37 - Microstructures of gravity castings (GC) of alloy C on position 1 of the ingot.

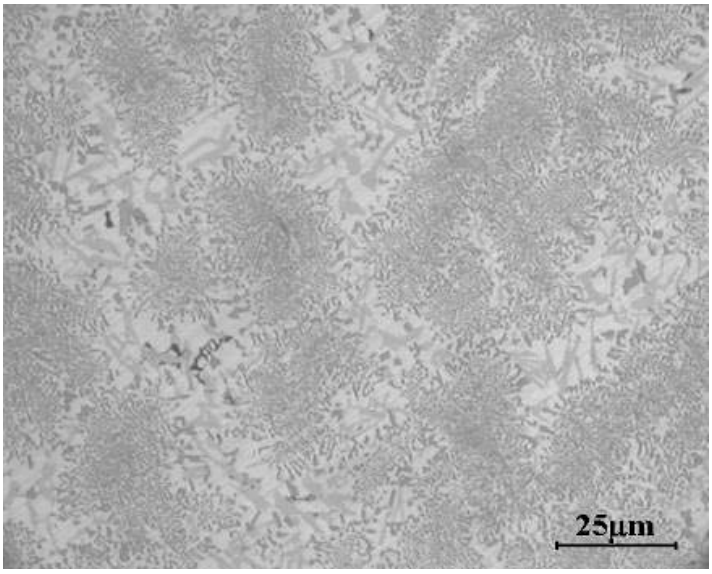

Figure 4.38 - Microstructures of centrifugal castings (CC) of alloy C on position 1 of the ingot.

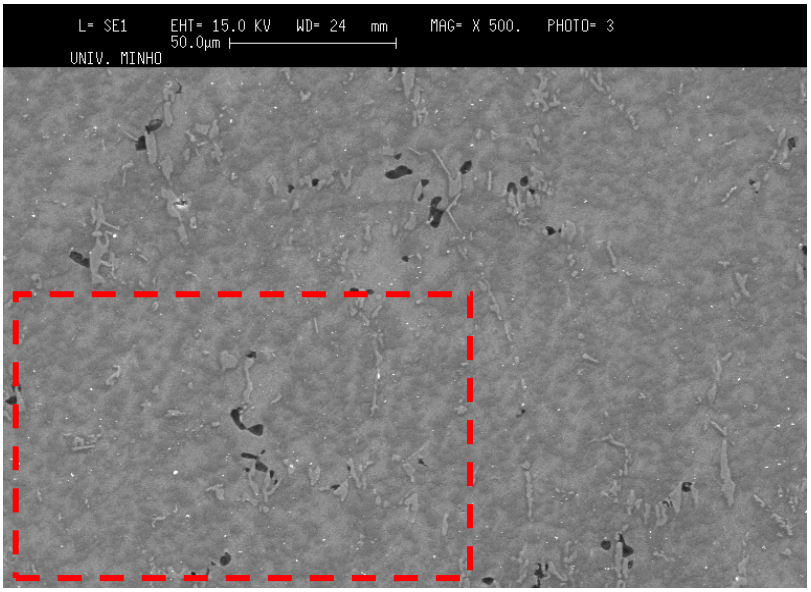

Figure 4.39 – SEM microstructure of centrifugal castings of alloy C in position 1: (500x)

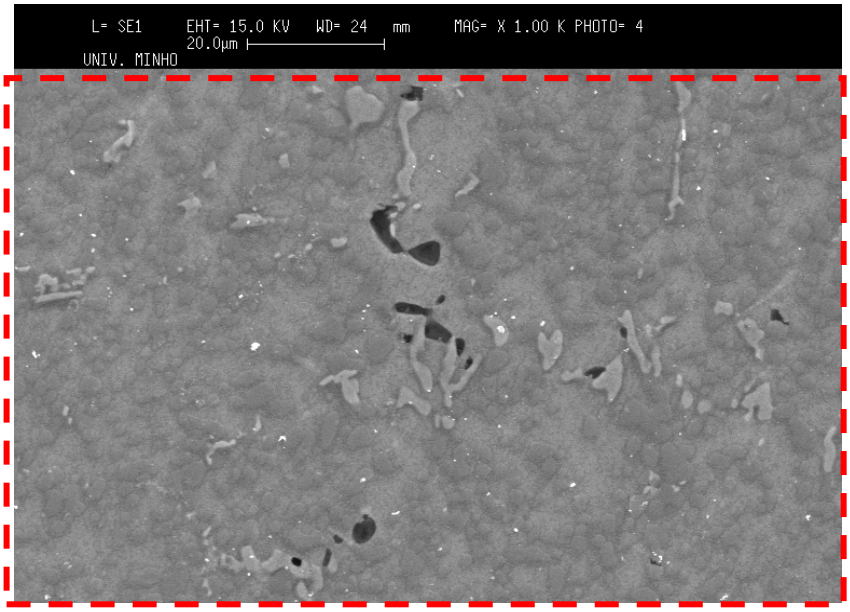

Figure 4.40– SEM microstructure of centrifugal castings of alloy C in position 1 (1000x)

4.4. Fatigue properties results

Microstructural, manufacturing, and environmental factors can cause high local stresses and therefore act as fatigue initiation sites. Typical microstructural factors in Al-Si alloys include brittle phases, for example primary Si particles, pores and oxides. Si particles have been shown to crack and decohere at the particle/matrix interface under cyclic loading and so act as initiation sites. Pores and other inclusions also act as stress raisers and are the most common reducer of fatigue life of the casting process.

In figures 4.41 to 4.43 it is shown the S-N (**S**tress vs. **N**umber of cycles) curves for the gravity and centrifugal castings of all three alloys studied.

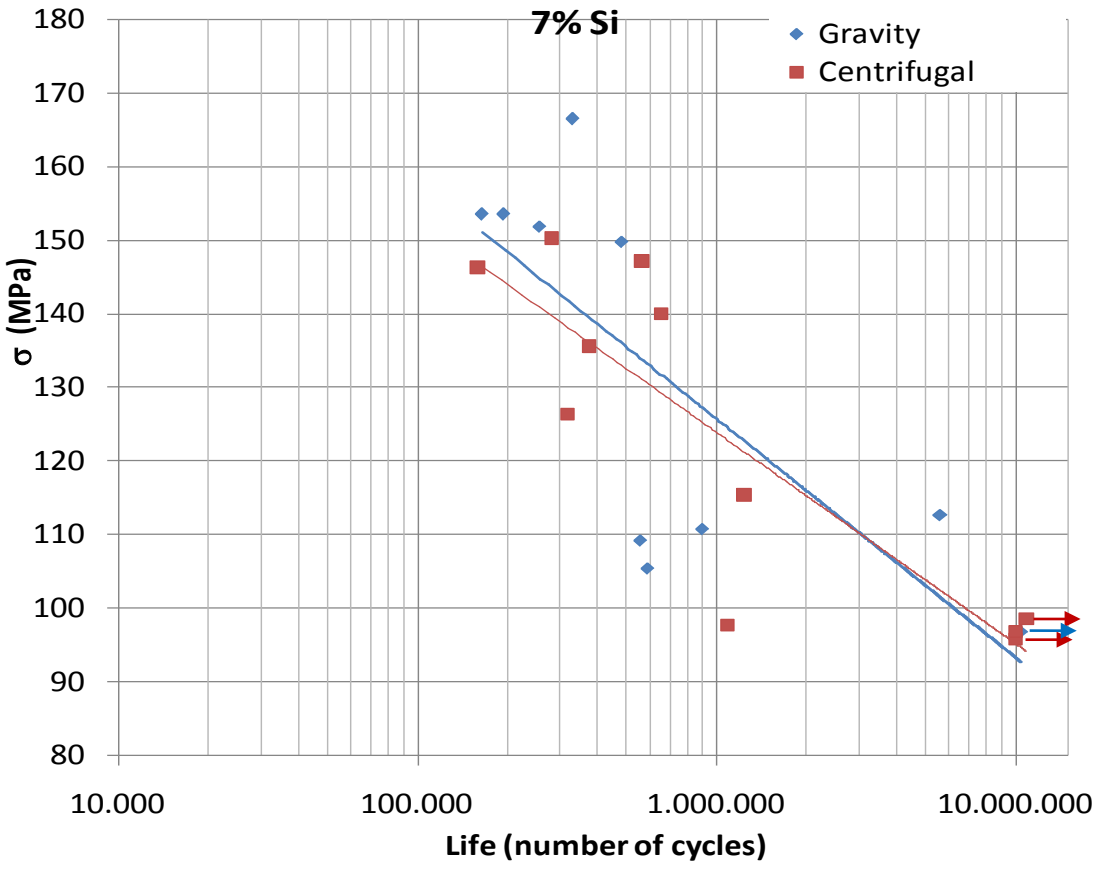

Figure 4.41 – S–N curves for centrifugal and gravity castings of alloy A

The rotating bending fatigue specimens obtained by centrifugal casting seem to resist longer than those obtained by gravity casting at same stress level applied, especially

in the case of alloy B and alloy C. In the case of alloy A (Figure 4.41) there is almost no difference between the two types of casting of alloy A having the same fatigue limit at around 95 MPa stress level.

The fatigue limit on centrifugal casting of alloy B (Figure 4.42) has increased with 24.5% compared with gravity casting and for alloy C the difference between castings techniques are even bigger showing an increasing with 31% compared with gravity casting (Figure 4.43).

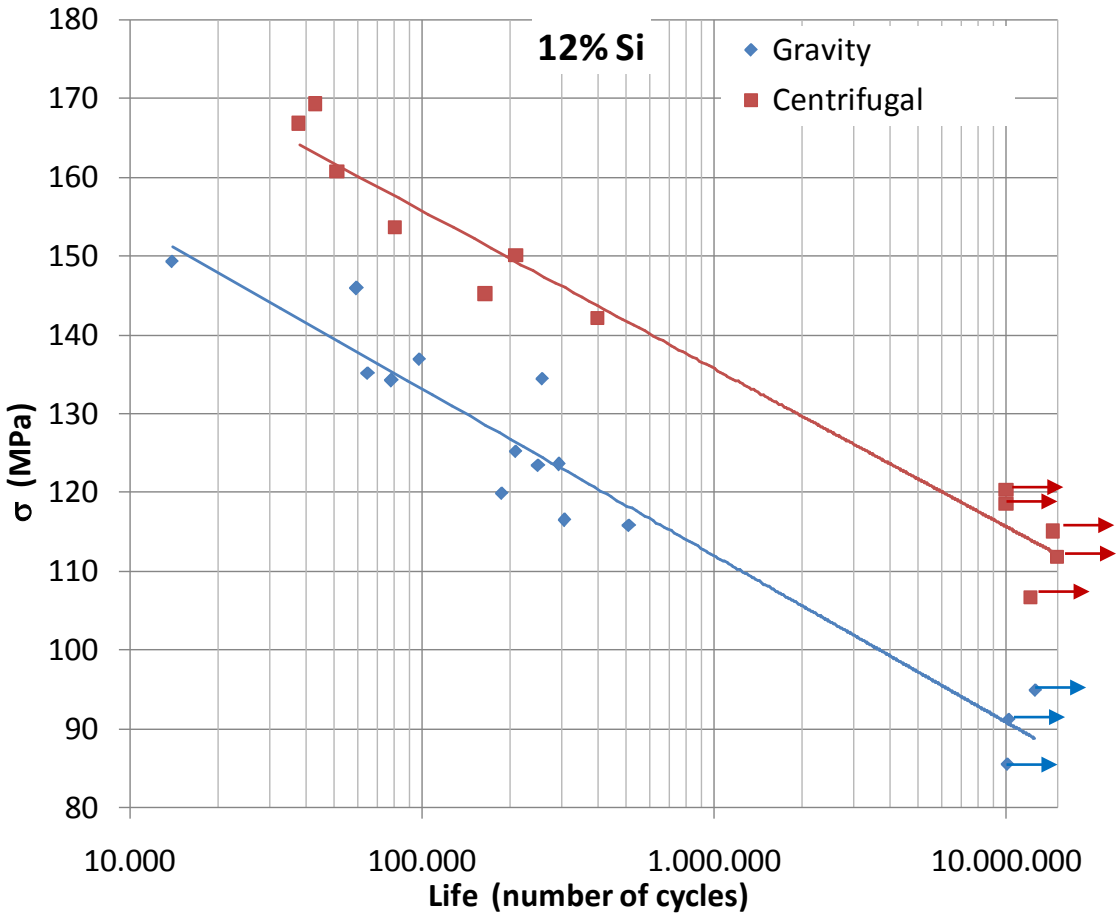

Figure 4.42 – S–N curves for centrifugal and gravity castings of alloy B

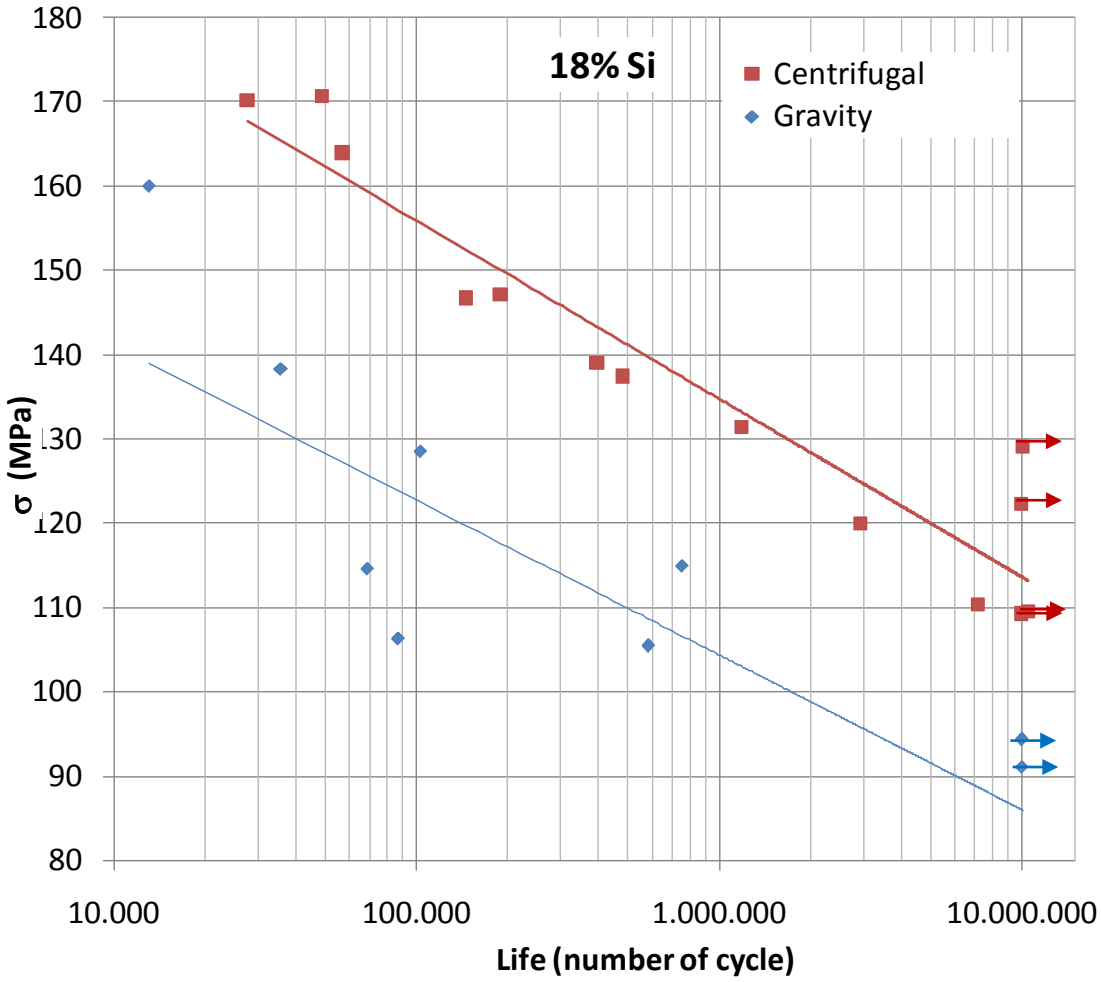

Figure 4.43 – S–N curves for centrifugal and gravity castings of alloy C, σ – stress amplitude.

The microstructural analysis near the crack initiation area reveals the fact that there are not the pores mainly responsible for initiation of cracks. The initiation sites are mainly the primary silicon particles (18%Si alloy) and it is not clear in 7%Si and 12%Si alloys what constituent is the most responsible (figures 4.44-4.46).

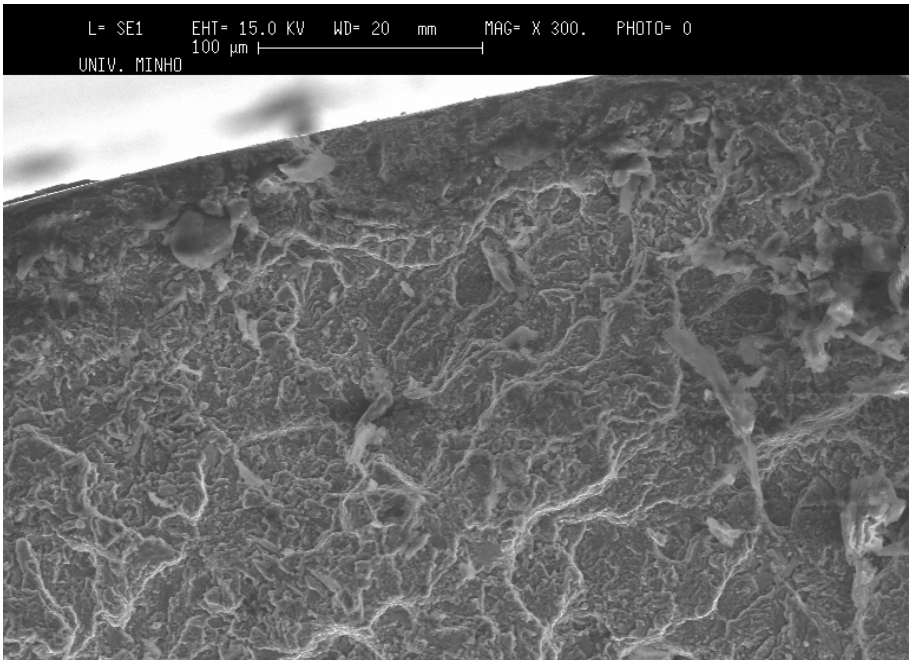

Figure 4.44– SEM microstructure of centrifugal castings of alloy A

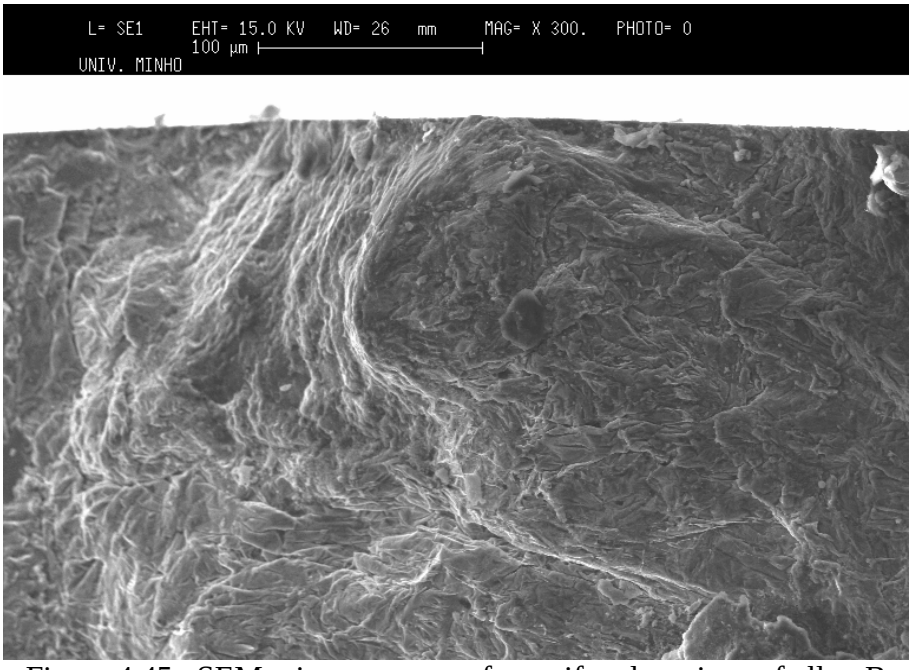

Figure 4.45– SEM microstructure of centrifugal castings of alloy B

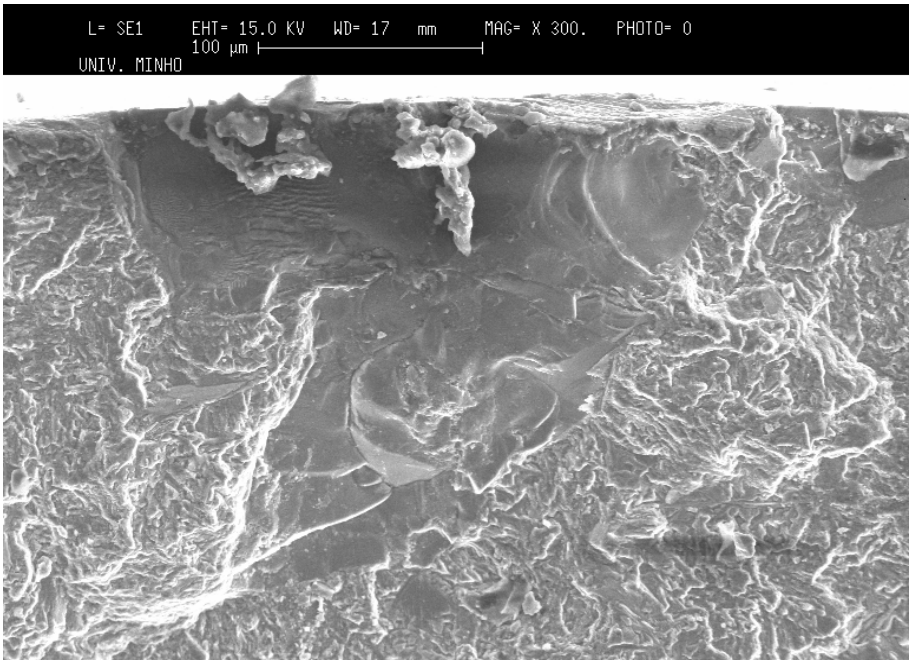

Figure 4.46– SEM microstructure of centrifugal castings of alloy C

CHAPTER 5

FURTHER RESULTS

5.1. Study on assessment of processing variables in vertical centrifugal casting technique

The aim of this study was to investigate the influence of the vertical centrifugal casting technique over mechanical and metallurgical properties of a hypereutectic Al18%Si alloy. In order to understand whether the centrifugal effect is due to the inherent vibration or to the centrifugal effect, or from both, three different tests were performed: gravity casting, gravity casting with vibration, and centrifugal casting. It was verified that both the inherent vibration of the centrifugal process as well as the centrifugal effect have an influence on the mechanical properties of the castings.

To isolate the inherent vibration from the centrifugal casting system and to determine the influence of the vibration, the mould was attached on a system that provides the mechanical vibration due to the eccentric of the shafts (Figure 3.3) during the molten metal pouring. The level of vibration (frequency and amplitude) of the centrifugal casting machine was measured with an accelerometer and was about 8Hz and 0.5 mm amplitude.

The results of ultimate tensile strength show that there is a tendency of increasing from position 3 to position 1 in all the casting techniques studied. This is exactly as it was expected because the position 1 is situated near the wall of the mould where the solidification rate is higher.

Although, the ultimate tensile strength shows a tendency to increase from position 3 to position 1 in all castings techniques; in centrifugal casting the slope is bigger. (Figure 5.1); in all positions the increasing of ultimate tensile strength for the centrifugal casting process is about 42% when compared to gravity and 28% compared with vibrated gravity castings (Figure 5.1);

The tendencies of the strain to failure results shows the same increasing as for ultimate tensile strength from the position 3 to position 1 in all the casting technique studied. Only the difference is bigger: for example in position 1 is about 280% compared with gravity vibrated casting and about 300% compared with gravity casting (Figure 5.2).

The microstructure examination was made on the middle part of the position 1 of each casting. The microstructures for the different castings techniques (gravity, vibrated gravity and centrifugal) are shown in figure 5.3. In most regular binary eutectic alloys, primary phase of either the base or the alloying element is not expected to exist. As it can be seen in figure 5.3 a, b and c, the morphology of eutectic silicon was modified from a much dispersed coral-like form to a finely but non-uniformly distributed coral-like form and to a more finely and uniformly coral-like eutectic form when centrifugal casting was used.

The volume fraction of α-Al phase shows a decreasing tendency from position 3 to position 1 in all the studied cases (centrifugal, gravity and vibrated gravity casting) (Figure 5.4). The eutectic's volume fraction has an increasing tendency from position 3 to position 1 in all the studied cases (Figure 5.4). Making a comparison between the three casting method it can be seen that the amount of the eutectic volume fraction, considering the gravity casting volume fraction as a comparison value, it is increasing with about 14% for vibrated casting and approximately 20% for centrifugal casting in all three position.

Eutectic silicon lamellas are thinner from the exterior position to the interior position of the castings (from position 3 to position 1) in each casting technique studied. Among the three casting processes (gravity, vibrated gravity and centrifugal) the finest eutectic

silicon lamellas are obtained on centrifugal casting followed by vibrating and than by gravity casting (Figure 5.5).

Figures 5.6 and 5.7 present the solidification curves for the three casting techniques used, and at the two (down and front) temperature reading positions. It is observed that on the gravity and vibrating gravity castings the solidification curves have an expected shape with starting and ending solidification points well defined. On the centrifugal solidification curve these points are not well defined. The starting point and solidification interval in centrifugal casting is not possible to identify due to the constant liquid movement (fluid dynamics) that does not allow a directional solidification from mould wall to the inner part of the casting as happens in the other casting techniques (gravity and vibrating gravity casting).

On ‘down’ position the centrifugal temperature curve reach a maximum lower temperatures (as compared to the other techniques) because the first liquid to touch the bottom (hot metal) is spread very fast along the whole mould dispersing the heat transfer to the whole mould, instead of concentrating on the bottom of the mould as it happens in gravity and vibrating gravity casting.

Contrarily, in ‘front’ region the maximum temperature is higher than for the other processing techniques because the liquid hot metal that is being poured is continuously renewed in this position Figure 5.10.

Due to this turbulent fluid dynamics there is a distribution of the solidification germens promoting a faster solidification time with thinner microstructure (silicon lamellas), higher eutectic volume fraction, and consequently with better mechanical properties.

The dynamics of the fluids may be very different between gravity castings and centrifugal castings. In the simulation carried out for atmospheric gravity casting and castings with a pressure level similar to the one existing in centrifugal castings, it is observed that the pressure results in a more turbulent filling inside the mould Figure 5.10. Due to the pressure level the filing time is shorter on centrifugal casting. After analysing the solidification graphs different solidification points and solidification intervals are

obtained for gravity, vibrated gravity and centrifugal casting. The solidification starts faster in centrifugal casting then gravity and then vibrating gravity (Table 5.1). The turbulent behaviour of the melt during pouring is contribute not only to a faster filling of the mould in case of centrifugal casting but also to promote o faster solidification due to distribute evenly in the mould the nuclei of solidification (Figures 5.8-5.10).

In the same simulation it is also observed that pressure casting promotes a quicker and a more turbulent mould filling (Figure 5.10). In pressure casting the mould is filled in less than 0.4 s and takes about 2s to fill in gravity atmospheric castings. Turbulence will be the responsible for the more uniform distribution of the solidification germens (that arise from first contact with the mould walls) and consequently will create a different solidification pattern and faster solidification rate of the casting.

Table 5.1 – Starting solidification point and interval for gravity, vibrated gravity and centrifugal casting

Down			***Front***		
gravity	***vibrating gravity***	***centrifugal***	***gravity***	***vibrating gravity***	***centrifugal***
Starting Solidification Point (s)					
9.625	5	2.25	4.875	6.5	2.5
Solidification Interval (s)					
9.5	9.25	5.5	22.25	20	7.25

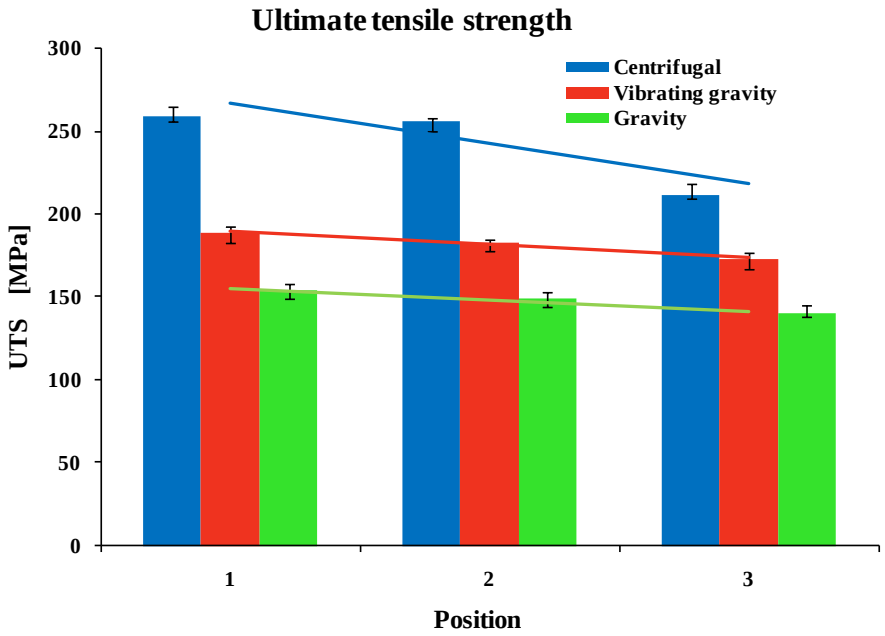

Figure 5.1 – Ultimate tensile strength for the three casting techniques: gravity; gravity with vibration; centrifugal casting.

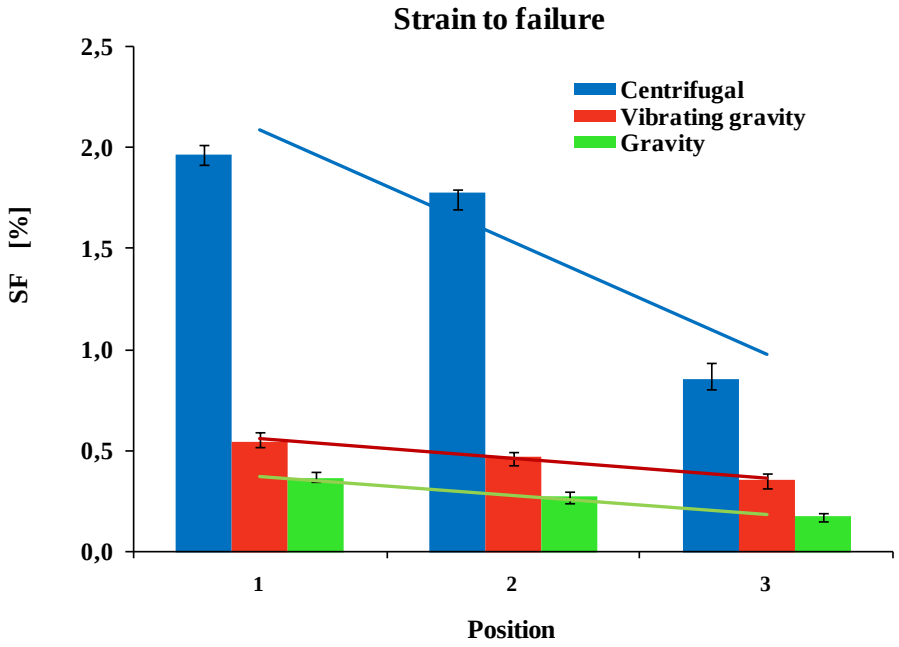

Figure 5.2 – Strain to failure for the three casting techniques: gravity; gravity with vibration; centrifugal casting.

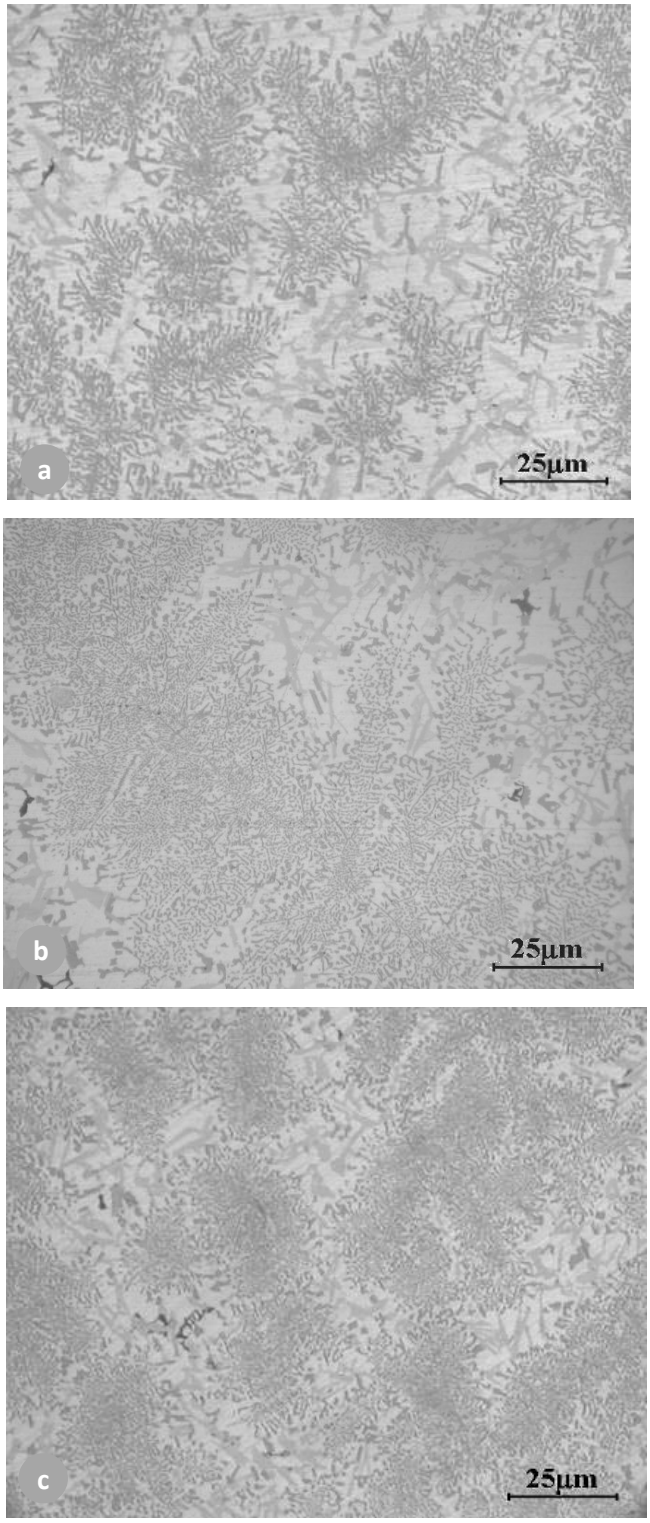

Figure 5.3 – Microstructures for the three casting techniques: a) gravity; b) gravity with vibration; c) centrifugal casting.

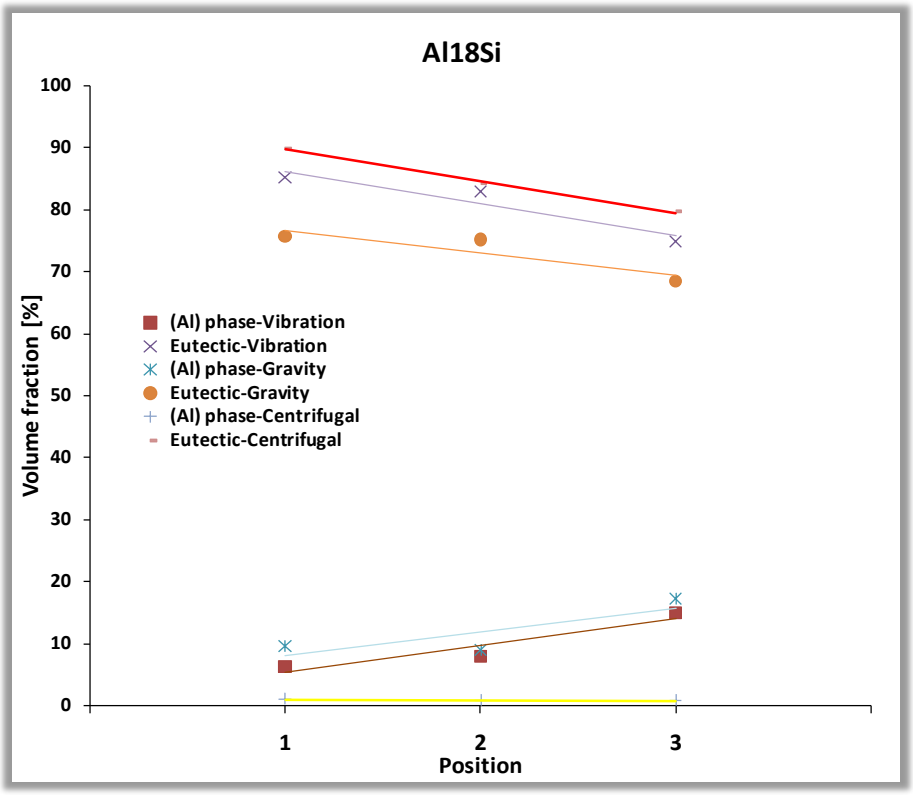

Figure 5.4 – Phases quantification for three casting techniques: gravity; gravity with vibration (8Hz); centrifugal casting.

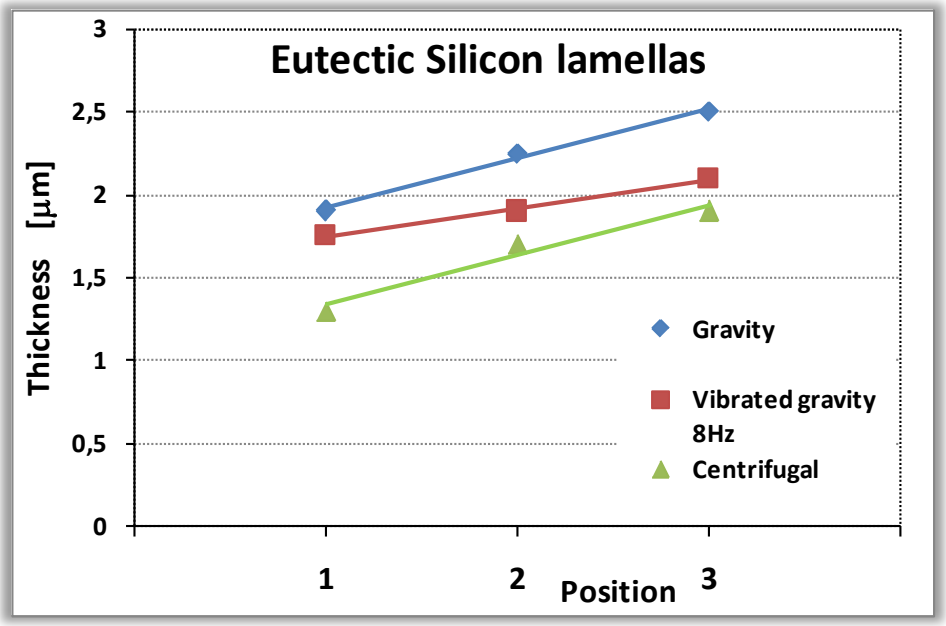

Figure 5.5 – Quantification of silicon lamellas thickness for the three casting techniques: gravity; gravity with vibration; centrifugal casting.

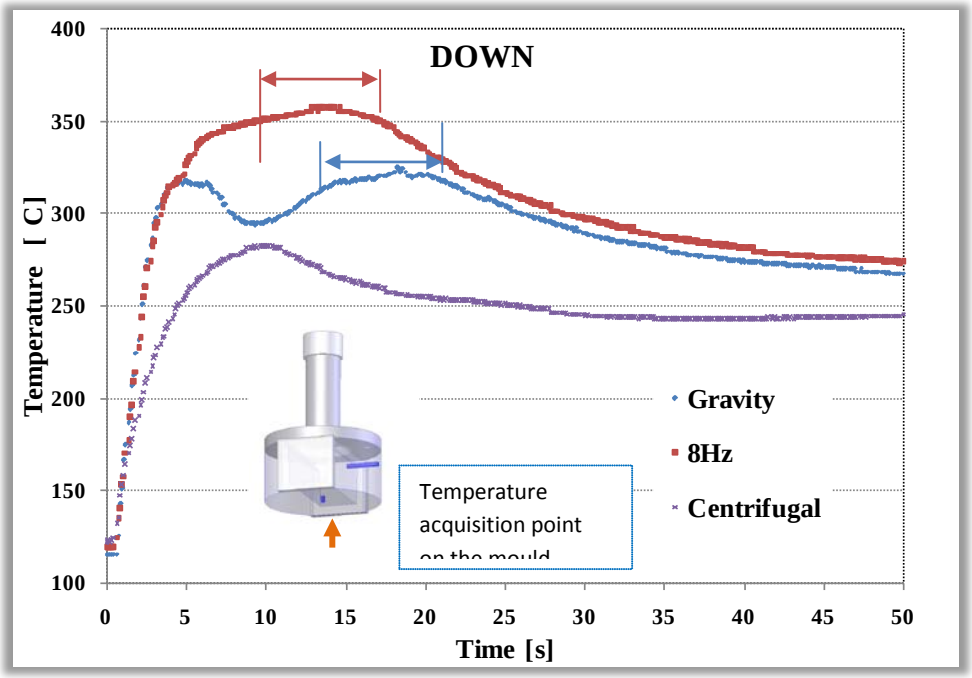

Figure 5.6 – Solidification curves for the studied casting techniques on the bottom of the mould

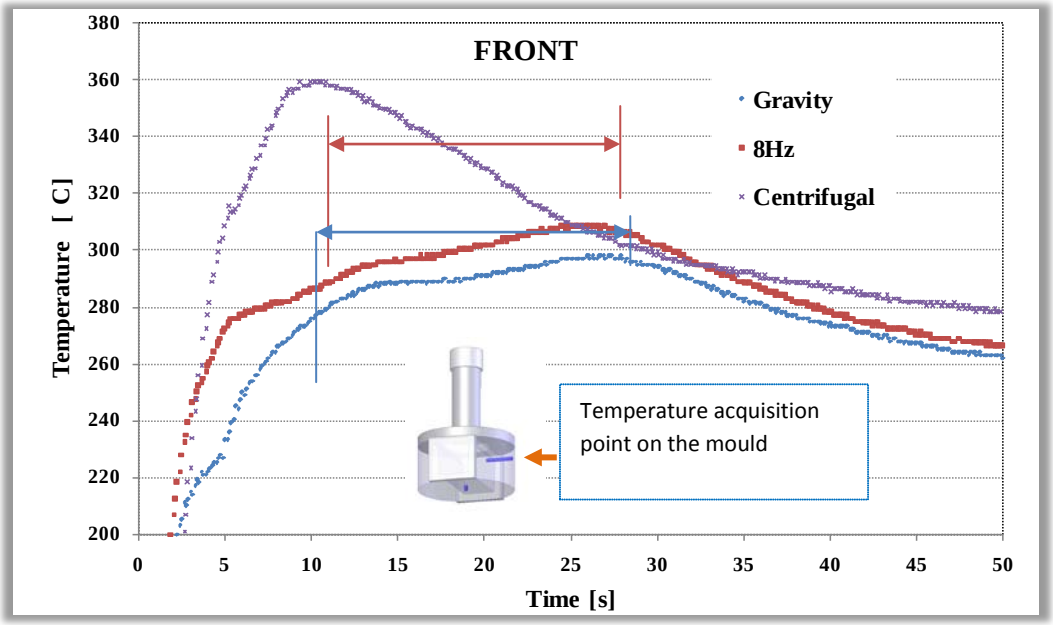

Figure 5.7 – Solidification curves for the studied casting techniques on the front of the mould

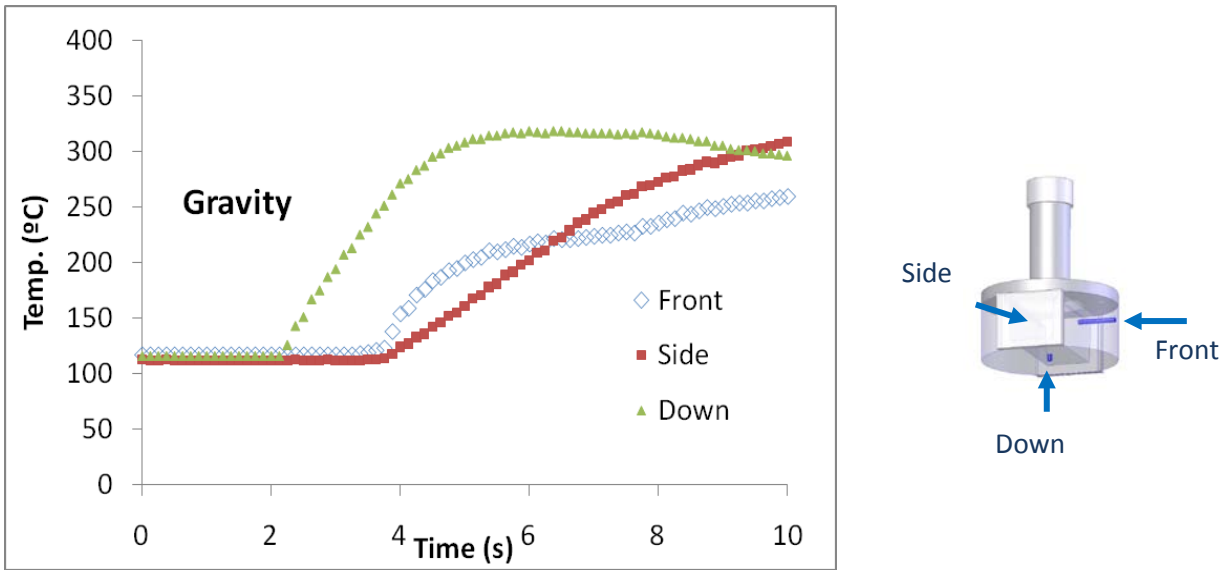

a) b)

Figure 5.8 – Temperature profile with time, for gravity casting a), in the different positions of the mould b).

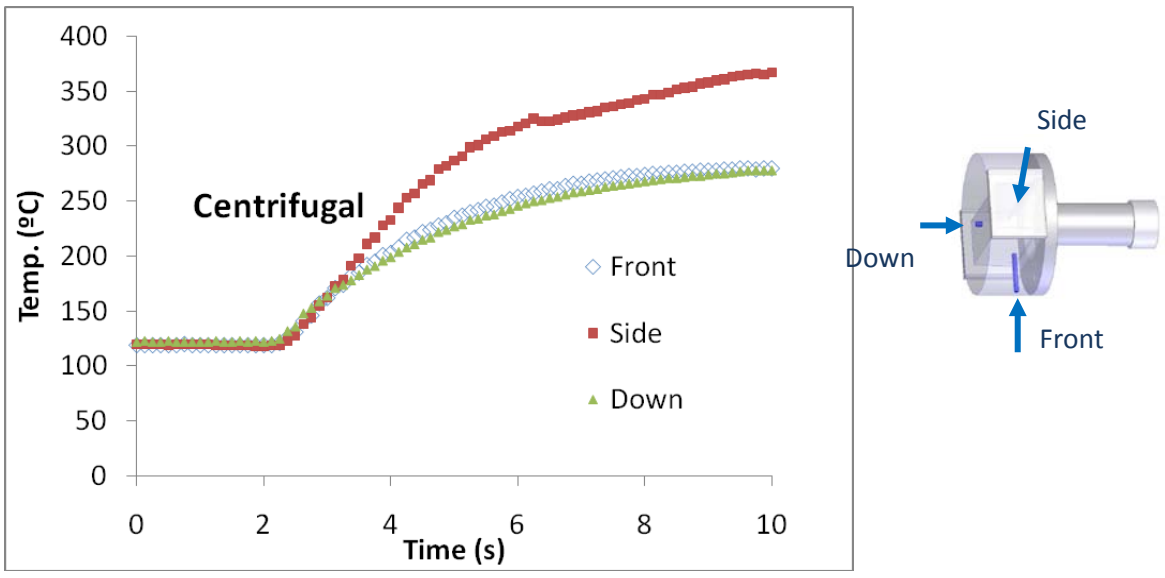

a) b)

Figure 5.9– Temperature profile with time, for centrifugal casting a), in the different positions of the mould b).

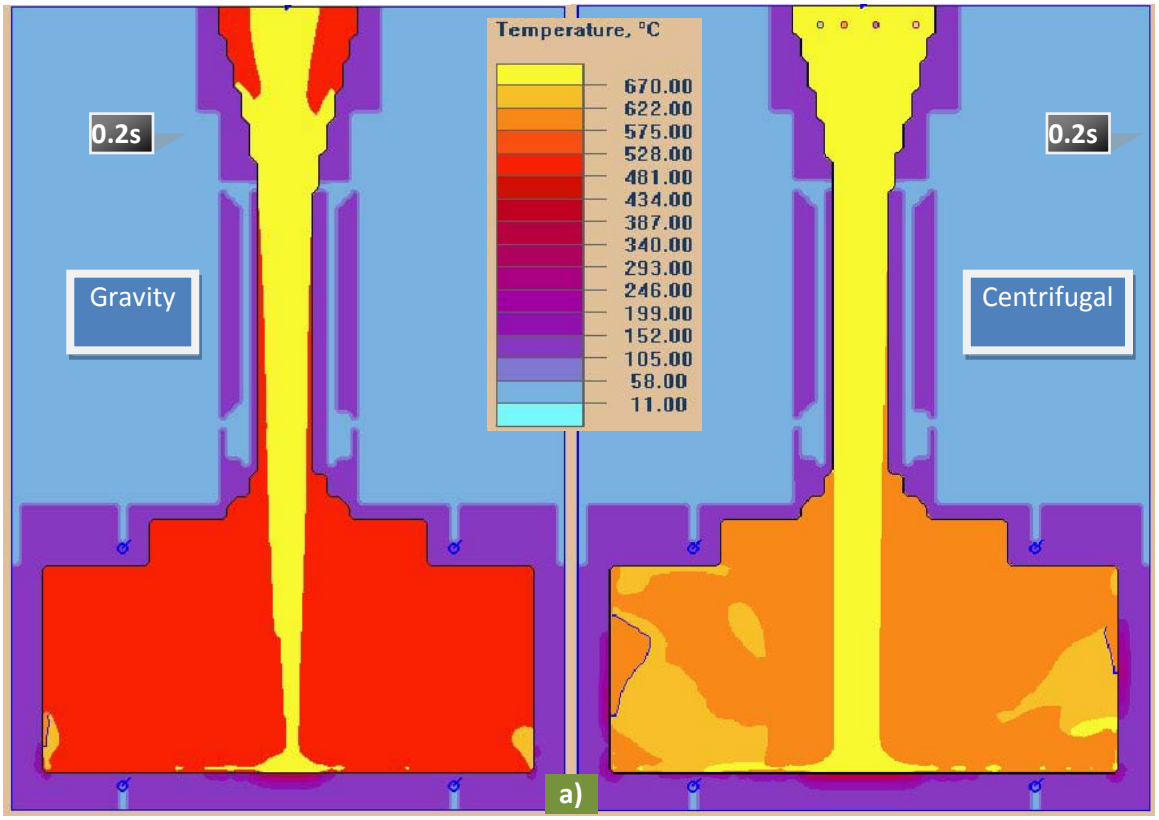
Temperature, °C
670.00
622.00
575.00
528.00
481.00
434.00
387.00
340.00
293.00
246.00
199.00
152.00
105.00
58.00
11.00
0.2s
0.2s
Gravity
Centrifugal
a)

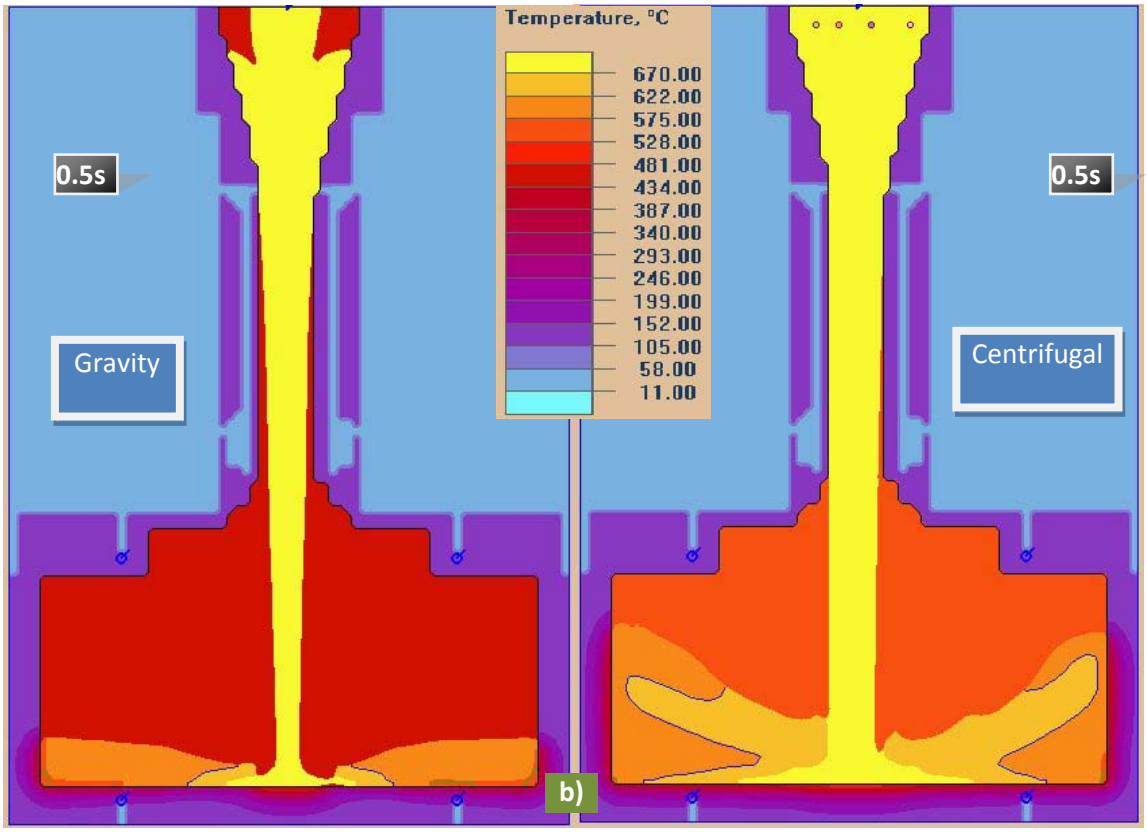
Temperature, °C
670.00
622.00
575.00
528.00
481.00
434.00
387.00
340.00
293.00
246.00
199.00
152.00
105.00
58.00
11.00
0.5s
0.5s
Gravity
Centrifugal
b)

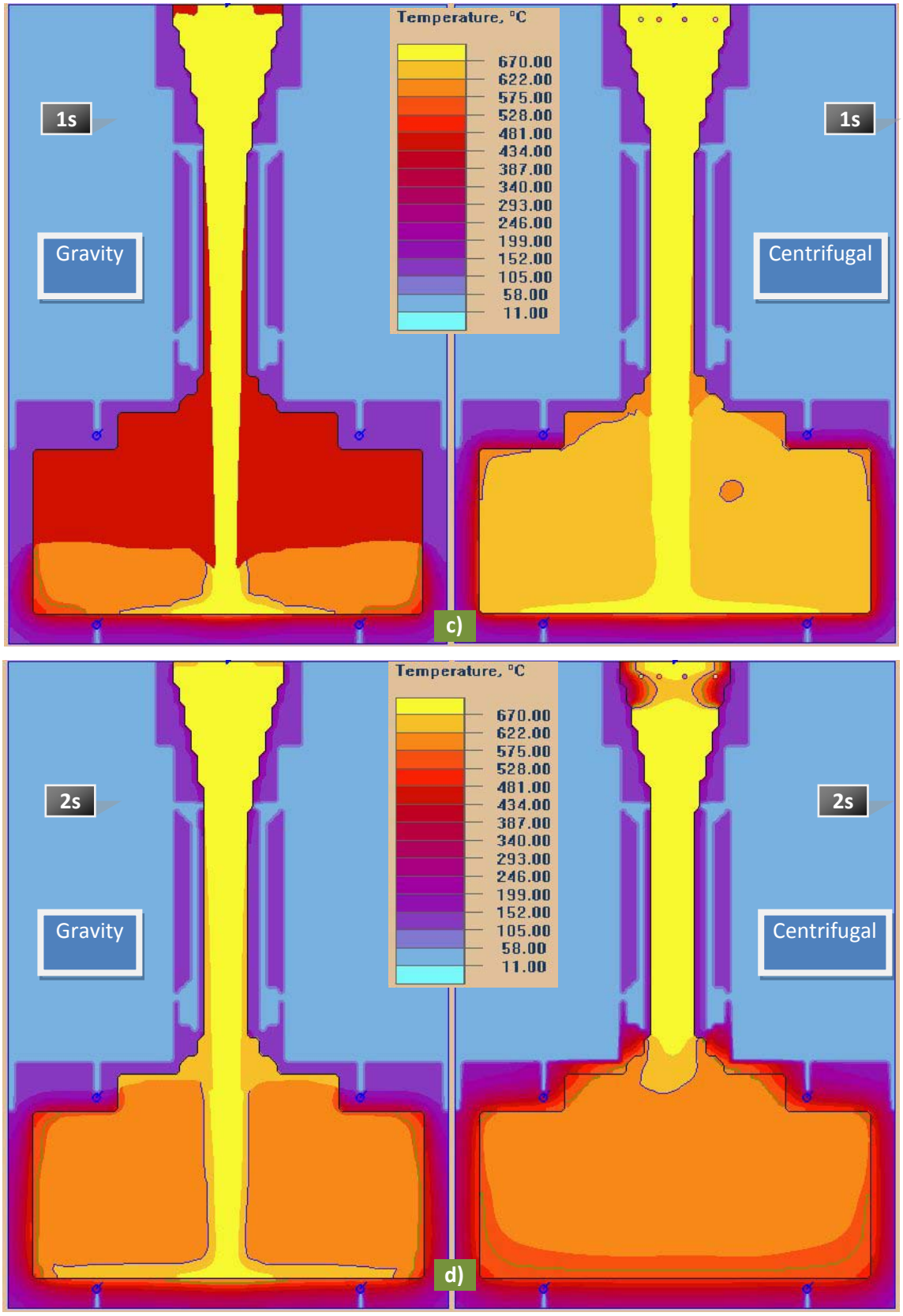

Figure 5.10 – Sequence of solidification simulation of gravity and centrifugal casting.

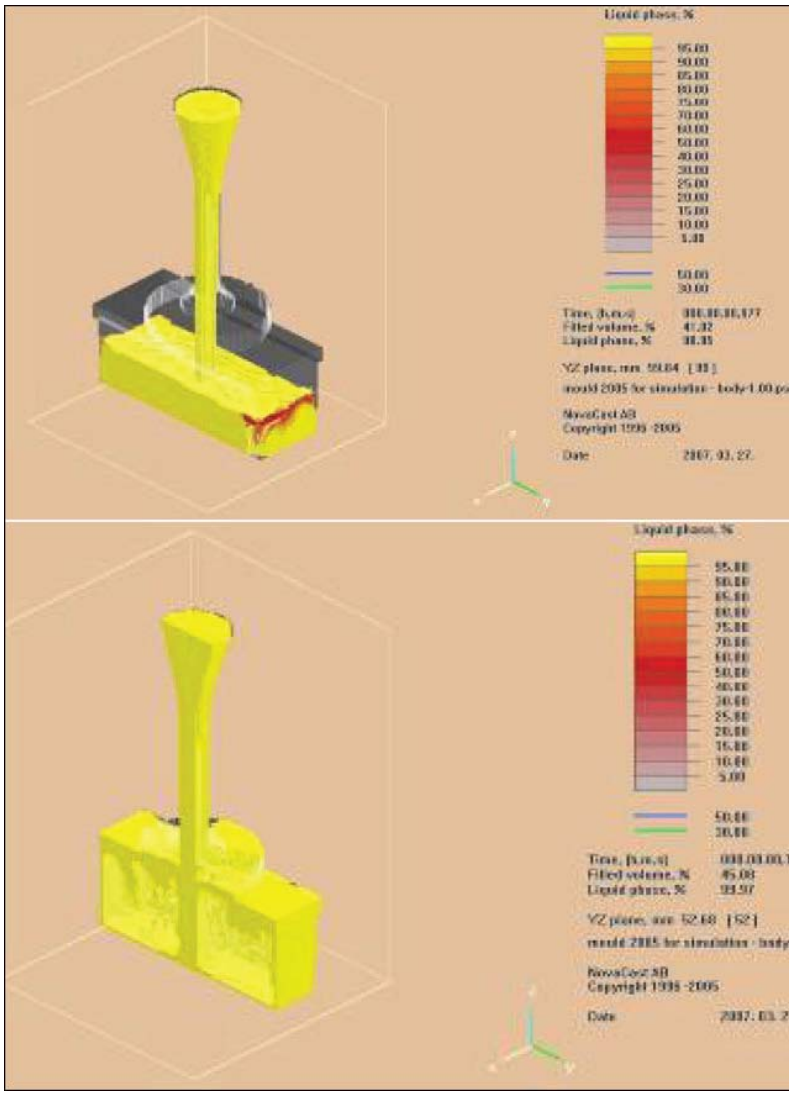

Figure 5.11 - Detail of filling of molten material on a gravity casting (time: 0.997 s) and casting with pressure (time: 0.192s)

5.2. The study of influence of vibration on the solidification behaviour and tensile properties of Al-18Si alloy

Has been observed with several types of metals, e.g. zinc, brass, aluminium that vibration is able to improve mechanical properties. The influence of vibration on mechanical properties is essentially based on amplitude and frequency. The main effects include: promotion of nucleation and thus reducing as-cast grain size; reduction of shrinkage porosities due to improve metal feeding; and production of a more homogenous metal structure.

In the present study, mechanical mould vibration were applied to an Al–Si hypereutectic alloy at a fixed amplitude of 0,5 mm and frequencies of 0 Hz, 8 Hz, and 24Hz. Tensile tests were done on specimens obtained with the different vibrating frequency levels. Experimental results show that mechanical properties were influenced by the level of applied frequency. The tensile strength was improved in 31% on lower frequency (8 Hz) and decreased in about 13% in the case of higher frequency used (24 Hz) as compared with the values of tensile strength of the specimens obtained with no vibration. A microstructure analysis, in particular a quantification of present phases was done, and correlated with the mechanical results.

The solidification curves of the vibrating gravity with 8 Hz show maximum temperatures (as compared to the other techniques) in both positions of the moulds (down and front – Figures 5.12 and 5.13) because the heat transfers in the liquid and on the interface liquid-mould is bigger. Bigger heat transfer is also observed in the 24Hz vibrating gravity solidification curve but less of heat transfer in the interface liquid-mould. As a matter a fact the wall 2 is more affected by the vibration effect than walls 1 and 3 (Figure 5.14).

Because the solidification starts faster in the 8Hz vibrating gravity and the interval of the solidification is shorter (Table 5.2), the volume fraction of eutectic is higher (Figure 5.17), the eutectic silicon lamellas are smaller (Figure 5.14), the microstructure is thinner (Figure 5.18) compared with 0Hz and 24Hz and lead to better mechanical properties (Figure 5.15 and 5.16).

Ultimate tensile strength results (Figure 5.15) show a clear tendency of increasing from position 3 to position 1 in the case of vibrated gravity with 8 Hz and 0 Hz but with no tendency on vibrated gravity with 24Hz. The ultimate tensile strength show higher values with about 31% for the vibrated gravity process with 8Hz in any position then gravity castings which also has higher values (≈13%) in all three positions compared with vibrated gravity with 24Hz.

Strain to failure results (Figure 5.16) show a tendency of increasing from position 3 to position 1 in all the studied cases with different slopes. The strain to failure is much higher (≈95%) for the vibrated gravity process with 8Hz in any position then vibrated gravity with 8Hz and 0Hz.

The volume fraction of α-Al phase shows a decreasing tendency from position 3 to position 1 in all the studied cases (0Hz, 8Hz and 24Hz) (Figure 5.17). An opposite behaviour show the eutectic's volume fraction which has an increasing tendency from position 3 to position 1 in all the studied cases (Figure 5.17). Considering the 0Hz frequencies as a comparison value, it is noticeable the fact that the amount of eutectic for the 8Hz is increasing with about 11% in all three positions and decreasing with about 8% for the 24 Hz.

The microstructure examination was made on the middle part of the position 1 of each casting. The microstructures for the different cases of vibrated castings (0Hz, 8Hz and 24Hz frequency) are shown in figure 5.19. In most regular binary eutectic alloys, primary phase of either the base or the alloying element is not expected to exist. As it can be seen in figure 5.19 the morphology of eutectic silicon was modified from a dispersed coral like form to a more finely and nested coral like form and to a coarse acicular plate-like form with less coral like eutectic form when mechanical vibration with 24Hz frequency was used. However, the most significant differences are the amount of eutectic that increases for 8Hz and decreases for 24 Hz, and a finer structure for 8Hz and courser structure for 24 Hz.

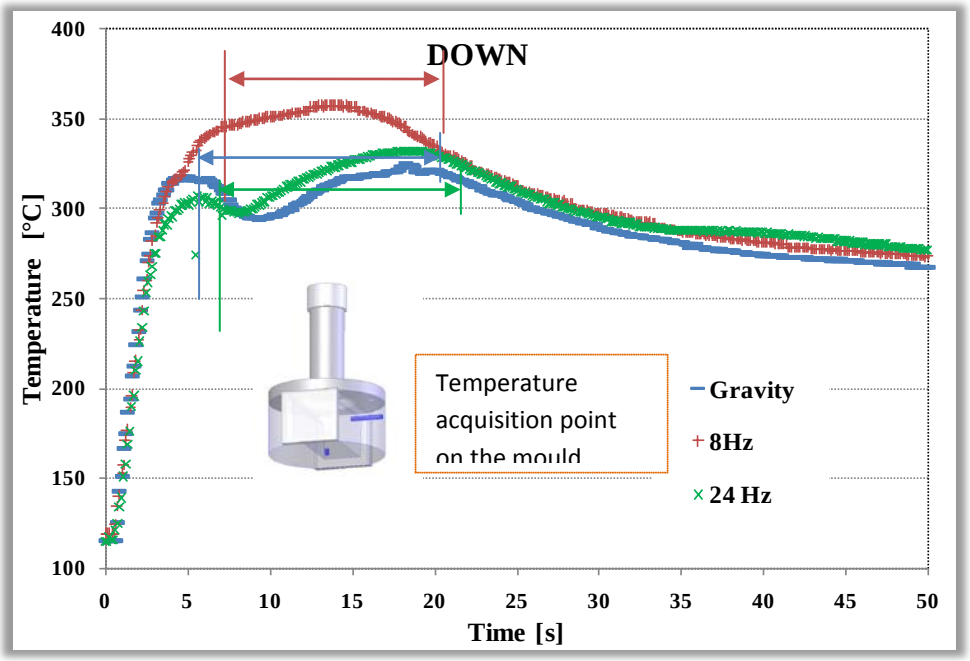

Figure 5.12 – Solidification curves for the studied casting techniques on the bottom of the mould

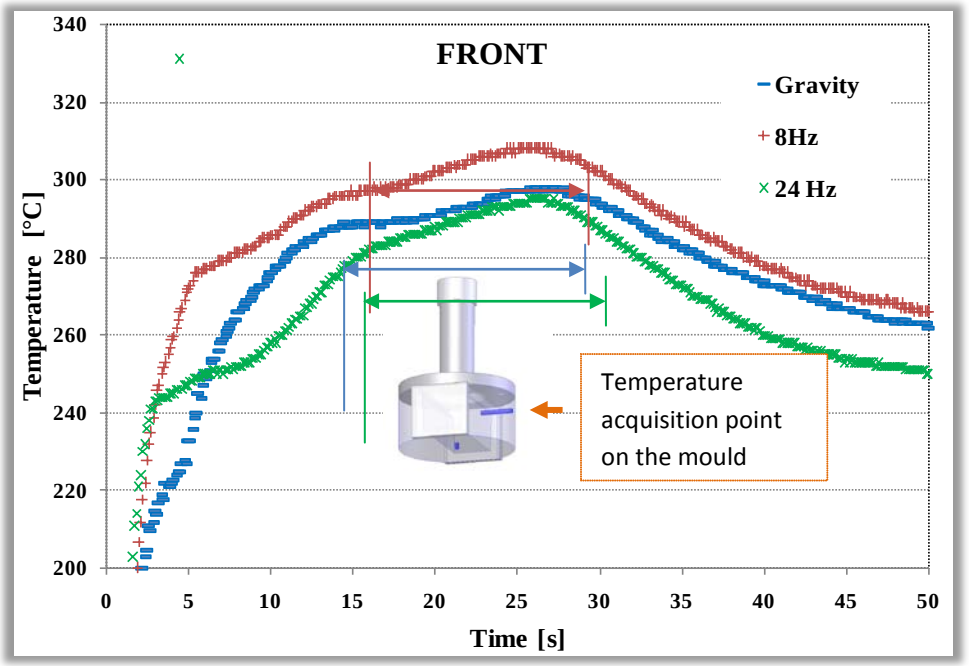

Figure 5.13 – Solidification curves for the studied casting techniques on the front of the mould

Table 5.2 – Starting solidification point and interval for gravity, vibrated gravity and centrifugal casting

Down			*Front*		
grav.	*8Hz*	*24Hz*	*grav.*	*8Hz*	*24Hz*
Starting Solidification Point (s)					
9,625	5	8.5	4,875	6,5	3.876
Solidification Interval (s)					
9,5	9,25	10.5	22,25	20	22.75

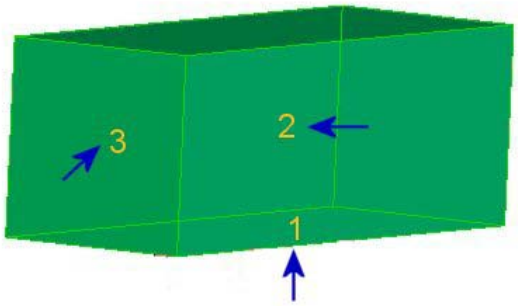

Figure 5.14 – Thermocouples insertion position on the mould

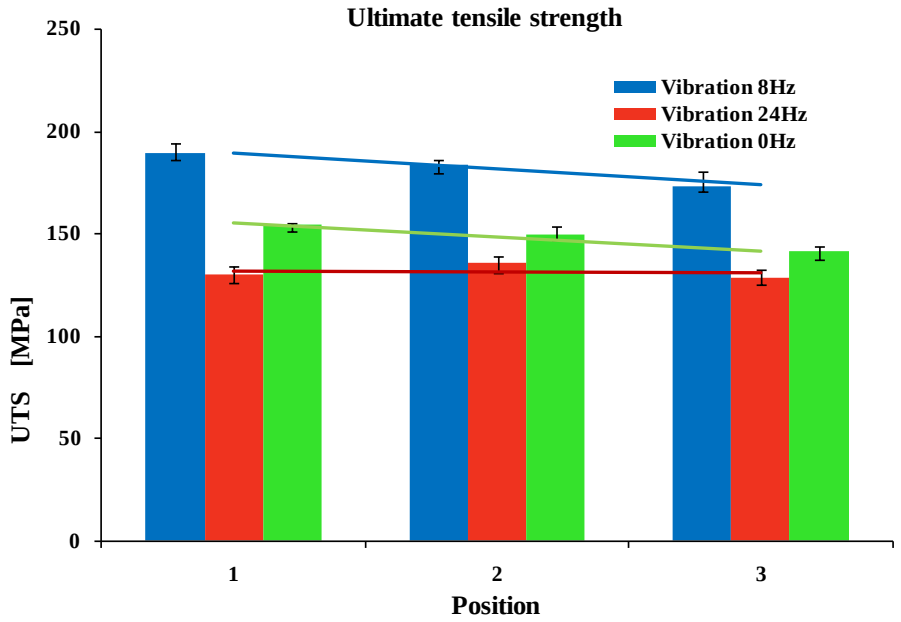

Figure 5.15 – Ultimate tensile strength for the three vibration level casting: 0Hz; 8Hz and 24 Hz.

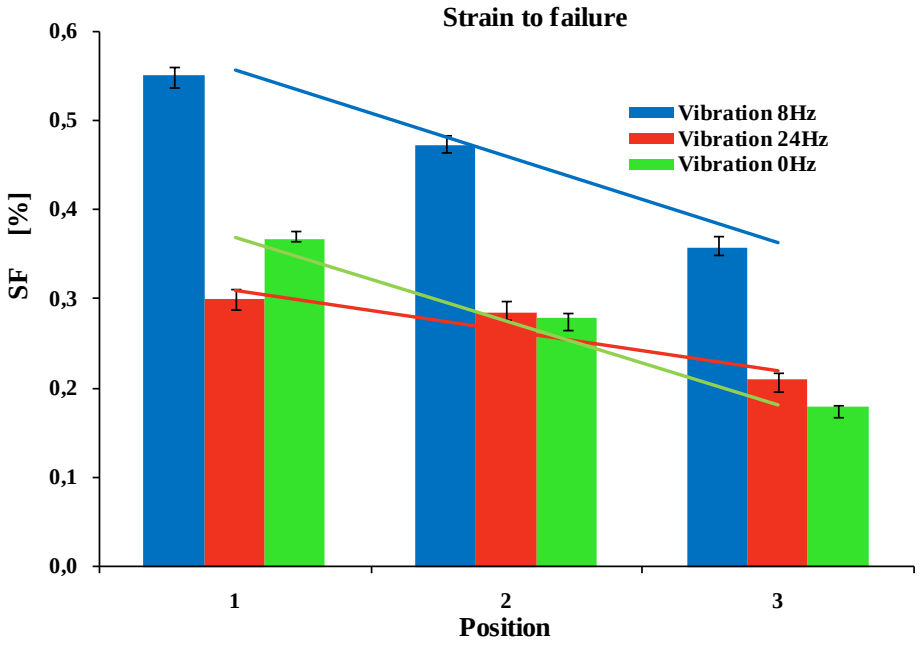

Figure 5.16 – Strain to failure for the three vibration level casting: 0Hz; 8Hz and 24 Hz.

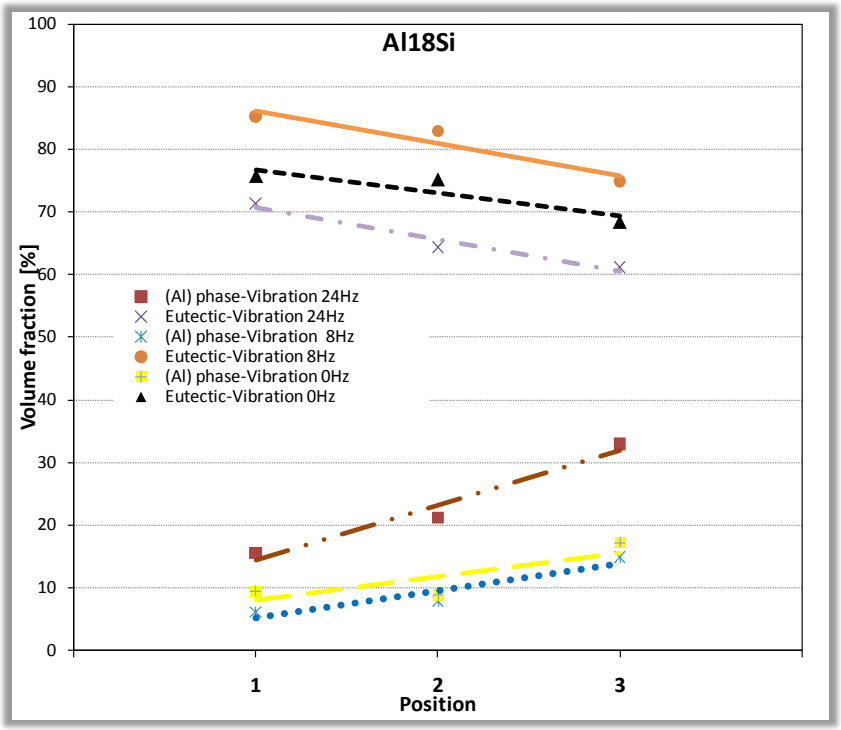

Figure 5.17 – Quantification of phases for the three vibration level casting: 0Hz; 8Hz and 24 Hz.

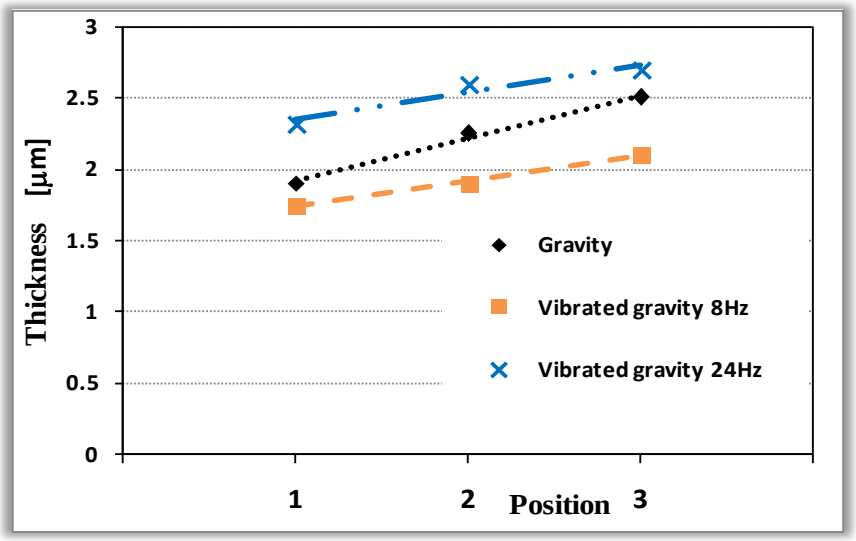

Figure 5.18 – Quantification of silicon lamellas thickness for three vibration level casting: 0Hz; 8Hz and 24 Hz.

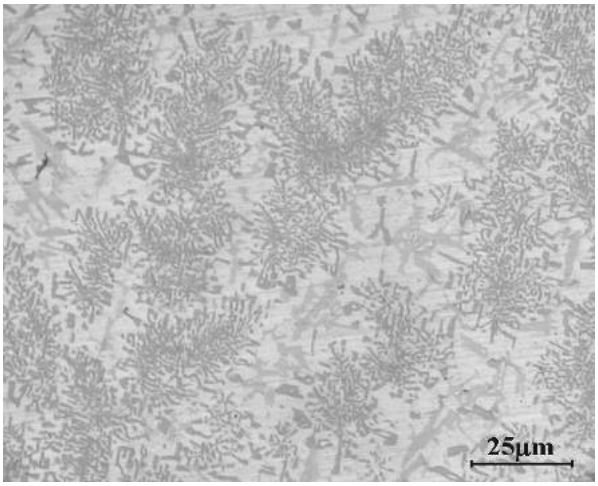

0Hz

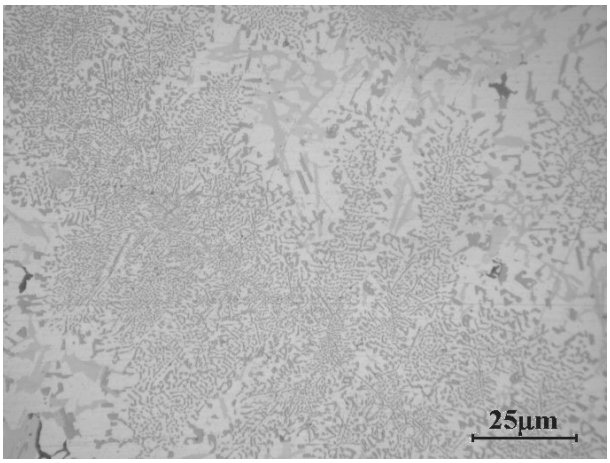

8Hz

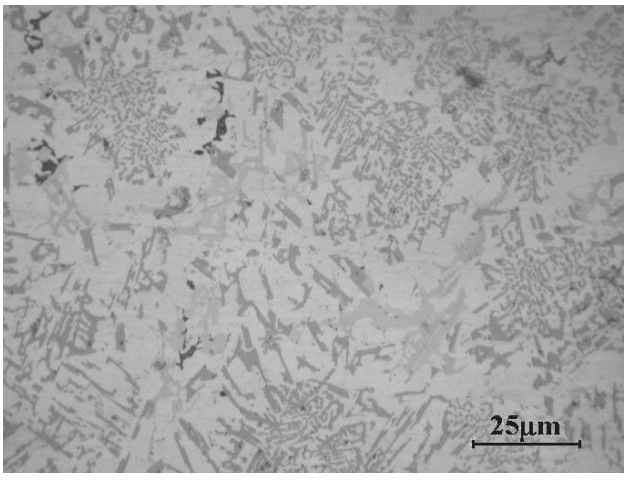

24Hz

Figure 5.19 – Microstructures for the three vibrations level casting: 0Hz; 8Hz and 24 Hz.

5.3. Discussion

5.3.1 Assessment of processing variables in vertical centrifugal casting technique

From the literature review, it could be stated that the centrifugal effect on the mechanical properties and microstructure of cast samples is not yet very well understood by the scientific community [16]. In order to better understand the centrifugal effect on castings this study focused its analysis in three main features: centrifugal pressure, intrinsic vibration of the process and fluid dynamics. The effect on mechanical properties of each of these variables will be subsequently discussed.

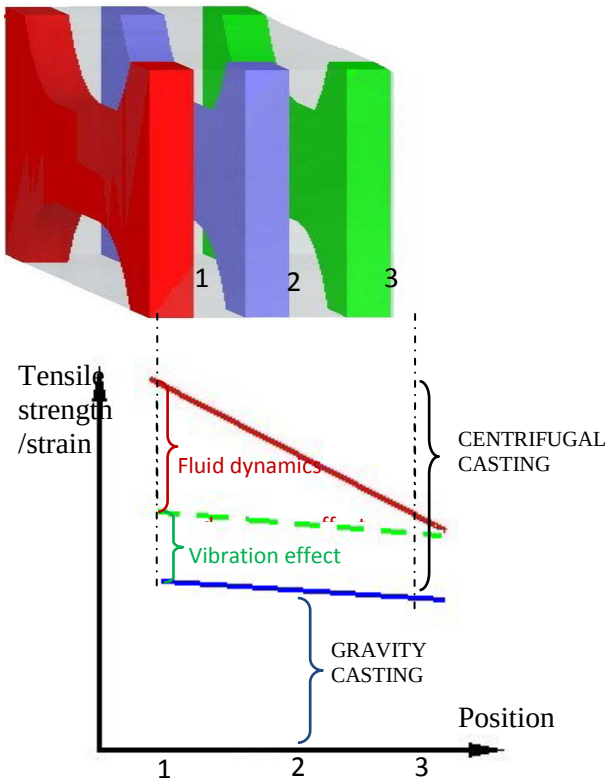

Figure 5.20 - Schematically representation of the main centrifugal effects.

Centrifugal pressure

The centrifugal pressure exerted over a certain region of a centrifugally cast sample during rotation depends on some variables, namely the angular speed, the distance from the mould cavity to the rotation axis, the quantity of poured material, the geometry of the sample and its position in the mould. For the specific case used in this study the pressure level is about 2 to 4 MPa. It is known that in squeeze casting pressure significantly improves the mechanical properties of the castings [37]. This improvement is attributed to the shift of the solidification diagram and to the reduction on microporosities.

However, in order to promote a shift in the solidification diagram a high pressure level would be needed, as it happens in squeeze casting where pressures may reach 50–200 MPa. In centrifugal casting the pressure is much lower when compared with the pressures used on squeeze casting (more than an order of magnitude lower), so it is expected and assumed that the low pressures on the centrifugal casting technique are not able to shift the solidification diagram.

On a previous study [33], it was observed that the microporosity level did not change significantly due to centrifugal pressure for the materials used in this study. It was also observed that in these alloys pressure does not promote a displacement of more dense solid phases along the direction of the centrifugal force [33]. Thus, if the centrifugal pressure does not seem to have any effect on mechanical and metallurgical properties, it must have been the melt fluid dynamics and the inherent vibration of the system those factors responsible for registered substantial changes.

The centrifugal effect seems to influence more the hypereutectic alloy: the silicon particle phase is more refined (Figure 5.3) compared to gravity case. This happens because as it was expose on chapter 2, on hypereutectic the first phase to solidify is the silicon phase but due to rapid cooling are not allowed to grow as much as in the gravity case.

Vibration

The vibration effect was assessed by introducing a linear vibrating movement, similar to the one measured on the centrifugal casting machine, on gravity casting. It was observed that it has a beneficial effect (Figures 5.1 and 5.2) on mechanical properties (an increase of about 20% on Ultimate tensile strength and about 40% on rupture strain),

when compared to gravity casting. It was also observed that the vibration effect also influences the microstructure (Figure 5.3) increasing the eutectic silicon volume fraction and reducing the eutectic lamellas thickness.

These effects are those that would be expected from a higher solidification rate [192]. As a fact, it can be seen from the solidification curves shown in Figure 5.6 and the results presented in Table 5.2 that a difference exists on the solidification behaviour between castings with and without vibration.

In gravity casting with vibration the solidification starts first and the solidification interval is shorter (Figure 5.6 and Table 5.2) if compared with simple gravity casting. This difference in the solidification pattern seems to be the responsible for the reduction of the silicon lamellas thickness (Figure 5.5) and the increase in the eutectic volume fraction (Figure 5.4). The mechanism that promotes the faster solidification behaviour due to vibration is that there exists an internal movement of the melt that promotes a quicker heat transfer inside the melt and to the mould, probably as a result of the elimination of the usually existing gap at the metal/mould interface, thus improving the metal–mould contact and the heat transfer rate. This vibration effect may also be attributed to a faster distribution of solidification germens inside the melt due to internal melt movement.

In general, the vibration effect is in accordance with most of the existing studies [99-101] which state that it improves the mechanical properties of the materials. However, a deeper study on the influence of the vibration effect under different acceleration values is provided in ref. [193]. In that study the mechanisms under which external vibration promotes higher or lower mechanical properties and the related mechanisms are presented.

Fluid Dynamics

The fluid dynamics may be very different between gravity castings and centrifugal castings The experimental solidification curves at the bottom of the casting/mould (Figure 5.6) show that for the three casting techniques used on this research, the gravity and vibrating gravity castings present an expected shape with starting and ending solidification points well defined. However, in the centrifugal solidification curve those points are not clearly defined. This is probably due to the constant liquid movement (see

fluid dynamics simulation shown in Figure 5.10) that does not allow a directional solidification from the mould wall to the inner part of the casting as it happens in the other casting techniques (gravity and vibrating gravity casting). On the other hand, the maximum attained temperature is lower than in the other curves because the first liquid to touch the bottom (hot metal) is spread very fast along the whole mould dispersing the heat transfer to the whole mould, instead of concentrating on the bottom as it happens in gravity and vibrating gravity casting. This is why the maximum temperature at the front part of the mould is now higher for centrifugal casting then for gravity and gravity with vibration casting (see Figure 5.7). This is also explained by the simulation in Figure 5.10.

While the gravity casting fills the mould from bottom to top in the pressure casting the metal is spread by the whole mould and it is filled from the walls to the inside of casting. In the same simulation, it is also observed that pressure casting promotes a quicker and a more turbulent mould filling (Figure 5.11). In pressure casting the mould is filled in less than 0.4 s and takes about 2 s to fill in gravity atmospheric castings. Turbulence will be the responsible for the more uniform distribution of the solidification germens (that arise from first contact with the mould walls) and consequently will create a different solidification pattern and faster solidification rate of the casting.

Due to this turbulent fluid dynamics there is a distribution of the solidification germens promoting a faster solidification time with thinner microstructure (silicon lamellas), higher eutectic volume fraction, and consequently with better mechanical properties.

This is in accordance with reference [107] where it is stated that in centrifugal castings the first melt that reaches the wall surface (bottom) of the mould (where the first germens of solidification appear) will came backwards to the side parts of the casting creating a fluid dynamics flow all around the casting. Furthermore, in the present study, the faster solidification rate will lead to a thinner microstructure (silicon lamellas), higher eutectic volume fraction, and consequently better mechanical properties. The difference between centrifugal and gravity casting techniques in what concerns the ultimate tensile strength and strain to failure is about 20 and 500% respectively.

It is worth to note that the results of centrifugal casting include the effect of the inherent vibration of the mould. Thus, as schematically shown in Figure 5.20, the centrifugal effect on mechanical properties (ultimate tensile strength and strain to failure)

can be understood as a sum of the vibration effect and the fluid dynamics effect. Starting from the gravity castings properties (blue line), the properties increase to the green line if the vibration effect is added, and increase again to the red line if the fluid dynamics is also added.

5.3.2. Influence of vibration on the solidification behaviour and tensile properties of Al-18Si alloy

Mechanical results depend on metallurgical features which itself depend on the solidification behaviour. Starting from the obtained solidification curves it is clear that the 8 Hz test is the one that starts and completely solidify first (and also has the smaller solidification interval) (Table 5.2). Thus a thinner microstructure in these castings (Figures 5.18 and 5.19), a higher amount of eutectic (Figure 5.17) [194] and, as a consequence, better mechanical properties (both ultimate tensile strength and rupture strain) are expected (Figures 5.15 and 5.16).

Regarding the comparison between 0 and 24 Hz, the results provide the same reasoning: 24 Hz is the one that takes longer time to solidify (Table 5.2), has the coarsest microstructure (Figures 5.18 and 5.19), has the lowest amount of eutectic (Figure 5.17), and consequently has the poorer mechanical results, in particular tensile strength (Figures 5.15 and 5.16). Thus, there is a perfect correlation between solidification behaviour, microstructure, and mechanical properties.

These results are basically in accordance with refs [26, 99], and [194]. Furthermore a peak shift in mechanical properties, after a certain frequency (acceleration), as reported in [26] is also observed. The differences between positions 1 and 3 are explained by the distance to the mould wall and by the consequent solidification behaviour. The material in position 1 solidifies first and then has the thinner microstructure (Figure 5.18), has the higher amount of eutectic phase (Figure 5.17), and consequently has the better mechanical properties (Figures. 5.15 and 5.16), among all positions. Position 3 obviously has the lower properties.

The main aspect is therefore to find an explanation that may provide a physical explanation for the phenomena of the mechanical properties shifting point with vibration

level. These results may be explained based on the heat-transfer mechanisms both in the liquid phase and in the mould wall interface.

The proposed mechanism is schematically provided in Figure 5.21, and is as follows:

- In the case of 0 Hz casting, there is a 'normal' contact between liquid metal and mould. The heat transfer is 'normal' and the solidification rate has a certain value giving rise to a determined microstructure;

- In the case of 8 Hz the vibration induces a higher heat transfer to the mould (higher cooling rate) due to the alternated movement of the liquid (see Figures. 5.12 and 5.13 with higher initial solidification temperatures in the mould). Furthermore, this movement may also provide displacement of the germen solidification sites providing a higher solidification rate. The contact between liquid metal and mould is about the same as for the 0 Hz case. However, as the heat convection in the liquid phase is improved by the vibration movements, the liquid temperature near the interface is higher which explains the higher temperatures in the mould obtained in the cooling curves for these experiments (Figures. 5.12 and 5.13). The lower cooling times (Table 5.2) resulted from the faster liquid cooling rate and the improved nucleation characteristics by germen distribution in the liquid. The consequence is that the microstructure is thinner (see Figures. 5.18 and 5.19) and the amount of eutectic is higher (see Figure 5.17). Consequently ultimate tensile strength and strain to failure increase (see Figures. 5.15 and 5.16);

- In the case of 24 Hz, the vibration should induce even a higher heat transfer inside the liquid to the mould interface due to the quicker alternated movement of the liquid. However, the relative acceleration between liquid metal and mould seems to be high enough in order to create a loss of contact (low pressure zones in the interface liquid metal and mould) (in front position) and even eventually low pressure bubbles as those originated in cavitations. This situation occurs when the surface tension (liquid–mould wall) is not low enough in order to keep the surface contact when high acceleration rates (frequency * amplitude) exist. A loss of contact means to switch the heat transfer mode from totally conductive to a conductive + convective transfer in the interface. Because the convective heat transfer is much lower than the conductive heat transfer, the heat transfer and consequent solidification rate substantially decrease (see mainly Figure 5.13 with lower initial solidification temperature in the mould). The consequence is a courser microstructure (see Figures. 5.18 and 5.19) and a lower eutectic content (see Figure 5.17).

Mechanical properties should then decrease (this is particularly evident for rupture strength) (Figures. 5.15 and 5.16).

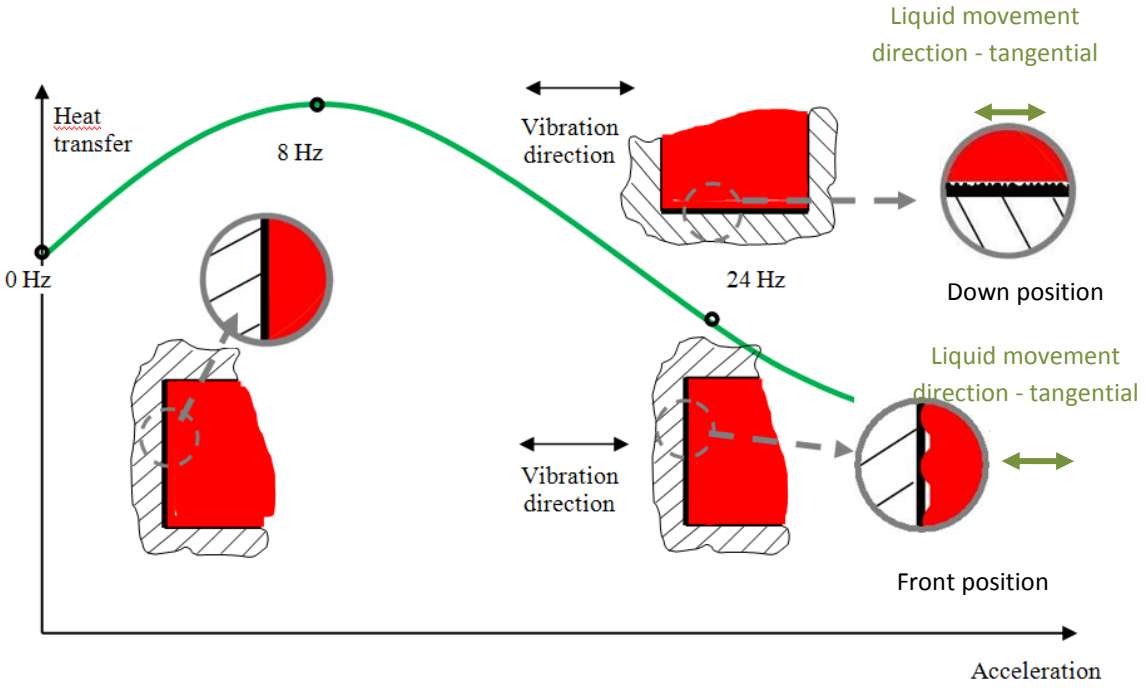

Figure 5.21 – Heat transfer representation.

Although with the same consequence, a different mechanism in the down position may occur. There is a loss of contact due to the tangential movement of the liquid (in front position there is a normal contact – see Figures. 3.3 and 5.14 with vibration direction and temperature readings/walls positions and details in Figure 5.20). This loss of contact is due to the liquid movement and roughness effect (for details see Figure 5.21).

This means that vibration can be beneficial as well as detrimental depending on the acceleration level between liquid metal and microstructure and surface tension of the liquid metal and mould material. This may be the reason why some papers attribute to vibration beneficial effects and others to detrimental effects on properties.

CHAPTER 6

DISCUSSION

6.1. Metallurgical Analysis

6.1.1. Chemical composition

It is clear on figures 5.14, 5.24 and 5.35 that the chemical composition of the ingots (Al and Si contents) in different positions (1, 2, and 3) of the three alloys is not substantially influenced by the casting process. Only alloy C shows a slight difference on the Si and on the Al content between the gravity and centrifugal castings in position 3 of the ingots. Thus, there is no significant displacement of Al or Si from the inner to the outer positions of the ingot due to the centrifugal effect or due to the gravity force. This displacement is common for materials with phases and/or chemical elements with different densities such as tin bronzes (the density of lead is higher than the density of copper – 11.3 vs 8.9 g/cm3) as presented by Halvae A.[35]. For Al-Si alloys this effect is not significant (Si and Al densities are similar - the density of Si is 2.34 g/cm^3 and the density of aluminium is 2.7 g/cm^3).

Because no significant difference on the chemical composition of samples was found among positions 1 to 3 it can be concluded that changes on mechanical properties are not due to chemical composition variation along the ingots but are dependent on constituent's volume fraction and morphology as will be presented subsequently.

6.1.2. Constituent's volume fraction

Many researchers already tried to establish relationships between some characteristics of constituents and mechanical properties in Al alloys.

Among those, perhaps the SDAS is the most studied. The secondary dendrite arm spacing (SDAS) versus tensile properties is discussed on reference [27] on A356 and A357 (ASTM) aluminium alloys. It was found that ultimate tensile strength decreases with SDAS. The same correlation was found for ultimate tensile strength and ductility on a sand cast A356-T6 obtained by hot isostatic pressing [126] and on an Al-7%Si-Mg alloys [148]. On this last reference the yield strength was found to be less influenced by the SDAS. Regarding other constituents, reference [74] provides a correlation of the amount of dendritic α-Al phase with ultimate tensile strength - UTS and strain to failure. However in this case the increase of UTS and strain to failure was also accompanied by a grain (SDAS) refinement. Thus it is not clear which feature - dendritic α-Al phase or SDAS refinement, caused the increase in properties. In another study, an increase in the strain to failure was attributed to the increase in the amount of eutectic in a 12,5% Si aluminium alloy [103].

Among the different previous studies, the one by Abu-Dheir [103] is the one where the results are similar to those obtained in present study. As a fact, in the present study, although there is also a grain refinement with increase in Si content (7% to 18%) and a change in shape of eutectic phase, particles in 7%, lamellas in 12% and coral-like form in 18%, it is clear that with the increase in amount of eutectic both UTS and strain to failure increase.

It is important to highlight that in most of the studies in which a correlation between mechanical properties and metallurgical features was tried, only one alloy was analysed. In the present study it is intended the establishment of a correlation that can be suitable for, at least, different grades of class of aluminium alloys (Al-Si alloys – series 4000) and for different casting processes. As a consequence it is tried a relation between a common denominators in all studied commercial Al-Si alloys. As can be seen in figures 4.15-4.19, 4.24-4.30 and 4.35-4.40 and tables 4.1, 4.2 and 4.3 the alloys are very different both in constituents as well as in morphology of the constituents: 7%Si alloy does not have intermetallics, the α-Al phase has the form of dendrites, and the eutectic constituent has

essentially a particle shape; the 12 % alloy has some intermetallics, the α-Al phase has also the form of dendrites, the silicon is present in the form of lamellar eutectic but also in the form of particles; finally in the 18% Si alloy there is some isolated α-Al phase, there is some intermetalics, and the silicon is essentially in an eutectic phase as coral-like morphology or primary silicon as particle.

However, although the substantial difference in terms of constituents and its morphology in the different alloys it was verified that there are common variations of mechanical properties evolution with some constituents, namely with eutectic volume fraction. Figures 4.15, 4.25, and 4.36 show this evolution. It is clear the qualitative match between eutectic volume fraction and mechanical properties for all three alloys. It is observed in tables 4.1, 4.2 and 4.3 and figure 4.9 that porosity is low and maximum equivalent diameter has comparable values (between gravity and centrifugal casting for each alloy type studied) does not seem to have any substantial influence on mechanical properties since there is no correlation with mechanical properties.

6.2 Mechanical Analysis

The centrifugal effect seems to be alloy sensitive (mainly on ultimate tensile strength and on strain to failure): alloy A is less influenced, (the maximum centrifugal effect in increasing ultimate tensile strength is approximately 13% and in strain to failure is approximately 45%); alloy B is substantially influenced (the maximum centrifugal effect in increasing ultimate tensile strength is approximately 18% and in strain to failure is approximately 65%); and alloy C is strongly influenced by the casting technique (the maximum centrifugal effect in increasing ultimate tensile strength is approximately 60% and in strain to failure is approximately 400%) (Figures 4.10-4.13, 4.20-4.23 and 4.31-4.34).

The difference in mechanical properties from positions 1 to 3 (slope of the tendency line), in centrifugal castings, is different. These differences are alloy chemical composition dependent: alloy A has small differences; alloy B has substantial differences; and alloy C has huge differences (Figures 4.10-4.13, 4.20-4.23 and 4.31-4.34). This is particularly evident in terms of strain to failure.

Mechanical properties are influenced by the centrifugal casting technique. As a fact, in general, the centrifugal castings have better mechanical properties (ultimate tensile strength and in particular strain to failure) then the gravity castings as can be observed on figures 4.10-4.13, 4.20-4.23 and 4.31-4.34.

To shorten the way to find the most suitable equation that can predict the fatigue strength, a sensitivity study was done over the experimental results.

This study is concerned with the sensitivity of different Al–Si alloys to centrifugal effect of the vertical centrifugal casting technique on castings as compared to the traditional gravity casting technique.

Correlations were established with the three main metallurgical constituent's: dendrites, eutectic, and intermetallics. Si particles were not considered because their amount is very small. The reason lies on the process characteristics and on the place from where specimens were taken from [194, 207]. In alloys/processes where Si particles volume fraction is high they must be included in relations.

The reason to quantify two types of features (amount and morphology) has explanation on the fact that the amount depends essentially on chemical composition of the alloy, and the geometry depends essentially on the casting process/solidification rate. Some thermal treatments such as ageing are also incorporated in the morphology feature. If it is considered, for example, an Al with 7% Si that is subjected to a thermal treatment of ageing, during treatment the Si particle aspect ratio changes but all the other features (amount, SDAS, etc) are kept constant.

The volume fraction of eutectic, dendrites and intermetalics, and one geometrical feature of eutectic, dendrites, and intermetallics were considered. They were considered isolated, namely by Vf_{eut}, Vf_{dend}, Vf_{int}, th_{eut}, *SDAS,* and th_{int}, but they were also correlated in conjunction by incorporating, for each metallurgical constituent, its volume fraction and one of its geometrical features, in the form of ratios, namely Vf_{eut}/th_{eut}, Vf_{int}/th_{int} and $Vf_{dend}/SDAS$. These relations incorporate simultaneously the chemical composition effect (amount of constituent) and the casting process/thermal treatment (geometry of constituent). Finally more global correlations considering more than one constituent and their geometrical features were also considered. These last correlations have the global form of $Vf_{eut}/Th_{eut} + Vf_{dend}/SDAS + Vf_{int}/Th_{int}$.

In figures 6.1 to 6.6 are presented different types of correlations between micro-structural features and mechanical properties: Ultimate Tensile Strength - *UTS* (Figures 6.1, 6.3, 6.5) and Strain to failure – *SF* (Figures 6.2, 6.4, 6.6). Correlations with mechanical properties (*UTS* and *SF*) are established with single metallurgical parameters, in quantity - volume fraction, and in terms of geometry – thickness of constituent and SDAS. They are also established with combined parameters including two or more internal microstructure features. Normalized values of Ultimate Tensile Strength – *UTS* (normalized to the minimum value) and of Strain to Failure - *SF* (normalized to the minimum value) and different metallurgical features (normalized to each minimum value) are used for two purposes: compare the sensitiveness of each correlation (sensitiveness is given by the slope of the curves); observe the error of the correlation (the R^2 value indicates the accuracy of the correlation or error of the readings as compared to the mean line/correlation value).

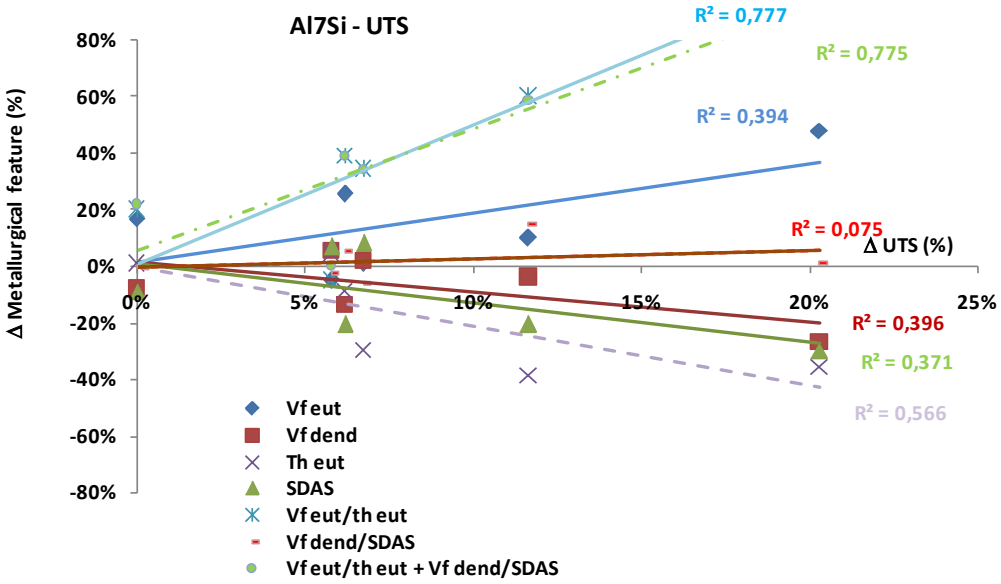

Figure 6.1 – Normalized values of Ultimate Tensile Strength – *UTS* (normalized to the minimum value) and different metallurgical features (normalized to each minimum value) for the Al-7%Si alloy.

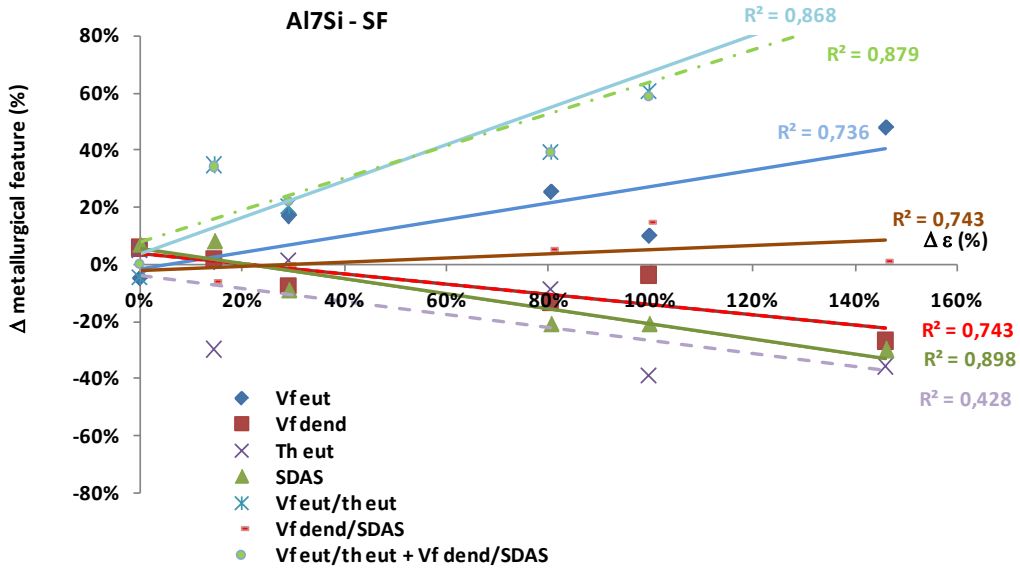

Figure 6.2 – Normalized values of Strain to Failure - *SF* (normalized to the minimum value) and different metallurgical features (normalized to each minimum value) for the Al-7%Si alloy.

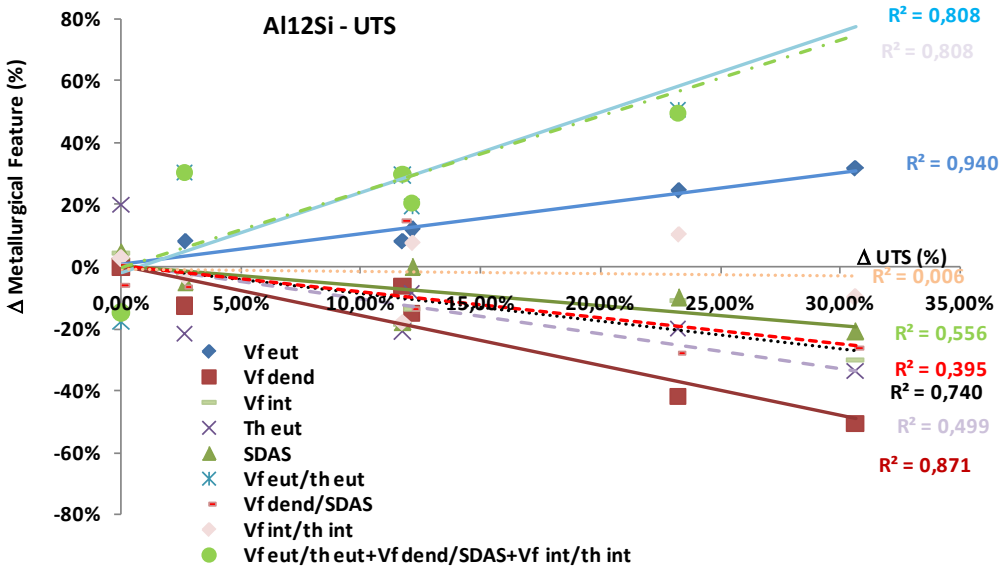

Figure 6.3 – Normalized values of Ultimate Tensile Strength – *UTS* (normalized to the minimum value) and different metallurgical features (normalized to each minimum value) for the Al-7%Si alloy.

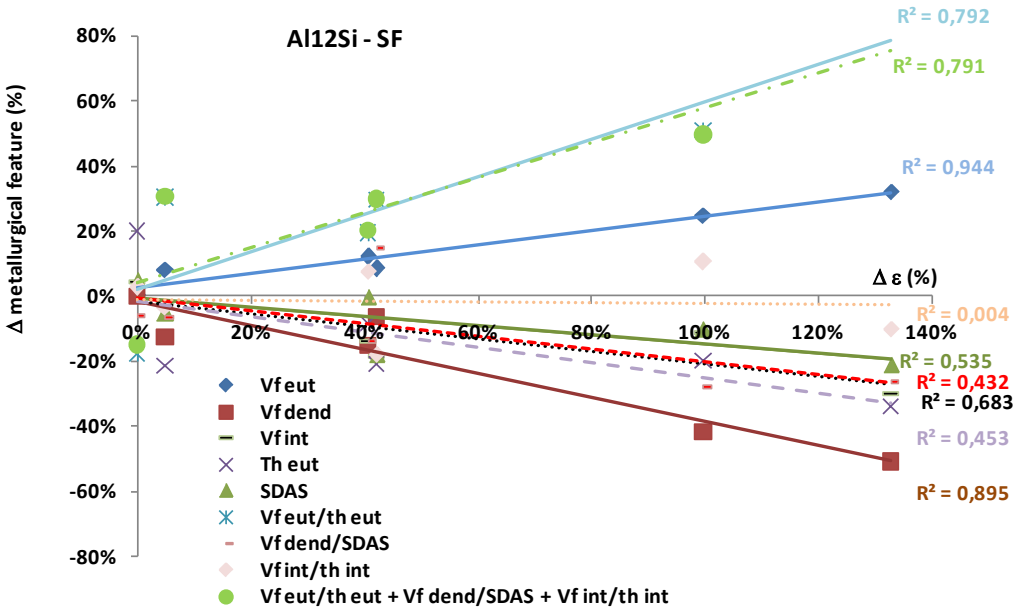

Figure 6.4 – Normalized values of Strain to Failure - *SF* (normalized to the minimum value) and different metallurgical features (normalized to each minimum value) for the Al-7%Si alloy.

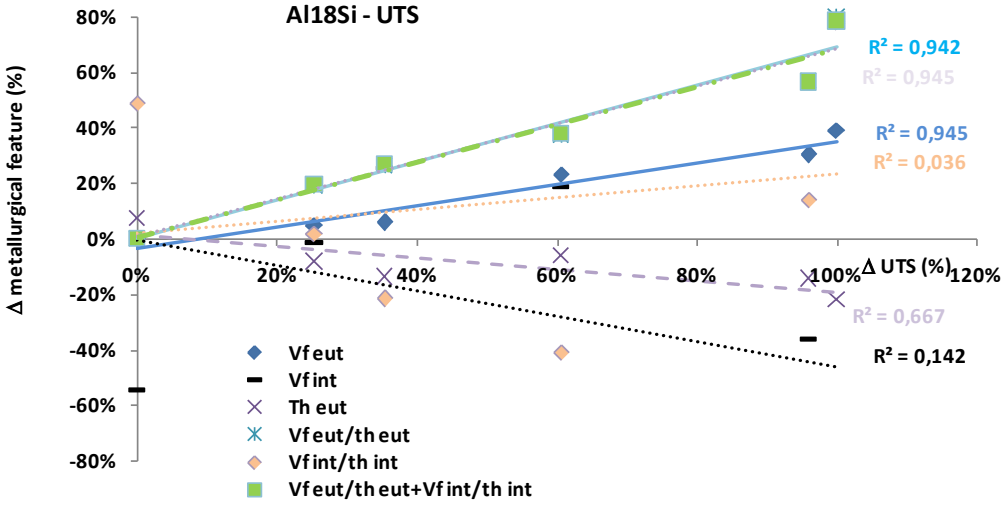

Figure 6.5 – Normalized values of Ultimate Tensile Strength – *UTS* (normalized to the minimum value) and different metallurgical features (normalized to each minimum value) for the Al-7%Si alloy.

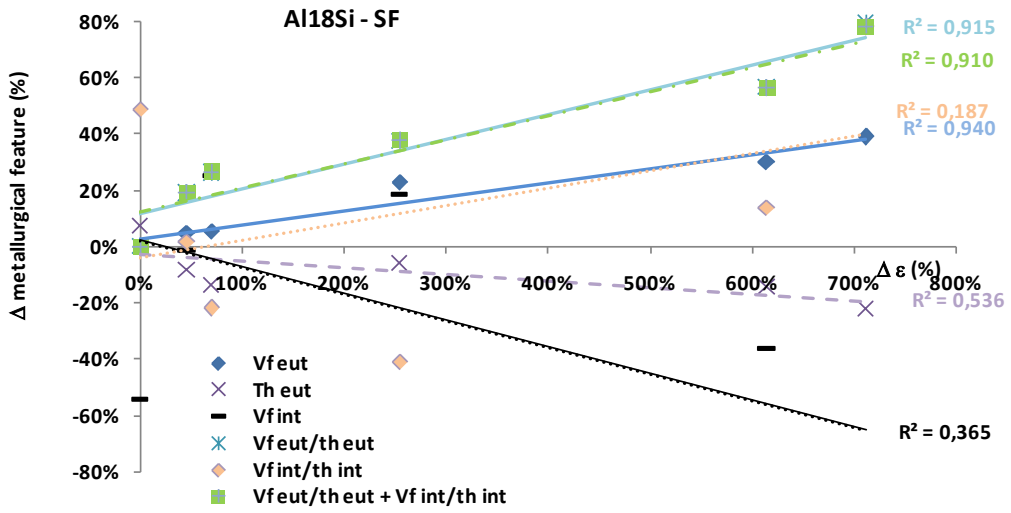

Figure 6.6 – Normalized values of Strain to Failure - *SF* (normalized to the minimum value) and different metallurgical features (normalized to each minimum value) for the Al-7%Si alloy.

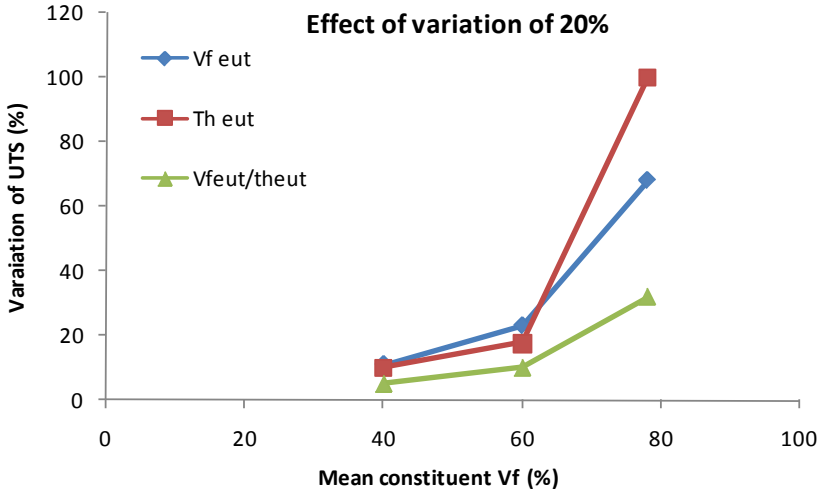

Figure 6.7 – Effect of variation of constituent (in 20%) parameter ((Vf_{eut}, th_{eut}, and Vf_{eut}/th_{eut}) in UTS for all three alloys (in *xx* axis is the mean volume fraction of eutectic for each alloy, 7%Si - 40% eut, 12%Si - 60% eut, and 18%Si - 80% eut).

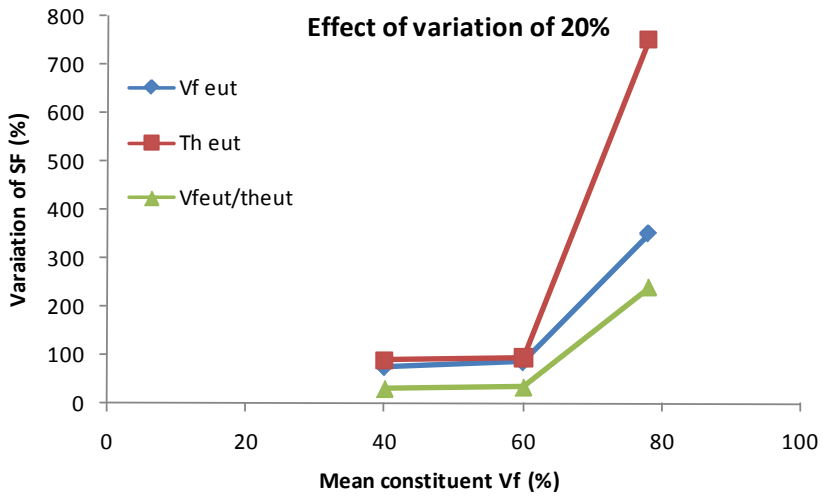

Figure 6.8 – Effect of variation of constituent (in 20%) parameter ((Vf_{eut}, th_{eut} , *and* Vf_{eut}/th_{eut}) in SF for all three alloys (in *xx* axis is the mean volume fraction of eutectic for each alloy, 7%Si - 40% eut, 12%Si - 60% eut, and 18%Si - 80% eut).

6.2.1. Mechanical properties vs. Eutectic volume fraction Model

Mechanical properties of aluminium alloys, both *UTS* and *SF* have widely been obtained by using material constituent's and their characteristics. The establishment of correlations between them is still a challenge. In literature it is possible to find out different types of relations essentially simple ones, but more elaborated ones, although scarce, can also be found. Simple relations are ones that correlate mechanical properties with one metallurgical feature such as SDAS [22, 27, 126] or eutectic volume fraction [26, 207] or Si and Fe intermetallics or even Si particles size and shape [22, 27, 126, 207].

The most used feature for metallographic measurement and quantification is *SDAS*. For example on reference [27] it is discussed the relationship between the secondary dendrite arm spacing (*SDAS*) and *UTS* and *SF*. Results show an increase of the ultimate tensile strength and strain to failure on both A356 and A357 (ASTM) alloys with the decrease of the secondary dendrite arm spacing (*SDAS*) [27]. On reference [126] it is also reported, for an A356-T6 alloy obtained by hot isostatic pressing, an increase of ultimate tensile strength and of ductility with a decrease of secondary dendrite arm spacing (*SDAS*). The same type of correlation was reported on an Al-7%Si-Mg alloy [148]. In this last study the yield strength was found to be less influenced by the *SDAS* then elongation. Other simple correlations have also been established between other constituents such as

eutectic volume fraction [26] or Si and Fe intermetallics, and Si particles size and shape [22, 27, 126, 207], and mechanical properties. On reference [147] there is a good correlation between the amounts of dendritic α-Al phase with mechanical properties of a Sr-modified Al alloy. In other study, an increase in the strain to failure was attributed to the increase in the amount of eutectic [26]. The amount of eutectic was also been mentioned to give good correlations with ultimate tensile strength and mainly with strain to rupture both in hypo and hyper eutectic alloys [207].

In literature, some quantitative relations between mechanical properties, phases and chemical composition were proposed. Mandal *et al*. [147], has established a correlation between tensile strength and primary silicon particle size [Equation 2.5]

Another relationship was proposed between ultimate tensile strength and secondary dendrite arm spacing and the size of silicon lamellas in interdendritic eutectic regions [Equation 2.6]:

These equations were derived for a specific type of alloys, for example hypoeutectic or hypereutectic Al-Si alloys.

As can be seen none of the previous equations would suit simultaneously the three Al-Si tested alloys in the present study. On the present work, the same type of equation was derived for the three tested alloys which have substantial different Si contents and different morphologies. An equation based on particle size as the one on equation 2.5 is not possible for all alloys since there are no non eutectic Si particles in alloy A and B (tables 4.1, 4.2 and 4.3 and figures 4.10-4.13, 4.20-4.23 and 4.31-4.34). An equation as equation 2.6 is also not possible for all three Al-Si alloys because there are no dendrites on alloy C (see figures 4.37-4.40). However, phases/constituent's volume fraction as shown on figures 4.15, 4.25, and 4.36, reveal that in all alloys A, B and C, and for both casting techniques, eutectic's volume fraction shows a clear tendency to increase from position 3 to 1. Further, regarding mechanical properties, figures 4.10-4.13, 4.20-4.23 and 4.31-4.34, show that ultimate tensile strength, Young modulus and hardness generally follow the same tendency of the eutectic volume fraction (an exception occurs for Young's modulus on alloy C). Strain to failure is particularly sensitive to the eutectics volume fraction.

Thus, from the sensitivity study result, a correlation between eutectic's volume fraction and mechanical properties (mainly ultimate tensile strength and strain to failure) could be established for all alloys. An equation with the type as shown on equation 6.1 may be derived for each alloy (for ultimate tensile strength and strain to failure):

$$\sigma;\varepsilon = k_{1(Stress\ or\ strain))} + V_{f\,eut} \cdot k_{2(Stress\ or\ Strain)} \quad (6.1)$$

where: σ is the ultimate tensile strength; ε is the strain to failure; k_1 is an empirical factor that introduces the influence of all other non eutectic metallurgical features (such as SDAS, primary silicon particles size; intermetallics type, size, and distribution); k_2 represents phase morphology and distribution on the eutectic constituent; and $V_{f\,eut}$ is the eutectic's volume fraction.

Table 6.1 presents the obtained values of k_2 for the three alloys and two casting processes. It should be emphasized that k_1 values are not in table 6.1 because they represent, in equation 6.1, the stress value for a volume fraction of eutectic equal to zero. And the equation is valid for values of eutectic silicon in the range that contains the ones obtained in the tested materials, e.g., between 30 and 90%. k_1 that represents the slope of the equation, is the value that is representative in the equation in its range.

It was found a characteristic k_2 value for each alloy, that is applied for both casting techniques. The difference in the k_2 values may correspond to the eutectic's morphology (see figures 5.15-5.19, 5.25-5.29 and 5.36-5.40) that is very different among the different alloys (for example, eutectic interlamellar distance on alloy C, is smaller than the one on the other alloys). These results show (same k_2 for both casting processes) that the mechanical properties are mainly defined by the eutectic volume fraction and that there is a significant change in the volume fraction between casting processes.

In order to compare the experimental results and calculated values, as obtained with the proposed equation (Equation 6.1), figures 6.9-6.14 shows the predicted and obtained results for ultimate tensile strength and strain to failure, respectively. It is important to highlight that although the slope of the equation is the same for each alloy, in figures 6.9-6.14 the slopes are different because the x axis identifies the positions and not the volume fraction of eutectic.

The relationship between eutectic's volume fraction and mechanical properties only applies to each alloy and cannot be extrapolated from alloy to alloy because there are other variables that were not considered here (for example, some low alloying elements content that are present in commercial alloys - see table 6.1).

It is worth to note that in the present study, a correlation between eutectic volume fraction and both ultimate tensile strength and strain to failure was found. However the sensitivity of the mechanical properties is different for the different alloys and casting processes.

In order to verify the sensitivity between stress or strain results with eutectics volume fraction the stress and strain results were normalized (see figures 6.1-6.6) in relation to the smallest value for each material/condition. It is possible to verify that strain to failure results are more sensitive to eutectics volume fraction then ultimate tensile strength results in all alloys and that the sensitivity increases from 7% Si aluminium alloy to 18% Si aluminium alloy. A similar conclusion was found on reference [103] for an Al12.5%Si. Abu-Dheir N. *et al.*, [103] also found that the dependence of strain to failure on eutectic volume fraction in a 12.5% Si aluminium alloy was more important than the dendritic structure and also than the eutectic structure that transformed from a flaky structure to a fibrous one.

Thus, the relationship found in this study between the mechanical properties (for both ultimate tensile strength and strain to failure) and the metallurgical parameter eutectic constituent, is a useful tool as a generalized prediction of mechanical properties since it is present in a wide range of Al-Si alloys, from hypoeutectic to hypereutectic. However more detailed equations could be defined for specific alloys.

By the results, it is also clear that the centrifugal force has a strong influence on mechanical and metallurgical properties of the obtained castings. As a general rule it can be said that the mechanical properties are improved by the use of the centrifugal casting technique and strain to failure is the most sensitive property to the centrifugal effect (figure 6.12-6.14). These differences may be properly correlated to the eutectics volume fraction along the ingots.

Table 6.1 – Correlation factor obtained for studied alloys between eutectics volume fraction and ultimate tensile strength and strain to failure.

	Casting process	$k_{2\ stress}$	$k_{2\ strain}$
Alloy A (7% Si)	Gravity Centrifugal	1.686	0.29
Alloy B (12% Si)	Gravity Centrifugal	3.758	0.054
Alloy C (18% Si)	Gravity Centrifugal	4.3	0.07

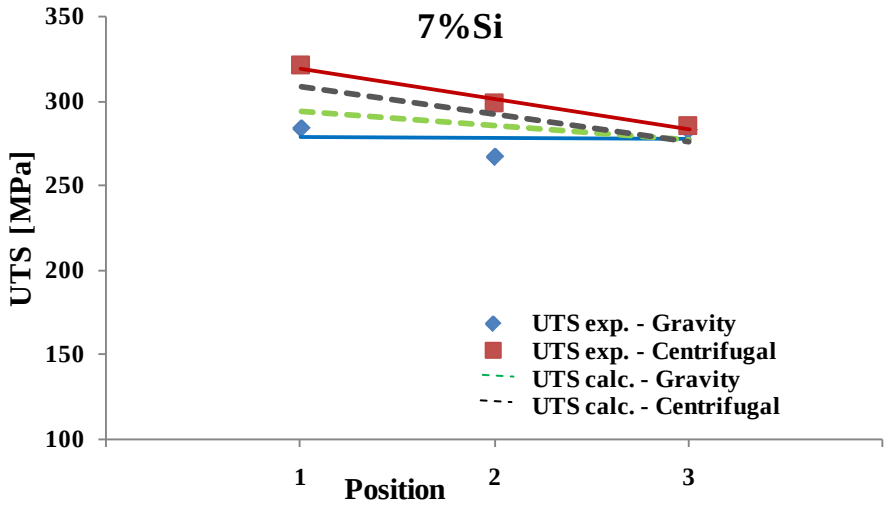

Figure 6.9 – Experimental and calculated (Eq. 6.1) values of ultimate tensile strength for centrifugal and gravity castings of alloy A in positions 1, 2 and 3 of ingot.

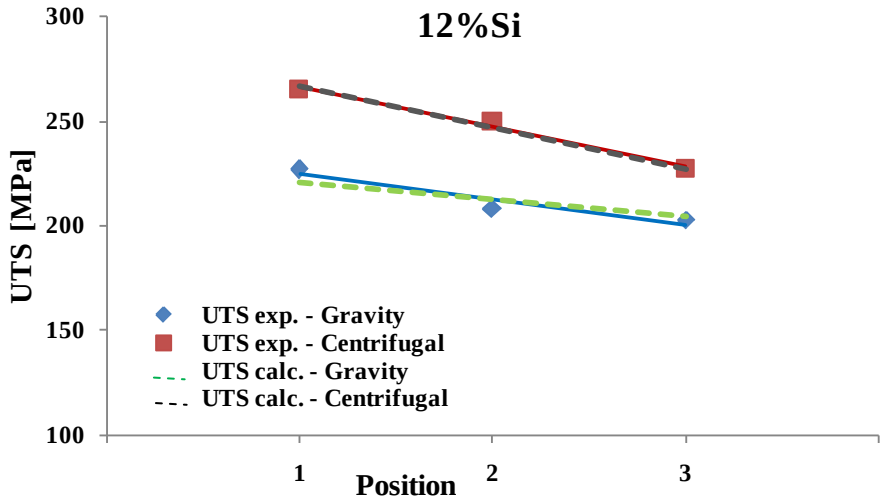

Figure 6.10 – Experimental and calculated (Eq. 6.1) values of ultimate tensile strength for centrifugal and gravity castings of alloy B in positions 1, 2 and 3 of ingot.

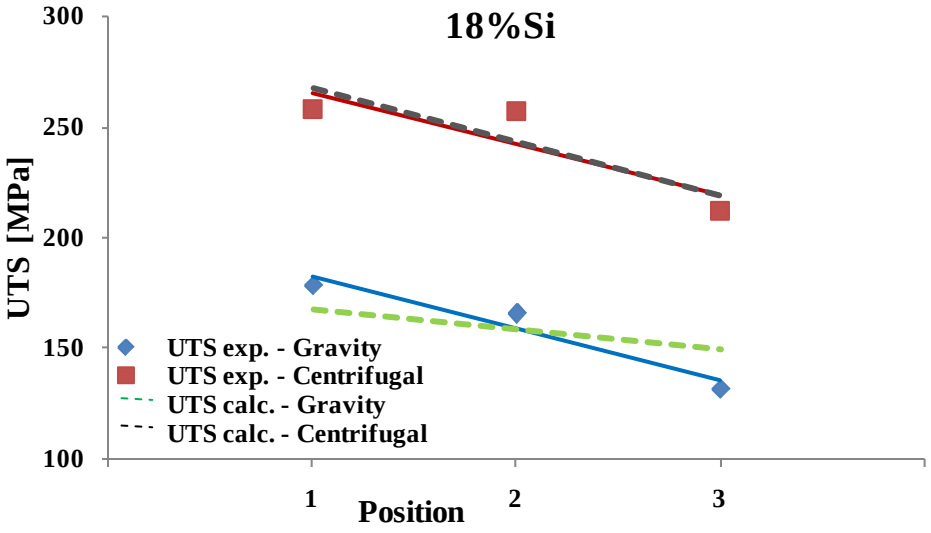

Figure 6.11 – Experimental and calculated (Eq. 6.1) values of ultimate tensile strength for centrifugal and gravity castings of alloy C in positions 1, 2 and 3 of ingot.

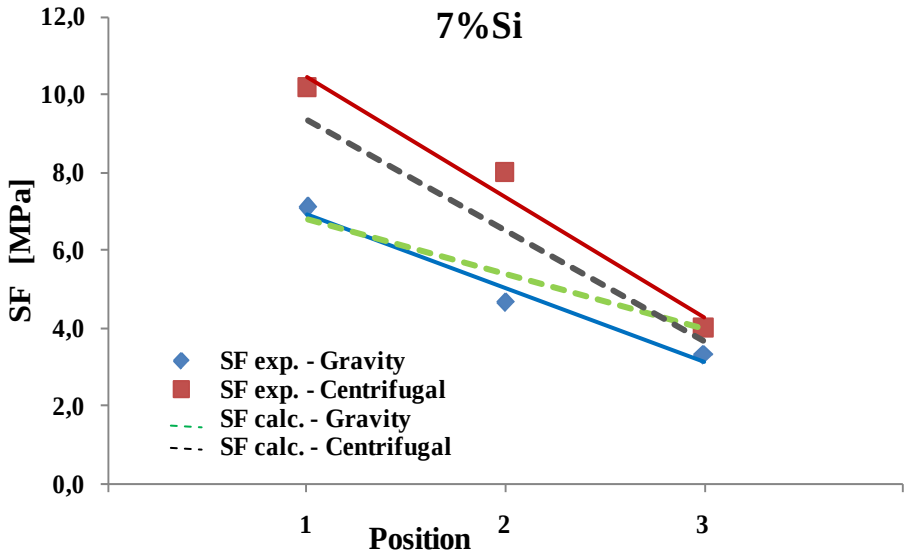

Figure 6.12 – Experimental and calculated (Eq.6.1) values of strain to failure for centrifugal and gravity castings of alloy A in positions 1, 2 and 3 of ingot.

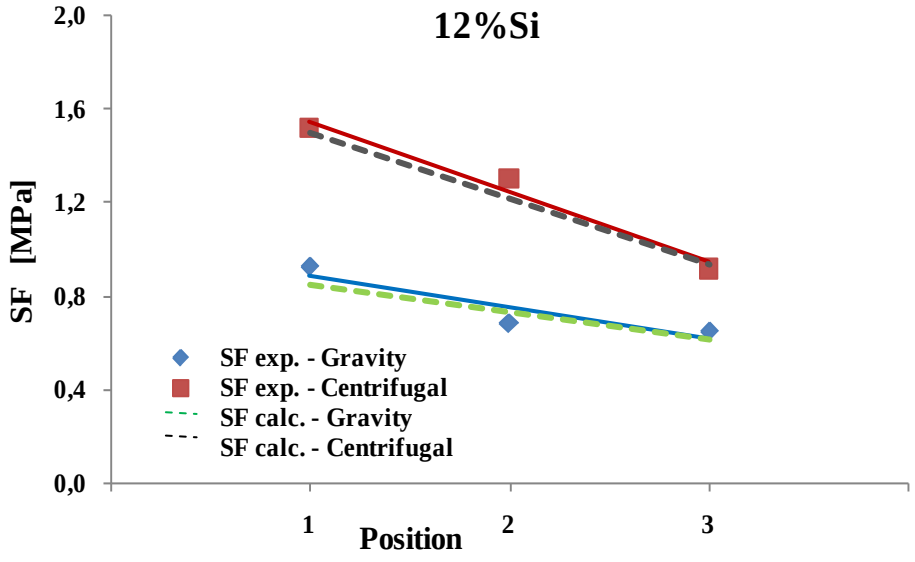

Figure 6.13 – Experimental and calculated (Eq.6.1) values of strain to failure for centrifugal and gravity castings of alloy B in positions 1, 2 and 3 of ingot.

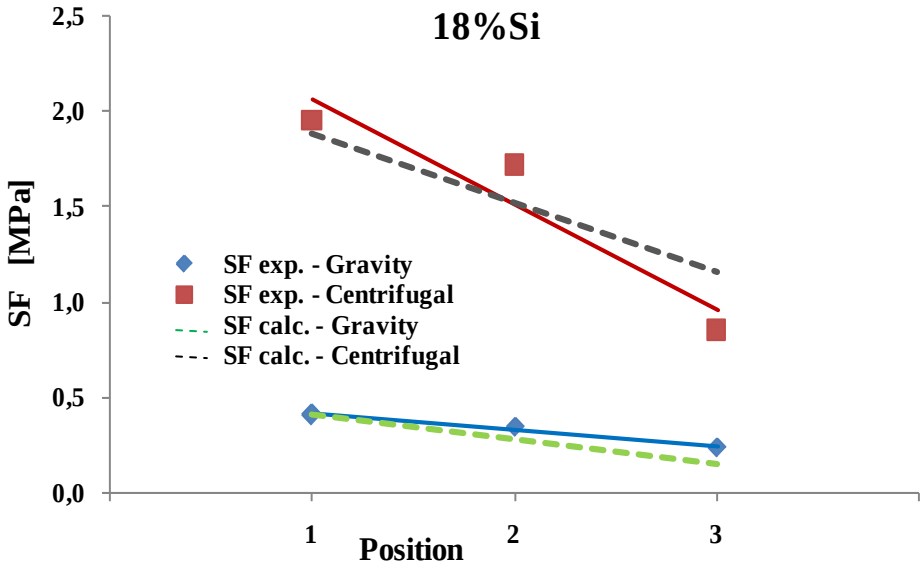

Figure 6.14 – Experimental and calculated (Eq.6.1) values of strain to failure for centrifugal and gravity castings of alloy C in positions 1, 2 and 3 of ingot.

6.2.2. Mechanical properties vs. Eutectic volume fraction/Thickness of eutectic silicon Model

The second model that was developed in this research incorporates simultaneously the chemical composition effect (amount of constituent) and the casting process/thermal treatment (geometry of constituent) (Equation 6.1). The reason to quantify two types of features (amount and morphology) has explanation on the fact that the amount depends essentially on chemical composition of the alloy, and the geometry depends essentially on the casting process/solidification rate. Some thermal treatments such as ageing are also incorporated in the morphology feature. If it is considered, for example, an Al with 7% Si that is subjected to a thermal treatment of ageing, during treatment the Si particle aspect ratio changes but all the other features (amount, SDAS, etc) are kept constant.

The prediction results based on equation 6.2 are presented in figures 6.14-6.16 together with the experimental results. The prediction of the UTS is good for all three alloys studied. For strain to failure prediction, the figures 6.17-6.19 show a good estimation compared with experimental results only for gravity casting results of SF shows some differences from experimental results. There are not big differences on

results based on equation 2.6 and 6.1 but each one has own advantage. Equation 6.1 is easy to use because is needed only the volume fraction of the eutectic but has the disadvantage of the increasing the error exponentially if the volume fraction readings include minor errors. In the case of equation 6.2 along with volume fraction of the eutectic is needed measuring of the thickness of the eutectic that require more time. The advantage of this equation resides in the fact that if small errors appear on measuring the microstructural features no important changes are observed on the prediction results. In conclusion both equations are useful: one for faster estimation with acceptable tolerance of prediction and the second one taking more time to determine all needed feature to calculate it but with less sensitivity and more precise results.

$$\sigma;\varepsilon = k_{1(Stress\ or\ strain))} + (V_{f\ eut} / Th_{eut}) \cdot k_{2(\ Stress\ or\ Strain)} \tag{6.2}$$

Table 6.2 – Correlation factor obtained for studied alloys between eutectics volume fraction/thickness of eutectic and ultimate tensile strength and strain to failure.

	Casting process	$k_{2\ stress}$	$k_{2\ strain}$
Alloy A (7% Si)	Gravity Centrifugal	3	2.15
Alloy B (12% Si)	Gravity Centrifugal	1.2	67
Alloy C (18% Si)	Gravity Centrifugal	0.5	105

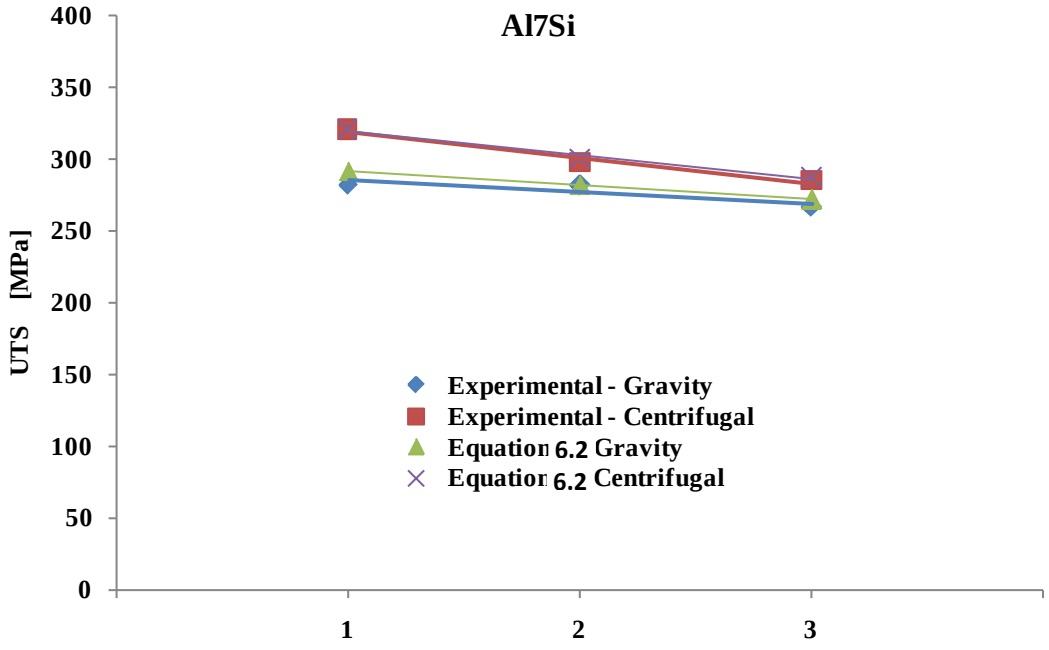

Figure 6.15 – Experimental and calculated values of ultimate tensile strength for centrifugal and gravity castings of alloy A in positions 1, 2 and 3 of ingot.

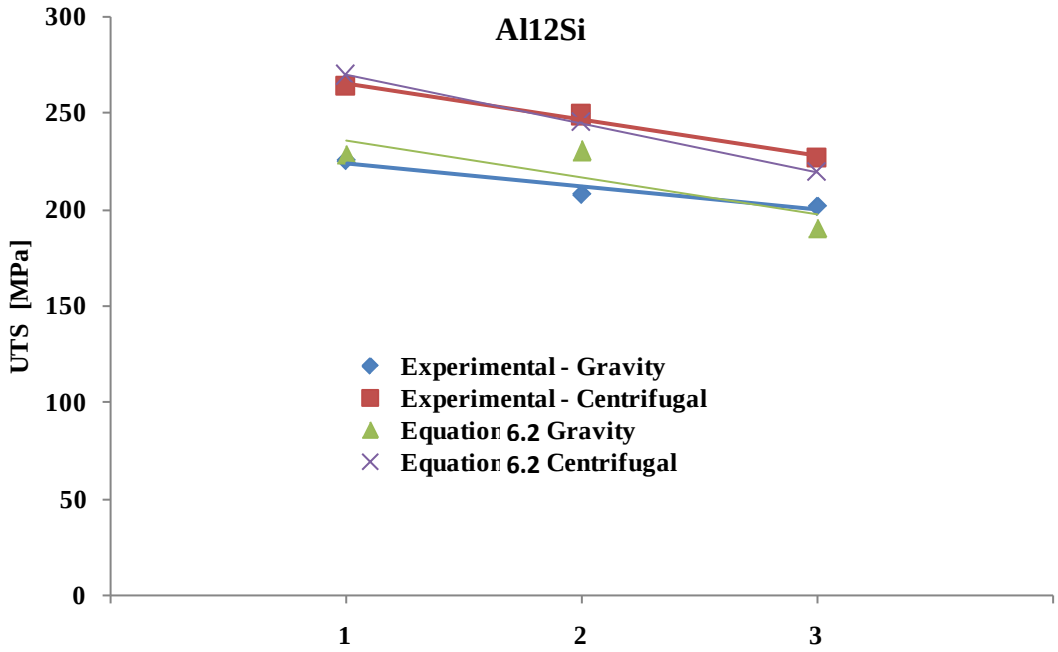

Figure 6.16 – Experimental and calculated values of ultimate tensile strength for centrifugal and gravity castings of alloy B in positions 1, 2 and 3 of ingot.

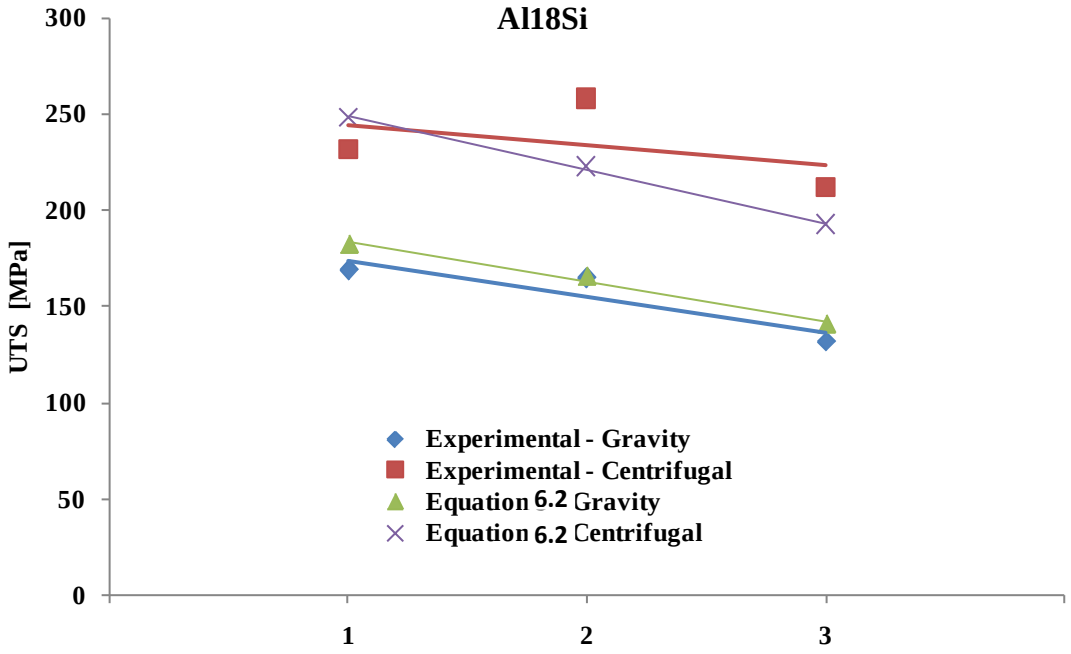

Figure 6.17 – Experimental and calculated values of ultimate tensile strength for centrifugal and gravity castings of alloy C in positions 1, 2 and 3 of ingot.

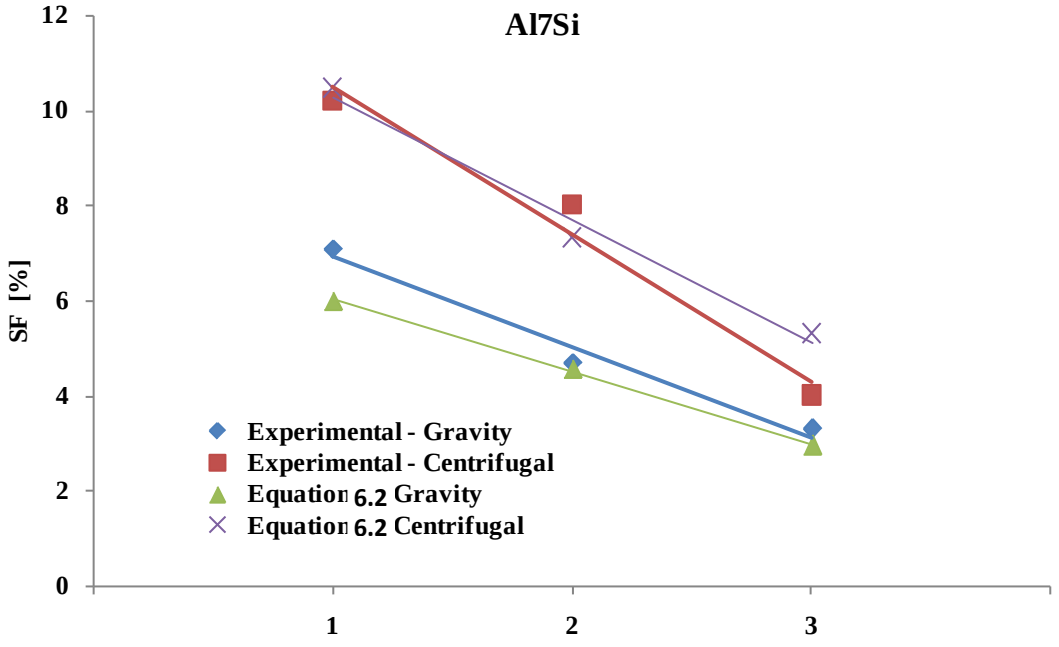

Figure 6.18 – Experimental and calculated values of strain to failure for centrifugal and gravity castings of alloy A in positions 1, 2 and 3 of ingot.

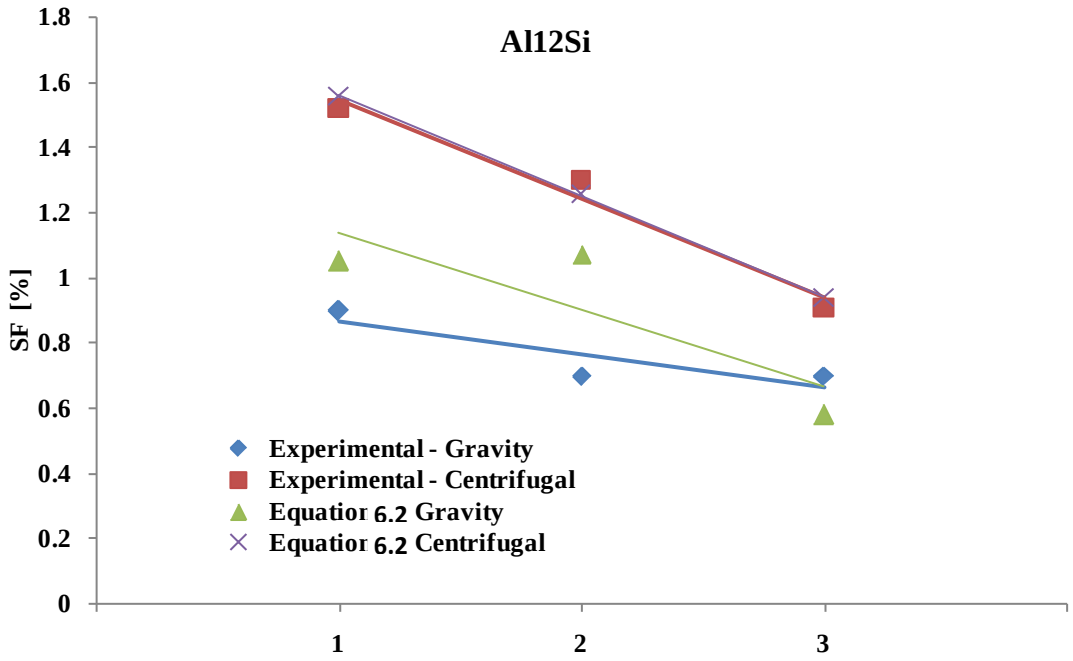

Figure 6.19– Experimental and calculated values of strain to failure for centrifugal and gravity castings of alloy B in positions 1, 2 and 3 of ingot.

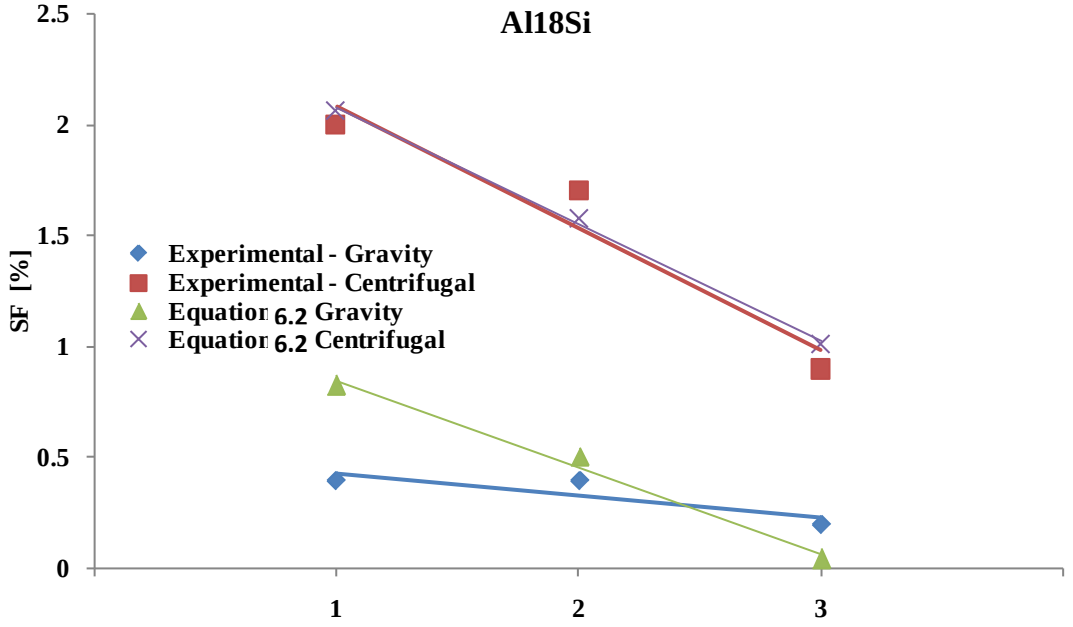

Figure 6.20 – Experimental and calculated values of strain to failure for centrifugal and gravity castings of alloy C in positions 1, 2 and 3 of ingot.

6.3 Fatigue Analysis

Many studies demonstrated that solidification defects (such as gas pores, cavity shrinkages and oxide films) strongly affect the mechanical behaviour, and mainly fatigue resistance, of cast aluminium alloys [121-128]. A number of papers have been published about the relationship between casting defects and fatigue resistance of A356 (AlSi7Mg0.3) and A357 (AlSi7Mg0.6) aluminium alloys [123-127]. Continuous improvement in casting techniques, however, has led to a decrease in casting defects. As a result, other microstructural parameters, including the secondary dendrite arm spacing (SDAS), the grain size, the size and morphology of eutectic Si particles, as well as the shape and distribution of intermetallic compounds, have to be considered in order to predict the mechanical behaviour of cast aluminium alloys [27, 129-136].

For aluminium alloys subjected to high cycle fatigue a significant portion of the life is consumed in microstructurally small fatigue damage evolution, which includes incubation-forming of a crack in a particle, nucleation–extension of a crack into the aluminium matrix, and propagation. It has been proposed that up to 90% of the fatigue life of structural components is consumed during the formation of a dominant fatigue crack [195]. Others have suggested that 50–70% of the total fatigue life elapses during the time that damage is microstructurally small [196–198]. A computationally demanding, scientifically based model for microstructurally small fatigue damage has been developed that incorporates fundamentals of materials science and mechanics with critical experimental observations of the highly stochastic damage phenomena [199]. Indeed, microstructurally small damage evolution is extremely complex; however, constituent particles in aluminium alloys are significant contributors to the process. The number of constituent particles per mm^2, with an area exceeding 1 μm^2, is approximately 2000 [200].

Several studies [75, 162-172] have shown that porosity is one of the key factors which control the fatigue properties in Al–Si casting alloys. Pores are preferential sites for crack initiation in these alloys, and thus constitute the main factor influencing fatigue performance, independently of the loading conditions and of the stress applied. Compared

with porosity situated on the surface, the eutectic structure and intermetallic phases play a minor role in crack initiation.

The effect of porosity on fatigue life has been summarized as follows: pores reduce the time for crack initiation by creating a high stress concentration in the material adjacent to the pores; because of this, most of the fatigue life is spent in crack growth [201].

Porosity has been classified according to the importance of crack initiation as follows: a single shrinkage pores close to or at the surface is considered the most critical, whereas a gas pore at the surface is considered the least critical.

Some researchers concluded that there exist thresholds of the pore size below which other microstructural features are likely to cause fatigue crack initiation. Zhang *et al.* [171] indicates the critical pore size as 100 μm, below which other microstructural features are responsibly of initiation of fatigue crack. Wang *et al*. [83] proposed a smaller critical pore size of approximately 25 μm. The reason for the discrepancy appears probably because different maximum oxide size results: ~1000 μm in [171] and ~250 μm [83]. It is therefore possible that oxides played a greater role in fatigue crack initiation in the alloys and this may influence (or mask) the critical pore size for fatigue crack initiation.

Empirical equations were used to estimate the values of the fatigue limit taking into consideration different features like dendrite arm spacing and the size of primary silicon particles [202, 203] and also porosity [204].

Most of the equations developed to predict the fatigue limit are using only one or maximum two experimental obtained parameters. Murakami [113] presents three most common used equations that are able to predict the fatigue limit of aluminium alloys (eq. 2.8-2.10). All three equations are estimating the value of the fatigue limit as a function of other experimental parameter such as rupture strength, hardness or diameter of pores. These equations are good to estimate the fatigue limit for a particular range of aluminium alloys with a silicon percentage from ~6% to ~24%.

In the present research a model to predict the fatigue limit was developed as a function of several microstructural features: volume fraction of the eutectic intermetalics and pores, eutectic silicon particles, thickness of intermetalics and pores dimension.

Thus, from the obtained experimental results a correlation between eutectic's volume fraction, thickness of eutectic silicon and volume fraction of pores and intermetalics was established for all alloys studied.

The volume fraction of the eutectic was considered in the equation as having a beneficial influence over fatigue strength because with the increasing of volume fraction is obtained a strengthening of the material that make more difficult for the crack to initiate and also to propagate. The equation development took also into consideration the detrimental effect of the increasing the thickness of the eutectic silicon particles and the volume fraction of pores that are the main site of fatigue crack initiation. According with some results reported on literature [84, 182, 190] intermetalics are also considered as initiators of fatigue cracks, so were added to the equation on denominator as volume fraction and thickness. A single equation matching with all the type of alloys studied was derived as can be seen in equation 6.3. A simplified version of equation 6.3 is expressed on equation 6.4 which is not as precise as the complete equation but is easier to calculate and can offer an acceptable error.

From these results it is clear that fatigue life in hypo-eutectic and eutectic Al-Si alloys can be better assessed when correlations take into consideration not only one single constituent as is the case of eutectic but consider different constituents at the same time. Previous results for static properties, namely for UTS-Ultimate Tensile Strength and SF-Strain to Failure, have shown the same logic, e.g., when more constituents are taken into consideration more accurate and robust predictions are obtained.

In this study it seems clear that eutectic silicon, either particles (7%Si alloy) or lamellae (12%Si alloy), plays a relevant role on fatigue life prediction (as obtained in eq. 6.5) because it gives a good correlation with fatigue limit. However better correlations can be obtained if other constituents are considered along with eutectic silicon. Intermetallics, because they are a fragile constituent being then prompt to break under large deformations (at for example crack tip), assume then an importance on fatigue crack propagation and initiation, and micro-pores because they are also stress raisers and good crack initiators. Again in this study they are considered important and detrimental.

Fracture surface examinations were performed and it is not clear that both the initiation as well as the propagation behavior is controlled by one single constituent. No large pores or primary Si particles were found on 7%Si alloy and 12%Si alloy (Figures

4.44 and 4.45). Thus it is assumed in this study that all the existing metallurgical constituents, considering small pores equivalent to a metallurgical constituent) play a role both on initiation as well as in propagation behavior.

The values of all the constituents used on equation 6.3 are presented in tables 4.1 to 4.3 and figures 4.4, 4.6 and 4.7.

$$\sigma_f = k \cdot V_{f\,eut} \cdot \left(Th._{eut\_silicon}\right)^{-\frac{1}{2}} \cdot \left(V_{f\,\mathrm{int}} \cdot Th_{\mathrm{int}}\right)^{-\frac{1}{2}} \cdot \left(V_{f\ pores} \cdot Th_{pores}\right)^{-\frac{1}{2}} \quad (6.3)$$

$$\sigma_f = k \cdot V_{f\,eut} \cdot \left(Th._{eut\_silicon}\right)^{-\frac{1}{2}} \quad (6.4)$$

Table 6.3 – Error and k values of the equations 6.5 and 6.6 for estimation of fatigue strength.

Equation	Alloy A (7% Si)		Alloy B (12% Si)		Alloy C (18% Si)		
	Casting process		Casting process		Casting process		
	G.	C.	G.	C.	G.	C.	
(6.3)	11.2		14.6		14.7		*k*
	2%	-2%	-2%	2%	-7%	8%	*Error*
(6.4)	3.26		1.38		0.6		*k*
	2%	-1%	4%	-4%	1%	-2%	*Error*

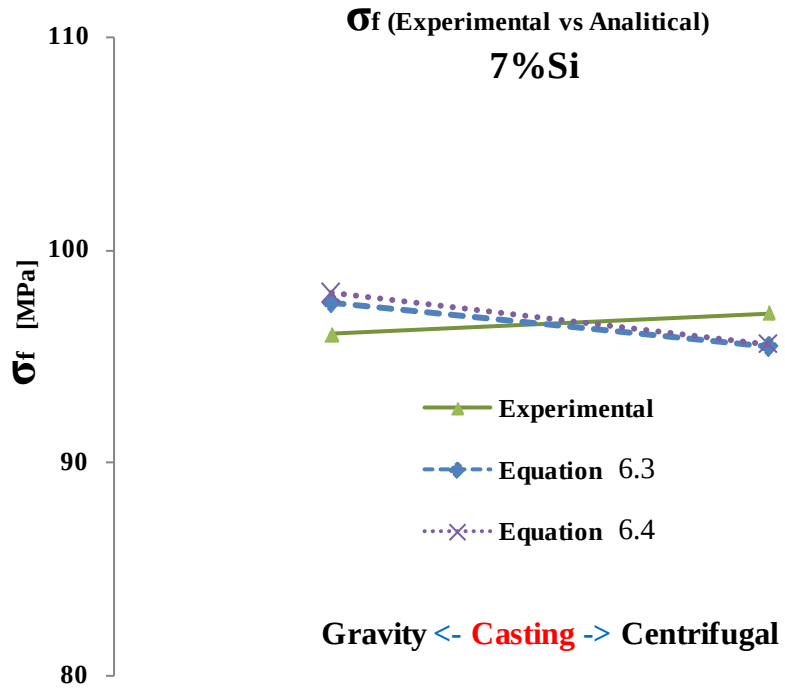

Figure 6.21 – Comparison of fatigue strength - Experimental vs. Models for gravity and centrifugal castings of alloy A.

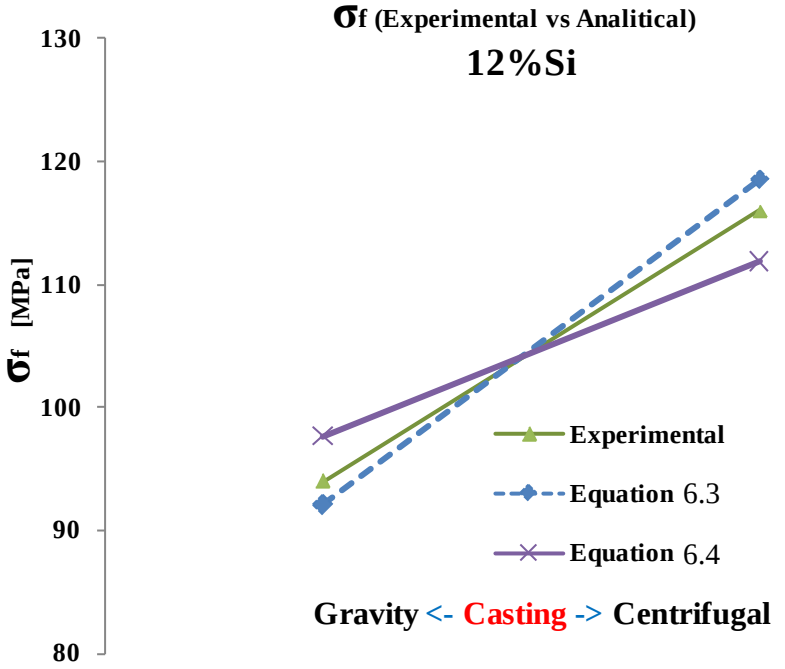

Figure 6.22 – Comparison of fatigue strength - Experimental vs. Models for gravity and centrifugal castings of alloy B.

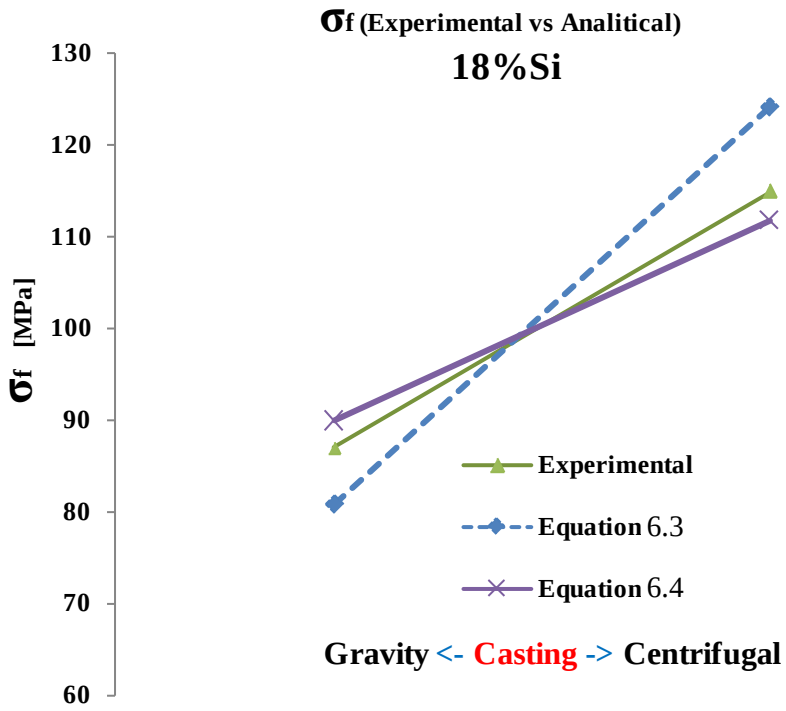

Figure 6.23 – Comparison of fatigue strength - Experimental vs. Models for gravity and centrifugal castings of alloy C.

Two most used analytical equations reported on literature (the correlation with ultimate tensile strength – equation 6.5 and correlation with hardness – equation 6.6) were also applied to have a global view of suitability of the model developed in this research. The k values for equation 6.5 and 6.6 are presented in table 6.4 along with the errors. In figures 6.24-6.26 is presented the experimental results of fatigue strength and also the predicted fatigue strength calculated with equation 6.3 and with equations based on UTS and Hv.

$$\sigma_f = k \cdot UTS \tag{6.5}$$

$$\sigma_f = k \cdot Hv \tag{6.6}$$

The most suitable equation as can be observed from figures 6.24 to 6.26 is equation 6.3 followed by equation based on UTS and than by the one with Hv compared with the experimental results.

Table 6.4 – Error of the equations 6.7 and 6.8 for estimation of fatigue strength

Equation	Alloy A (7% Si)		Alloy B (12% Si)		Alloy C (18% Si)		
	Casting process		Casting process		Casting process		
	G.	C.	G.	C.	G.	C.	
(6.5)	0.5		0.5		0.5		*K*
	0%	0%	4%	-4%	0%	-1%	*Error*
(6.6)	0.9		0.9		0.9		*K*
	-5%	5%	6%	-5%	12%	-11%	*Error*

The equation that is simultaneously the best one and that is more universal (good for different alloys and casting techniques) is equation 6.3. Can be observed that equation 6.3 is also independent of the casting technique and gives good predictions for substantially different microstructures obtained with different casting processes - mainly for 12%Si alloy (see tables 6.3). *k* value is the same for both casting techniques not withstand the substantially different results for the fatigue limit.

Can be stated that the equation 6.3 can be successfully used to estimate the fatigue limit for 7%Si alloy and 12%Si alloy and on a lesser extent for 18%Si alloy. The analysis of crack initiation area reveals the fact that there are not the pores mainly responsible for initiation of cracks for the three alloys studied. In the case of 18%Si alloy there are other micro structural factors that are most responsible as can be seen on figure 4.46, for initiation of cracks, like primary silicon particle that are not included in the equation. In the case of 7%Si and 12%Si alloys it is not clear what constituent is the most responsible for the crack initiation (figures 4.44-4.45).

Further development of the equation may take into account also those feature that is common only for specific Al-Si alloys.

It is worth to note that the hardness based equation does not provide the best relations in all cases, as compared to UTS based equation and equation 6.3. It is also worth to highlight that when local properties are needed, for example in failure analysis where it is needed to obtain the properties where the failure/fatigue crack started, it is not

always possible to obtain local specimens and perform tensile tests. Only the hardness based equation may be used. Thus between hardness based equations and microstructure based ones, although the first are simpler to obtain since it is easy to obtain hardness measurements from small local obtained specimens, the microstructure based ones seem to be more accurate. To obtain microstructure features seem a little more complex and time consuming. However, nowadays with computer software programmes and image processing it is equally easy to obtain microstructure features.

Moreover, if it is considered that it is expected in the near future all Al alloys, even obtained by casting processes, may have only small porosity, due to casting improvements and due to hot isostatic pressing processes to components, thus it seems feasible to use microstructure based approaches to predict fatigue life or fatigue limit in Al-Si alloys.

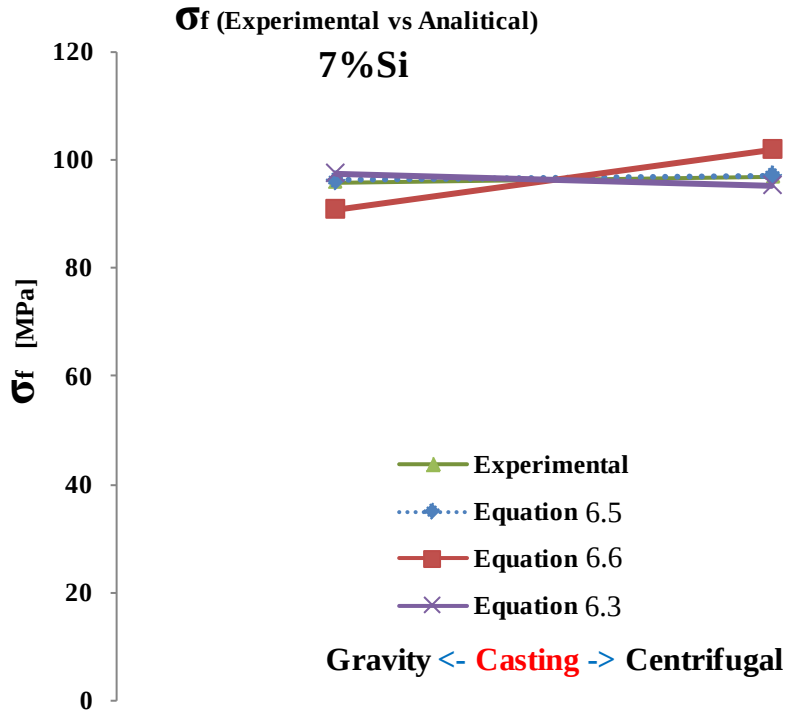

Figure 6.24 – Comparison of fatigue strength - Experimental vs. Models for gravity and centrifugal castings of alloy A.

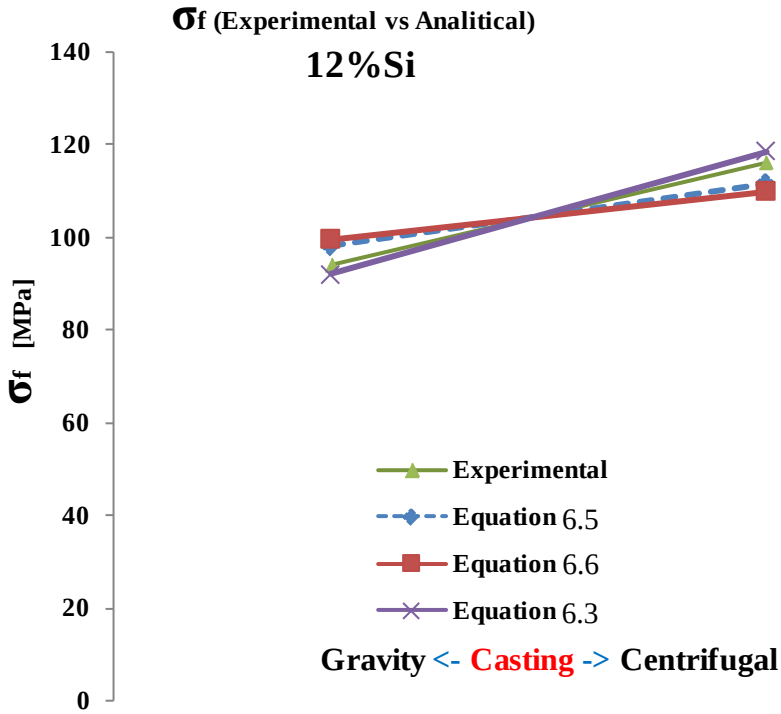

Figure 6.25 – Comparison of fatigue strength - Experimental vs. Models for gravity and centrifugal castings of alloy B.

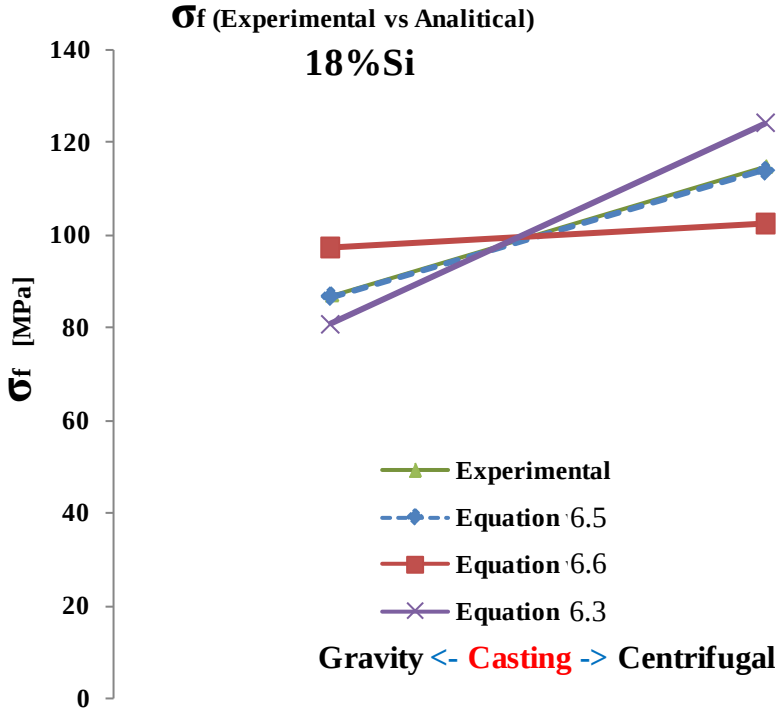

Figure 6.26 – Comparison of fatigue strength - Experimental vs. Models for gravity and centrifugal castings of alloy C.

It is worth to highlight that other different correlations between fatigue limit and other microstructure constituents were tried in this study and it was found that the best correlations are the ones proposed on equation 6.3 and 6.4.

Finally can be concluded the fact that eutectic constituent as a resistance controlling parameter and intermetallics and pores as fatigue detrimental parameters, taking both quantity (volume fraction) and geometrical features of constituents, seem to be adequate to correlate fatigue limit for the Al-Si alloys used in this study, obtained with different casting techniques.

CHAPTER 7

CONCLUDING REMARKS

7.1 Conclusions

The mechanical and fatigue properties improvements of the three aluminium silicon alloys studied in this research are obtained by the presence of several forces applied to the melt during the pouring and solidification due to a combination of the dynamics of fluid (melt), the vibration and centrifugal pressure.

This can be explained by the fact that, the fluid dynamics due to the inherently vibration of the equipment and respectively due to the centrifugal pressure make the melt during solidification to initiate more nuclei of solidification. Then, the centrifugal pressure concentrate the nuclei of solidification to the furthest point of the mould (where the pressure is higher) fact that explains the obtained results which are higher on one side of the ingots which corresponds with the side of the mould where the pressure is higher and smaller on the other side where the pressure is smaller. Actually the composition is graded on centrifugal direction which provides also graded properties.

The centrifugal effect seems to be alloy sensitive. Alloy C is much more sensitive then alloys A and B and affects phases/constituents distribution and morphology along the ingot.

Strain to failure and ultimate tensile strength can be satisfactorily correlated with the eutectic's volume fraction (for alloys with eutectic volume fraction between 30 and 90%). Strain to failure is the most sensitive mechanical property, although ultimate tensile strength is also affected by the centrifugal process.

A correlation of the mechanical properties with the volume fraction of the eutectic phase has been found and a model that can calculate the ultimate tensile strength and strain to failure based on this feature was developed.

The mechanical and fatigue properties seem to be essentially dependent on microstructure and not so largely influenced by the presence of material inhomogeneities such as pores or inclusions.

This study makes also a prediction of fatigue life by establishing a correlation within some of the characteristics of the micro structural features of studied aluminium silicon alloys such as: volume fraction of eutectic phase, the size of thickness silicon lamellas in interdendritic eutectic regions, the volume fraction and thickness of intermetalics and the volume fraction and the dimension of pores. It was done a comparison of the formulas from this research with the more used formulas from literature.

Due to centrifugal force it is possible to obtain much better mechanical and fatigue properties along the whole casting, especially on the outer layers where the centrifugal force is higher; this fact is easy to observe also on the microstructure that is thinner on the direction of centrifugal force.

Solidification behaviour as obtained by solidification curves and microstructure analysis and mechanical results seem to point out that vibration affects the solidification rates and its characteristics and has an influence on mechanical properties. Its influence seems to be due to heat transfer related aspects. Vibration increases heat transfer in the liquid and substantially reduce heat transfer in the interface metal–wall due to the loss of contact under mainly two hypothetic mechanisms: high surface tension and wall roughness effect.

The present work is emphasizing the fact that the centrifugal process could be successfully used for obtaining functionally graded materials also for metallic materials (alloys) with moderate solubility and small differences of density of the different phases, as is the case of most aluminium alloys. In terms of direct industrial application, the centrifugal casting can be successfully used to obtain engine pistons with gradation of properties on one direction (see figure 7.2) by positioning the engine piston mould inside

of the rotating vacuum chamber as it is presented in figure 7.1. In terms of mechanical and fatigue properties, engine pistons would be obtained by vertical centrifugal casting with obvious advantages over the traditional gravity castings.

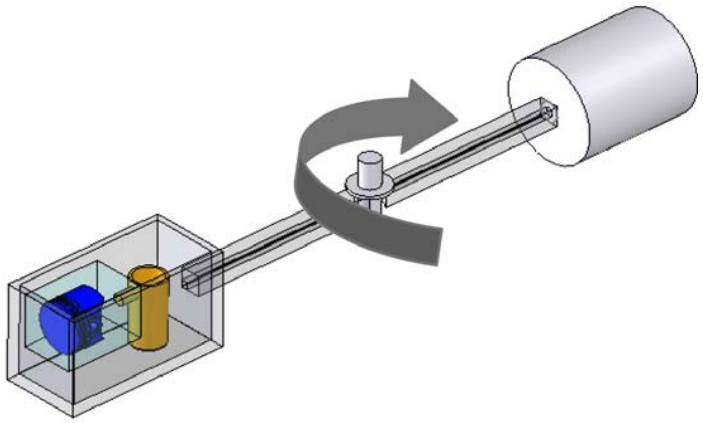

Figure 7.1 – Schematic representation of casting of an engine piston using the vertical centrifugal casting technique.

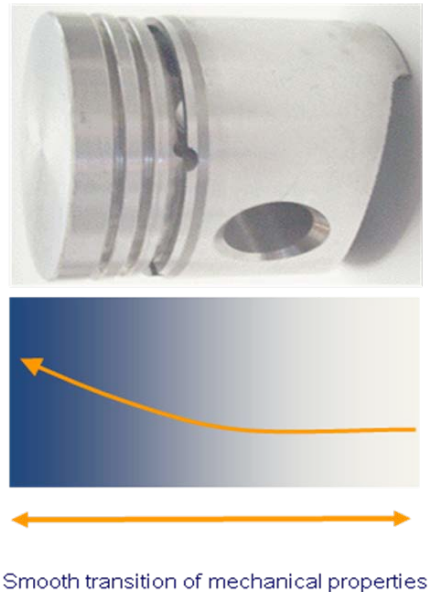

Figure 7.2 - Example of gradation of mechanical properties of an engine piston using vertical centrifugal casting technique.

7.2 Recommendations for future work

The first issue that is important for future work on functionally graded materials is to test the cast aluminium alloys obtained by vertical centrifugal casting at different temperatures.

The high temperature properties of Al-Si alloys are of particular importance because the normal operating temperature of these materials is between 200°C and 440°C. At these temperatures the mechanisms of fatigue crack propagation have been shown to be slightly different to those at room temperature.

Another issue is to analyse the crack growth along the gradient. It is good to know the behavior of the crack along the gradient of the FGM in order to precisely predict the life of the final component.

The next step in this research is to cast and test real pistons to confirm the equation obtained in real components.

The last suggestion for the future of this research is to develop software that can output the mechanical and fatigue properties based on some microstructure feature of the functionally graded materials.

REFERENCES

[1] Dieter G.E., *Engineering Design, A Materials and Processing Approach*, 2nd ed., McGraw-Hill, 1991

[2] Junker H, Issler W. Pistons for high loaded direct injection diesel engines. MAHLE Technical Information.

[3] *** http://www.kspg-ag.de

[4] Chiriţă G., Stefănescu I., Soares D., Silva F.S., „Mechanical resistance as a function of local properties", The Annals of University "Dunărea De Jos" Of Galaţi, Fascicle VIII, 2007 (XIII), ISSM 1221-4590 Tribology, pp. 45-49.

[5] Silva FS. „Fatigue on engine pistons – A compendium of case studies", Engineering Failure Analysis 13 (2006) 480–492

[6] Silva FS. Analysis of a vehicle crankshaft failure. Engineering Failure Analysis 2003;10(5):605–16.

[7] Suresh S.,"Graded materials for resistance to contact deformation and damage", Science, vol.292, pp. 2447-2451, 2001.

[8] Suresh S. and Mortensen A., "Fundamentals of functionally graded materials", London: Institute of Materials, 1998.

[9] Paulino G. H. and Kim J.H., "A new approach to compute T-stress in functionally graded materials by means of interaction integral method", Engineering Fracture Mechanics, vol.71, pp. 1907-1950, 2004.

[10] Nai S, Gupta M, Lim C. Synthesis and wear of Al based, free standing functionally gradient materials: effects of different reinforcements. Mater Sci Technol 2004;20:57 – 67.

[11] Fukui Y.; JSME Inst.J.Series III,34(1991)144-148.

[12] Fukui Y.,Y.Oya-Seimiya,and K.Nakanishi; Transaction of the Japan Society of Mechanical Engineers, Ser. A, 57 (1991) 1790-1793.

[13] Watanabe Y., N. Yamanaka, and Y.Fukui; "Control of composition gradient in a metal-ceramic functionally graded material manufactured by the centrifugal method", Composites Part A, 29A (1998)595-601.

[14] Wenzhou C., W. Qudong, Z. Chunquan, M Chunjiang, Z. Yanping, and H. Wei, "Functionally Graded Zn-Al-Si in-situ Composites Fabricated by Centrifugal Casting," Journal of Materials Science Letters 20. 2001, 823-826.

[15] Watanabe, Y., R. Sato, I. Kim, S. Miura and H. Miura, „ Functionally Graded Material Fabricated by Centrifugal Casting Method from ZK60A Magnesium Alloy," Materials Transactions 46. 2005. 944-949.

[16] Janco, N. (1998) *Centrifugal Casting*, American Foundrymen Society, Inc., ISBN 0-87433-110-2

[17] Nairobi B. Duque, Z. Humberto Melgarejo, O. Marcelo Suarez, "Functionally graded aluminum matrix composites produced by centrifugal casting", Materials Characterization 55 (2005) 167– 171

[18] Zenón Humberto Melgarejo Pinto, "Fabrication and characterization of functionally graded al/alb_2 matrix composites for high wear aerospace applications using centrifugal casting", Master of Science, 2006.

[19] Tunde Kingsley Adelakin, "An experimental study of aluminum boride particles distribution in centrifugally cast al/albx composites", Master of Science, 2009.

[20] Humberto Melgarejo Z., O. Marcelo Suárez, Kumar Sridharan, "Microstructure and properties of functionally graded Al–Mg–B composites fabricated by centrifugal casting", Composites: Part A 39 (2008) 1150–1158.

[21] Yoshihiro Oya-Seimiya, Tetsumori Shinoda, and Yoshimi Watanabe, "Optimization of the In-Situ Al-Si Base Functionally Graded Material Fabricated by Centrifugal Casting", Materials Research Society. Symp. Proc. Vol. 702., 2002.

[22] ASM International, Metal Handbook, Ninth Edition, Vol. 15 Casting, 1997, pag. 296-307.

[23] Haque M.M., M.A. Maleque, "Effect of process variables on structure and properties of aluminium–silicon piston alloy", Journal of Materials Processing Technology 77 (1998) 122–128.

[24] Haque M.M., A. Sharif," Study on wear properties of aluminium–silicon piston alloy",Journal of Materials Processing Technology 118 (2001) 69–73.

[25] Jian X., T.T. Meek, Q. Han, "Refinement of eutectic silicon phase of aluminum A356 alloy using high-intensity ultrasonic vibration", Scripta Materialia 54 (2006) 893–896.

[26] Numan Abu-Dheir, Marwan Khraisheh, Kozo Saito, Alan Male,"Silicon morphology modification in the eutectic Al-Si alloy using mechanical mold vibration", Materials Science and Engineering A 393 (2005) 109–117.

[27] Wang Q.G., "Micro structural effect on the tensile and fracture behaviour of aluminium casting alloy A 356/357", Metallurgical and Materials Transaction, Vol. 34 A, December 2003, 2887-2899.

[28] A.J. Moffat, S. Barnes, B.G. Mellor, P.A.S. Reed , "The effect of silicon content on long crack fatigue behavior of aluminium–silicon piston alloys at elevated temperature" , International Journal of Fatigue 27 (2005) 1564–1570.

[29] Juan Asensio-Lozano, Beatriz Suarez-Pena, "Effect of the addition of refiners and/or modifiers on the microstructure of die cast Al–12Si alloys", Scripta Materialia 54 (2006) 943–947.

[30] Lee Y.C., A.K. Dahle, D.H. StJohn, J.E.C. Hutt, "The effect of grain refinement and silicon content on grain formation in hypoeutectic Al–Si alloys", Materials Science and Engineering A259 (1999) 43–52.

[31] Lim Ying Pio, Shamsuddin Sulaiman, Abdel Majid Hamouda, Megat Mohamad Hamdan Megat Ahmad, "Grain refinement of LM6 Al–Si alloy sand castings to enhance mechanical properties", Journal of Materials Processing Technology 162–163 (2005) 435–441.

[32] Mohanty P. S., J. E. Gruzleski, "Grain refinement mechanisms of hypoeutectic Al-Si alloys", Acta mater. Vol. 44, No. 9, pp. 3749-3760, 1996.

[33] Chirita G., D. Soares, F.S. Silva, Advantages of the centrifugal casting technique for the production of structural components with Al–Si alloys, Materials and Design, Materials & Design, Volume 29, Issue 1, 2008, Pages 20-27.

[34] Abou El-khair M.T., "Microstructure characterization and tensile properties of squeeze-cast AlSiMg alloys", Materials Letters 59 (2005) 894– 900.

[35] Halvaee A., Talebi A., "Effect of process variables on microstructure and segregation in centrifugal casting of C9220 alloy", Journal of Materials Processing Technology,118 (2001) 123-127.

[36] Maleki A., Niroumand B., Shafyei A., “Effects of squeeze casting parameters on density, macrostructure and hardness of LM13 alloy”, Materials Science and Engineering A 428 (2006) 135–140.

[37] Ghomashch M.R., Vikhrov A., “Squeeze casting: an overview”, Journal of Material Processing and Technology, 101, (2000), 1-9.

[38] Watanabe, Y. and Fukui Y.., “Microstructures and Mechanical properties of Functionally Graded Material Fabricated by Centrifugal Casting Method,” Metallurg.& Materials Sci 4. 2000, 51-93.

[39] Sehitoglu H. Thermal and thermomechanical fatigue of structural alloys. ASM Handbook – fatigue and fracture v.9, Ohio, 1996.

[40] Thomas JJ, Verger L, Bignonnet A, Charkaluk E. Thermomechanical design in the automotive industry. Fatigue Fract Eng Mater Struct 2004;27:887–95.

[41] Sermage JP, Lemaitre J, Desmorat R. Multiaxial creep-fatigue under anisothermal conditions. Fatigue Fract Eng Mater Struct 2000;23:241–52.

[42] Neu RW, Sehitoglu H. Thermo-mechanical fatigue, oxidation and creep: Part II: Life prediction. Metall Trans A 1989;20A: 1769–83.

[43] Tohriyama S, Kumano M. Influence of material and mechanical properties on thermal fatigue life of aluminum casting. In: Proceedings of the aluminum application for automotive design, Warrendale, SAE; 1995. p. 47–57.

[44] Gundlach RB, Ross B, Hetke A, Valtierra S, Mojica JF. Thermal fatigue resistance of hypoeutectic aluminum–silicon casting alloys. AFS Trans 1994;102:205–23.

[45] Sehitoglu H, Engler-Pinto Jr CC, Maier HJ, Foglesong T. Thermomechanical deformation of Al319 alloys with different iron contents. In: Proceedings of the high temperature fatigue, CAMP2002, Bad Lippspringe; 2002. p.76–83.

[46] Wickberg A, Gustafson G, Larson LE. Microstructural effects on the fatigue properties of a cast Al7SiMg alloy. SAE Trans 1984;93:728–35.

[47] Vorren O, Evensen JE, Pedersen TB. Microstructure and mechanical properties of AlSi(Mg) casting alloys. AFS Trans 1984;92:459–66.

[48] Sehitoglu H, Qing X, Smith TJ, Maier HJ, Allison JA. Stress–strain response of a cast 319-T6 aluminum under thermomechanical loading. Met Trans A 2000;31A:139–51.

[49] BARNES, S. (2002) Manufacturing pistons. WIPO patent number WO/2002/001059.

[50] BUFFIERE, J.-Y., SAVELLI, S., JOUNEAU, P. H., MAIRE, E. & FOUGIERES, R. (2001) Experimental study of porosity and its relation to fatigue mechanisms of model Al-Si7-Mg0.3 cast Al alloys. Materials Science & Engineering A (Structural Materials: Properties, Microstructure and Processing), A316, 115-26

[51] CONLEY, J. G., HUANG, J., ASADA, J. & AKIBA, K. (2000) Modelling the effects of cooling rate, hydrogen content, grain refiner and modifier on microporosity. formation in Al A356 alloys. Materials Science and Engineering A, 285, 49-55.

[52] CHEN, C. L., WEST, G. & THOMSON, R. C. (2006) Characterisation of intermetallic phases in multicomponent Al-Si casting alloys for engineering applications. Materials Science Forum, 519-521, 359-64.

[53] DAYKIN, C. R. S. (1998) PhD thesis: Microstructural Modelling of Commercial Aluminium - Silicon Alloys for Piston Design. Department of Materials Science and Metallurgy. Cambridge, Magdalene College, Cambridge.

[54] RAVI, M., PILLAI, U. T. S., PAI, B. C., DAMODARAN, A. D. & DWARAKADASA, E. S. (2002) The effect of mischmetal addition on the structure and mechanical properties of a cast Al-7Si-0.3Mg alloy containing excess iron (up to 0.6 pct). 2 ed. San Diego, CA, USA, Minerals, Metals, Materials Society & ASM International.

[55] CACERES, C. H., DAVIDSON, C. J., GRIFFITHS, J. R. & WANG, Q. G. (1999) The effect of Mg an the microstructure and mechanical behavior of Al-Si-Mg casting alloys. Metallurgical and Materials Transactions A (Physical Metallurgy and Materials Science), 30A, 2611-2618.

[56] ELLIOT, R. (1983) Eutectic Solidification Processing Crystalline and Glassy Alloys, London, Butterworths.

[57] EDWARDS, W. M. (2002) PhD Thesis: Microstructural and Mechanical Property Modelling for the Processing of Al-Si Alloys. Institute of Polymer Technology and Materials Engineering. Loughborough, Loughborough University.

[58] ESHELBY, J. D. (1957) The determination of the elastic field of an ellipsoidal inclusion, and related problems. Proceedings of the Royal Society of London, Series A (Mathematical and Physical Sciences), 241, 376-396.

[59] GREER, A. L., COOPER, P. S., MEREDITH, M. W., SCHNEIDER, W., SCHUMACHER, P., SPITTLE, J. A. & TRONCHE, A. (2003) Grain refinement of aluminium alloys by inoculation. Advanced Engineering Materials, 5, 81-91.

[60] GUPTA, M. & LING, S. (1999) Microstructure and mechanical properties of hypo/hyper-eutectic Al-Si alloys synthesized using a near-net shape forming technique. Journal of Alloys and Compounds, 287, 284-294.

[61] HAN, S.-W., KUMAI, S. & SATO, A. (2002) Effects of solidification structure on short fatigue crack growth in Al-7%Si-0.4%Mg alloy castings. Materials Science and Engineering A, 332, 56-63.

[62] HARUN, M., DAUD, A. R. & TALIB, I. A. (1996) Effect of element additions on wear property of eutectic aluminium-silicon alloys. Wear, 194, 54-59.

[63] JOYCE, M. R., STYLES, C. M. & REED, P. A. S. (2002) Elevated temperature fatigue of Al-Si piston alloys. Aluminium Alloys 2002 Their Physical and Mechanical Properties: Proceedings of the 8th International Conference ICAA8, Jul 2-5. Cambridge, United Kingdom, Trans Tech Publications Ltd.

[64] JOYCE, M. R., STYLES, C. M. & REED, P. A. S. (2002b) Microstructural and mechanical property modelling for the processing of Al-Si Alloys: Final report on MAPEA EPSRC grant GR/M38667. Southampton, University of Southampton.

[65] KEARNEY, A. & ROOY, E. L. (1990) Aluminum foundry products. ASM handbook 2. Ohio, USA, ASM.

[66] BAMBERY, H. M. (1932) Piston for internal combustion engine and the like, U.S. Patent No. 1852602. USA.

[67] KIM, H. R., SEO, M. G. & BAE, W. B. (2002) A study of the manufacturing of tie- rod ends with casting/forging process. Journal of Materials Processing Technology, 125-126, 471-476.

[68] SUAREZ-PENA, B. & ASENSIO-LOZANO, J. (2006) Microstructure and mechanical property developments in Al-12Si gravity die-castings after Ti and/or Sr additions. Materials Characterization, 57, 218-226.

[69] STOLARZ, J., MADELAINE-DUPUICH, O. & MAGNIN, T. (2001) Microstructural factors of low cycle fatigue damage in two phase Al-Si alloys. Materials Science and Engineering A, 299, 275-286.

[70] PACZ, A. (1921) Alloy, US Patent No. 1387900. USA.

[71] POLMEAR, I. J. (1989) Light Alloys, London, Edward Arnold.

[72] LASAGNI, F., LASAGNI, A., HOLZAPFEL, C., CKLICH, F. & DEGISCHER, H. (2006) Three Dimensional Characterization of Unmodified and Sr-Modified Al-Si Eutectics by FIB and FIB EDX Tomography. Advanced Engineering Materials, 8, 719-723.

[73] LI, X.-D. & EDWARDS, L. (1996) Theoretical modelling of fatigue threshold for aluminium alloys. Engineering Fracture Mechanics, 54, 35-48.

[74] LIAO, H., SUN, Y. & SUN, G. (2002) Correlation between mechanical properties and amount of dendritic [alpha]-Al phase in as-cast near-eutectic Al-11.6% Si alloys modified with strontium. Materials Science and Engineering A, 335, 62-66.

[75] LEE, M. H., KIM, J. J., KIM, K. H., KIM, N. J., LEE, S. & LEE, E. W. (2003) Effects of HIPping on high-cycle fatigue properties of investment cast A356 aluminum alloys. Materials Science and Engineering A, 340, 123-129.

[76] LOPEZ, I. A., ZEPEDA, C. M., GONZALEZ REYES, J. G., FLORES, A. M., RODRIGUEZ, J. S. & GOMEZ, L. B. (2007) TEM microstructural characterization of melt-spun aged Al-6Si-3Cu-xMg alloys. Materials Characterization, 58, 509-518.

[77] LEE, F. T., MAJOR, J.F., SAMUEL, F.H. (1995) Effect of silicon particles on the fatigue crack growth characteristics of Al-12 wt pct Si-0.35 wt pct Mg-(0 to 0.02) wt pct Sr casting alloys. Metallurgical and Materials Transactions A: Physical Metallurgy and Materials Science, 26A, 1553-1570.

[78] LUDWIG, W., BUFFIERE, J.-Y., SAVELLI, S. & CLOETENS, P. (2003) Study of the interaction of a short fatigue cracks with grain boundaries in a cast Al alloy using X-ray microtomography. Acta Materialia, 51, 585-98.

[79] ZHANG, D. L., ZHENG, L. H. & STJOHN, D. H. Effect of a short solution treatment time on microstructure and mechanical properties of modified Al-7wt.%Si-0.3wt.%Mg alloy. Journal of Light Metals, 2, 27-36,(2002)

[80] YE, H. (2003) An overview of the development of Al-Si-alloy based material for engine applications. Journal of Materials Engineering and Performance, 12, 288-297.

[81] VERDU, C., CERCUEIL, H., COMMUNAL, S., SAINFORT, P., FOUGERES, R. (1996) Microstructural aspects of the damage mechanisms of cast Al-7Si-Mg alloys. Materials Science Forum: Proceedings of the 1996 5th International Conference, ICAA5. Part 3 (of 3), Jul 1-5 1996, 217-222, 1449-1454.

[82] WANG, J., HE, S., SUN, B., GUO, Q. & NISHIO, M. (2003) Grain refinement of Al-Si alloy (A356) by melt thermal treatment. Journal of Materials Processing Technology, 141, 29-34.

[83] WANG, Q. G., APELIAN, D. & LADOS, D. A. (2001a) Fatigue behavior of A356-T6 aluminum cast alloys. Part I. Effect of casting defects. Journal of Light Metals, 1, 73-84.

[84] WANG, Q. G., APELIAN, D. & LADOS, D. A. (2001) Fatigue behavior of A356/357 aluminum cast alloys. Part II - Effect of microstructural constituents. Journal of Light Metals, 1, 85-97.

[85] ROY, N., SAMUEL, A. M. & SAMUEL, F. H. (1996) Porosity formation in Al-9 wt pct Si-3 wt pct Cu alloy systems: Metallographic observations. Metallurgical and Materials Transactions A: Physical Metallurgy and Materials Science, 27A, 415-429.

[86] Campbell J., Castings, 2nd Ed, Butterworth-Heinemann Ltd, Oxford (2003), ISBN 0 75064790 6.

[87] Kumar P., J.L. Gaindhar, AFS Transaction, (1997), pp. 635-638.

[88] Uzun O., T. Karaaslan, M. Gogebakan, M. Keskin, "Hardness and microstructural characteristics of rapidly solidified Al–8–16 wt.%Si alloys", Journal of Alloys and Compounds 376 (2004) 149–157..

[89] Takayama S., J. Mater. Sci. 11 (1976) 164–168.

[90] Lu S., A. Hellawell, Metall. Trans. A 18 (1987) 1721–1733.

[91] Nogita K., S.D. McDonald, A.K. Dahle, Mater. Trans. 45 (2004) 323–326.

[92] Xu C.L., H.Y. Wang, F. Qiu, Y.F. Yang, Q.C. Jiang, "Cooling rate and microstructure of rapidly solidified Al–20 wt.% Si alloy", Materials Science and Engineering A 417 (2006) 275–280.

[93] Gruzleski J.E., Closset B.M., *The Treatment of Liquid Aluminum-Silicon Alloys,* American Foundrymen's Society, Inc., Des Plaines, IL, USA, 1990. pp. 16; 25-55.

[94] Bãckerud L., Chai G., Tamminen J., *Solidification Characteristics of Aluminum Alloys, Volume 2: Foundry Alloys,* AFS/SKANALUMINUM, Des Plains, IL, 1990.

[95] Jorstad J.L., Rasmussen W.M., *Aluminum Casting Technology*, 2n d Edition, American Foundrymen's Society, Des Plaines, IL, 1993.

[96] Kissling RJ., Wallace J.F., "Grain Refinement of Aluminum Castings", *Foundry*, June 1963, pp. 78-82.

[97] Boileau J.M., "The Effect of Solidification Time on the Mechanical Properties of a Cast 319 Aluminum Alloy", *Ph.D Dissertation*, Wayne State University, 2000.

[98] Moffat A. J., Barnes S., Mellor B. G. and Reed P.A.S.: "The effect of silicon content on long crack fatigue behaviour of aluminium–silicon piston alloys at elevated temperature", International Journal of Fatigue, 2005, vol. 27, 1564–1570.

[99] Fisher T.P., Effects of vibrational energy on the solidification of aluminium alloys, Br. Foundryman 66 (3) (1973), pp. 71–83.

[100] Ivanov A.A. and Krushenka G.G., Preparation of Al–Si alloying composition by means of vibration, Liteinoe Proizvod 3 (1993), pp. 7–8 [in Russian].Met. Abs. 46-0019; 1992.

[101] Kocatepe Kadir, Effect of low frequency vibration on porosity of LM25 and LM6 alloys, Mater Des 28 (6) (2006), pp. 1767–1775

[102] Pillai R.M., Biju Kumar K. S. and Pai B. C., "A simple inexpensive technique for enhancing density and mechanical properties of Al-Si alloys", Journal of Material processing Technology, vol 146, 2004, pp 338-348.

[103] Abu-Dheir Numan, Marwan Khraisheh, Kozo Saito, Alan Male,"Silicon morphology modification in the eutectic Al-Si alloy using mechanical mould vibration", *Materials Science and Engineering* A393 pp. 109-117, (2005).

[104] Dommaschk C, Ph.D. Thesis, University of Freiburg, Germany, 2003.

[105] Bast et all, Advanced engineering materials, 2004, vol.6, no.7, pp 550-554.

[106] Abu-Dheir N et all, Solidification of aluminium alloys, TMS 2004, pp 361-368.

[107] Chang S. R., Kim J. M. and Hong C. P.: ISIJ Int., 2001, 41, (7),738–747.

[108] Kim J. K. and Rohatgi P. K.: Mater. Sci. Eng. A, 1998, A244, 168–177.

[109] Liu G, Ma YC, Gao M, Rao GB, Li YY, Wei K, et al. Single step centrifugal casting TiAl automotive valves. Intermetallics 2005;13: 925–8.

[110] Gao JW, Wang CY. Modelling the solidification of functionally graded materials by centrifugal casting. Mater Sci Eng 2000;A292: 207–15.

[111] Cay F, Kurnaz SC. Hot tensile and fatigue behaviour of zinc–aluminium alloys produced by gravity and squeeze casting. Mater Des 2005;26(6):479–85.

[112] Beghi ME, Caglioti G, Barone S, Mus C. Microstructural and mechanical effects on liquid hot isostatic pressing on AA356 samples. Met Sci Technol 2001;19(1):6–11.

[113] Murakami Y. Metal fatigue: effects of small defects and non-metallic inclusions. Elsevier Science; 2002, ISBN 0-08-044064-9. p. 1–9.

[114] Radhakrishna K., S. Seshan, M. Seshardi, "Effect of Porosity on Mechanical Properties of Aluminum Alloy Castings", *Transactions of the Indian Institute of Metals*, 1981, vol. 34(2), pp. 169-171

[115] Wang QG. Micro structural effect on the tensile and fracture behaviour of aluminium casting alloy A 356/357, Metallurgical and Material Transactions 2003;34A(12):2887–2899.

[116] Liao H, Sun Yu, Sun G. Correlation between mechanical properties and amount of dendritic a-Al phase in as-cast near-eutectic Al–11.6% Si alloys modified with strontium. Mater Sci Eng 2002;A335:62–6.

[117] Shabestari SG, Moemeni H. Effect of copper and solidification conditions on the microstructure and mechanical properties of Al–Si–Mg alloys. J Mater Proc Technol 2004;153–154:193–8.

[118] Cantor B., O'Reilly K., Solidification and Casting, IOP, 2003.

[119] Alexopoulos N.D., Pantelakis Sp.G., Quality evaluation of A357 cast aluminum alloy specimens subjected to different artificial aging treatment, Materials and Design 25 (2004) 419–430.

[120] Granger D. A., Elliott R., Solidification of Eutectic Alloys: Aluminum-Silicon Alloys in: Metals Handbook, Vol 15, 9th ed., ASM International, Warrendale, PA, 1988, 159-181

[121] Tiryakioglu M., Campbell J., Staley J.T., The influence of structural integrity on the tensile deformation of cast Al–7wt.%Si–0.6wt.%Mg alloys; Scripta Materialia 49 (2003) 873-878.

[122] Lee C. D., Effects of microporosity on tensile properties of A356 aluminum alloy; Materials Science and Engineering: A 464 (2007) 249-254.

[123] Wang Q.G., Apelian D., Lados D.A., Fatigue behavior of A356-T6 aluminum cast alloys Part I. Effect of casting defects, J. Light Metals 1 (2001) 73-84.

[124] Yi J.Z., Lee P.D., Lindley T.C., Fukui T., Statistical modeling of microstructure and defect population effects on the fatigue performance of cast A356-T6 automotive components, Materials Science and Engineering: A, 432, Issues 1-2 (2006) 59-68.

[125] Ammar H.R., Samuel A.M., Samuel F.H., Effect of casting imperfections on the fatigue life of 319-F and A356-T6 Al–Si casting alloys, Materials Science and Engineering: A, 473, Issues 1-2, (2008) 65-75.

[126] Guang Ran, Jingèn Zhou, Q.G. Wang, The effect of hot isostatic pressing on the microstructure and tensile properties of an unmodified A356-T6 cast aluminum alloy, Journal of Alloys and Compounds, V. 421, Issues 1-2 (2006) 80-86.

[127] Ceschini L., Morri A., Sambogna G., The effect of hot isostatic pressing on the fatigue behaviour of sand-cast A356-T6 and A204-T6 aluminum alloys; Journal of Materials Processing Technology, 204, Issues 1-3 (2008) 231-238.

[128] Linder J., Axelsson M., Nilsson H., The influence of porosity on the fatigue life for sand and permanent mould cast aluminium, International Journal of Fatigue, 28, Issue 12, (2006) 1752-1758.

[129] Shabestari S.G., Moemeni H., Effect of copper and solidification conditions on the microstructure and mechanical properties of Al–Si–Mg alloys, Journal of Materials Processing Technology, 153-154 (2004) 193-198.

[130] Shabestari S. G., Shahari F., Influence of modification, solidification conditions and heat treatment on the microstructure and mechanical properties of A356 aluminum alloy; Journal of Materials Science 39 (2004) 2023-2032.

[131] Wang Q. G., Apelian D., Lados D. A., Fatigue behavior of A356/357 aluminum cast alloys. Part II. Effect of microstructural constituents, Journal of Lights Metals 1, 2001, p.85-97.

[132] Wang Q. G., Cáceres C. H., The fracture mode in Al–Si–Mg casting alloys, Materials Science and Engineering A, 241, Issues 1-2 (1998) 72-82.

[133] Li Z., Samuel A.M., Samuel F.H., Ravindran C., Valtierra S., Doty H.W., Parameters controlling the performance of AA319-type alloys Part I. Tensile properties, Materials Science and Engineering A 367 (2004) 96–110.

[134] Ogris E., Wahlen A., Luchinger H., Uggowitzer P.J., On the silicon spheroidization in Al–Si alloys ; Journal of light Metals 2 (2002) 263–269.

[135] The Properties of Aluminum and its Alloys, 9th ed., Aluminum Federation Ltd., Birmingham, 1993.

[136] Zhu X., Shyam A., Jones J.W., Mayer H., Lasecki J.V., Allison J.E., Effects of microstructure and temperature on fatigue behavior of E319-T7 cast aluminum alloy in very long life cycles, International Journal of Fatigue 28 (2006) 1566–1571.

[137] Voigt, R.C. and Bye, D.R. “Microstructural aspects of fracture in A356", AFS Transactions, 91-125, pp 33-50 (1991).

[138] Oswalt, K.J. and Misra, M.S. “Dendrite arm spacing: A non destructive test to evaluate tensile properties of premium quality aluminum alloy (Al-Si-Mg) castings", AFS Transactions, 80-51, pp 845-861 (1980).

[139] Radhakrishna, K. and Seshan, S. “Dendrite arm spacing and mechanical properties of aluminum cast alloys", Cast Metals., 2(1), pp 34-38 (1989).

[140] Flemings, M.C., Kattamis, T.Z. and Bardes, B.P. “Dendrite arm spacing in aluminum alloys", AFS Transactions, 90-176, pp 501-506 (1991).

[141] Caceres, C.H. “Microstructural effects on the strength-ductility relationship of Al-7Si-Mg casting alloys", Materials Science Forum, 331-337, pp 223-228 (2000).

[142] Pan, E.N., Hsieh, M.W., Jang, S.S. and Loper, Jr., C.R. “Study of influence of processing parameters on the microstructure and properties of A356 aluminum alloy", AFS Transactions, 89-73, pp 397-414 (1989).

[143] Hetke, A. and Gundlach, R.B. “Aluminum casting quality in alloy 356 engine components", AFS Transactions, 94-137, pp 367-380 (1994).

[144] Khomamizadeh F. and Ghasemi A., “Evaluation of Quality Index of A-356 Aluminum Alloy by Microstructural Analysis”, Scientia Iranica, Vol. 11, No. 4, pp 386-391

[145] Caceres, H., Wang, L., Apelian, D. and Makhlouf, M.M. “Alloy selection for die castings using the quality index", AFS Transactions, 107, 99-147, pp 239-247 (1999).

[146] Bernsztejn L. and Zajmowskij W.A., , 1973 Struktura i własnos´ci mechaniczne metali (Structure and Mechanical Properties of Metals),Wyd. Naukowo-Techniczne, Warsaw.

[147] Mandal P., A. Saha, M. Chakraborty, 1991, Size of primary silicon particles and mechanical properties of as-cast high Silicon Al alloys, AFS Trans.33, p 99.

[148] Takahashi T., Sugimura Y., Sasaki K., 2004, Thermal plastic-elastic analysis in consideration of metallurgical microstructure, Journal of Manufacturing Science and Engineering Vol.126 (2004) 25-32.

[149] YI, J. Z., GAO, Y. X., LEE, P. D., FLOWER, H. M. & LINDLEY, T. C. (2003) Scatter in fatigue life due to effects of porosity in cast A356-T6 aluminumsilicon alloys. *Metallurgical and Materials Transactions A: Physical Metallurgy and Materials Science,* 34 A**,** 1879-1890.

[150] JOYCE, M. R., STYLES, C. M. & REED, P. A. S. (2003) Elevated temperature short crack fatigue behaviour in near eutectic Al-Si alloys. *International Journal of Fatigue,* 25**,** 863-869.

[151] GALL, K., YAN, N., HORSTEMEYER, M., MCDOWELL, D. L. & FAN, J. (2000) The influence of modified intermetallics and Si particles on fatigue crack paths in a cast A356 Al alloy. *Fatigue and Fracture of Engineering Materials and Structures,* 23**,** 159-172.

[152] Armstrong G.L., SAE Technical Paper, No. 780249, Society of Automotive Engineers, 1987.

[153] Properties and Selection: Nonferrous Alloys and Special-Purpose Materials, ASM Handbook, vol. 2, ASM International, The Materials Information Society, USA, 1990.

[154] Boileau J.M., Allison J.E., SAE Trans. 110 (2001) 648–659.

[155] Kim J.M., Kwon H.W., Kim D.G., Loper C.R. Jr., AFS Trans. 105 (1997) 825–831.

[156] Sigworth G.K., Wang C., Huang H., Berry T., AFS Trans. 102 (1994) 245–260.

[157] Kubo K., Pehlke R.D., AFS Trans. 94 (1986) 753–756.

[158] Huang Y.J., Lu S.Z., Proceedings of the 2nd International Aluminum Casting Technology Symposium, 2002, Columbus, OH, USA, ASM International, 2002, 4 pp.

[159] Roy N., Zhang L., Louchez P.R., Samuel F.H., J. Mater. Sci. 31 (5) (1996) 1243–1254.

[160] Samuel A.M., Samuel F.H., AFS Trans. 100 (1992) 657–666.

[161] Lampman S.R., Fatigue and Fracture, ASM International, The Materials Information Society, Materials Park, OH, USA, 1996.

[162] Wang Q.G., Crepeau P.N., Griffiths J.R., Davidson C.J., in: M. Tiryakioglu, P.N. Creapeau (Eds.), Proceedings of the Shape Casting: The John Campbell Symposium, TMS, Warrendale, PA, 2005, pp. 205–214.

[163] Wang Q.G., Crepeau P.N., Gloria D., Valtierra S., Proceedings of the 2nd International Aluminum Casting Technology Symposium, 2002, Columbus, OH, ASM International, Materials Park, OH, USA, 2002, pp. 209–218.

[164] Boileau J.M., Allison J.E., Metall. Mater. Trans. A 34A (2003) 1807–1820.

[165] Boileau J.M., Zindel J.W., Allison J.E., SAE Paper No. 970019, SAE, Warrendale, PA, 1997.

[166] Odegard J.A., Pedersen K., Proceedings of the Conference on Metal Matrix Composites, Detroit, MI, USA, 1994, pp. 25–35.

[167] Rading G.O., Li J., Berry J.T., AFS Trans. 102 (1994) 57–61.

[168] Major J.F., AFS Trans. 105 (1997) 901–906.

[169] Savelli S., Buffiere J.-Y., Maire E., Fougeres R., Proceedings of the 6th International Conference on Aluminum Alloys, 1998, pp. 571–576.

[170] Skallerud, B., T. Iveland, and G. Harkegard, *Fatigue life assessment of aluminum alloys with casting defects.* Engineering Fracture Mechanics, 1993. 44(6): p. 857-874.

[171] ZHANG, B., POIRIER, D. R. & CHEN, W. (1999) Microstructural effects on highcycle fatigue-crack initiation in A356.2 casting alloy. Metallurgical and Materials Transactions A: Physical Metallurgy and Materials Science, 30**,** 2659-2666.

[172] Seniw M.E., Fine M.E., Chen E.Y., Meshii M., Gray J., Proceedings of the TMS Fall Symposium, Indianapolis, Indiana, USA, ASM International, Materials Park, OH, 1997, pp. 371–379.

[173] Annual Book of ASTM Standards, Section 3: Metal Test Methods and Analytical Procedures, E466-82. 3.1 (1995) 470–471.

[174] SONSINO CM, ZIESE J. Fatigue strength and applications of cast aluminium alloys with different degree of porosity. International Journal of Fatigue; 15:75-84, 1993.

[175] MURAKAMI, Y. Metal Fatigue: Effects of Small Defects and Nonmetallic Inclusions, Elsevier, Oxford, 2002. p. 320.

[176] Caton, M.J., et al., *The effect of solidification rate on the growth of small fatigue cracks in a cast 319-type aluminum alloy.* Metall. Trans. A, 1999. 30(12): p. 3055-3068.

[177] Boileau, J.M. and J.E. Allison, *The Effect of Solidification Time and Heat Treatment on the Fatigue Properties of a Cast 319 Aluminum Alloy.* Metallurgical and Materials Transactions A, 2003. 34A(9): p. 1807-1820.

[178] Couper, M.J., A.E. Neeson, and J.R. Griffiths, *Casting Defects and the Fatigue Behaviour of an Aluminium Casting Alloy.* Fatigue Fract. Engng Mater. Struct., 1990. 13(3): p. 213-227.

[179] Murakami, Y. and M. Endo, *Effects of defects, inclusions and inhomogeneities on fatigue strength.* International Journal of Fatigue, 1994. 16(3): p. 163-182.

[180] Caton, M.J., J.W. Jones, and J.E. Allison, *Use of small fatigue crack growth analysis in predicting the S-N response of cast aluminium alloys*, in *Fatigue Crack Growth Thresholds, Endurance Limits, and Design, ASTM STP 1732*, J.C.J. Newman and R.S. Piascik, Editors. 2000, ASTM: West Conshohocken, PA. p. 285-303.

[181] Lados, D.A., D. Apelian, and J.K. Donald, *Fatigue crack growth mechanisms at the microstructure scale in Al-Si-Mg cast alloys: Mechanisms in the near-threshold regime.* Acta Materialia, 2006. 54(6): p. 1475-1486.

[182] Caton, M.J., J.W. Jones, and J.E. Allison, *The influence of heat treatment and solidification time on the behavior of small-fatigue-cracks in a cast aluminum alloy.* Materials Science and Engineering A, 2001. 314(1-2): p. 81-85.

[183] Gall, K., et al., *Environmentally influenced microstructurally small fatigue crack growth in cast magnesium.* Materials Science and Engineering A, 2005. 396(1-2): p. 143-154.

[184] Ting, J.C. and F.V.J. Lawrence, *Modeling the Long-Life Fatigue Behavior of a Cast Aluminum Alloy.* Fatigue and Fracture of Engineering Materials and Structures, 1993. 16(6): p. 631-647.

[185] Boileau, J.M., J.W. Zindel, and J.E. Allison, *The effect of solidification time on the mechanical properties in a cast A356-T6 aluminum alloy*, in *SAE Technical Paper #970019*. 1997.

[186] Ting, J.C., *The long-life regime fatigue analysis for lost foam cast Al- Si Alloy 319*. 1991, University of Illinois-Champaign, IL. p. 1-86.

[187] Lados, D.A. and D. Apelian, *Fatigue crack growth characteristics in cast Al-Si-Mg alloys: Part I. Effect of processing conditions and microstructure.* Materials Science and Engineering A, 2004. 385(1-2): p. 200-211.

[188] Kim, S.-W., et al., Mater. Lett., 2003. 58: p. 257-261.

[189] Kumai, S., et al., *Effects of dendrite cell size and eutectic Si particle morphology on fatigue crack growth in cast and HIPed AC4CH alloys.* Materials Transactions, JIM, 1999. 40(7): p. 685-691.

[190] Yi, J.Z., *Effect of microstructure and defects on the fatigue behavior of cast A356-T6 aluminium-silicon alloy,* in *Department of Materials*. 2004, Imperial College: London, UK.

[191] Kumai, S., et al., *Effects of solidification structure on fatigue crack growth in AC4CH cast aluminum alloys.* Journal of Japan Institute of Light Metals, 1995. 45(4): p. 198-203.

[192] Chirita G., Stefanescu I., D. Cruz, D. Soares and F. S. Silva: Submitted to J. Eng. Mater. Technol.

[193] Chirita G., I. Stefanescu, D. Soares and F. S. Silva: Materials and Design 30 (2009) 1575–1580

[194] Chirita G, Stefanescu I, Barbosa J, Puga N, Soares D, Silva, FS. „On the assessment of precessing variables in a vertical centrifugal casting technique", International Journal of Cast Metals Research 2009 vol. 22 no. 5, pp.382-389.

[195] Suresh S. Fatigue of materials. 2nd ed. Cambridge University Press; 1998.

[196] Brockenbrough JR, Hinkle AJ, Magnusen PE, Bucci RJ. Microstructurally based model of fatigue and growth. In: NASA conference publication 3274; 1994. p. 71–84.

[197] Fan J, McDowell DL, Horstemeyer MF, Gall K. Computational micromechanics analysis of cyclic crack-tip behavior for microstructurally small cracks in dualphase Al–Si alloys. Eng Fract Mech 2001;68:1687–706.

[198] McDowell DL, Gall K, Horstemeyer MF, Fan J. Microstructure-based fatigue modeling of cast A356-T6 alloy. Eng Fract Mech 2003;70:49–80.

[199] Liu M, Bozek JE, Hochhalter JD, Veilleux MG, Heber G, Sintay SD, et al. A geometric approach to modeling microstructurally small fatigue crack formation. Part I: Probabilistic simulation of constituent particle cracking in AA 7075-T651. Model Simulat Mater Sci Eng 2008;16:1–28.

[200] Harlow DG, Wang MZ, Wei RP. Statistical analysis of constituent particles in 7075-T6 aluminum alloy. Metall Mater Trans A 2006;37A:3367–73.

[201] GAO Y. X., YI J. Z., LEE P. D. and LINDLEY T. C., „The effect of porosity on the fatigue life of cast aluminium-silicon alloys", 2004 Blackwell Publishing Ltd. Fatigue Fract Engng Mater Struct 27, 559–570.

[202] Reinhart T L, ASM Handbook, 19, (Fatigue and Fracture), (1996), p.813-822.

[203] Chen W, Zhang B, Wu T, Poirier D R and Fang Q T: *Materials Solutions Conference*, ASM, International, (1998).

[204] Promise N E: Evaluation of non-ferrous materials (1956), cited by H. E. Boyer in *Atlas of Fatigue Curves*, American Society of Metals, (1960).

[205] Zhang, B., Chen, W., Poirier, D.R., "Effect of solidification cooling rate on the fatigue life of A356.2-T6 cast aluminium alloy", Fatigue Fract Engng Mater Struct 23, pp. 417-423, 2000.

[206] Ceschini L., Morri A., Gamberini A., Messieri S., "Correlation between ultimate tensile strength and solidification microstructure for the sand cast A357 aluminium alloy", Materials & Design, Volume 30, Issue 10, pp. 4525-4531, Dec. (2009).

[207] G. Chirita, I. Stefanescu, D. Cruz, D. Soares, F.S. Silva, Sensitivity of different Al–Si alloys to centrifugal casting effect, Materials & Design, Volume 31, Issue 6, Pages 2867-2877, (2010)

LIST OF PUBLICATIONS

Papers in international scientific periodicals with referees

[1] Chirita, G; Stefanescu, I; Soares, D, Silva, FS,. *Effect of Gravity/Vibration/Centrifugal Process on Mechanical Properties of an Al-Si Alloy,* ADVANCED MATERIALS FORUM IV Volume: 587-588 Pages: 395-399, 2008.

[2] Chirita, G; Stefanescu, I; Soares, D, Silva, FS,. *Centrifugal casting features/metallurgical characterization of aluminum alloys*, MULTISCALE AND FUNCTIONALLY GRADED MATERIALS Volume: 973 Pages: 598-603, 2008.

[3] Chirita, G; Soares, D; Silva, FS, *Advantages of the centrifugal casting technique for the production of structural components with Al-Si alloys,* MATERIALS & DESIGN Volume: 29 Pages: 20-27, 2008.

[4] Chirita G, Stefanescu I, Barbosa J, Puga H, Soares D, Silva FS, "*On assessment of processing variables in vertical centrifugal casting technique*", INTERNATIONAL JOURNAL OF CAST METALS RESEARCH Volume: 22 Issue: 5 Pages: 382-389, 2009.

[5] Chirita G, Stefanescu I, Soares D, Silva FS, "*Influence of vibration on the solidification behaviour and tensile properties of an Al-18 wt%Si alloy*", MATERIALS & DESIGN Volume: 30 Issue: 5 Pages: 1575-1580, 2009.

[6] Chirita G, Stefanescu I, Cruz, D, Soares D, Silva FS, "*Sensitivity of different Al-Si alloys to centrifugal casting effect* ", MATERIALS & DESIGN Volume: 31 Issue: 6 Pages: 2867-2877, 2010.

[7] Chirita G, Stefanescu I, Soares D, Silva FS, *" On the ability of producing FGMs with an AlSi12 aluminium alloy by using centrifugal casting "*, International Journal of Materials & Product Technology, Volume: 39, Issue: 1-2, Pages:30-43, 2010.

[8] Silva FS, Chirita G, N. Costa, Stefanescu I, Soares D, , *" Guidelines for establishment of correlations between mechanical properties and microstructure in Al-Si alloys "*, Materials Science & Technology, in press, (2010), DOI: 10.1179/1743284710Y.0000000003.

Papers in conference proceedings

[1] Chirita, G. , Stefanescu, I, Soares, D., Barbosa, J. , Silva, F.S.*"Particular features of the centrifugal casting technique over mechanical properties of obtained castings"*, Proceedings of 10th Portuguese Conference on Fracture, Guimaraes, 22-24 februarie 2006, ISBN: 972-99596-1-7, Ref. S6-A-3.

[2] Chirita, G., Stefanescu, I, Soares, D., Silva, F.S., *„Centrifugal versus gravity casting techniques over mechanical properties"*, Proceedings of XXIII Encuentro de Grupo Español de Fractura, Albarracin, 29-31 Martie 2006, vol. I, 2006, pp. 317-322.

[3] Chirita, G., Stefanescu, I, Cruz, D., Soares, D., Silva, F.S. *„The centrifugal effect over mechanical properties on aluminium castings"*, Proceedings of 5th International Conference on Mechanics and Materials in Design, Porto, 24–26 July 2006, ISBN: 972-8826-10-9 Ref: A1001.0008.

[4] Chirita, G., Stefanescu, I., Soares, D., Cruz, D., Silva, F.S., *„Centrifugal casting features/metallurgical characterization on aluminum alloys*", Proceedings of Multiscale and Functionally Graded Materials Conference, Hawaii, 15-18 October 2006.

[5] Chirita, G., Stefanescu, I, Soares, D., Silva, F.S., „Effect of gravity/ vibration/ centrifugal process on mechanical properties of an al-si alloy", Proceeding of the Materials 2007 Conference, Porto , 1-4 April.

[6] Chirita, G., Stefanescu, I, Soares, D., Silva, F.S., „Mechanical resistance as a function of local properties", 1st International Conference on Diagnosis and Prediction in Mechanical Engineering Systems (DIPRE'07), 26-27 October 2007, Galati, Romania.

[7] Chirita, G., Stefanescu, I, Soares, D., Silva, F.S., „Mechanical properties modification in a hypereutectic Al–Si alloy using mechanical mold vibration", Proceeding of the 11TH PORTUGUESE CONFERENCE ON FRACTURE, Lisbon, 13-15 february 2008.

Oral communications

[1] Chirita, G. , Stefanescu, I, Soares, D., Barbosa, J. , Silva, F.S."*Particular features of the centrifugal casting technique over mechanical properties of obtained castings"*, 10th Portuguese Conference on Fracture, February 22-24, University of Minho, Guimarães, Portugal, (2006).

[2] Chirita, G., Stefanescu, I, Soares, D., Silva, F.S., „*Centrifugal versus gravity casting techniques over mechanical properties",* XXIII Encuentro de Grupo Español de Fractura, Albarracin, 29-31 March 2006.

[3] Chirita, G., Stefanescu, I, Cruz, D., Soares, D., Silva, F.S. *„The centrifugal effect over mechanical properties on aluminium castings"*, 5th International Conference on Mechanics and Materials in Design, Porto, 24–26 July 2006.

[4] Chirita, G., Stefanescu, I., Soares, D., Cruz, D., Silva, F.S., „*Centrifugal casting features/metallurgical characterization on aluminum alloy*s", Multiscale and Functionally Graded Materials Conference, Hawaii, 15-18 october 2006.

[5] Chirita, G., Stefanescu, I, Soares, D., Silva, F.S., „Effect of gravity/ vibration/ centrifugal process on mechanical properties of an Al-Si alloy", Proceeding of the Materials 2007 Conference, Porto , 1-4 April.

[6] Chirita, G., Stefanescu, I, Soares, D., Silva, F.S., „Mechanical resistance as a function of local properties", 1st International Conference on Diagnosis and Prediction in Mechanical Engineering Systems (DIPRE'07), 26-27 October 2007, Galati, Romania.

[7] Chirita, G., Stefanescu, I, Soares, D., Silva, F.S., „Mechanical properties modification in a hypereutectic Al–Si alloy using mechanical mold vibration", 11TH PORTUGUESE CONFERENCE ON FRACTURE, Lisbon, 13-15 february 2008.

[8] Chirita, G., Stefanescu, I, Soares, D., Silva, F.S., „Improvement of Mechanical and Fatigue Properties by Centrifugal Casting Process on Al-Si Alloys", Materials Science and Engineering Congress, 1 - 4 September 2008 , Nürnberg, Germany.

[9] Chirita, G., Stefanescu, I, Soares, D., Silva, F.S.,, "Casting technique influence over fatigue life of Al12Si", 2nd International Conference on Diagnosis and Prediction in Mechanical Engineering Systems (DIPRE'09), 22-23 October 2009, Galati, Romania.

[10] Chirita, G., Stefanescu, I, Soares, D., Silva, F.S.,, "Functionally graded material's of Al18Si obtained by centrifugal casting", 2nd International Conference on Diagnosis and Prediction in Mechanical Engineering Systems (DIPRE'09), 22-23 October 2009, Galati, Romania.